CHARACTERIZATION OF ATAXIN-2 AND ITS INTERACTION PARTNERS

DISSERTATION

ZUR ERLANGUNG DES DOKTORGRADES

DER NATURWISSENSCHAFTEN

VORGELEGT BEIM FACHBEREICH BIOWISSENSCHAFTEN

DER JOHANN WOLFGANG GOETHE -UNIVERSITÄT

IN FRANKFURT AM MAIN

VON MELANIE VANESSA HALBACH (GEB. HECK)

AUS KARLSRUHE

FRANKFURT AM MAIN, 2015

(D30)

Vom Fachbereich Biowissenschaften (15) der Johann Wolfgang Goethe - Universität als Dissertation angenommen.

Dekanin: Prof. Dr. rer. nat. Meike Piepenbring

Gutachter: Prof. Dr. rer. nat. Anna Starzinski-Powitz
Prof. Dr. med. Georg Auburger

Datum der Disputation:

Table of contents

1 Introduction

1.1 Cerebellum: the movement coordination system

The cerebellum is a quite striking part of the brain due to its extraordinary structure and separated position. It accounts for ~10% of the total brain volume in humans and rodents but contains more than 50% of the total number of neurons (Kandel et al., 2000). The cerebellum is essential for coordination and movement control, specifically for the coordination and timing of different voluntary body movements, for motor learning, and balance maintaining (Kandel et al., 2000; Purves et al., 2001). In the past, the cerebellum was considered as a structure only dedicated to these motor control functions. However, functional imaging studies revealed that it is also implicated in language and other cognitive functions (Kandel et al., 2000). Furthermore, a role in signal processing for perception and emotional behavior has been proposed (Bhanpuri et al., 2012; D'Angelo and Casali, 2012; Kandel et al., 2000; Schmahmann, 2010). However, the function that has been the most reviewed and the best understood remains the motor control (Kandel et al., 2000).

1.2 Structure and connectivity of the cerebellum

Due to differences in their functional responsibilities and their input sources, the cerebellum is subdivided into three parts: the cerebrocerebellum, the spinocerebellum, and the vestibulocerebellum (Figure 1). The cerebrocerebellum is the largest of the three compartments and is necessary for motor learning and memory of skilled tasks but also for voluntary eye movement. The spinocerebellum is the only part that receives input directly from the spinal cord. It is responsible for maintaining muscle tone as well as routine movement coordination like walking and running. The vestibulocerebellum is the most primitive and phylogenetically oldest part. It is involved in postural maintenance, balance, coordination of gait, and eye movements (Kandel et al., 2000; Mendoza, 2008; Purves et al., 2001).

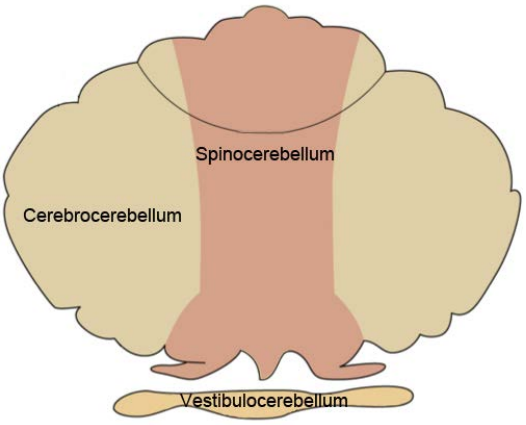

Figure 1. Compartmentalization of the cerebellum. Functional partition of the cerebellum into cerebrocerebellum, spinocerebellum, and vestibulocerebellum (adapted from (Kandel et al., 2000)).

Apart from the functional partition, the cerebellum is morphologically divided into the cerebellar cortex and the deep nuclei. The cerebellar cortex is strongly folded and is composed of three layers: a superficial molecular layer, followed by a single line of Purkinje cells and the granule cell layer as the deepest layer (Figure 2 A) (Apps and Garwicz, 2005). Mossy fibers deriving from the pontine nuclei or the spinal cord but also from other brain regions and climbing fibers originating from the inferior olive generate the cerebellar input (Herrup and Kuemerle, 1997). More precisely, mossy fibers form excitatory synapses on the glutamatergic granule cells as well as on the deep cerebellar nuclei cells (Purves et al., 2001). The axons of the granule cells extend to the molecular layer and branch like a “T”. These branches are arranged in parallel and are, therefore, called parallel fibers. The parallel fibers form excitatory synapses with the Purkinje cell dendrites but only one synapse per cell. However, due to the large number of parallel fibers passing by, one Purkinje cell still receives about 100 000 synapses in total (Bear, 2001). Climbing fibers directly innervate the cerebellar nuclei cells and the Purkinje cells. They make hundreds of excitatory synapses on the dendritic tree of one Purkinje cell by winding around the dendrites. A Purkinje cell is always innervated by only one climbing fiber in the adult brain (Purves et al., 2001) and the innervation of a Purkinje neuron by a climbing fiber generates a strong postsynaptic activity. A parallel stimulation of Purkinje cells by climbing and parallel fibers together results in long term depression (Bear, 2001). The GABAergic Purkinje cells are the most prominent cells in the cerebellum due to their size and their morphology. Their large dendritic tree is almost two-dimensional, oriented in parallel, and only extends into the molecular layer (Apps and Garwicz, 2005). The axons of the Purkinje cells create the sole output of the cerebellar cortex projecting to the deep cerebellar nuclei with an inhibitory synaptic contact (Figure 2 B). Thus, while mossy and climbing fibers make excitatory projections onto the Purkinje cells and the deep cerebellar nuclei, the Purkinje cells form inhibitory synapses on the deep cerebellar nuclei creating a

feedback loop. The cerebellar nuclei cells in turn create the sole output of the complete cerebellum projecting to diverse brain regions like the upper motor neurons in the cortex and the spinal cord (Purves et al., 2001). Apart from these main players in cerebellar connectivity, there are also several inhibitory (basket, Golgi, Lugaro, and stellate cells) and excitatory (unipolar brush cells) interneurons as well as specialized astrocytes (Bergmann glia) that enable efficient signaling (Reeber et al., 2013).

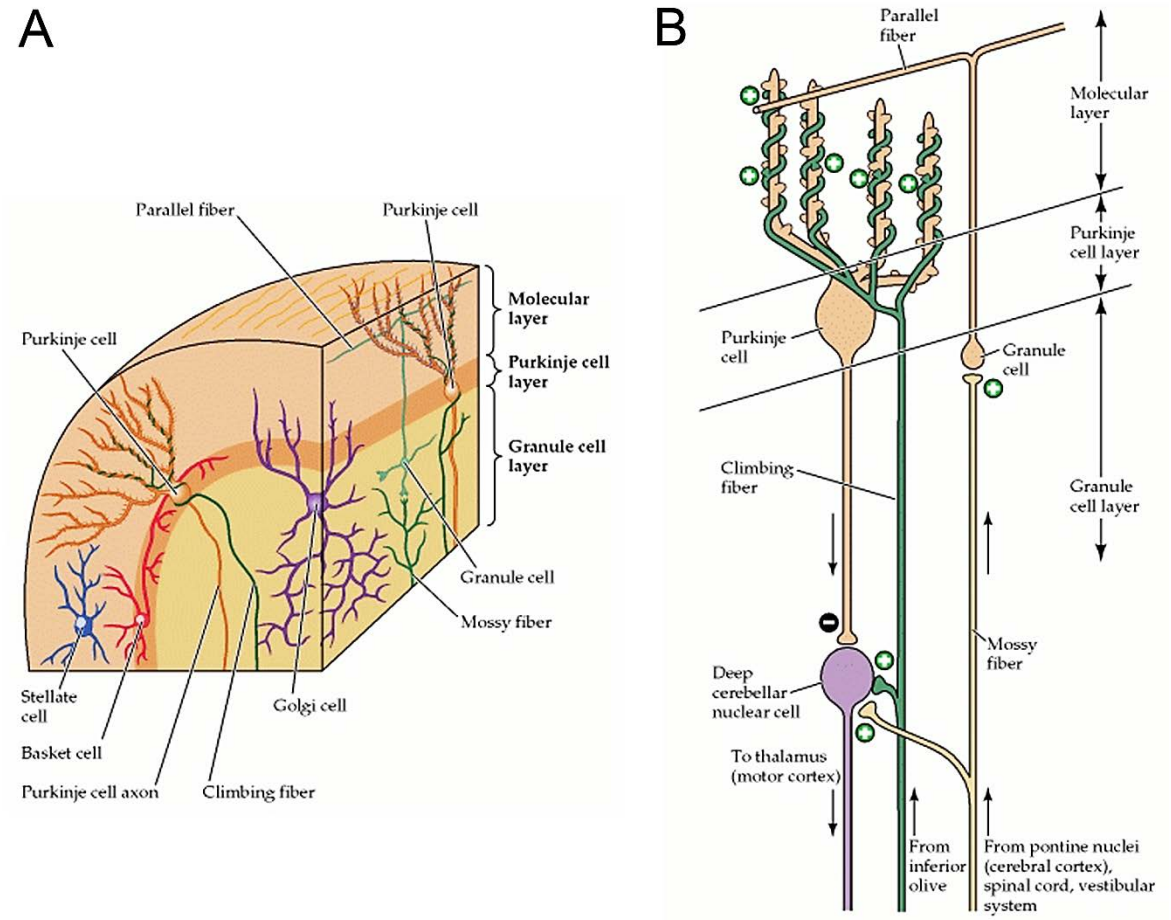

Figure 2. Structure and connectivity of the cerebellum. (A) Morphological division of the cerebellum into molecular, Purkinje cell, and granule cell layer. (B) Purkinje cells receive excitatory input from climbing fibers and parallel fibers and make inhibitory connections with the cerebellar nuclei cells which create the sole output of the cerebellum projecting for example to the motor cortex. The granule cells with their parallel fibers are innervated by the mossy fibers deriving from the brain stem nuclei and spinal cord. Furthermore, the mossy fibers as well as he climbing fibers make excitatory connections to the cerebellar nuclei cells (adapted from (Purves et al., 2001)).

1.3 Cerebellar ataxias and their classification

Although cerebellar dysfunction maybe involved in several motor and non-motor diseases such as Multiple sclerosis, Tourette's and autism spectrum disorders, schizophrenia, and sleep apnea, the most prominent disorder evoked by the cerebellum remains the ataxia (Reeber et al., 2013). The term ataxia derives from the Greek word ἀταξία which means

lack of order and refers to the movement incoordination of the patients (Bushara and Bower, 2008). The cerebellar ataxias comprise a group of disorders with high variety. In the following section the different types of cerebellar ataxias and their causes are described briefly (compare Figure 3).

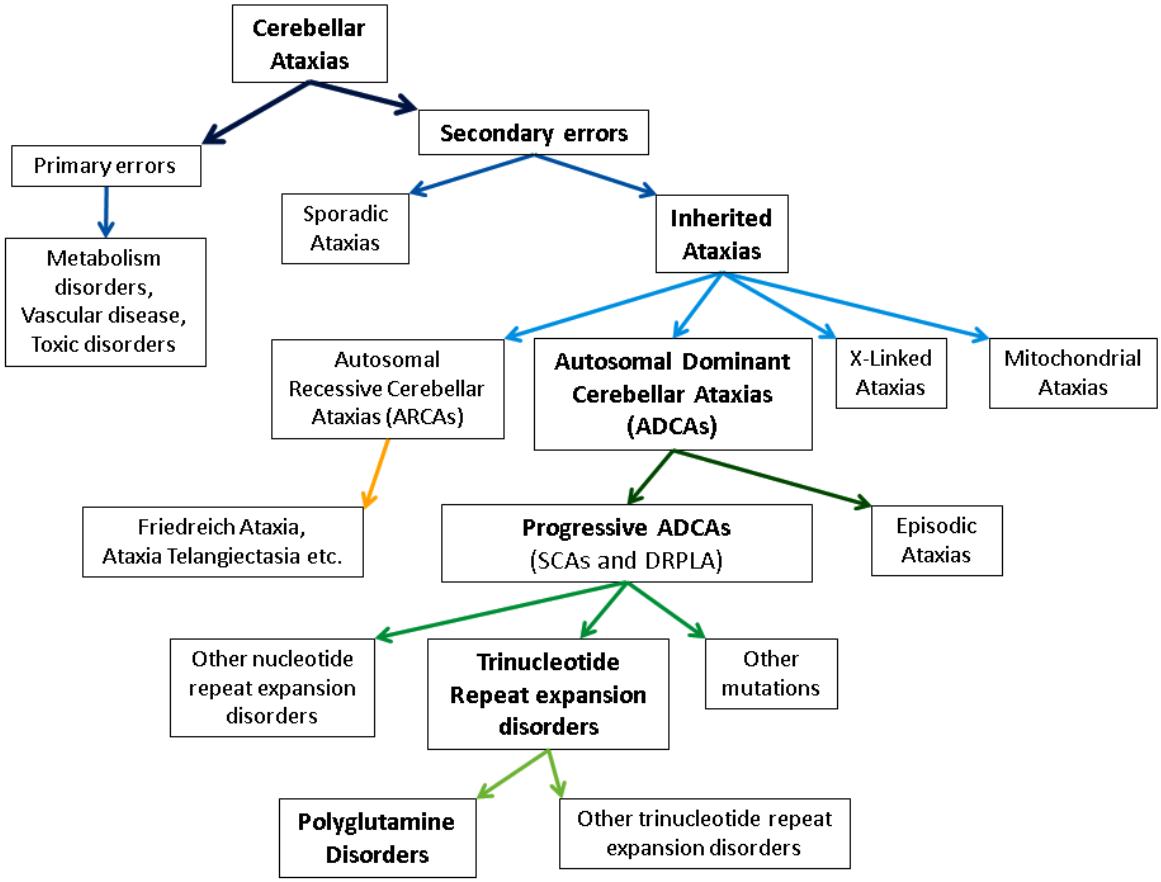

Figure 3. Classification of the cerebellar ataxias. Cerebellar ataxias are divided into ataxias with primary or with secondary errors. The latter one can manifest as sporadic or inherited ataxias. Inherited ataxias are divided into autosomal recessive, autosomal dominant, X-linked, and mitochondrial forms. Among the autosomal dominant ataxias, the Spinocerebellar ataxias (SCAs) make the largest part including almost 40 subtypes. The SCAs are furthermore subdivided according to their mutation type into trinucleotide repeat expansion disorders, other nucleotide repeat expansion disorders, and other mutations like insertions or deletions. Polyglutamine disorders are quite prominent among the trinucleotide repeat expansions. ARCAs = Autosomal recessive cerebellar ataxias, ADCAs = Autosomal dominant cerebellar ataxias, SCAs = Spinocerebellar ataxias, DRPLA = Dentatorubral-pallidoluysian atrophy.

Ataxias can be triggered either by primary or by secondary errors; they can be inherited or sporadic, progressive or episodic. Cerebellar ataxias evoked by (primary) inborn metabolism errors are inherited in an autosomal recessive manner and appear most often in childhood (Parker and Evans, 2003). The metabolic pathways that are affected in this ataxia type comprise for instance the urea cycle as well as the pyruvate and lactate pathway (Hoffmann et al., 2010; Parker and Evans, 2003).

In contrast to that, sporadic and inherited ataxias of secondary errors mostly develop during adulthood or mid-age. The inherited cerebellar ataxias are separated by their mode

of inheritance into autosomal recessive, autosomal dominant, X-linked, and mitochondrial forms. The mitochondrial ataxias (e.g. Leigh syndrome or Mitochondrial recessive ataxia syndrome (MIRAS)) are in the majority of cases evoked by alterations in the respiratory chain or by oxidative phosphorylation (Finsterer, 2009b). The X-linked ataxias are a group of very heterogeneous ataxias including X-linked sideroblastic anemia with ataxia (XLAS) and Fragile-X-associated tremor/ataxia syndrome (FXTAS) (Finsterer, 2013). They are primarily expressed in males as they do not have a second X allele that could replace the mutated one. Two well-known examples for autosomal recessive ataxias are Friedreich's Ataxia (FRDA) and Ataxia Telangiectasia (AT) (Jayadev and Bird, 2013). FRDA is the most common hereditary ataxia (~50% of all hereditary ataxias; prevalence of 1 - 2 individuals per 50 000) and is caused by a loss of function mutation in the *FRATAXIN* gene, a factor responsible for mitochondrial iron-sulfur cluster biogenesis (Campuzano et al., 1996; Jayadev and Bird, 2013). AT is named after the two main symptoms it evokes: ataxia (poor coordination of movement) and telangiectasia (dilatation of small blood vessels). The disease is caused by a defect in the *ATM* gene which is involved in DNA damage repair. AT symptoms most often start in early childhood.

1.3.1 Autosomal dominant cerebellar ataxias

The autosomal dominant cerebellar ataxias (ADCAs) form probably the biggest group among the inherited ataxias combining almost 40 Spinocerebellar ataxias (SCAs) and Dentatorubral-pallidoluysian atrophy (DRPLA) as progressive ADCAs together with seven varieties of episodic autosomal dominant ataxias (Finsterer, 2009a). The episodic ADCAs all have in common that the symptoms are only present for a certain period of time (Jen et al., 2007; Kerber et al., 2007). These intervals can vary between a few seconds, hours and several days (Jen et al., 2007).

Contrarily, when symptoms of progressive ADCAs have started once in life, they continuously worsen. Progressive ADCAs are often hard to distinguish among each other by clinical or neuroimaging studies due to their similar phenotypes. Therefore, molecular genetic testing is the current method for discrimination (Jayadev and Bird, 2013). Nevertheless, they can be grouped depending on different parameters. In 1993, Harding proposed three classes for ADCAs according to their symptoms and mode of inheritance (Harding, 1993). Class I (ADCA type I) comprises disorders with cerebellar and variable additional signs like optic atrophy, ophthalmoplegia, slow saccades, fasciculation, bulbar signs, spasticity, extrapyramidal features, peripheral neuropathy, pontine signs, sphincter disturbance, and dementia (Schols et al., 2004; Whaley et al., 2011). SCA1, 2, 3, 4, 8, 10,

12, 13, 14, 15/16, 17, 18, 19, 20, 21, 22, 23, 25, 27, 28, and DRPLA belong to this group. In contrast to the first class, the second one (ADCA type II) only consists of one disorder: SCA7, the only syndrome that is continuously associated with pigmentary macular degenerations. The third and last group (ADCA type III) consists of ataxias with pure cerebellar symptoms like SCA5, 6, 11, 26, 29, 30, and 31 (Fujioka et al., 2013). Apart from the classification proposed by Harding, ADCAs can also be divided by the type of their mutations into disorders with coding repeat expansions (SCA1, 2, 3, 6, 7, 17, and DRPLA), noncoding repeat expansions (SCA8, 10, 12, 31, and 36), other mutations (point mutations, deletions and duplications; SCA5, 11, 13, 14, 15, 16, 18, 19, 20, 22, 23, 26, 27, 28, 29, and 35) and unknown mutations (SCA4, 21, 25, 30, 32, 34, and 37) (Bettencourt et al., 2014).

1.3.2 Spinocerebellar ataxias

SCAs are a heterogeneous group of disorders characterized by ataxia and variable additional symptoms but with a focus on cerebrospinal deficits. To date, ~35 different SCAs are known, each of them caused by a mutation in a varying gene (apart from SCA15/16/29 and SCA19/22 that arise from the same gene). They are named by the order of their discovery SCA1 through SCA40 (Table 1). The number of SCAs, however, is steadily increasing. SCA37 has just been identified in a family from Spain, SCA38 in an Italian family, and SCA40 in a Chinese family in 2013/2014 (Di Gregorio et al., 2014; Serrano-Munuera et al., 2013). For 26 of these SCAs the causative genes and their mutations are known, for the rest of them the chromosomal localization was determined but the exact gene has not been identified, yet. The type of mutation in these 26 SCA genes varies. Many SCAs are caused by nucleotide repeat expansions in the respective gene, others by missense mutations, deletions or insertions. In nucleotide repeat expansion disorders the expanded repeats lead, upon a certain threshold, sooner or later to the respective disease. The age of onset is thereby often depending on the length of the repeat (Storey, 2014). So far, trinucleotide, pentanucleotide, and hexanucleotide repeat expansions are known.

Table 1. Overview of Spinocerebellar ataxias. Known SCAs with their gene/locus and the mutation type (adapted from (Storey, 2014)).

SCA	Gene / Locus	Mutation
SCA1	ATXN1	exonic CAG repeat
SCA2	ATXN2	exonic CAG repeat
SCA3	ATXN3	exonic CAG repeat

SCA	Gene / Locus	Mutation
SCA4	16q22, PLEKHG4?	?
SCA5	SPTBN2	missense
SCA6	CACNA1A	exonic CAG repeat
SCA7	ATXN7	exonic CAG repeat
SCA8	ATXN82OS ATXN8	CTG repeat CAG repeat
(SCA9)	empty	-
SCA10	ATXN10	intronic ATTCT repeat
SCA11	TTBK2	insertion / deletion
SCA12	PPP2R2B	CAG repeat
SCA13	KCNC3	missense
SCA14	PRKCG	missense / deletion
SCA15	ITPR1	large deletion
(SCA16)	= SCA15	-
SCA17	TBP	exonic CAG repeat
SCA18	7q22-q32	?
SCA19	KCND3	missense / small deletion
SCA20	11q12	multigene duplication
SCA21	TMEM240*	missense/stop mutation*
(SCA22)	= SCA19	-
SCA23	PDYN	missense
(SCA24)	= SCAR4/SCASI	-
SCA25	2p21-p13	?
SCA26	EEF2	missense
SCA27	FGF14	missense / nonsense
SCA28	AFG3L2	missense
SCA29	ITPR1	missense
SCA30	4q34-q35	?
SCA31	BEAN1	insertion with TGGAA repeat
SCA32	7q32-q33	?
(SCA33)	empty	-
SCA34	ELOVL4*	missense*
SCA35	TGM6	missense
SCA36	NOP56	intronic GGCCTG repeat
SCA37	1p32	?
SCA38	ELOVL5*	missense*
(SCA39)	empty	
SCA40	CCDC88	missense*

*SCA21, 34, 38, and 40 genes have just been identified (Cadieux-Dion et al., 2014; Delplanque et al., 2014; Di Gregorio et al., 2014; Tsoi et al., 2014)

Among the SCAs, SCA3 is the most prevalent worldwide, followed by SCA2, SCA1, and SCA8 (Whaley et al., 2011). However, there are known founder effects for example for SCA2 with an incidence of 183 in 100 000 in a region called Holguín on Cuba (Durr, 2010). The overall incidence of the SCAs is about 5 - 7 per 100 000 inhabitants (Velazquez-Perez et al., 2011).

1.3.3 Trinucleotide repeat expansion disorders

The group of trinucleotide repeat expansion disorders is the largest and most prominent group among the SCAs. It accounts for at least eight SCAs as well as some non-SCA disorders. SCA1, 2, 3, 6, 7, 8, 12, and 17 belong to this group. Additionally, the non-SCA disorders Huntington's disease (HD), Fragile X syndrome (FRAXA), Fragile-X-associated tremor / ataxia syndrome (FXTAS), Fragile XE mental retardation (FRAXE), Dentatorubral-pallidoluysian atrophy (DRPLA), Myotonic dystrophy (DM), Friedreich's ataxia (FRDA), and Spinal and bulbar muscular atrophy (SBMA) form part of this group.

About half of the trinucleotide repeat expansion disorders are caused by an exonic polyglutamine repeat and, therefore, belong to the subgroup of polyglutamine (polyQ) disorders (SCA1, 2, 3, 6, 7, 17, HD, DRPLA, and SBMA). The polyglutamine disorders are characterized by an expanded CAG/CAA repeat encoding glutamine but do not share protein structure or motif homologies. Although CAG and CAA both encode the amino acid glutamine, it was found that CAA interrupted CAG repeats are more stable and therefore less prone to expansion than pure CAG repeats are (Choudhry et al., 2001; Dorsman et al., 2002; Menon et al., 2013; Sobczak and Krzyzosiak, 2005). The critical length of the glutamine repeat varies among all polyQ diseases (Table 2). While in CACNA1A a length of ~20 polyQs is sufficient to cause SCA6, more than 51 polyQs are necessary in ATXN3 to cause SCA3.

Anticipation is a known feature of polyglutamine disorders. It implies that the symptoms in the next generation appear earlier and are more severe (Koshy and Zoghbi, 1997). Anticipation occurs more likely when the male part of the first generation harbors the mutation and, besides, depends on the type of ataxia (Rub et al., 2013). In SCA2 and SCA7 this feature is most pronounced (Rub et al., 2013). Regarding the clinical manifestation, each polyQ disease has its distinct main features that primarily result from the function of the mutated gene and the responsibility of the brain area that is the most affected. Although all polyQ proteins are expressed in many different brain areas only specific areas exhibit the pathology. The reason for this regional specificity is not yet resolved and may refer to the role of the affected protein.

Table 2. Overview of polyglutamine disorders. PolyQ disorders with their respective protein, their main clinical features, and the normal as well as the disease-causing CAG repeat range (adapted from (Almeida et al., 2013; Gatchel and Zoghbi, 2005; Storey, 2014)).

Disorder	Protein	Main clinical features	Normal	Affected
SCA1	ATXN1	Ataxia, slurred speech, spasticity, cognitive impairment	6 - 44	39 - 91
SCA2	ATXN2	Ataxia, slow saccades, decreased reflexes, polyneuropathy, motor neuropathy, infantile variant, parkinsonian features	14 - 32	33 - ≥200
SCA3 (MJD)	ATXN3	Ataxia, parkinsonian features, severe spasticity	12 - 47	51 - 89
SCA6	CACNA1A	Ataxia, dysarthria, nystagmus, tremor	3 - 18	20 - 33
SCA7	ATXN7	Ataxia, retinal degeneration, cardiac involvement in infantile variant	4 - 35	36 - 460
SCA17	TBP	Ataxia, behavioral changes or psychosis, intellectual deterioration, seizures	25 - 44	47 - 63
DRPLA	ATN1	Ataxia, epilepsy, choreoathetosis, dementia	7 - 34	49 - 88
SBMA	AR	Motor weakness, swallowing difficulty, gynecomastia, hypogonadism	9 - 36	38 - 62
HD	HTT	Severe movement abnormalities, chorea, dystonia, cognitive decline, psychiatric features	6 - 34	36 - 121

1.3.4 Pathomechanism of polyglutamine disorders

There are many mechanisms that have been postulated for the pathology of polyQ diseases, for example protein accumulation, transcriptional dysregulation, altered calcium homeostasis or mitochondrial dysfunction (Figure 4). Several of the mechanisms discussed in the following sections may be limited to or being more pronounced in some of the polyQ diseases while others are generally disturbed in polyQ disorders. This difference refers to the fact that the involved mechanisms are dependent on the cellular function of the respective protein. For example, ATXN1, TBP, and AR (SCA1, SCA17, and SBMA, respectively) as transcription factors may have an additional or stronger effect on transcriptional dysregulation. In SCA2, RNA translation and metabolism are probably specifically affected due to the role of ATXN2 in these processes. Effects on the UPS are likely to be more pronounced in SCA3 given that ATXN3 itself is involved in this system. Nevertheless, how exactly all these mechanism in the end lead to altered synaptic signaling and neurodegeneration is still unclear.

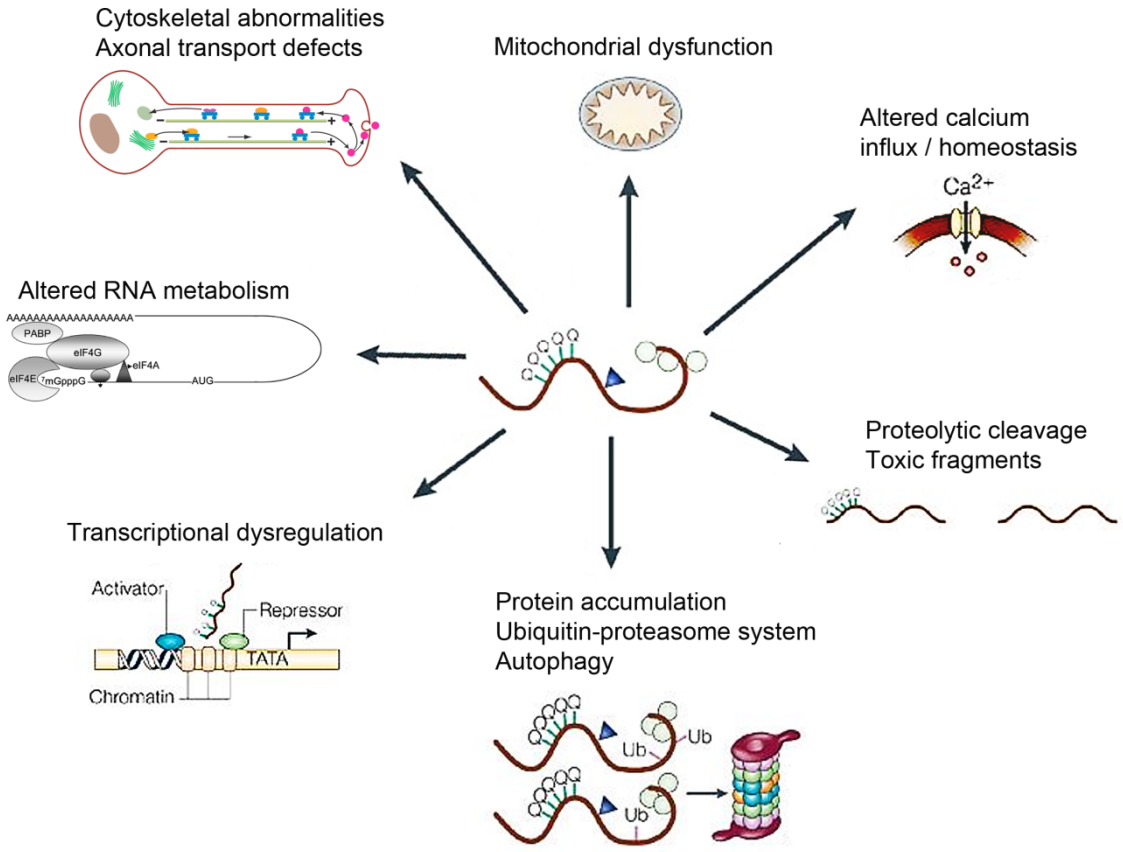

Figure 4. Mechanisms involved in polyQ pathology. The CAG repeat expansion of polyQ genes can result in altered calcium homeostasis as well as protein accumulation in the cytoplasm or nucleus. Mitochondrial dysfunction and cytoskeletal abnormalities were also shown to be consequences of polyQ expansion. For some polyQ proteins, proteolytic cleavage has been suggested to participate in pathology by producing toxic fragments. Furthermore, RNA metabolism and transcription are affected by polyQ expansions (adapted from (Gatchel and Zoghbi, 2005; Lopez-Lastra et al., 2005; Schliwa and Woehlke, 2003).

1.3.4.1 The question of gain- or loss-of-function

A (toxic) gain-of-function as well as a (partial) loss-of-function theory have been proposed regarding the pathomechanism of polyQ and other neurodegenerative disorders (Di Prospero and Fischbeck, 2005; Lieberman et al., 2002; Orr and Zoghbi, 2007; Zuccato et al., 2010). The (toxic) gain-of-function theory is mainly based on the fact that the expanded polyQ proteins form nuclear and/or cytoplasmic aggregates in various brain regions and that these aggregates may exert a toxic effect on the cell leading to neuronal dysfunction and cell death. Due to these protein accumulations, the polyQ diseases also belong to the more general group of proteinopathies like Parkinson's and Alzheimer's disease for both of which a similar hypothesis has been proposed. However, the role of aggregates in polyQ diseases is a disputed issue (Michalik and Van Broeckhoven, 2003). Several studies indicate that inclusion bodies of mutant proteins are not the bad guys they were suspected to be. Instead they may help cells to survive longer as revealed in SCA1 and SCA7 mice (Bowman et al., 2005; Watase et al., 2002; Yoo et al., 2003).

Furthermore, no association between inclusions and neurodegeneration was observed in a study using HD mice challenging the hypothesis of toxic aggregates (Slow et al., 2005).
The (partial) loss-of-function of the mutant protein due to an altered conformation and subsequent altered or disturbed interactions is the basis for the second theory. When the first knock-out (KO) models of various polyQ genes were generated, it was argued that a loss-of-function theory is not appropriate to explain the pathology because these models did not show a typical disease phenotype (Kiehl et al., 2006; Lastres-Becker et al., 2008a; Matilla et al., 1998) in contrast to transgenic and knock-in (KIN) models (Damrath et al., 2012; Farrar et al., 2014; Huynh et al., 2000; Sathasivam et al., 1999; Watase et al., 2002). However, since that time various similarities between KO and disease models have been identified. Comparing *Atxn1*-deficient and *Atxn1*-Q154-KIN mice, for example, a common pool of 197 dysregulated transcripts was found (Crespo-Barreto et al., 2010). Furthermore, in *Atxn2*-KO mice, a slight but significant deficiency in motor performance on the rotarod was detected (Kiehl et al., 2006) similar to *Atxn2*-Q58 (Huynh et al., 2000) transgenic and *Atxn2*-CAG42-KIN mice (Damrath et al., 2012; Huynh et al., 2000). Consequently, the question of gain- or loss-of-function is still up for debate.

1.3.4.2 Involvement of the ubiquitin-proteasome system and autophagy

As mentioned before, aggregation of the mutant protein is a common hallmark of polyQ disorders. Components of the protein degradation pathway are probably included in these aggregates in order to degrade the mutant proteins. Two main routes for protein clearance of damaged, misfolded, and mislocated proteins exist: the ubiquitin-proteasome system (UPS) and autophagy (Dantuma and Bott, 2014; Ortega and Lucas, 2014). The difference between the two systems is that the UPS also degrades short-lived proteins while autophagy is important for the degradation of long-lived proteins and whole organelles (Beau et al., 2008). A crosstalk between these two systems seems to exist as it has been observed that they can compensate each other's activity (Dantuma and Bott, 2014). Furthermore, both systems use the tagging of proteins with ubiquitin as a signal for degradation although this mechanism is way more common in the UPS pathway (Dantuma and Bott, 2014; Riley et al., 2010).
The process of ubiquitin tagging is known as ubiquitination or ubiquitylation and is accomplished in three steps involving the enzymes E1 to E3 (Figure 5). The E1 enzyme binds and activates ubiquitin using ATP (Adenosine triphosphate). In the next step, the ubiquitin is transferred to the ubiquitin-conjugating enzyme E2 that associates with the E3 ligase and conjugates the ubiquitin to the target protein. The ubiquitin-protein ligase E3 ensures the target specificity by binding the target protein as well as the E2 enzyme. The ubiquitinated target protein is subsequently recognized and degraded by the proteasome

or the ubiquitin is bound by p62/Sequestosome1 (Sqstm1) inducing autophagy of the ubiquitinated protein (Bjorkoy et al., 2005; Bjorkoy et al., 2006; Pankiv et al., 2007). Furthermore, ubiquitinated proteins can be dedicated to other cellular processes like endocytosis and DNA repair (Lilienbaum, 2013). The consequences of protein ubiquitination are thereby dependent on the number of ubiquitins (mono- or poly-ubiquitination) and the type of their linkage (Lys11-, Lys48-, Lys63-linked) (Dantuma and Bott, 2014).

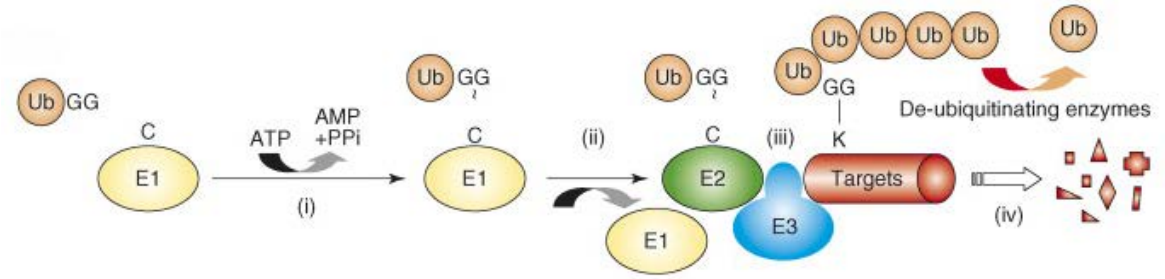

Figure 5. Ubiquitination of target proteins. The E1 enzyme activates ubiquitin using ATP. E2 is the conjugating enzyme that attaches the ubiquitin to the target protein. The E3 enzyme is an ubiquitin-protein ligase that binds the E2 enzyme as well as the target protein and is therefore important for target specificity. Ubiquitinated proteins can either be de-ubiquitinated again or degraded. Ubiquitination is also a recognition motif for other cellular processes (adapted from (Beau et al., 2008)). ATP = Adenosine triphosphate, AMP = Adenosine monophosphate, Ub = ubiquitin.

Ubiquitin and p62 are proteins commonly found in aggregates of polyQ disorders (Chai et al., 1999; Ciechanover and Brundin, 2003; Schmidt et al., 2002; Stenoien et al., 2002; Waelter et al., 2001). Thus, the protein degradation machinery seems to be strongly involved in the process of polyQ protein aggregation and there is probably a crosstalk between the UPS and autophagy in this process. Originally, it was thought that the sequestration of UPS components blocks UPS function thereby disturbing normal protein homeostasis. Consequently, different research groups tried to show an impairment of the UPS but no consistent results were obtained. Possibly, UPS activity is decreased but there is no overall impairment (Maynard et al., 2009; Ortega et al., 2010; Schipper-Krom et al., 2014). It should also be taken into account that maybe not the aggregated but the remaining soluble mutant proteins are toxic and aggregation helps to remove them from critical cellular processes (Ciechanover and Brundin, 2003; Dantuma and Bott, 2014). Consequently, if the aggregation of the mutant protein and the subsequent sequestration of UPS and autophagy components are for the sake or for the fate of the cell, needs to be further elucidated.

1.3.4.3 Disturbances in calcium homeostasis

Transcriptional changes of calcium homeostasis factors were among the first features observed in various polyQ mouse models (Hansen et al., 2013; Lin et al., 2000). Decreased expression of many calcium homeostasis factors has been noted in SCA1 (Crespo-Barreto et al., 2010; Lin et al., 2000; Serra et al., 2004), SCA2 (Hansen et al., 2013), SCA3 (Chou et al., 2008), SCA7 (Friedrich et al., 2012; Gatchel et al., 2008), HD (Friedrich et al., 2012; Luthi-Carter et al., 2002a), and DRPLA (Luthi-Carter et al., 2002b) mouse models. These downregulations may result in altered calcium signaling thereby disturbing signal transduction. The involvement of the calcium signaling pathway in the pathology of ataxia is further strengthened by the fact that many participants of this pathway are causative genes for SCAs like CACNA1A (SCA6), a calcium channel subunit in the plasma membrane or ITPR1 (SCA15/16/29), a receptor in the endoplasmic reticulum (ER) that mediates calcium release from the ER. Among the SCAs in general, there is PRKCG (SCA14), a protein kinase that can be activated by calcium and diacylglycerol and phosphorylates glutamate receptors. Furthermore, the protein causative for SCA5 (SPTBN2) functions in stabilization of the glutamate transporter SLC1A6. Mutations in the two potassium channel subunits KCNC3 and KCND3 turned out to be the genetic cause for SCA13 and SCA19/22, respectively.

Additionally, proteins that are not directly involved in this pathway have, however, been credibly associated with it. For example, in SCA1, an interaction with a transcription factor named Rorα that is strongly downregulated in many polyQ diseases has been shown (Serra et al., 2006). RORA is furthermore known to regulate the expression of some other calcium signaling pathway targets (Gold et al., 2003; Gold et al., 2007). It is of interest that a KO of *Rora* leads to severe ataxia observed for the first time in the so called “staggerer” mouse (Hamilton et al., 1996). Therefore, it was suggested that the downregulation of *Rora* may also be responsible for the downregulation of many transcripts and the resulting ataxic phenotype in SCA1 (Gehrking et al., 2011; Serra et al., 2006). Indeed, the authors demonstrated that the partial loss of the ATXN1/RORA interactor TIP60 leads to an increase in *Rora* and *Rora*-mediated transcript expression and slows down SCA1 progression (Gehrking et al., 2011). Consequently, ATXN1 may be indirectly involved in this pathway via TIP60 and RORA.

Further association between calcium signaling and ataxia is based on the fact that apart from *Rora* a KO of several other genes implicated in this pathway (*Grm1, Itpr1, Atp2b2,* and *Ca8*) also leads to an ataxic phenotype (Guergueltcheva et al., 2012; Matsumoto et al., 1996; Rossi et al., 2010; Street et al., 1998; Turkmen et al., 2009). Thus, it seems like calcium disturbances are a global effect in polyQ disorders that may be mediated either directly or via specific protein-dependent interactors. Interestingly, several of these

downregulations have also been observed in *Atxn1*-KO mice stimulating the discussion about gain- or loss-of-function.

1.3.4.4 Altered RNA metabolism

It is of note that in several polyQ diseases like SCA1 or HD the causative gene is involved in miRNA regulation thereby altering the expression of specific proteins (Johnson et al., 2008; Packer et al., 2008; Rodriguez-Lebron et al., 2013). Additionally, different miRNAs have been shown to modify expression and/or cytotoxicity of ATXN1 (Lee et al., 2008; Persengiev et al., 2011), ATXN3 (Huang et al., 2014), and HTT (Kozlowska et al., 2013; Sinha et al., 2011). miRNAs are essential for neuronal survival and depletion of miRNAs in Purkinje cells was demonstrated to result in neurodegeneration and ataxia (Schaefer et al., 2007). Therefore, miRNAs are probably strong modifiers of cerebellar pathology and miRNA silencing strategies could be used as therapeutic agents but these strategies are still under development (Dumitrescu and Popescu, 2015).

Splicing is another component of RNA metabolism that may be implicated in polyQ disorders as well. For example, it is known that ATXN1 interacts with the RNA-splicing factors RBM17 and U2AF65 (de Chiara et al., 2009; Lim et al., 2008) and ATXN2 interacts with A2BP1 and TDP43 (Elden et al., 2010; Shibata et al., 2000). In a KIN mouse model for SBMA altered splicing was implicated in skeletal muscle pathology (Yu et al., 2009b). Furthermore, aberrant splicing of the mutant transcript itself was implicated in SCA3 and HD (Ramani et al., 2015; Sathasivam et al., 2013).

Alterations in translation regulation have been limited to SCA2 up to now. Therefore, this aspect is covered later on (see section 1.4.2.1).

1.3.4.5 Other mechanisms implicated in polyQ pathology

Recently, it has been proposed that transcriptional dysregulation may be the main common mechanism of polyQ diseases (Mohan et al., 2014). Indeed many polyQ proteins are implicated in transcription regulation acting as (co-) activators, (co-) repressors or directly as transcription factors (Carlson et al., 2009). A role in transcription regulation has especially been studied in SCA1 where the causative protein, ATXN1, displayed interaction with various transcription factors like CIC, TIP60, BOAT, and LANP (Lam et al., 2006; Matilla et al., 1997; Mizutani et al., 2005; Serra et al., 2006). However, it should be considered that although there are effects on transcription in all polyQ diseases some of them may not be directly caused by the mutant protein but could be feedback mechanisms.

Other mechanisms that have been proposed to contribute to pathology are mitochondrial dysfunction (Laco et al., 2012; Panov et al., 2002; Simon et al., 2007; Weber et al., 2014; Yu et al., 2009a) and impaired axonal transport (Gunawardena and Goldstein, 2005; Gunawardena et al., 2003; Reddy and Shirendeb, 2012; Seidel et al., 2010). Apart from the fact that mitochondria are directly involved in calcium homeostasis the sequestration of caspases into protein aggregates leads to the activation of mitochondrial apoptotic pathways (Chou et al., 2006; Sanchez et al., 1999; Wang et al., 2006). Regarding axonal transport, it was found that expression of mutant HTT (HD) or ATXN3 (SCA3) leads to axonal blockage in *D. melanogaster* models (Gunawardena et al., 2003). Furthermore, proteolytic cleavage of mutant proteins resulting in fragments that are more prone to aggregation than full-length proteins is likely to be involved in the pathological process as well (Ellerby et al., 1999; Haacke et al., 2006; Kubodera et al., 2003; Nucifora et al., 2003; Wellington et al., 2000; Young et al., 2007). All these dysfunctions may be somehow associated with each other resulting in the observed pathology.

1.3.5 Spinocerebellar ataxia type 2

In 1971, Spinocerebellar ataxia type 2 has been described for the first time in nine families from India (Wadia and Swami, 1971). It is nowadays the most common ataxia in India, Korea, southern Italy, Spain, and Cuba (Storey, 2014). Slowing of eye movement had already been found in these first patients and is now known as a characteristic feature of SCA2 observed in 90% of all patients (Velazquez-Perez et al., 2011). The main clinical symptoms of SCA2 are gait, stance, trunk, and limb ataxia (Gierga et al., 2005). Other features of this disease are intention and postural tremor, dysmetria, dysarthria, hyporeflexia, and dysdiadochokinesia (Estrada et al., 1999; Orozco Diaz et al., 1990; Velazquez-Perez et al., 2011). Fasciculation and distal amyotrophy are signs of motor neuron involvement (Velazquez-Perez et al., 2011). Furthermore, sleep disturbances including restless legs syndrome, muscle cramps, ophthalmoplegia, and dysphagia are quite common (Abele et al., 2001; Iranzo et al., 2007; Lastres-Becker et al., 2008b). Patients with moderate repeat expansions and CAA interruptions often develop Parkinsonian features (Charles et al., 2007; Takao et al., 2011; Wang et al., 2015).

Disease onset is usually in the third decade of life but depends on the polyQ repeat length (Lastres-Becker et al., 2008b; Storey, 2014). Furthermore, the disease onset of SCA2 also varies depending on the CAG repeat length of other polyQ proteins like CACNA1A (Pulst et al., 2005) and ATXN7 (Tezenas du Montcel et al., 2014). SCA2 shows a strong progression and most patients die within 15 - 20 years after the appearance of the first

symptoms due to respiratory failure (Auburger, 2012; Velazquez-Perez et al., 2011). Magnetic resonance imaging (MRI) and pathological examinations show neurodegeneration in the cerebellum (Figure 6), pons, medulla oblongata, frontal lobe, cranial nerves, and substantia nigra (Estrada et al., 1999; Gierga et al., 2005). In the end stage, neuronal loss is also found in the thalamus, striatum, and spinal cord (Lastres-Becker et al., 2008b; Rub et al., 2006; Rub et al., 2005). Within the cerebellum, the dendritic arborisation decreases early in disease together with a shrinking of molecular layer thickness and finally loss of the large Purkinje cells (Estrada et al., 1999).

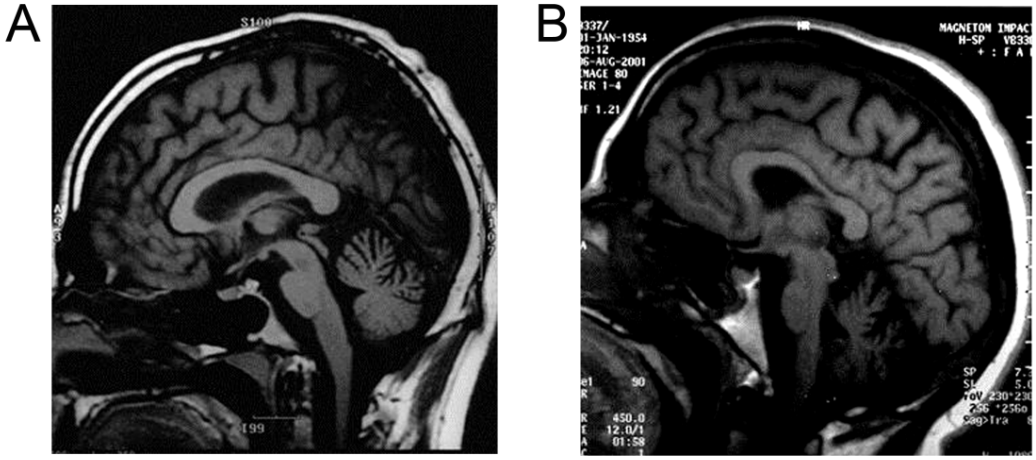

Figure 6. Sagittal MRIs of two SCA2 patients from Turkey. MRI of (A) a 49-year-old female and (B) her 26-year-old son, both with 41 CAGs in one ATXN2 allele but with strong difference in the degree of neurodegeneration (adapted from (Agan et al., 2006)).

In contrast to other SCAs, SCA2 shows little nuclear inclusions of the mutant protein. If so, they are mostly observed in the inferior olive, substantia nigra, pontine nuclei, and anterior horn but not or barely in the cerebellum (Huynh et al., 2000; Koyano et al., 2002; Koyano et al., 2014; Pang et al., 2002). Contrarily, a strong cytoplasmic aggregation especially in the Purkinje neurons is observed (Damrath et al., 2012; Huynh et al., 2000).

1.3.6 Therapy of Spinocerebellar ataxia type 2

At present, there is no cure for SCA2. Consequently, only symptomatic treatment is possible using 5-Hydroxytryptophan and buspirone against ataxia and levodopa or dopamine agonists against Parkinsonian features. Furthermore, magnesium, chinine or mexiletine can be administered against muscle cramps and budipine, clonazepam, and clozapine against tremor (Schols et al., 2004). Riluzole may also reduce ataxic symptoms (Ristori et al., 2010; van de Warrenburg et al., 2014) and deep brain stimulation has been discussed as being helpful for tremor but may worsen the ataxic phenotype (Freund et al.,

2007; Oyama et al., 2014). However, most of the treatments are of limited effect and several different therapeutics have to be tested in each case before a positive effect is observed. Apart from the pharmacotherapy, regular physiotherapy has been shown to be helpful for ataxia of gait, stance, and limbs and logopedics for dysarthria (Ilg et al., 2012; Synofzik and Ilg, 2014). Innovative approaches like RNA interference, overexpression of chaperones, and application of histone deacetylase inhibitors are still in the testing phase but all aim to prevent protein misfolding and neurodegeneration at different stages (Matilla-Duenas et al., 2010).

1.4 Ataxin-2

1.4.1 The Ataxin-2 gene and its protein ATXN2

In 1996, the SCA2 causing CAG trinucleotide repeat expansion in the *ATXN2* gene was detected by three independent groups (Imbert et al., 1996; Pulst et al., 1996; Sanpei et al., 1996). The *ATXN2* gene is localized on chromosome 12q24 (Belal et al., 1994; Gierga et al., 2005; Gispert et al., 1995; Hernandez et al., 1995) and consists of 25 exons with an exon size ranging from 37 to 800 bp. Exon 1 is the largest and harbors the CAG repeat (Sahba et al., 1998). The usual polyQ length is around 22/23 repeats (in 90% of individuals) and the CAG repeats are normally interrupted by a CAA triplet: $(CAG)_8CAA(CAG)_4CAA(CAG)_8$ (Pulst et al., 1996). Individuals with an expansion of more than 32 CAGs probably develop SCA2 (Auburger, 2012) with a longer repeat being related to an earlier onset and a more severe course of disease (Cancel et al., 1997; Sasaki et al., 1998; Schols et al., 1997; Velazquez-Perez et al., 2004). Similar to other SCA genes, loss of the CAA interruptions in *ATXN2* may result in repeat instability rendering the gene more prone to expansion (Pujana et al., 1999). Therefore, the ataxia causing repeat expansions of ATXN2 are most often pure CAG repeats while intermediate repeat expansions (27 to 31 CAGs) are mostly interspersed and associated with a higher risk for other neurodegenerative diseases (see section 1.4.3).

In humans only three splice variants of Atxn2 are known while four variants have been detected in mouse (Affaitati et al., 2001; Nechiporuk et al., 1998; Sahba et al., 1998). Isoform I is the full-length form, isoform II lacks exon 10 and isoform IV exon 21 (Affaitati et al., 2001). Isoform III has only been observed in mouse and lacks exon 10 and 11 (Nechiporuk et al., 1998). This splicing pattern suggests a quite similar structure of *Atxn2*

in humans and mice. Indeed, the identity between the human and the mouse gene is 89% on nucleotide level and 91% on protein level except for the N-terminal part of the gene (amino acids 1 - 151) where only 79% similarity have been observed (Nechiporuk et al., 1998). This difference may result from the fact that mice only possess one CAG and, consequently, repeat expansion does not occur. In both species, the *Atxn2* gene is expressed widely in the CNS including cerebellum, cerebral cortex, medulla, spinal cord, striatum, hippocampus, substantia nigra, and thalamus (Huynh et al., 1999; Nechiporuk et al., 1998). In mice, *Atxn2* expression was also shown in heart, liver, placenta, skeletal muscle, and pancreas (Nechiporuk et al., 1998).

In the past, the ATXN2 protein was believed to consist of 1312 amino acids starting at an ATG translation initiation codon at the beginning of exon 1 (Albrecht et al., 2004). However, in 2012, a second ATG codon located 480 bp downstream of the first one was identified and could be the actual translation initiation start codon. Usage of this second codon results in a full length protein of 1152 amino acids (Scoles et al., 2012). Given that most studies used the original ATG codon, in this work all specifications regarding structural domains or sizes are given depending on this first ATG codon.

Figure 7. Protein structure of ATXN2. The polyQ domain of ATXN2 is located at the N-terminal end, followed by the Lsm and LsmAD domains that are responsible for RNA-binding. The PAM2 motif at the C-terminal end mediates binding to PABP while the different proline-rich domains (2 PRDI and 2 PRDII) establish connections to other proteins via their SH3-domain.

ATXN2 has a molecular mass of about 140 kDa and is a highly basic protein with only one acidic region spanning between exon 2 and 7 (amino acids 254-475). This region consists of an Lsm (Like Sm, amino acids 254 - 345) and an LsmAD (Lsm associated domain, amino acids 353 - 475) domain (Figure 7). Apart from a clathrin-mediated *trans*-Golgi signal, the LsmAD also consists of an ER exit signal (both between amino acids 414 and 428). These two domains are essential for the RNA binding function of ATXN2 (Albrecht et al., 2004). Located more at the C-terminal end is the PAM2 motif (amino acids 908 - 925) that mediates the binding of ATXN2 with the Poly(A)-binding protein PABPC1 (Albrecht et al., 2004; Damrath et al., 2012). Furthermore, there are four proline-rich domains (PRDs) in ATXN2: two type 1 domains (PRDI) and two type 2 domains (PRDII). One of each is located at the C-terminal end, before the polyQ repeat. The second PRDI is at the N-terminal end and the second PRDII between the Lsm domains and the PAM2 motif. The PRDs interact with SH3 (src homology 3) domains of various other proteins (Nonis et al., 2008). Regarding post-translational modifications, a phosphorylation of

human ATXN2 at S860 and S864 has been observed but no glycosylation (Turnbull et al., 2004). ATXN2 protein expression is similar to transcript expression with a strong presence in Purkinje cells in contrast to a weak expression in granule layer. On a subcellular level, a perinuclear distribution and no nuclear staining were detected for ATXN2 in the adult mouse brain (Nechiporuk et al., 1998). Furthermore, it showed co-localization with ER-markers in immunocytochemical stainings *in vitro* and an association with the rough ER (more than with the smooth ER) and membrane-bound polysomes (more than with free polysomes) in centrifugation studies using mouse brain (van de Loo et al., 2009). Under stress conditions, ATXN2 re-localizes to stress granules (Nonhoff et al., 2007; Ralser et al., 2005a).

1.4.2 The function of ATXN2

To be able to understand the molecular basis of SCA2 pathology it is essential to unravel the function of ATXN2, but up to now the exact cellular function of ATXN2 is unknown. Several domains of the ATXN2 protein and diverse interaction partners have been identified and used to get insight into the role of this protein. Subsequently, it has been implicated in several pathways including translation regulation, splicing, stress response, receptor endocytosis, and lipid metabolism which will be discussed in the following sections (compare Figure 8).

1.4.2.1 ATXN2 function in mRNA translation and splicing

As proteins exhibiting an Lsm or LsmAD domain are normally involved in RNA modification, pre-mRNA splicing, mRNA decapping, and degradation (Albrecht et al., 2004), a role for ATXN2 in RNA metabolism was proposed. The *Saccharomyces cerevisiae* homolog of ATXN2, PBP1 (Pab1-binding protein 1), possesses an Lsm domain like human and mouse ATXN2 does. Furthermore, it has been shown to interact with PAB1, the *S. cerevisiae* homolog of the poly(A)-binding protein PABP (Mangus et al., 1998; Satterfield and Pallanck, 2006) and a deletion of PBP1 suppressed the lethal effect of PAB1 deletion (Mangus et al., 1998). Therefore, in 2005, Ralser et al. tested for a putative interaction between human ATXN2 and PABP (Ralser et al., 2005a). Using a yeast-two-hybrid system as well as a mammalian cell line, they could show that human ATXN2 indeed interacts with the C-terminal domain of PABP. In yeast and human PAB1/PABP is essential for poly(A)-shortening (to trigger mRNA degradation) and translation initiation as it binds the eIF4G (eukaryotic initiation factor 4 G) translation initiation complex thereby circularizing the mRNA (Mangus et al., 1998; Tarun and Sachs,

1996). The hypothesis of an bidirectional effect between ATXN2 and PABP is strengthened by the fact that a knockdown of ATXN2 resulted in an increase of *PABP* transcript levels in HEK293T cells whereas an overexpression of ATXN2 led to a decrease of *PABP* transcript levels (Nonhoff et al., 2007). Thus, ATXN2 seems to be somehow involved in translation via PABP but it remains unclear if it participates in the regulation of all mRNAs or only of selected ones.

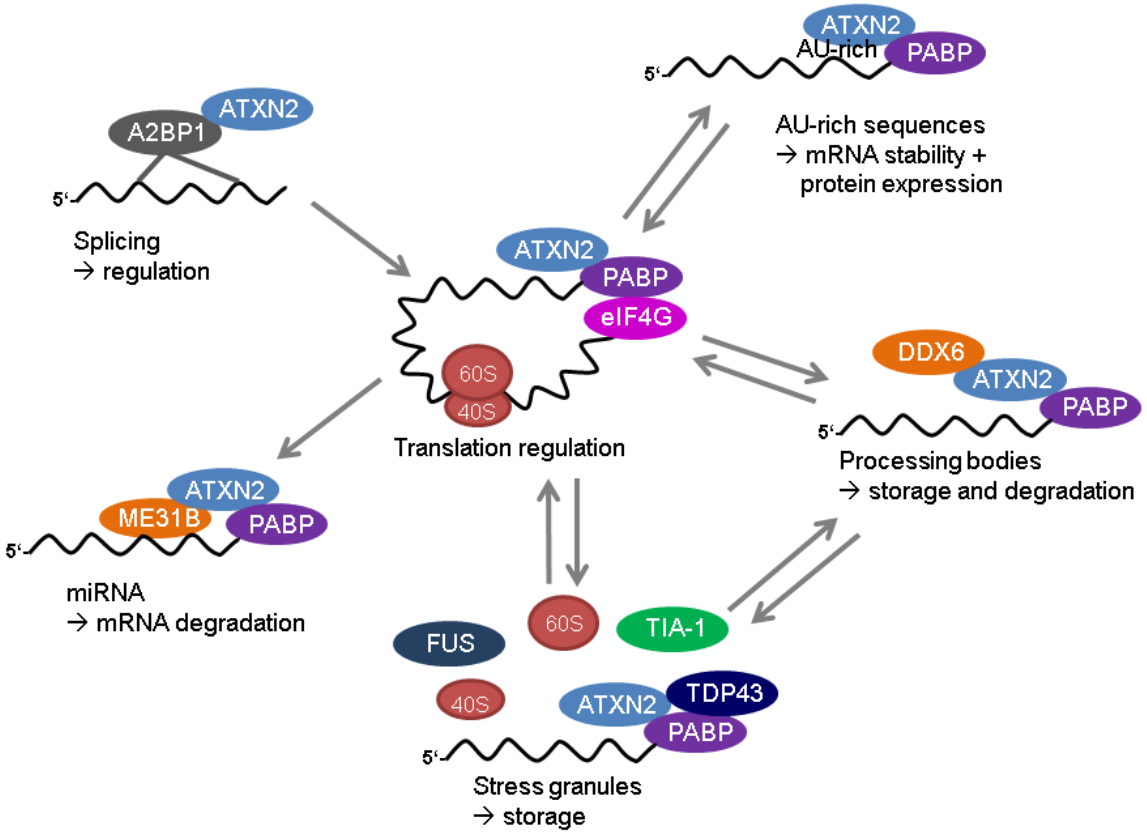

Figure 8. Functions of ATXN2 in RNA metabolism. ATXN2 functions in translation regulation by binding to PABP thereby regulating PABP-dependent processes. Furthermore, ATXN2 is involved in mRNAs stabilization, protein expression regulation, and miRNA-mediated mRNA degradation. Under stress conditions, ATXN2 has been found in stress granules and processing bodies were translationally silent mRNAs are stored and degraded. The interaction of ATXN2 and A2BP1 suggests an implication of ATXN2 in splicing regulation.

Recently, this question was addressed in a study about RNA-binding proteins (RBPs) (Yokoshi et al., 2014). While miRNAs bind the 3'UTR to repress translation or promote degradation (Kim et al., 2009), RBPs bind this region to enhance mRNA stability and protein abundance (Barreau et al., 2005). The authors found that ATXN2 is such an RBP that binds preferentially to uridine-rich elements, for example AU-rich elements (AREs) in the 3'UTR thereby stabilizing the mRNAs (Yokoshi et al., 2014). A depletion of ATXN2 in HEK293T cells consequently reduced the amount of target mRNAs whereas an overexpression increased their stability. Dependent on the stability of the mRNAs, the protein expression was decreased or increased, respectively. Furthermore, they showed that a polyQ expansion did not strongly decrease the ability of ATXN2 to bind target

mRNAs but that protein expression was, however, slightly reduced due to the mutation. It is interesting to note that PABP contributed to the effects of ATXN2 on mRNA stability and protein expression but that it was not essential as the effects were also present in the absence of PABP. In contrast to the positive regulation, the *Drosophila melanogaster* ATXN2 homolog, dATX2, was shown to be necessary for miRNA function involved in the repression of several translational reporters probably via binding to PABP or ME31B, a DDX6 homolog (DEAD box helicase 6) (McCann et al., 2011). Consequently, ATXN2 is either involved in both stabilizing of mRNAs and repression and the effects may be transcript specific or ATXN2 function varies between different species.

Apart from its function in translation regulation and mRNA stability, ATXN2 has been associated with mRNA splicing since an interaction with the Ataxin-2 binding protein 1 (A2BP1 or RBFOX1) was shown in a yeast-two-hybrid assay (Shibata et al., 2000). The function of A2BP1 is not yet known but its homolog in *Caenorhabditis elegans*, FOX1, binds RNA and is implicated in alternative splicing regulation (Jin et al., 2003). The NMDA1 receptor exon 5 is one of these splicing targets of A2BP1/FOX1 (Lim et al., 2006). Interestingly, A2BP1 as well as another ATXN2 interaction partner and SCA protein, ATXN1, both interact with RBM9 (RNA-binding motif protein 9; RBFOX2) which is also involved in RNA splicing (Lim et al., 2006). In conclusion, there are several data that point to a role for ATXN2 in splicing or splicing regulation but the mechanisms behind this regulation need to be clarified.

1.4.2.2 ATXN2 participation in stress response

Another function of ATXN2 in RNA metabolism is its involvement in stress response. As a reaction to environmental stress cells form distinct cytoplasmic granules named stress granules (SGs) (Anderson and Kedersha, 2002; Anderson and Kedersha, 2006; Kedersha and Anderson, 2002; Kedersha et al., 2005). SGs are highly dynamic structures in which mRNAs are stalled during stress conditions together with several translation initiation factors, ribosomal subunits, and other mRNA stabilizing and destabilizing proteins (Kedersha et al., 2000). Prominent markers of stress granules are TIA1 (T-cell restricted intracellular antigen 1) and its related protein TIAR but also PABP as an mRNA-associated protein is found in these tiny granules. Given that PABP and ATXN2 interact with each other, Ralser et al. analyzed and demonstrated the presence of ATXN2 in mammalian SGs (Ralser et al., 2005a). *In vitro* studies in a carcinoma cell line showed an effect of ATXN2 loss on the number and size of SGs, while no interference was detected when WT (Q22) or pathogenic (Q79) ATXN2 were overexpressed. However, in the same approach overexpression of ATXN2 slightly changed TIA1 localization in the nucleus suggesting an interaction of the two stress granule components (Nonhoff et al., 2007). In

contrast to the observation in SGs, an overexpression of Q22 or Q79 ATXN2 altered the presence of P-bodies (processing bodies) (Nonhoff et al., 2007). P-bodies are dynamic structures similar to SGs that store and degrade translationally silenced mRNAs and can co-localize with SGs under stress conditions (Kedersha et al., 2005; Teixeira et al., 2005; Wilczynska et al., 2005). Typical components of P-bodies are de-capping enzymes and RNases as well as the DEAD/H-box RNA helicase DDX6 which is essential for P-body assembly (Andrei et al., 2005). Interestingly, DDX6 was shown to interact with ATXN2 via its Lsm/LsmAD domain and the two proteins co-localize in SGs and P-bodies (Nonhoff et al., 2007). Thus, ATXN2 forms part of several structures involved in mRNA storage and processing under stress conditions but its role in these tiny structures is not yet resolved.

1.4.2.3 Other functions of ATXN2

Apart from these direct RNA-related functions, ATXN2 has also been implicated in various other cellular mechanisms that – at first sight – do not seem to be directly associated with RNA. For example, a role in receptor endocytosis has been proposed due to the interaction of ATXN2 with endophilin A1 and endophilin A3 in *S. cerevisiae*, human HEK293T cells, and mouse brain (Nonis et al., 2008; Ralser et al., 2005a). Both proteins are predominantly expressed in the brain (Giachino et al., 1997) and function in the formation of plasmatic membrane curvature for clathrin-mediated endocytosis (Schmidt et al., 1999). ATXN2 interacts with the two endophilins via its PRDs and their SH3-domains (Ralser et al., 2005b). They co-localize at the ER as well as at the plasma membrane as shown in *in vitro* studies (Nonis et al., 2008). To investigate the role of ATXN2 in endocytosis, Nonis et al. measured the endocytosis of the EGFR (epidermal growth factor receptor) in presence and in absence of ATXN2. Overexpression of ATXN2 slowed down EGFR endocytosis while it was enhanced in murine embryonic fibroblasts of *Atxn2*-KO mice. Consequently, ATXN2 seems to affect receptor endocytosis maybe via an interaction with the endophilins or via direct interaction with the receptor.

Furthermore, ATXN2 has been strongly implicated in diabetes, lipid metabolism, and obesity because the *Atxn2*-KO mice show increased weight as well as higher serum insulin and cholesterol levels compared to WT (Lastres-Becker et al., 2008a). Besides, these animals are characterized by marked lipid accumulation in liver, reduced insulin receptor expression, elevated sphingomyelin and ganglioside levels in cerebellum, and decreased fertility (Lastres-Becker et al., 2008a). Moreover, in diverse genome-wide association studies (GWAS) the region around the *ATXN2* locus was associated with a broad spectrum of diseases (Auburger et al., 2014) including kidney disease (Kottgen, 2010; Liu et al., 2011), hypertension and coronary heart disease (Ikram et al., 2010), obesity (Figueroa et al., 2009), and myocardial infarction (Gudbjartsson et al., 2009).

Aside from its function in obesity-related disorders, ATXN2 has been shown to play a role in the regulation of circadian rhythm and megakaryopoiesis. Studies in *D. melanogaster* revealed that dATX2 is crucial for the period length determination of circadian behavior in pacemaker neurons (Zhang et al., 2013). Specifically, it is involved in the coordination of the translation complex for PERIOD expression, an important protein in circadian rhythm control (Lim and Allada, 2013). Regarding megakaryopoiesis, a role for ATXN2 in protein accumulation and proper platelet function was proposed (Zeddies et al., 2013). Reduction of ATXN2 decreased the protein synthesis in a megakaryotic cell line resulting in a reduced amount of total protein content per cell. In conclusion, ATXN2 may function in various cellular pathways that are not directly RNA-related but may be affected due to the regulation of translation and protein expression by ATXN2.

1.4.3 Involvement of ATXN2 in other neurodegenerative diseases

An association of ATXN2 with various non-CNS diseases has already been discussed in the last section. Additionally, ATXN2 has been implicated in various neurodegenerative disorders. For example, intermediate repeat expansions of ATXN2 were shown to be a risk factor for Amyotrophic lateral sclerosis (ALS) (Elden et al., 2010; Gispert et al., 2012; Lee et al., 2011), Frontotemporal dementia (FTD) (Lattante et al., 2014; van Blitterswijk et al., 2014), Progressive supranuclear palsy (Ross et al., 2011), and Levodopa-responsive idiopathic Parkinson's disease (PD) (Charles et al., 2007; Gwinn-Hardy et al., 2000; Kim et al., 2007; Yamashita et al., 2014). Moreover, a role for ATXN2 in other SCAs like SCA1 and SCA3 was proposed (Al-Ramahi et al., 2007; Lessing and Bonini, 2008).

1.4.3.1 Role of ATXN2 in ALS

ALS is a neurodegenerative disease characterized by the selective loss of motor neurons from brain and spinal cord. This massive loss of neurons typically leads to paralysis and death one to five years after the disease has been diagnosed (Cleveland and Rothstein, 2001). There is not only one gene or protein that is causative for ALS, but there are many, for example, TDP43 (Sreedharan et al., 2008), FUS (Kwiatkowski et al., 2009; Vance et al., 2009), SOD1 (Rosen et al., 1993), VCP (Johnson et al., 2010; Koppers et al., 2012), and C9ORF72 (DeJesus-Hernandez et al., 2011; Renton et al., 2011). Additionally, ALS can either be inherited or occur sporadically. The sporadic cases are much more complicated to study since association studies in affected families are not possible. Therefore, less gene associations have been found compared to familial cases (Sreedharan and Brown, 2013). Unfortunately, the majority of ALS cases (~90%) is

caused by sporadic mutations (Sreedharan and Brown, 2013). Like in many other neurodegenerative diseases, affected neurons in ALS show aggregation of the mutant protein. Additionally, TDP43 is a major component of these aggregates in about 90% of all (sporadic and familial) ALS cases independent of its mutation (Neumann et al., 2006; Tollervey et al., 2011)

A first association between ATXN2 and ALS was found in 2010 by Elden et al., who identified an increased number of intermediate CAG repeat expansion carriers (27 - 33 glutamines) among 915 ALS patients compared to controls (Figure 9). They initiated this study based on former results that determined the *S. cerevisiae* homolog of ATXN2, PBP1, as well as the *D. melanogaster* homolog, dATX2, as dose-sensitive modifiers of TDP43 toxicity (Elden et al., 2010). Subsequently, several independent studies confirmed the ALS risk association with ATXN2 in different etiological groups (Bonini and Gitler, 2011; Gellera et al., 2012; Gispert et al., 2012; Lahut et al., 2012; Lattante et al., 2014; Liu et al., 2013). Moreover, ATXN2 was associated with a shortened survival in ALS (Chio et al., 2014). However, in a recent meta-analysis of nine former studies, an increased risk for ALS was only verified for CAG repeats between 29 and 32 while for smaller expansions (27 - 28 CAGs) the risk was even slightly decreased (Neuenschwander et al., 2014). It should be taken into account that these bigger intermediate repeat expansions are prone to meiotic expansion and that the higher risk could therefore result from repeat expansions occurring during mitosis or DNA repair (Neuenschwander et al., 2014).

It is of interest that Atxn2 was not only identified as a risk factor for ALS but SCA2 and ALS were found in individuals of the same family (Baumer et al., 2014; Tazen et al., 2013). In two reported cases both family members exhibited a pathological CAG repeat expansion in ATXN2 but one individual of each family presented with ALS and the other one with SCA2. These observations indicate that there is an overlap between SCA2 and ALS. Besides, a difference in the pathological subtype between ALS cases with and without *ATXN2* polyQ expansion was reported: ALS cases with ATXN2 expansion exhibited primarily skein-like or filamentous TDP43 aggregates whereas in cases without ATXN2 pathology large round and skein-like inclusion of TDP43 were observed (Hart et al., 2012). Already in the first association study, a perturbation of ATXN2 localization in motor neurons from ALS patients was found and an RNA-dependent interaction between ATXN2 and TDP43 was proven (Elden et al., 2010). TDP43 is a DNA and RNA-binding protein that is involved in transcription regulation and splicing (Buratti and Baralle, 2008). It shuttles between the nucleus and the cytoplasm but is mainly found in the nucleus in healthy state, while it is aggregated in the cytoplasm in diseased state. TDP43 inclusions have not only been found in ALS but also in Alzheimer's disease (AD) (Amador-Ortiz et

al., 2007; Arai et al., 2009; Higashi et al., 2007), Corticobasal degeneration (Uryu et al., 2008), Lewy body-related diseases (Arai et al., 2009; Higashi et al., 2007), Huntington's disease (HD) (Schwab et al., 2008) as well as in SCA2 (Toyoshima et al., 2011). Moreover, in an SCA2 case, neuronal inclusions with TDP43 were indistinguishable from those in ALS (Toyoshima et al., 2011). Thus, it seems like the two RNA-binding proteins, ATXN2 and TDP43, are both involved in a range of other neurodegenerative diseases and may also influence each other's pathology.

However, while ATXN2 always seems to be mutated (increased polyQ size) when associated with other diseases, no mutation was found in TDP43 that could account for its cytoplasmic aggregation in diverse disorders. Even in ALS, where TDP43 aggregates are frequently shown, mutations in this gene only account for less than 1% of the sporadic and about 4% of the familial ALS cases (Lagier-Tourenne et al., 2010). Instead, it has been shown that independent of a TDP43 mutation, shuttling of TDP43 between the nucleus and the cytoplasm is unbalanced resulting in cytoplasmic TDP43 accumulation (Barmada et al., 2010). Furthermore, TDP43 can be C-terminally cleaved thereby creating fragments that are more prone to aggregation than the full-length protein (Igaz et al., 2008; Zhang et al., 2009b). ATXN2 with intermediate-length repeats was shown to enhance this stress-induced C-terminal cleavage of TDP43 in human cells and may also activate multiple caspases that are involved in ALS pathology rendering TDP43 more prone to aggregations (Hart et al., 2012).

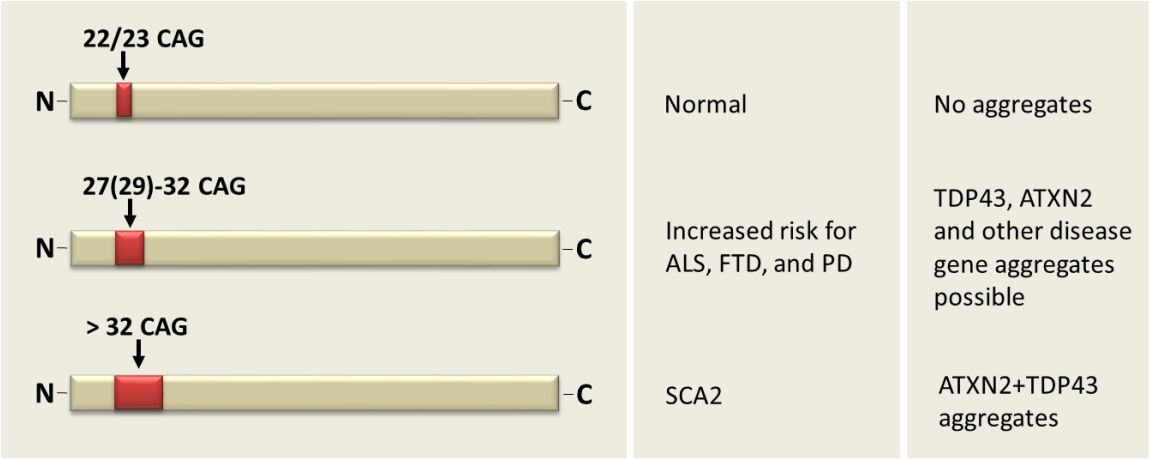

Figure 9. Involvement of Ataxin-2 polyQ length in disease. In healthy individuals the polyQ length is about 22/23 CAGs while intermediate repeat expansions (27-32 CAGs) increase the risk for neurodegenerative diseases like ALS, FTD, and PD and >32 CAGs most probable result in SCA2 (adapted from (Elden et al., 2010)). ALS = Amyotrophic lateral sclerosis, FTD = Frontotemporal dementia, PD = Parkinson's disease, SCA2 = Spinocerebellar ataxia type 2.

A modifier effect for intermediate-length ATXN2 has also been investigated for another ALS-causing protein called FUS (fused in sarcoma) which behaves quite similar to TDP43 regarding its cellular distribution. When co-expressed in a cell model, ATXN2[Q31]

enhanced ER stress and translocation of FUS to the cytoplasm. Furthermore, it co-localized with FUS in neuronal cell lines (Farg et al., 2013). In another *in vitro* study, overexpressed ATXN2 was shown to increase the cytoplasmic concentration of TDP43 and FUS, while their nuclear presence was decreased (Nihei et al., 2012). Besides, Atxn2, TDP43, and FUS are among the differentially spliced transcripts that were detected in ALS motor neurons (Highley et al., 2014). These three proteins further have in common that they re-localize to stress granules under conditions of environmental stress. Based on this fact, a "precursor model" for TDP43 aggregate formation was proposed where the stress granules serve as "seeds" for TDP43 aggregates that arise due to chronic stress (Dewey et al., 2012). The presence of intermediate-length ATXN2 could then further promote this aggregation (Hart and Gitler, 2012). Up to now, no evidence has been found for this theory and that is why the authors also proposed a model in which TDP43 aggregate formation occurs stress granule independent (Dewey et al., 2012). Nevertheless, one year later, another research group proposed three similar models also including stress granules (Li et al., 2013). They emphasized that many SG proteins harbor RNA-binding as well as prion-like domains, for example TDP43, FUS, ATXN2, and TIA1. These prion-like domains could be responsible for the rapid formation of SGs under conditions of stress given that they likely aggregate. In their first model TDP43 and FUS are depleted from the nucleus and form pre-inclusions in the cytoplasm. These pre-inclusions may interact with SGs and SG components like proteases and kinases might modify TDP43 and FUS thereby accelerating aggregation. In the second model, aggregation of TDP43 and FUS in the cytoplasm leads to interference with SGs disturbing their proper function and disassembly after stress. In the last model, the depletion of TDP43 from the nucleus results in altered gene expression of SG components. It is for example known that TDP43 regulates the expression of G3BP (McDonald et al., 2011), a protein required for normal SG assembly and an alteration in G3BP expression could therefore alter SG assembly. Besides, G3BP is associated with calcium homeostasis and neuronal plasticity and, therefore, may link SG formation with neurodegenerative disease (Martin et al., 2013). These models are not exclusive but might be responsible for many disturbances at different levels of pathology.

1.4.3.2 Involvement of ATXN2 in SCA1 and SCA3

SCA1 and SCA2 share a similar disease phenotype known as cerebellar plus syndrome although it can vary between patients (Rub et al., 2013). However, the two causative proteins, ATXN1 and ATXN2 do not share any sequence homology apart from the polyQ domain, and they show a different subcellular localization. ATXN1 is mainly implicated in transcription regulation, localized in the nucleus, and shows many nuclear inclusions in

disease state in contrast to ATXN2 (Cummings et al., 1999). First evidence for an interaction between ATXN1 and ATXN2 came up in a yeast-two-hybrid study (Lim et al., 2006). Later on, the interaction was confirmed via GST (Glutathione S-transferase) pulldown as well as in co-immunoprecipitation studies using a SCA1 *D. melanogaster* model with human ATXN1[Q82] and the ATXN2 *D. melanogaster* homolog dATX2 (Al-Ramahi et al., 2007). This interaction was proven to occur in cytoplasm as well as in the nucleus, meaning that both proteins need to shuttle between these two subcellular compartments. Indeed, a re-localization of dATX2 to the nucleus was shown in the same model but only when it was overexpressed together with expanded and not with WT ATXN1. Accumulation of dATX2 in nuclear inclusions caused severe eye toxicity. In the same model, the authors observed that a decrease of ATXN2 reduced the dysfunction caused by pathological ATXN1 while an increase in ATXN2 worsened SCA1 pathology. Similar effects were observed in an SCA3 *D. melanogaster* model in which upregulation of dATX2 enhanced and reduction of dATX2 mitigated neurodegeneration. The two proteins further showed a PAM2 motif dependent interaction in this study and dATX2 was also observed in intranuclear inclusions of dATX3 (Lessing and Bonini, 2008).

1.5 Mouse models

Several cell lines and mouse models have been employed for this doctoral thesis to examine the function and interactions of ATXN2. Cell culture experiments nowadays are the initial approach and a good way for mechanistic understanding. However, it is still necessary to analyze the respective genes and pathways in animal models as well. The reason is that isolated two-dimensional cell cultures cannot mimic the complicated processes that occur in a living creature with three-dimensional synaptic interactions and neural circuitry of diverse differentiation, especially when modeling age-associated insidiously progressive disorders (Yang et al., 2014a). Especially diseases with yet unknown mechanisms are hard to model in cell culture. In contrast, model organisms like *S. cerevisiae*, *D. melanogaster* or *C. elegans* are easy to modify genetically so that they develop features of the human disease. They have a short breeding time, a limited lifespan, and several genes are conserved from yeast to human. However, many lower organisms lack complex pathways that exist in humans and conclusions drawn in yeast are sometimes hard to transfer into humans. Therefore, besides patient material, the genetically modified mice were the model of choice for this doctoral thesis because they are closer to humans regarding their genetics (most human genes have homologs in

mice) and still easy to breed. The genetic basis and key features of the employed animal models are described in the following sections, in cases where their characterization was not part of this work.

1.5.1 ATXN2 mouse models

Given that mice do not harbor a CAG repeat in their *Atxn2* gene and are therefore not prone to develop SCA2, the CAG repeat needs to be introduced genetically. The first SCA2 mouse model, generated in 2000, was a transgenic one with random genomic insertion of human *ATXN2*[58Q] cDNA, overexpressed under control of the Purkinje cell specific promoter Pcp2 (Huynh et al., 2000). This mouse model was reported to show a rotarod phenotype at 26 weeks of age. However, in independent experiments we could not confirm this phenotype until 46 weeks of age using descendants of this line. Therefore, studies with *ATXN2*[Q58] mice were excluded from this work. In 2012, the first *Atxn2*-KIN mouse line harboring an expansion of 42 CAGs was published (Damrath et al., 2012). Since this mouse line was generated with a KIN approach, it ubiquitously expressed expanded *Atxn2* in a proper spatial and temporal pattern. However, another consequence of this approach was that the mutated gene was not overexpressed as in most transgenic models. Therefore, and due to the relatively short CAG repeat, this mouse line showed a quite late behavioral phenotype with motor performance deficits on the rotarod starting at 18 months of age. Further behavioral studies, like open field or grip strength test, did not reveal any differences between wild type (WT) and *Atxn2*-CAG42-KIN mice until 24 months of age. Anatomically, these mice showed slight aggregation of ATXN2 in the Purkinje cells starting at 14 months of age. Furthermore, *Atxn2*-CAG42-KIN mice were characterized by a pronounced weight loss, while no significant alteration in the survival rate was observed.

To study the effect of *Atxn2* loss, two independent *Atxn2*-KO mice were generated (Kiehl et al., 2006; Lastres-Becker et al., 2008a). Mice from both lines were viable but with decreased fertility and an obese phenotype. No ataxia or other pathological symptoms in the CNS were observed. However, *Atxn2*-KO mice showed a slightly reduced motor performance on the rotarod which was not related to the obese phenotype as the animals had been set on a low fat diet before (Kiehl et al., 2006). Furthermore, a deranged insulin metabolism as mentioned in section 1.4.2.3 and hyperactivity were demonstrated (Lastres-Becker et al., 2008a). The latter *Atxn2*-KO mice as well as the *Atxn2*-CAG42-KIN mice were employed in this doctoral thesis.

1.5.2 ATXN1 mouse models

The *Atxn1*-Q154-KIN mouse model was the second KIN mouse line that was generated for SCA1 after some transgenic models. The first KIN mice only harbored 78 polyQs resulting in a mild phenotype that appeared late in life (Lorenzetti et al., 2000). Therefore, a new line with an almost twofold longer repeat expansion was generated (Watase et al., 2002). In heterozygous mice of this mouse line, the first symptoms appeared at 5 weeks of age (decreased rotarod performance) and none of the mice survived 50 weeks of age due to premature death (Watase et al., 2002). Furthermore, the mice showed growth retardation and kyphosis, abnormal gait, and a clasping phenotype. The reduced body and brain weight as well as the reduced brain size resulted from the enormous neurodegeneration in the brain. The authors also observed muscle wasting, learning and memory deficits, and intranuclear inclusions of ATXN1 in various brain regions. Further studies of this mouse line showed transcriptional downregulation of several calcium homeostasis factors in the cerebellum (Lin et al., 2000). *Atxn1*-Q54-KIN mice were not characterized independently regarding their motor performance. Therefore, in contrast to the original study where heterozygous mice had been employed, homozygous animals were used in this work to increase the pathology and assure an early phenotype.

1.5.3 TDP43 mouse models

As mentioned before, TDP43 changes its distribution from predominantly nuclear in healthy state to predominantly cytoplasmic in disease state. There is an ongoing discussion about whether the loss of nuclear TDP43 or the gain of TDP43 in the cytoplasm causes ALS. Therefore, several mouse models with deletion or mutation of TDP43 have been generated (Arnold et al., 2013; Chiang et al., 2010; Kraemer et al., 2010; Sephton et al., 2010; Stallings et al., 2010; Swarup et al., 2011; Wils et al., 2010; Wu et al., 2010; Xu et al., 2010) in order to elucidate the pathomechanism. Nevertheless, there were only transgenic mouse lines for TDP43 until in 2014 the first TDP43-KIN mouse (hTDP43-A315T-KIN) was published (Stribl et al., 2014). In this mouse line the mouse *Tardbp* (TDP43) was exchanged with the human *TARDBP* that additionally had an A315T transition, a common mutation causative for ALS. Unfortunately, when this mouse line was generated, it was not known that TDP43 has a self-regulating mechanism: it binds to its own 3'UTR thereby regulating its transcription levels (Ayala et al., 2011; Stribl et al., 2014). In hTDP43-A315T-KIN mice, the insertion of the human *TARDBP* open reading frame cDNA without 3'UTR results in absent expression autoregulation and thus in an increased human *TARDBP* and decreased murine *Tardbp* transcript abundance in

heterozygous mice. Apart from the altered transcript levels, this mouse line shows TDP43 aggregates in brain and spinal cord, neurodegeneration in motor neurons, and altered lipid metabolism. These features were all observed in heterozygous mice as TDP43 seems to be necessary for development and therefore homozygotes were not viable (Stribl et al., 2014).

1.6 Aim of the thesis

Almost 20 years after its genetic mapping, SCA2 is still far from being understood. Nevertheless, to find suitable therapies it is necessary to conceive the mechanisms that lead to SCA2 pathology. As for all other neurodegenerative disorders, it is difficult to study a disease without being able to examine the relevant tissue. The complexity of the neuronal network cannot be displayed exclusively using cell culture. Consequently, to generate and study adequate animal models for these diseases is quite important. As long as it is not completely clear to which extend gain- and loss-of-function are implicated in SCA2, both *Atxn2*-KIN and *Atxn2*-KO mouse mutants together with human patient tissue should be studied to be able to receive a thorough picture of ATXN2 function. Therefore, the first aim of this thesis was to study the effect of *Atxn2* mutation or loss on genes of pathways ATXN2 is involved in:

1) Components of the UPS were shown to form part of protein aggregates in many SCAs. In a microarray transcriptome study, the expression of a specific component of this pathway, named *Fbxw8*, was strikingly upregulated in *Atxn2*-CAG42-KIN mice. Therefore, the following questions were addressed:
    a. Do ATXN2 and FBXW8 influence each other's expression by interacting with each other?
    b. Is FBXW8 relevant for ATXN2 degradation?
    d. Could *FBXW8* serve as a biomarker in SCA2 patients?

2) Transcripts of calcium homeostasis factors show a downregulation in many other SCAs and independently were found among the 100 most downregulated transcripts in an RNAseq of cerebellar tissue from *Atxn2*-KO mice. This finding raised the questions whether:
    a. The downregulation of calcium homeostasis factors is an age-dependent and/or cerebellum-specific effect?
    b. Loss and mutation of ATXN2 similarly affect calcium homeostasis factors?
    c. The formerly proposed model of a repeat length dependent interaction of ATXN2 and ITPR1 can be confirmed in *Atxn2*-CAG42-KIN mice?

3) The main function of ATXN2 seems to be translation regulation. Several transcripts involved in translation were upregulated in a whole transcriptome analysis of *Atxn2*-KO cerebellum and liver.
    a. Are protein levels of these transcripts similarly affected?

4) TBC1 domain family proteins are dysregulated in several stress or disease related mouse models.
    a. Can similar effects be observed in Atxn2 mouse models?

5) An effect of ATXN2 on SCA1 and SCA3 pathology was already observed in *D. melanogaster*. Thus, the question was raised:
    a. Are there SCA genes that are altered by or that influence SCA2 pathology?
    b. Is ATXN2 relevant for human SCA2 pathology?

The second aim of this thesis was to characterize two new mouse models to get a better insight into the functional mechanisms of SCA2 and ALS pathology. Specifically, two issues were addressed:

6) ATXN2 and TDP43 have been shown to interact with each other and ATXN2 is a modifier of TDP43 toxicity.
    a. Is there a potentiation effect of ATXN2 and TDP43 mutations that is reflected in a stronger pathology on behavioral level in double mutants?

7) The *Atxn2*-CAG42-KIN mouse shows ubiquitous expression of ATXN2 but a quite late pathology. To reach an earlier and stronger pathology, the *Atxn2*-CAG100-KIN mouse was generated.
    a. Does the *Atxn2*-CAG100-KIN mouse fulfill the criteria of an early and strong pathology on behavioral, immunohistochemical, and molecular level?

2 Material and Methods

2.1 Material

2.1.1 General equipment and chemicals

Table 3. General instruments used in the laboratory

Instrument	Company / Distributor
Analytical Balance 474-32	Kern & Sohn
Analytical Balance PE1600	Mettler Toledo
Analytical Precision Balance A120S	Sartorius
Autoclave Tuttnauer 2540EL	Systec
Autoclave Varioklav 400	H+P Labortechnik
BioPhotometer 6131	Eppendorf
Centrifuge 5415 C	Eppendorf
Centrifuge 5415 D	Eppendorf
Centrifuge 5415 R	Eppendorf
Drying oven T5025	Heraeus
Drying oven T5028	Heraeus
Freezer (-80 °C) Forma900	Thermo Scientific
Freezer (-80 °C) HERAfreeze	Thermo Scientific
Freezer AEG Arctis	AEG
Ice machine Scotsman AF80	Hubbard Systems
Incubator BD23	Binder
Incubator Modell 200	Memmert
KontesTM Pellet Pestle™ Cordless Motor	Sigma-Aldrich
Magnetic stirrer and heater Ikamag RCT	IKA Werke
Magnetic stirrer REO basic C	IKA Werke
Megafuge 1.0 R	Heraeus
Microwave R-234	Sharp
Milli-Q Ultrapure Water System	Millipore
Minishaker MS1	IKA Werke
pH Bench Meter Microprocessor ATC PH210	HANNA Instruments
Pipet Boy accu-jet	Brand
Power pack Consort E122	Consort
Power pack Pac 200	Biorad

Instrument	Company / Distributor
Rotator 2-1175	Neolab
Rotator 34528E	Neolab
Thermomixer comfort	Eppendorf
Thermomixer compact	Eppendorf
Vortex Genie 2	Bender & Hobein

Table 4. General material used in the laboratory

Product	Cat. No.	Company / Distributor
Aluminium foil alupro	A0621	Ecopla
Cellstar® Tubes sterile, 15 ml	188271	Greiner Bio-One
Cellstar® Tubes sterile, 50 ml	227261	Greiner Bio-One
Cellstar® Tubes sterile, 50 ml brown	227 280	Greiner Bio-One
Combitips Advanced, 0.1 ml	0030089405	Eppendorf
Combitips Advanced, 0.2 ml	0030089413	Eppendorf
Combitips Advanced, 2.5 ml	0030089448	Eppendorf
Combitips Advanced, 5 ml	0030089456	Eppendorf
Combitips Advanced, 10 ml	0030089464	Eppendorf
Feather disposable scalpel No. 11	02.001.30.011	Pfm medical
Finnpipette® F1, 1-10 µl	613-2732	Thermo Scientific
Finnpipette® F1, 2-20 µl	613-2735	Thermo Scientific
Kim Precision Wipes	05511	Kimberly-Clark
Laboratory glassware	-	Fisherbrand
Microtube Easy Cap 1.5 ml	72.690550	Sarstedt
Microtube rack	C772.1	Carl Roth
Microtube Safe Seal 2.0 ml	72.695	Sarstedt
Multipette® plus	4981000019	Eppendorf
Parafilm	PM-996	Pechiney Plastic Packaging
Pellet pestles polypropylene	Z359947	Sigma-Aldrich
Pipetman Classic™ pipettes, 2 µl	F144801	Gilson
Pipetman Classic™ pipettes, 10 µl	F144802	Gilson
Pipetman Classic™ pipettes, 20 µl	F123600	Gilson
Pipetman Classic™ pipettes, 200 µl	F123601	Gilson
Pipetman Classic™ pipettes, 1000 µl	F123602	Gilson
Pipette tips TipOne, 10 µl	S1111-3700	Starlab
Pipette tips TipOne, 200 µl	S1111-0706	Starlab
Pipette tips TipOne, 1000 µl	S1111-2721	Starlab
Pipette tips TipOne, sterile, 10 µl	S1120-3810	Starlab
Pipette tips TipOne, sterile, 20 µl	S1120-1810	Starlab
Pipette tips TipOne, sterile, 200 µl	S1120-8810	Starlab
Pipette tips TipOne, sterile, 1000 µl	S1122-1830	Starlab

Product	Cat. No.	Company / Distributor
Plastic ware	-	Vitlab
Plastic wrap	10518	PapStar
Serological pipet, non-sterile, 5 ml	CLS4050	Sigma-Aldrich
Serological pipet, non-sterile, 10 ml	CLS4100	Sigma-Aldrich
Serological pipet, non-sterile, 25 ml	CLS4250	Sigma-Aldrich
Serological pipet, sterile, 5 ml	CLS4487	Sigma-Aldrich
Serological pipet, sterile, 10 ml	CLS4488	Sigma-Aldrich
Serological pipet, sterile, 25 ml	CLS4251	Sigma-Aldrich
Tongue depressor	NOBA-SEME-7-210	NOBA Verbandmittel
UV-Cuvette micro	759200	Brand
Vasco® Nitril White	9208410	Braun
Weigh Boat	611-9189	VWR International
Welted glasses	-	Carl Roth

Table 5. General chemicals used in the laboratory

Chemical	Cat. No.	Company / Distributor
2-Mercaptoethanol (C_2H_6OS)	12006	Merck
2-Propanol (C_3H_8O)	33539	Sigma-Aldrich
Boric acid (H_3BO_3)	191411	MP Biomedicals
Bovine serum albumin (BSA)	A7906	Sigma-Aldrich
Bromophenol Blue ($C_{19}H_{10}Br_4O_5S$)	B6131	Sigma-Aldrich
Calcium chloride ($CaCl_2$)	A1428	Applichem
Citric acid ($C_6H_8O_7$ * H_2O)	100243	Merck
Dimethylsulfoxid (DMSO) (C_2H_6OS)	41639	Sigma-Aldrich
di-Potassium hydrogen phosphate (KH_2PO_4)	A3620	Applichem
di-Sodium hydrogen phosphate (Na_2HPO4)	106559	Merck
Distilled water (“DNase/RNase free”) (H_2O)	109977-035	Life Technologies
Ethanol (C_2H_6OH)	32205	Sigma-Aldrich
Ethylenediamine tetraacetic acid (EDTA) ($C_{10}H_{16}N_2O_8$)	E5134	Sigma-Aldrich
Ethyleneglycol tetraacetic acid (EGTA) ($C_{14}H_{24}N_2O_{10}$)	A0878	Applichem
Gelatin solution	G1393	Sigma-Aldrich
Glycerol ($C_3H_8O_3$)	G8773	Sigma-Aldrich
Glycine ($C_2H_5NO_2$)	A1377	Applichem
Hydrochloric acid 1 M (HCl)	3528	Sigma-Aldrich
Hydrogen peroxide 30% (H_2O_2)	8070.1	Carl Roth
Magnesium chloride ($MgCl_2$)	814733	Merck
Methanol (CH_4O)	32213	Sigma-Aldrich
Potassium chloride (KCl)	A2939	Applichem
Sodium azide (NaN_3)	S8032	Sigma-Aldrich
Sodium chloride (NaCl)	31434	Sigma-Aldrich

Chemical	Cat. No.	Company / Distributor
Sodium hydroxide (NaOH)	30620	Riedel-de-Haën
Sucrose ($C_{12}H_{22}O_{11}$)	84100	Sigma-Aldrich
Tris (Trizma® base) ($C_4H_{11}NO_3$)	T1503	Sigma-Aldrich
Trisodium citrate dihydrate ($Na_3C_6H_5O_7$ * 2 H_2O)	71402	Sigma-Aldrich
Triton® X-100 reduced ($C_{30}H_{60}O_9$)	282103	Sigma-Aldrich
Tween® 20 ($C_{58}H_{114}O_{26}$)	A1389	Applichem

2.1.2 Mouse models

Table 6. Mouse models described before

Mouse model	Mutation	Background	Reference
Atxn2-knock-out	Excision of *Atxn2* exon 1	C57BL/6J	Lastres-Becker et al., 2008
Atxn2-CAG42-knock-in	Replacement of *Atxn2* exon 1 with an CAG42-containing fragment	C57BL/6J	Damrath et al., 2012
hTDP43-A315T-knock-in	Insertion of human full length *TARDBP43*(A315T) cDNA	C57BL/6N	Stribl et al., 2014
Atxn1-Q154-knock-in	Replacement of *Atxn1* exon 8 with an CAG154-containing fragment	C57BL/6J	Watase et al., 2002 Lorenzetti et al., 2000
Tia1-knock-out	Replacement of parts of Tia1 exon 3 and exon 4	C57BL/6J	Piecyk et al., 2000

Table 7. Newly introduced mouse models

Mouse model	Mutation	Background
Atxn2-CAG42-knock-in / hTDP43-A315T-knock-in	Replacement of *Atxn2* exon 1 with an CAG42-containing fragment and insertion of human full length *TARDBP43*(A315T) cDNA	Mixed C57BL/6J and C57BL/6N
Atxn2-CAG100-knock-in	Replacement of *Atxn2* exon 1 with an CAG100-containing fragment	C57BL/6J

2.1.3 Equipment used for behavioral studies, perfusion, and dissection

Table 8. Instruments used for behavioral studies, perfusion, and dissection

Instrument	Company / Distributor
Dewar Carrying Flask Type B	KGW Isotherm
Digital Scale GT-KSt-01	Globaltronics
Peristaltic Pump Minipuls 3	Gilson
Rotarod 7650	Ugo Basile
Versamax Animal Acitivity Monitoring System	Accuscan Instruments

Instrument	Company / Distributor
Video Camera HC-V707M	Panasonic

Table 9. Material used for perfusion and dissection

Product	Cat. No.	Company / Distributor
Dumont precision forceps	K344.1	Carl Roth
Forceps	LH56.1	Carl Roth
Forceps	1151	Bochem
Heparin-Natrium 2500	-	Ratiopharm
Microlance™ 3 Nr. 20	302200	BD
Narcoren®	-	Merial
Utility drape	700330	Barrier
Paraformaldehyde	16005	Sigma-Aldrich
Plastipak™ Syringe, 1 ml	300013	BD
Precision scissors	3534.1	Carl Roth
Safety-Multifly®-Set	851638235	Sarstedt
Scissors	3577.1	Carl Roth
Transportation cages d|series	04109	Allentown

2.1.4 Blood samples

Blood samples were taken after approval of the local ethics committee and written informed consent of the donors.

Table 10. Blood samples of SCA2 patients and healthy controls

Blood Sample	Gender	Age	Ethnicity	Reference
162 polyQ-expansion CAG: 35	male	52	Turkish	NDAL, Boğaziçi University, Istanbul, Turkey
721 polyQ-expansion CAG: 40	male	66	Turkish	
958 polyQ-expansion CAG: 44	female	19	Turkish	
718 healthy control	male	72	Turkish	
719 healthy control	male	69	Turkish	NDAL, Boğaziçi University, Istanbul, Turkey
163 healthy control	female	48	Turkish	
722 healthy control	female	27	Turkish	
957 healthy control	female	37	Turkish	

2.1.5 Cell lines

Skin biopsies were taken after approval of the local ethics committee and written informed consent of the donors or were obtained commercially.

Table 11. Cell lines

Cell type	Gender	Ethnicity	Source	Reference
HeLa	-	-	cervix carcinoma	DSMZ
SCA2 Patient fibroblasts				
5106 polyQ-expansion CAG: 41	female	Dutch	skin biopsy	Ewout Brunt, Groningen, Netherlands
5107 polyQ-expansion CAG: 38	male	Dutch		
5109 polyQ-expansion CAG: 14/41	male	German		
5110 polyQ-expansion CAG: 22/40	female	German		
Healthy Control Fibroblasts				
02222	male	Caucasian	skin biopsy	Coriell
02261	male	Caucasian		Coriell
20445	male	Caucasian		Coriell
4573	female	Dutch		Ewout Brunt, Groningen, Netherlands

2.1.6 Equipment and reagents used in cell culture

Table 12. Instruments used in cell culture

Instrument	Company / Distributor
Cell culture bench Envirco	Envirco
Cell culture bench Lamin Air HB2448	Heraeus
Cell culture bench MSC Advantage	Thermo Scientific
Centrifuge 5702	Eppendorf
Centrifuge MinifugeTM	Labnet
CO_2-Incubator HERAcell 240i	Thermo Scientific
Freezing Container, Nalgene 5100, Cryo 1°C	Thermo Scientific
Nitrogen tank Cryosystem 2000	MVE Cryosystem
Nitrogen tank RS Series	Welabo
Water bath GFL 1083	Gemini BV Laboratory

Table 13. Material used in cell culture

Product	Cat. No.	Company / Distributor
6-well cell culture plate sterile, with lid	657160	Greiner Bio-One
Cell scraper	83.1830	Sarstedt
Cellstar Cell culture dishes, 100x20 mm	664160	Greiner Bio-One
Cellstar cell culture flasks, 25 cm^2	690175	Greiner Bio-One
Cellstar cell culture flasks, 75 cm^2	658175	Greiner Bio-One
CryoTube™ Vials, 2 ml	377224	Thermo Scientific
Neubauer counting chamber, 20 x 26 mm	728.1	Carl Roth
Pasteur pipette 145 mm	747715	Brand
Pasteur pipette 225 mm	747720	Brand

Table 14. Media and reagents used in cell culture

Product	Cat. No.	Company / Distributor
DME Medium high glucose (DMEM)	21969-035	Life Technologies
Effectene Transfection Reagent Kit	301425	Qiagen
Fetal Calf Serum Gold (FCS)	A15-151	PAA
Hepes Buffer Solution (1M)	S11-001	PAA
L-glutamine 200mM	25030-024	Life Technologies
Liquid Trypsin EDTA 0.05%	25300-054	Life Technologies
MEM medium + Earle´s Salts	31095	Life Technologies
Non-essential amino acids	11140	Life Technologies
Penicillin-streptomycin solution (Pen-Strep)	15140-122	Life Technologies
Phosphate Buffered Saline (PBS)	H15-001	PAA

2.1.7 Vector constructs and competent cells

Table 15. Vector constructs used for transient transfections

Construct	Selection Antibiotic	Restriction Enzyme	Enzyme Buffer	Company / Distributor	Cat. No.
ATXN2-Q22-GFP (pCMV)	Ampicillin	Gift from M. Azizov	-	custommade *	-
ATXN2-Q22-Myc (pCMV)	Ampicillin	Sac II	NEBuffer 4	custommade **	-
ATXN2-Q74-GFP (pCMV)	Ampicillin	Gift from M. Azizov	-	custommade *	-
ATXN2-Q74-Myc (pCMV)	Ampicillin	Sac II	NEBuffer 4	custommade **	-
Control-Cherry (pCMV)	Ampicillin	Xcm I	NEBuffer 2	Genecopeia	EX-mCHER-M56
Control-HA (pCMV)	Ampicillin	Bcg I	NEBuffer 3 + SAM	Genecopeia	EX-EGFP-M07
Control-Myc (pCMV)	Ampicillin	Nde1	NEBuffer 4	Clontech	631604
FBXW8-3xHA (pCMV)	Ampicillin	BamH I	NEBuffer 3	Genecopeia	EX-H4905-M07
FBXW8-Cherry (pCMV)	Ampicillin	BamH I	NEBuffer 3	Genecopeia	EX-H4905-M55

Construct	Selection Antibiotic	Restriction Enzyme	Enzyme Buffer	Company / Distributor	Cat. No.
PARK2-Cherry-GFP (pCMV)	Kanamycin	Gift from M. Jendrach	-	custommade ***	-

* published in Halbach et al., 2015; ** published in Nonis et al., 2008; *** published in Klinkenberg et al., 2012

Table 16. Competent cells used for transformation

Strain	Cat. No.	Company / Distributor
DH5α Chemically Competent Cells	18265-017	Life Technologies
SURE Competent Cells	200238	Agilent Technologies

2.1.8 Equipment and reagents used for cloning

Table 17. Instruments used for cloning

Instrument	Company / Distributor
Incubator Shaker G 25	New Brunswick Scientific
Labogaz 206	Camping Gaz
Sorvall refrigerated superspeed centrifuge RC-5B	DuPont Instruments

Table 18. Material used for cloning

Product	Cat. No.	Company / Distributor
Agar	A7002	Sigma-Aldrich
DNA the Jetstar Plasmid Purification MIDI kit	210025	Genomed
GenElute HP Plasmid Midiprep Kit	NA0200	Sigma-Aldrich
Isopropyl-β-D-thiogalactopyranosid (IPTG)	2316	Carl Roth
N,N-Dimethylformamide	D4551	Sigma-Aldrich
NEBuffer 2	B7002	New England Biolabs
NEBuffer 3	B7003	New England Biolabs
NEBuffer 4	B7004	New England Biolabs
Peptone from Casein	8986.1	Carl Roth
pGEM®-T Easy Vector Systems	A1360	Promega
Restriction Enzyme BamH I	R0136	New England Biolabs
Restriction Enzyme Bcg I	R0545	New England Biolabs
Restriction Enzyme Nde I	R0111	New England Biolabs
Restriction Enzyme Sac II	R0157	New England Biolabs
Restriction Enzyme Xcm I	R0533	New England Biolabs
S-adenosylmethionine (SAM)	B9003	New England Biolabs
Wizard® SV Gel and PCR Clean-Up System	A9281	Promega

Product	Cat. No.	Company / Distributor
Yeast extract	2363.2	Carl Roth
β-X-Gal	2315	Carl Roth

2.1.9 Equipment and reagents used for DNA isolation, PCR, and agarose gel electrophoresis

Table 19. Instruments used for PCR and agarose gel electrophoresis

Instruments	Company / Distributor
GeneAmp® PCR System 2700	Life Technologies
Horizontal Gel Electrophoresis System Agagel	Biometra
Horizontal Gel Eletrophoresis System Owl™ Easy Cast™	Thermo Scientific
Polaroid Direct Screen Instant Camera DS34	Polaroid
UV-light	Bachofer

Table 20. Material used for PCR and agarose gel electrophoresis

Product	Cat. No.	Company / Distributor
8-Lid chain, flat	65.989.002	Sarstedt
Fujifilm instant Black & White	FP-3000B	Fujifilm
Multiply®-µStrip 0.2 ml chain	72.985.002	Sarstedt

Table 21. Reagents used for DNA isolation, PCR, and agarose gel electrophoresis

Product	Cat. No.	Company / Distributor
10x PCR Buffer	58002026-01	Life Technologies
5Prime Master Mix	2200100	5Prime
Agarose	A9539	Sigma-Aldrich
AmpliTaq® DNA Polymerase	58002040-01	Life Technologies
Cresol Red sodium salt	50100	Sigma-Aldrich
dNTP set (dATP, dCTP, dGTP, dTTP; 100 mM each)	R0181	Thermo Scientific
Ethidium bromide	2218.1	Carl Roth
TrackIt™ 100 bp DNA Ladder	10488-058	Life Technologies
TrackIt™ 1 Kb DNA Ladder	10488-072	Life Technologies
Proteinase K (Fungal)	25530-015	Life Technologies
Purified BSA 100x	B9001S	New England Biolabs
TaKaRa LA Taq®	RR002M	Takara
UltraPure Low Melting Point Agarose	15517-014	Life Technologies

2.1.10 Oligonucleotide primer

Table 22. Oligonucleotide primer used for PCR and SYBR Green

Name	Sequence
Atxn2-KIN_Fwd	*5'-TGA GTT GAC TCC ACA GGG AGG TGA GC-3'*
Atxn2-KIN_Rev	*5'-CCA TCT CGC CAG CCC GTA AGA TTC-3'*
Atxn2-KO_Fwd1	*5'-TTG CCC CTT CTT GAG ACT GG-3'*
Atxn2-KO_Rev1	*5'-GTA GAA CTG GGT GAT GGG GT-3'*
Atxn2-KO_Rev2	*5'-TGA GTA GCA AAA GCA AGG CC-3'*
Fbxw8_Fwd	*5'-ACT GGT GTC CGT CTG GGA CT-3'*
Fbxw8_Rev	*5'-GCT ATC CAG GTC GGC ATT TC-3'*
M13_Rev	*5´-CAGGAAACAGCTATGAC-3´*
Atxn1-Q154_Fwd	*5'-CAC CAG TGC AGT AGC CTC AG-3'*
Atxn1-Q154_Rev	*5'-AGC TCT GTG GAG AGC TGG AA-3'*
Sca2Ex1_Fwd5	*5'-CCC CGC CCG GCG TGC GAG CCG GTG TAT-3'*
Sca2Ex1_Rev2	*5'-CGG GCT TGC GGC CAG TGG-3'*
T7 Promotor	*5´-TAATACGACTCACTATAGGG- 3´*
TDP43-KIN_Fwd	*5'-GCC AAA CCT ACA GGT GGG GTC TTT-3'*
TDP43-KIN_Rev	*5'-ATC AAG GAA ACC CTG GAC TAC TG-3'*
Tia1_WT_Fwd	*5'-TAT GAG TTC AAG GCC AGC CAA-3'*
Tia1_WT_Rev	*5'-TAG ACC CTC TGG ATT AGC ATC-3'*
Tia1_KO_Fwd	*5'- GTC GTG ACA AGC CAC ACT TG-3'*
Tia1_KO_Rev	*5'- AAT TCC ATC AGA AGC TTA TCG AT-3'*

2.1.11 Equipment and Reagents used for RNA isolation, cDNA synthesis, and RT-qPCR

Table 23. Material used for RNA isolation, cDNA synthesis, and RT-qPCR

Product	Cat. No.	Company / Distributor
96-well Multiply® Fast PCR plate	72.1981.202	Sarstedt
Adhesive qPCR seal	95.1999	Sarstedt
QIAshredder tubes	79654	Qiagen
RNase Zap Wipes	AM9788	Life Technologies
StepOnePlus™ Real-Time PCR System	4376600	Life Technologies

Table 24. Reagents used for RNA isolation, cDNA synthesis, and RT-qPCR

Product	Cat. No.	Company / Distributor
0.1 M DTT	18080-044	Invitrogen
10x DNAse I Reaction Buffer	18068-015	Invitrogen

Product	Cat. No.	Company / Distributor
5x FirstStrand Buffer	18080-044	Invitrogen
Chloroform	1.02445	Merck
DNase I Amplification Grade	18068-015	Invitrogen
dNTP-mixture (10 mM)	18427-088	Invitrogen
EDTA 25 mM (pH 8.0)	18068-015	Invitrogen
Fast Start Universal Probe Master (Rox)	04914058001	Roche
Oligo(dT)20 primer	18418-020	Invitrogen
qPCR™ Mastermix for SYBR® Green I	RT-SN2X-03T	Eurogentec
Random primer	48190-011	Invitrogen
RNeasy Mini Kit	74106	Qiagen
SuperScript III reverse transcriptase	18080-044	Invitrogen
TRI Reagent®	T9424	Sigma-Aldrich

2.1.12 TaqMan® assays

Table 25. Murine TaqMan® assays

Gene symbol	Assay No.	Gene symbol	Assay No.
Afg3l2 (SCA28)	Mm01258204_m1	*Itpr1*	Mm00439907_m1
Atp2a2	Mm01201431_m1	*Kcnc3 (SCA13)*	Mm00434614_m1
Atp2b2	Mm00437640_m1	*Kitlg*	Mm01232341_m1
Atxn1 (SCA1)	Mm00485928_m1	*Nop56 (SCA36)*	Mm00458467_m1
Atxn10 (SCA10)	Mm00450332_m1	*Park2*	Mm00450186_m1
Atxn2 (SCA2)	Mm01199894_m1	*Pdyn (SCA23)*	Mm00457573_m1
Atxn3 (SCA3)	Mm00804702_m1	*Plcb4*	Mm00649825_m1
Atxn7 (SCA7)	Mm01315281_m1	*Plekhg4 (SCA4)*	Mm00614486_m1
Bean1 (SCA31)	Mm01250908_m1	*Ppp2r2b (SCA12)*	Mm00511698_m1
Ca8	Mm00801469_m1	*Prkcg (SCA14)*	Mm00440861_m1
Cacna1a (SCA6)	Mm00432190_m1	*Rora*	Mm01173766_m1
Calb1	Mm00486647_m1	*Sptbn2 (SCA5)*	Mm01239117_m1
Calm1	Mm00486655_m1	*Tbc1d1*	Mm00497989_m1
Fbxw8	Mm00554876_m1	*Tbc1d24*	Mm00557451_m1
Fgf14 (SCA27)	Mm00438914_m1	*Tbc1d8b*	Mm01305807_m1
Fxn	Mm00784016_s1	*Tbc1d9b*	Mm00659608_m1
Grm1	Mm00810219_m1	*Tbp*	Mm00446973_m1
Homer3	Mm00803747_m1	*Tgm6 (SCA35)*	Mm00624922_m1
Hprt1	Mm00446968_m1	*Trpc3*	Mm00444690_m1
Inpp5a	Mm00805812_m1	*Ttbk2 (SCA11)*	Mm00453709_m1

Table 26. Human TaqMan® assays

Gene symbol	Assay Number
ATXN2	Hs00268077_m1
FBXW8	Hs00395480_m1
ATXN1	Hs00165656_m1
TBP	Hs99999910_m1
PARK2	Hs01038318_m1
HPRT1	Hs99999909_m1

2.1.13 Equipment and reagents used for protein isolation, Western Blot and co-immunoprecipitation

Table 27. Material used for protein isolation, Western Blot, and co-immunoprecipitation

Product	Cat. No.	Company / Distributor
Blot Absorbent Filter Paper	1703958	Bio-Rad
ImmunobBlot® PVDF membrane	1620177	Bio-Rad
Super RX medical X-Ray film	Super RX	Fujifilm
Microliter™ syringe Model 710	7638-01	Hamilton
Microtest-Plate 96-well flat bottom	82.1581	Sarstedt
Microtest-Plate 96-well lid	82.1584	Sarstedt
Protran® Nitrocellulose Membranes BA83	10401396	Sigma-Aldrich

Table 28. Reagents used for protein isolation, Western Blot, and co-immunoprecipitation

Product	Cat. No.	Company / Distributor
Acrylamide/Bis-Acrylamide 29:1	161-0124	Bio-Rad
Ammonium persulfate (APS)	9592.2	Carl Roth
Complete Mini, EDTA-free	11836170001	Roche
Developer G153A+B	HT536	AGFA
Igepal® CA-630	I3021	Sigma-Aldrich
N,N,N',N'-Tetramethylethylenediamine (TEMED)	T9281	Sigma-Aldrich
Phenylmethylsulfonyl fluoride (PMSF)	78830	Sigma-Aldrich
Precision Plus Protein™ Standards, all blue	161-0373	Bio-Rad
Precision Plus Protein™ Standards, dual color	161-0374	Bio-Rad
Protein A-Agarose	sc-2001	Santa Cruz
Protein quantification Kit MicroBC Assay	UP75860A	Interchim
Rapid Fixer G354	2828Q	AGFA
RestoreTM Western Blot Stripping Buffer	21059	Thermo Scientific

Product	Cat. No.	Company / Distributor
SDS Pellets	CN30.2	Carl Roth
Sodium deoxycholate	D5670	Sigma-Aldrich
Sucofin milk powder	-	TSI
SuperSignal® West Femto Maximum Sensitivity Substrate	34095	Thermo Scientific
SuperSignal® West Pico Chemiluminescent Substrate	34080	Thermo Scientific

2.1.14 Equipment and reagents used for immunocyto- and immunohistochemistry

Table 29. Instruments used for immunochemistry

Instrument	Company / Distributor
Dekloaking Chamber™ Pro	Biocare Medical
Heated forceps T40/E	SWS
Heating plate Hp100	Guwina
Microscope Eclipse 90i	Nikon
Microscope 090-135-001	Leica
Microscope Axiovert 200M	Carl Zeiss
Microscope BX61	Olympus
Microscope Primo Star	Carl Zeiss
Microtome 21518	Jung
Vibratome VT1000S	Leica

Table 30. Material used for immunochemistry

Product	Cat. No.	Company / Distributor
Feather Microtome Blade S35	0207500000	Pfm medical
Histosette® Tissue Embedding cassettes	H0542	Sigma-Aldrich
Microscope Cover Slides, 24 x 60 mm	BB024060A1	Menzel/Thermo Scientific
Microscope Slides SuperFrost® Plus	J1800AMNZ	Menzel/Thermo Scientific
Paraplast X-tra Tissue Embedding Medium	503002	McCormick
Plastic Pipettes	H109M	Copan
Snap Cap Vials 45 x 22 mm	548-0625	VWR International

Table 31. Reagents used for immunochemistry

Product	Cat. No.	Company / Distributor
VECTOR NovaRED Peroxidase (HRP) Substrate Kit	SK-4800	Vector Laboratories
Bull's Eye Decloaker 20x	BULL1000L2JX	Biocare Medical

Product	Cat. No.	Company / Distributor
DAKO Fluorescent Mounting Medium	S3023	DAKO
DAKO Pen	S2002	DAKO
DL-Lysine	L-6001	Sigma-Aldrich
Formic Acid 98-100%	A3153	Applichem
Hoechst 33342	B2261-25MG	Sigma-Aldrich
Immersion Oil for Microscope Type A	MXA20233	Nikon
Immersion oil Immersol 518 N, 100 ml	000000-1111-807	Carl Zeiss
Shandon™ EZ-Mount™ Mountant	9999120	Thermo Scientific
Xylenes	16446	Sigma-Aldrich

2.1.15 Antibodies

2.1.15.1 Primary antibodies

Table 32. Primary antibodies used for Western Blot, co-immunoprecipitation, and immunohistochemistry

Antibody	Cat. No.	Company / Distributor	Dilution	Pred. Mol. Weight	Antigen Retrieval
1C2	MAB1574	Millipore	IHC 1:800		30' Citrate Buffer + 3' Formic Acid
ATAXIN-1	PA5-17094	Thermo Scientific	WB: 1:500	100 kDa	
ATAXIN-2	611378	BD Biosciences	WB 1:500 IHC 1:50	150 kDa	Decloaker
ATAXIN-2	-	custommade	IP: 50 µl / sample		
CA8	PA3-852	Thermo Scientific	WB: 1:1000	37 kDa	
CALB1	LS-B6725	LSBio	WB: 1:1000	25 kDa	
CALB1	AB1778	Millipore	WB: 1:1000	25 kDa	
FBXW8	HPA038851	Prestige	WB: 1:1000 IHC: 1:20 IP: 5 µl / sample	75 kDa	Decloaker
GRM1	12551	Cell Signaling	WB: 1:500	132 kDa	
HOMER3	OAAB04116	Aviva	WB: 1:500	40 kDa	
INPP5A	MBS716862	MyBioSource	WB: 1:800	48 kDa	
ITPR1	ab5804	Abcam	WB: 1:1000 IHC: 1:800	310 kDa	Decloaker
ITPR1	abs55	Millipore	WB: 1:1000 IP: 10 µl / sample	310 kDa	
NOP10	LS_C154663	LSBio	WB: 1:700	8 kDa	
p62	sc-25575	Santa Cruz	IHC: 1:50		Decloaker
PABPC1	ab21060	Abcam	WB: 1:500	71 kDa	
PARKIN	2132S	Cell Signaling	WB: 1:800	52 kDa	

Antibody	Cat. No.	Company / Distributor	Dilution	Pred. Mol. Weight	Antigen Retrieval
PARKIN	4211S	Cell Signaling	WB: 1:800 IP: 10 µl / sample	52 kDa	
RACK1	610177	BD Biosciences	WB: 1:500	35 kDa	
RPS10	PA5-21390	Thermo Scientific	WB: 1:700	19 kDa	
RPS18	AP17722PU-N	Acris	WB: 1:500	18 kDa	
RPS3	9538	Cell Signaling	WB: 1:500	27 kDa	
RPS6	2217	Cell Signaling	WB 1:1000	29 kDa	
ß-ACTIN	a5441	Sigma	WB 1:10 000	42 kDa	
UBIQUITIN	Z0458	Dako	IHC: 1:100		Decloaker

2.1.15.2 Secondary antibodies

Table 33. Secondary antibodies used for Western Blot and immunohistochemistry

Antibody	Cat. No.	Company / Distributor	Dilution
Anti-Goat IgG HRP (from donkey)	sc-2020	Santa Cruz	1:10 000
Cy-3 conjugated AffiniPure donkey anti-mouse IgG (H+L)	711-225-152	Dianova	1:1000
Cy-2 conjugated AffiniPure donkey anti-rabbit IgG (H+L)	715-165-150	Dianova	1:1000
ECL™ Anti-Mouse IgG HRP (from sheep)	NA931V	GE Healthcare Life Sciences	1:10 000
ECL™ Anti-Rabbit IgG HRP (from donkey)	NA934V	GE Healthcare Life Sciences	1:10 000
IRDye 680 goat anti-mouse	926-32220	LI-COR	1:15 000
IRDye 680 goat anti-rabbit	926-32221	LI-COR	1:15 000
IRDye 800CW donkey anti-goat	926-32214	LI-COR	1:15 000
IRDye 800CW goat anti-mouse	926-32210	LI-COR	1:15 000
IRDye 800CW goat anti-rabbit	926-32211	LI-COR	1:15 000
VECTASTAIN ABC Kit (Rabbit IgG)	PK-4001	Vector Laboratories	1:200
VECTASTAIN Elite ABC Kit (Mouse IgG)	PK-6102	Vector Laboratories	1:200

2.1.16 Buffers and Solutions

2.1.16.1 Perfusion

Buffer / Solution	Ingredients
Phosphate buffer	161.8 mM Na_2HPO_4 x 2 H_2O 37.7 mM NaH_2PO_4 x H_2O pH 7.4
8% PFA	8% PFA

Buffer / Solution	Ingredients
	2 pellets NaOH
4% PFA	50% Phosphate buffer
	50% PFA 8%
Storing solution	10% PBS (10x)
	10% Sucrose
	0.05% NaN_3
	Store at 4 °C

2.1.16.2 Transformation

Buffer / Solution	Ingredients
5x KCM buffer	500 mM KCl
	150 mM CaCl2
	250 mM MgCl2
	Autoclave
LB Medium	1% Peptone
	0.5% Yeast Extract
	1% NaCl
	0.75 mM NaOH
	Autoclave
LB Agar plates	98.5% LB Medium
	1.5% Agar
	Autoclave
	100 µg / ml Ampicillin or 50 µg / ml Kanamycin

2.1.16.3 DNA extraction

Buffer / Solution	Ingredients
Proteinase K buffer	10 mM Tris-HCl
	100 mM NaCl
	10 mM EDTA
	0.5% SDS
	pH 8.0

Buffer / Solution	Ingredients
TE buffer	10 mM Tris-HCl
	1 mM EDTA
	pH 7.5-8.0

2.1.16.4 Genotyping

Buffer / Solution	Ingredients
Pink Juice	2 mM Cresol
	12.5% 10x PE buffer
	2 mM dNTPs
	15% Sucrose

2.1.16.5 Agarose gel electrophoresis

Buffer / Solution	Ingredients
TBE buffer	890 mM Tris
	890 mM Boric acid
	20 mM EDTA

2.1.16.6 Protein isolation

Buffer / Solution	Ingredients
RIPA lysis buffer	50 mM Tris-HCl pH 8.0
	150 mM NaCl
	1 mM EDTA
	1 mM EGTA
	1% Igepal CA-630
	0.5% Sodium deoxycholate
	0.1% SDS
	1 mM PMSF
	1 tablet / 10 ml Complete Mini Protease Inhibitor Cocktail
SDS lysis buffer	68.5 mM Tris-HCl pH 6.8
	2% SDS

Buffer / Solution	Ingredients
	10% Glycerol
	1 tablet / 10 ml Complete Mini Protease Inhibitor Cocktail
NP40 lysis buffer	20 mM Tris-HCl pH 8.0
	137 mM NaCl
	1% Glycerol
	0.1% Igepal CA-630
	2 mM EDTA
	1 tablet / 10 ml Complete Mini Protease Inhibitor Cocktail

2.1.16.7 Co-immunoprecipitation

Buffer / Solution	Ingredients
Blocking buffer	0.2% NaCl
	0.1% Gelatine
	0.05% NaN3
	50 mM Tris
	0.1 % Triton
Lysis buffer	120 mM NaCl
	0.1% Triton X 100
	50 mM Tris-HCl pH 7.5
	1 tablet / 10 ml Complete Mini Protease Inhibitor Cocktail

2.1.16.8 SDS-PAGE

Buffer / Solution	Ingredients
Running gel buffer	1.5 M Tris
	0.4% SDS
	pH 8.8
Stacking gel buffer	0.5 M Tris
	0.4% SDS
	pH 6.8
Running gel	24.2% Running gel buffer
	23.2 – 40.3% Acrylamide/Bis-acrylamide (30%)

Buffer / Solution	Ingredients
	0.36% APS
	0.05% Temed
Stacking gel	24.2% Stacking gel buffer
	14.4% Acrylamide/Bis-acrylamide (30%)
	0.97% APS
	0.12% Temed
Running buffer (10x)	25 mM Tris pH 8.2
	192 mM Glycine
	0.1% SDS
Loading Buffer (2x)	25% Stacking gel buffer
	20% Glycerol
	4% SDS
	5% 2-Mercaptoethanol
	0.05 % Bromophenol blue

2.1.16.9 Western Blot

Buffer / Solution	Ingredients
Transfer buffer (10x)	25 mM Tris
	192 mM Glycine
	10% Methanol
Transfer buffer (1x)	25 mM Tris
	192 mM Glycine
	10% Methanol
PBS (10x)	137 mM NaCl
	2.7 mM KCl
	4.3 mM Na2HPO4
	1.4 mM KH2PO4
	pH 7.4
PBST (1x)	10% PBS (10x)
	0.1% Tween
Blocking buffer	5% Milk powder

Buffer / Solution	Ingredients
	95% PBST (1x)

2.1.16.10 Immunohistochemistry

Buffer / Solution	Ingredients
Tris/HCl pH 7.6	0.605% Tris
	0.9% NaCl
	4.4% 1 M HCl
	pH 7.6
Citrate buffer	100 mM C6H8O7 * H2O (A)
	100 mM Na3C6H5O7 * 2 H2O (B)
	Mix A:B:H2O at the ratio of 18:82:900
	pH 6.0

2.1.17 Software and online databases

Table 34. Software and online databases

Software/ Database	Source
Acrobat Reader	Adobe
Allen brain atlas	http://www.brain-map.org/
ApE 1.13	http://biologylabs.utah.edu/jorgensen/wayned/ape/
Axio Vision	Carl Zeiss
ClustalW	http://www.ebi.ac.uk/Tools/msa/clustalw2/
DNAStar	DNAStar Inc.
Endnote X4	Thomson Reuters
GeneCards	http://www.genecards.org/
GraphPad Prism 4.03	GraphPad Software Inc.
GraphPad Software	http://www.graphpad.com/quickcalcs/)
Image Studio™ Lite 3.1	LI-COR Biosciences
ImageJ	http://rsbweb.nih.gov/ij/
MS Office	Microsoft
NCBI tools	http://www.ncbi.nlm.nih.gov/
NetAffx Analysis Center	http://www.affymetrix.com/analysis/index.affx
Peak Scanner Software 1.0	Life Technologies
Photoshop	Adobe

Software/ Database	Source
PictureFrame Application 2.3	Optronics
Primer3	http://frodo.wi.mit.edu/primer3/
NIS-Elements Imaging Software 4.20.00	Nikon
Spidey	http://www.ncbi.nlm.nih.gov/spidey/
Step One Software 2.1	Life Technologies
StepOnePlus Software	Applied Biosystems
Versadat Version 1.90	Accuscan Instruments

2.2 Methods

2.2.1 Mouse models

2.2.1.1 Generation of *Atxn2*-CAG42-KIN / hTDP43-A315T-KIN double mutants

The generation of *Atxn2*-CAG42-KIN and hTDP43-A315T-KIN mice has already been described (Damrath et al., 2012; Stribl et al., 2014). For the double mutants homozygous *Atxn2*-CAG42-KIN mice were bred with heterozygous hTDP43-A315T-KIN mice to receive *Atxn2*$^{CAG42/CAG42}$ / hTDP43$^{+/A315T}$ (HOM/HET) and *Atxn2*$^{CAG42/CAG42}$ / hTDP43$^{+/+}$ (HOM/WT) mice. Furthermore, WT mice of the *Atxn2*-CAG42-KIN strain and heterozygous hTDP43-A315T-KIN mice were bred together to obtain *Atxn2*$^{+/+}$ / hTDP43$^{+/+}$ (WT/WT) and *Atxn2*$^{+/+}$ / hTDP43$^{+/A315T}$ (WT/HET) mice. Thus, WT, single mutants of both strains, and double mutants were generated with only two different breeding pairs. Since both, Atxn2 and TDP43 single mutants, had already been crossed back to C57BL/6 background (BL6/J and BL/6N, respectively), double mutants were not backcrossed further.

2.2.1.2 Generation of *Atxn2*-CAG100-KIN mice

The generation of the *Atxn2*-CAG100-KIN mouse line was outsourced to Genoway (Lyon, France) and was performed similarly to the generation of *Atxn2*-CAG42-KIN mice (Damrath et al., 2012).

2.2.1.2.1 Vector construct

The pKO-Sca2 vector previously used for the generation of *Atxn2*-KO mice (Lastres-Becker et al., 2008a) was applied. In this vector the Atxn2 exon 1 is flanked by a distal LoxP site and a FRT-Neo-FRT-LoxP selection cassette (Figure 10 A). The original vector was modified by insertion of 100 CAG repeats into exon 1 at amino acid position Q156 (Geneart, Regensburg). Furthermore, one nucleotide 42 bp upstream the CAG repeat was changed from G to A to produce an additional SphI restriction site for Southern Blot validation. The already inserted FRT-flanked neomycin gene is a positive selection and the Diphtheria Toxin A (DTA) at the 3' end a negative selection marker. The LoxP sites were originally introduced for excision of exon 1 and therefore had no relevance for the generation of *Atxn2*-CAG100-KIN mouse. The new vector was named NOW1-HR (Figure 10 B).

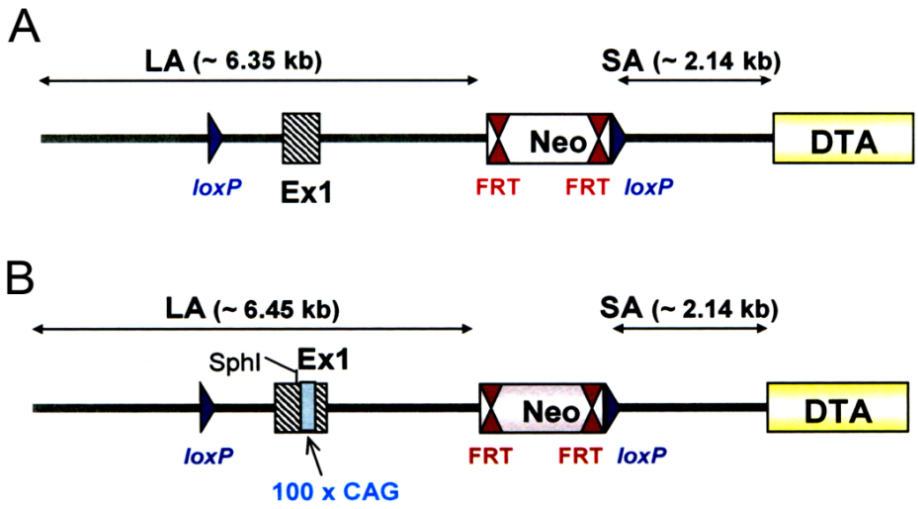

Figure 10. Structure of the original pKO-Sca2 and the modified NOW1-HR vector. The original pKO-Sca2 vector (A) was used for generation of *Atxn2*-KO mice and therefore harbors loxP sites (blue triangles) for excision of exon1 (hatched rectangle). (B) The modified NOW1-HR vector had an elongated CAG repeat (light blue rectangle) and a newly introduced SphI restriction site. The FRT-flanked neomycin cassette (double red triangles) was used for positive selection and the Diphtheria Toxin A (DTA) for negative selection. The long arm (LA) and short arm (SA) of homology are indicated (Genoway).

2.2.1.2.2 ES cell electroporation and verification of homologous recombination

The modified NOW1-HR vector was linearized by digestion with the restriction enzyme KpnI and the resulting fragment was isolated. The linearized NOW1-HR targeting construct was then inserted into 129Sv ES cells by electroporation. Positive selection was started 48 h after electroporation using G418. The selection identified 1016 ES cell clones. Subsequently, the correct homologous recombination of the target construct at the 3' end as well as of the CAG repeat were examined via two different PCRs (Figure 11).

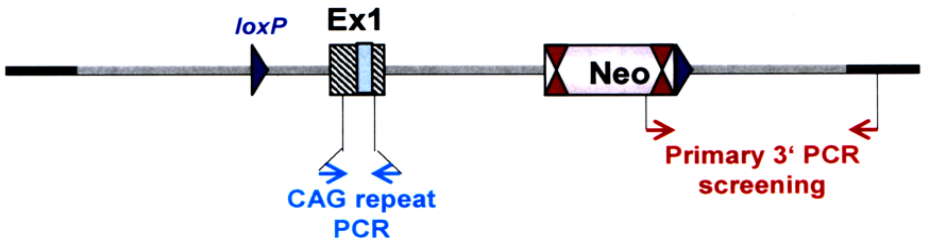

Figure 11. Confirmation of correctly recombined Sca2 locus by PCR. For confirmation of correct recombination events PCR screening was applied. 3’ (red) and CAG repeat (blue) PCR screening confirmed correct insertion of the target construct and CAG repeat, respectively (Genoway).

A PCR over the 3’ short arm of homology detected the expected integration in 48 clones. The CAG repeat PCR was used to check for the integration of the complete CAG repeat.

In a next step, the homologous recombination event was verified by Southern Blot analysis at the 3’ and 5’ end. This screening was based on SpeI or SphI digestion as well as hybridization using a SA-I-B or LA-E-A probe, respectively. The 3’ SA-I-B probe showed correct recombination events (10 059 bp for the WT and 7192 bp for the recombined allele) for most of the ES cell clones (Figure 12 A). In contrast to that, the 5’ LA-E-A probe detected the expected WT and recombined hybridization signals at 6198 bp and 4811 bp in only six of the 39 analyzed ES cell clones (Figure 12 B). The six clones that were found to be correctly recombined at the 5’ end were also among the ones confirmed at the 3’ end. A randomly inserted copy of the targeting construct was not detected by the two Southern Blot approaches.

Subsequently, the neomycin cassette was removed using FLP-mediated excision. The excision was verified using PCR and Southern Blot. For the PCR a primer pair flanking the FRT-Neo-FRT-loxP sequence was used resulting in a 2944 bp fragment for alleles with neomycin cassette and 948 bp for neomycin-excised alleles (Figure 13 A). Southern Blot validation was again performed using SpeI digestion and the SA-I-B probe. For the Flp-mediated excision the expected fragment size was 5576 bp (Figure 13 B).

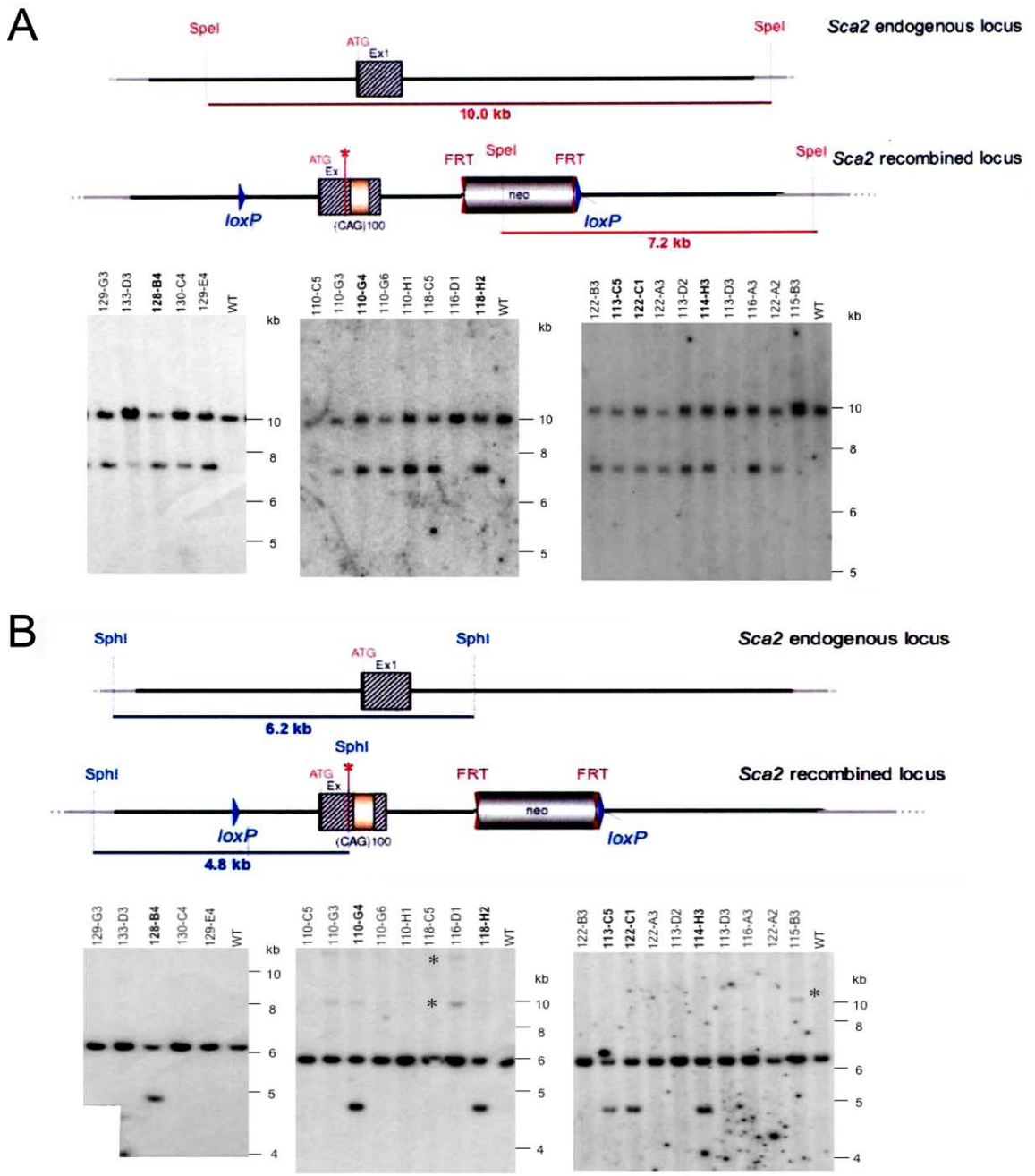

Figure 12. Confirmation of correct recombination events via Southern Blot. Correct recombination was also analyzed via Southern Blot at the 3' (A) and 5' (B) ends. For the 3' Southern Blot, digestion using SpeI and hybridization with the SA-I-B probe was performed confirming correct recombination events for most ES clones. Southern Blot analysis of the 5' end was conducted via digestion with SphI and hybridization with the LA-E-A probe resulting in six correctly recombined ES clones (Genoway).

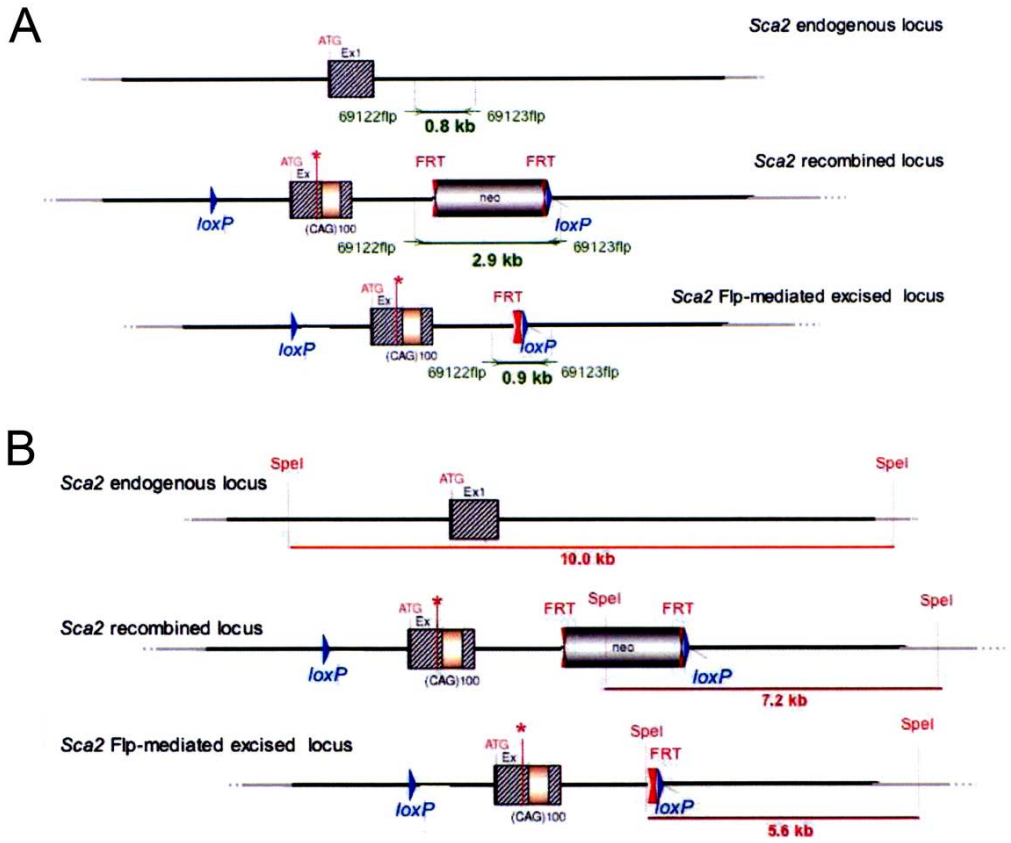

Figure 13. Confirmation of neomycin cassette removal. The excision of the neomycin cassette was confirmed via PCR screening (A) and Southern Blot analysis (B). For PCR screening primers flanking the FRT-Neo-FRT cassette were applied. For Southern Blot analysis, again SpeI digestion and SA-I-B hybridization were conducted. Both approaches resulted in a smaller fragment for the Neo-excised locus.

2.2.1.2.3 Blastocyst injection and further breeding

One of the validated clones (#128-B4) was used for sequencing analysis showing the correct length of 100 CAG with only one point mutation at position 71 leading to a proline instead of a glutamine. However, this ES cell clone was used for blastocyst injection into a C57BL/6J mouse. The male chimeric offspring thereof was bred with female C57BL/6J mice and germ line transmission was controlled. As the color marker of 129Sv is dominant over the black coat of C57BL/6J mice, the color of the offspring provides information whether the ES cells have contributed to the germ cells or not. The selected mice were again validated by PCR and shipped to the animal facility (ZFE) in Frankfurt am Main as founder breeders. Animals used for behavioral, molecular and immunohistochemical studies were crossed back four times in C57BL/6J.

2.2.1.3 Animal housing and breeding

All animals were either housed at the Central Animal Facility (ZFE) of the Goethe University Medical School, Frankfurt am Main or at mfd Diagnostics GmbH in Wendelsheim, Germany, both FELASA-certified facilities. They were kept in individually

ventilated cages at a 12-h-light / 12-h-dark cycle under routine health monitoring and fed *ad libitum.* The cages were supplemented with bedding and paper chipping and were cleaned weekly. Breeding either took place in homozygous (for *Atxn2*-CAG100-KIN mice) or heterozygous matings (for all other mouse lines). Apart from the *Atxn2*-CAG100-KIN mice and the double mutants, all mouse lines were backcrossed into C57Bl/6 for more than eight generations. All procedures were in accordance with the German Animal Welfare Act, the Council Directive of 24th November 1986 (86/609/EWG) with Annex II and the ETS123 (European Convention for the Protection of Vertebrate Animals).

2.2.2 Phenotype analyses

Behavioral analyses were always conducted in a separated, ventilated room at the same daytime to avoid variances caused by circadian clock. If not otherwise stated, male as well as female animals were used for phenotype studies without separation.

2.2.2.1 Body and brain weight

Mice were weighed with a digital kitchen balance. Brain weight was measured after dissection and after removal of the olfactory bulbus an analytical balance. In contrast to all other measurements, male and female animals were separated for weight analyses due to strong gender-specific weight differences.

2.2.2.2 Survival curve

To analyze the survival rate of animals, a fixed group of mice was assessed regarding their life and death over a period of 20 weeks (starting at birth). Sudden death of animals was noted together with the age at death.

2.2.2.3 Rotarod

For behavioral analysis of the motor performance an accelerating rotarod was used. The performance was measured within a period of 6 min while the rod was accelerating from 4 to 44 rpm. Every mouse had four consecutive trials interrupted by at least 10 min of break. The latency to fall was recorded for each trial; the mean value of the four trails was calculated and used for statistical analysis.

2.2.2.4 Open field

For recording of spontaneous motor activity a Versamax animal activity monitor and the Versadat software were used. The Versamax consists of a 20 x 20 cm area in a plexiglass box with infrared beams at each side. Every movement, horizontal or vertical, was counted and analyzed by the software through the beam breaks the animal causes during a 5 min trial. The following parameters were measured: horizontal activity, total distance, number of movements (horizontal), movement time, rest time, vertical activity, number of vertical movements, vertical time, stereotype counts, number of stereotypes, stereotype time, clockwise revolutions, anti-clockwise revolutions, margin distance, margin time, center distance, center time, left-front time, right-front time, left-rear time, and right-rear time.

2.2.2.5 Clasping

For the clasping test mice were suspended by their tails for about 1 min. The performance of the mice was videotaped and fixed images thereof were used to compare WT and mutant mice.

2.2.2.6 Balance beam

The balance beam normally assesses the ability of animals to walk along a narrow beam. Here, it was used to compare walking behavior and position of WT and mutant mice on a beam via videotaping. The beam had a length of ~1 m and a diameter of 18 mm.

2.2.3 Perfusion, dissection, and preparation

If the tissue was designated for immunohistochemical staining, mice were perfused to avoid unspecific background signal due to hemoglobin and to pre-fix the tissue. Therefore, mice were anesthetized with an overdose of the narcotic Narcoren via intraperitoneal injection (~10 µl per gram body weight). The chest was opened and the ventral aorta was branched off. Then, 0.1 µl Heparin were directly injected into the left ventricle to avoid blood coagulation. Subsequently, 4% PFA solution was injected similarly and immediately after the right atrium was opened to enable the efflux of the blood and PFA. Thus, the PFA can flush the blood circuit of the upper body, thereby fixing the tissue. To assure a constant flux of the PFA a peristaltic pump was used. After the perfusion, mice were decapitated; brain and spinal cord were removed and postfixed in 4% PFA at 4 °C overnight. Subsequently, tissues were stored in 10% sucrose solution with 0.25% NaF for

at least 24 h. For paraffin embedding, the fixed tissue had to be dehydrated. Therefore, it was washed three times with demineralized water to remove the sucrose and consecutively stored in 70%, 96%, and 100% ethanol as well as 100% xylenes for 24 h each. Afterwards, it was incubated in paraplast for 24 h at 56 °C und subsequently embedded in paraplast in sagittal direction for brains and vertical direction for spinal cords. All tissues were cut into 7-µm-thick slices using a microtome, mounted onto object slides in a 45 °C-warm water bath, and dried at room temperature (RT). To remove the paraffin, slices were incubated at 60 °C in a drying oven and subsequently kept at RT until further use.

For all other applications (e.g. RNA and protein isolation), animals were not perfused but sacrificed by cervical dislocation. The respective tissues were removed in minimal time, frozen immediately in liquid nitrogen, and stored at -80 °C.

2.2.4 Genotype analyses

Tail biopsies were taken at ten days of age as well as during the dissection step for verification of the genotype. Tails were incubated in 500 µl Proteinase K buffer containing 25 µl Proteinase K for more than 3 hours at 55 °C and 800 rpm. Then, 250 µl of 6 M NaCl were added and the samples were mixed vigorously for 1 - 2 min by hand following incubation on ice for 10 min. After a centrifugation step of 10 min at 2300 xg and RT, 500 µl of the supernatant were transferred into a new tube and 1 ml of 100% ethanol was added for precipitation. The samples were gently mixed several times and centrifuged for 10 min at 16 000 xg. Subsequently, the ethanol was removed and the pellet was washed once with 500 µl of 70% ethanol followed by another centrifugation step at 16 000 xg for 5 min. Again, the ethanol was removed, this time thoroughly and the dry pellet was dissolved in 100 µl TE buffer either at 4 °C overnight or at 50 °C for 10 min. DNA samples were kept at -20 °C until further use.

2.2.4.1 *Atxn2*-CAG42- and *Atxn2*-CAG100- KIN mice PCR

For *Atxn2*-CAG42- and *Atxn2*-CAG100-KIN mice the same protocol was applied using Atxn2-KIN_Fwd and Atxn2-KIN_Rev primers. The reaction mix and conditions are listed in Table 35. Fwd and Rev primers flank the Neo-excised *Atxn2* locus that still contains a FRT and a loxP site in the KIN and is therefore 155 bp longer than the same sequence in the *Atxn2* WT locus. The predicted lengths for the WT and KIN allele are 793 bp and 984 bp, respectively.

Table 35. Reaction mix and PCR conditions for Atxn2-KIN genotyping

Reaction Mix		**Conditions**			
DNA	~ 50 ng	**Step**	**Temperature**	**Time**	**Cycles**
10x LA PCR Buffer	2.5 µl	Initial denaturation	94 °C	3'	1x
dNTPs (2.5 mM each)	4 µl	Denaturation	94 °C	15"	
Primers	5 pmol each	Annealing	68 °C	3'	30x
LA Taq Polymerase (5 U/µl)	0.25 µl	Elongation	68 °C	1'	
Reaction volume	25 µl	Final elongation	68 °C	9'	1x

2.2.4.2 *Atxn2*-KO mice PCR

The PCR for the *Atxn2*-KO mice was conducted using Atxn2-KO_Fwd and Atxn2-KO_Rev1 or Atxn2-KO_Rev2 for the WT or KO allele, respectively, in one reaction. Volumes and conditions are listed in Table 36. Forward and reverse primers for the WT are located before exon 1 while the reverse primer for the KO is located behind exon 1. The predicted size for the WT allele is 443 bp and for the KO allele 239 bp.

Table 36. Reaction mix and PCR conditions for Atxn2-KO genotyping

Reaction Mix		**Conditions**			
DNA	~ 50 ng	**Step**	**Temperature**	**Time**	**Cycles**
Pink Juice	16 µl	Initial denaturation	95 °C	3'	1x
Primers	5 pmol each	Denaturation	94 °C	30"	
AmpliTaq® Polymerase (5 U/µl)	0.1 µl	Annealing	57 °C	30"	35x
Reaction volume	20 µl	Elongation	72 °C	50"	
		Final elongation	72 °C	7'	1x

2.2.4.3 hTDP43-A315T-KIN mice PCR

For the genotyping of hTDP43-A315T-KIN mice a human-specific primer pair was used: TDP43-KIN_Fwd and TDP43-KIN_Rev. Primers flank the A315T exchange position in human TDP43 and result in a KIN allele band of 312 bp and no band for the WT or the mouse TDP43 allele when applying the conditions listed in Table 37.

Table 37. Reaction mix and PCR conditions for hTDP43-A315T-KIN genotyping

Reaction Mix		**Conditions**			
DNA	~ 50 ng	**Step**	**Temperature**	**Time**	**Cycles**
Primers	5 pmol each	Initial Denaturation	94 °C	5'	1x
5 Prime Master Mix	10 µl	Denaturation	94 °C	30''	
Reaction volume	25 µl	Annealing	60 °C	30''	35x
		Elongation	72 °C	1'	
		Final Elongation	72 °C	10'	1x

2.2.4.4 *Atxn1*-Q154-KIN mice PCR

The primers Atxn1-Q154_Fwd and Atxn1-Q154_Rev were applied. Further components of the reaction as well as PCR conditions are given in Table 38. Primers flank the CAG repeat producing a PCR fragment of 238 bp for the WT allele and 694 bp for the KIN allele.

Table 38. Reaction mix and PCR conditions for Atxn1-Q154-KIN genotyping

Reaction Mix		**Conditions**			
DNA	~ 50 ng	**Step**	**Temperature**	**Time**	**Cycles**
Pink Juice	17 µl	Initial Denaturation	95 °C	3'	1x
Primers	5 pmol each	Denaturation	95 °C	30''	
AmpliTaq® Polymerase (5 U/µl)	0.75 µl	Annealing	60 °C	30''	35x
Reaction volume	20 µl	Elongation	72 °C	1'	
		Final Elongation	72 °C	7'	1x

2.2.4.5 *Tia1*-KO PCR

For *Tia1*-KO mice two different primer pairs and PCR conditions were applied, one for WT and one for KO animals. For the WT PCR the primer pair Tia1_WT_Fwd and Tia1_WT_Rev was used and the conditions listed in

Table 39 were applied. The KO PCR was conducted with Tia1_KO_Fwd and Tia1_KO_Rev primers under the conditions depicted in Table 40. Both primer pairs bind around the excised exon 4. The WT PCR resulted in a product with a length of 953 bp, the KO PCR in a product with 400 bp.

Table 39. Reaction mix and PCR conditions for Tia1 WT genotyping

Reaction Mix		**Conditions**			
DNA	~ 50 ng	**Step**	**Temperature**	**Time**	**Cycles**
Pink Juice	17 µl	Initial Denaturation	94 °C	2'	1x
Primers	5 pmol each	Denaturation	94 °C	15''	
AmpliTaq® Polymerase (5 U/µl)	0.25 µl	Annealing	62 °C	30''	33x
Reaction volume	20 µl	Elongation	72 °C	2'	
		Final Elongation	72 °C	10'	1x

Table 40. Reaction mix and PCR conditions for Tia1 KO genotyping

Reaction Mix		**Conditions**			
DNA	~ 50 ng	**Step**	**Temperature**	**Time**	**Cycles**
Pink Juice	17 µl	Initial Denaturation	94 °C	2'	1x
Primers	5 pmol each	Denaturation	94 °C	15''	
AmpliTaq® Polymerase (5 U/µl)	0.25 µl	Annealing	58 °C	30''	33x
Reaction volume	20 µl	Elongation	72 °C	1'	
		Final Elongation	72 °C	10'	1x

2.2.5 Cell culture

2.2.5.1 Cell culture media

All cell lines were cultured under standard conditions (95% air, 5% CO_2, 37 °C) using the following growth media:

HeLa
MEM
10% FBS Gold
10 mM Hepes
1% NEAA

Primary skin fibroblasts:
DMEM (4.5 g/l glucose)
10% FBS Gold
2 mM L-glutamine
100 U/ml penicillin G
100 µg/ml streptomycin

Cells were stored in a freezing medium containing 80% FBS Gold and 20% DMSO in liquid nitrogen when not in use. For culturing, they were thawed in 10 ml pre-warmed medium, centrifuged for 4 min at 200 xg and re-suspended in 3 ml fresh medium. Subsequently, cells were seeded in 25 mm^2 flasks coated with FBS Gold 30 min before seeding and incubated under standard conditions.

2.2.5.2 Transfection

Cells were always seeded 16 h prior to transfection using 200 000 cells per 6-well and 1.5 million cells per 10-cm-dish. Transfection was conducted with Effectene Transfection Reagent Kit using 1 µg plasmid DNA for the 6-wells and 5 µg for the 10-cm dishes diluted in 100 µl and 500 µl of EC buffer, respectively. Samples were vortexed and shortly centrifuged. Subsequently, 3.2 µl or 16 µl Enhancer were added, samples were incubated for 4 min and 2.5 µl or 12.5 µl of Effectene were added. After another incubation step of 8 min, 800 µl cell culture media from the dish were added and the mixture was dripped gently into the dish. Cells were then incubated under standard conditions for 48 h before they were harvested for RNA or protein isolation.

2.2.6 DNA techniques

2.2.6.1 PCR for CAG repeat amplification

For amplification of the CAG repeat the primers Sca2Ex1_Fwd5 and Sca2Ex1_Rev2 were used. Reaction mix and PCR conditions are listed in Table 41. Alleles with ~100 CAG have a predicted length of 400 bp, WT alleles have 94 bp.

Table 41. Reaction mix and PCR conditions for CAG repeat amplification

Reaction Mix		**Conditions**			
Primer	5 pmol each	**Step**	**Temperature**	**Time**	**Cycles**
10x LA PCR Buffer II	2.5 µl	Initial Denaturation	98 °C	3’	1x
dNTPs	2.5 mM each	Denaturation	98 °C	40’’	39x
BSA (100x)	0.25 µl	Annealing	60 °C	40’’	
LA Taq Polymerase (5 U / µl)	0.25 µl	Elongation	72 °C	1’	
Reaction volume	25 µl	Final Elongation	72 °C	7’	1x

2.2.6.2 cDNA synthesis

Before cDNA synthesis was performed using 1 µg RNA, the remaining DNA was digested by incubation with DNase I Amplification Grade for 15 min at RT. DNase I was inactivated by adding 1 µl of 25 mM EDTA and incubation for 10 min at 65 °C. Subsequently, the RNA was incubated with 1 µl of oligo(dT) primer (250 ng/µl), 1 µl random primer (200 ng/µl) and 1 µl of dNTPs (10 mM) for 5 min at 65 °C for annealing. After 1 min of incubation on ice and short centrifugation 4 µl 5x First strand buffer, 1 µl 0.1 M DTT and 1 µl SuperScript III Reverse Transcriptase (200 U/µl) were carefully added and the samples were incubated first for 5 min at 25 °C, then for 1 h at 50 °C and finally for 15 min at 70 °C.

2.2.6.3 Quantitative real-time reverse transcriptase PCR (RT-qPCR)

Expression levels were measured in 96-well plates with the StepOnePlus Real-Time PCR System using 25 ng of cDNA, 10 µl of FastStart Universal Probe Master (Rox) Mix, and 1 µl of one of the respective TaqMan® Assays for each reaction in a volume of 20 µl. The PCR conditions were 50 °C for 2 min, 95 °C for 10 min followed by 40 cycles of 15 s at 95 °C and 60 s at 60 °C. Analysis of the gene expression data was conducted according to the $2^{-\Delta\Delta Ct}$ method (Livak and Schmittgen, 2001). Mean Ct (cycle threshold) values from the two housekeeping genes *Tbp* and *Hprt1* used in all mouse tissue were averaged to avoid false positive results in one of them. Then, Ct values from the respective transcript were normalized to *Tbp+Hprt* and to the average of the WT values.

2.2.6.4 SYBR® Green Assay

For transcript level determination of overexpressed FBXW8 in HeLa cells, SYBR® Green assay was used since the plasmid codon had been optimized and TaqMan® probes could not be applied. The same qPCR system as for TaqMan® assays was used with 25 ng of cDNA, 1 µl of each, Fbxw8_fwd and Fbxw8_rev primer, and 10 µl SYBR® Green Master Mix in a volume of 20 µl. PCR conditions and analysis of gene expression data are described in passage 2.2.6.3.

2.2.6.5 Transformation

Transformations were performed under sterile conditions using a Bunsen burner.

2.2.6.5.1 Transformation of standard plasmids

For transformation of standard plasmids 20 µl 5x KCM buffer, 80 µl H_2O, and 10 - 50 ng plasmid DNA were mixed and added to 50 µl of competent *E. coli* DH5α bacteria. The bacteria were then incubated for 20 min on ice and subsequently for 10 min at RT. After adding 1 ml LB medium, the mixture was incubated for 50 min at 37 °C and 300 rpm. Between 50 and 100 µl of the solution were plated on LB agar plates containing the respective antibiotic(s) and incubated at 37 °C overnight.

2.2.6.5.2 Transformation of plasmids with CAG repeats

For plasmids containing CAG repeats a special bacteria type and different incubation conditions were used to ensure the replication of the complete CG-rich repeat. LB medium was pre-warmed in a water bath at 42 °C and 50 µl of competent SURE cells were mixed with 1.7 ml 2-Mercaptoethanol. During a 10-min-incubation of the bacteria on ice they were gently swirled every two minutes. After adding 10 - 50 ng of plasmid DNA and incubation for 30 min on ice, the bacteria were heat-pulsed for 45 s at 45 °C in a water bath. Immediately after, the bacteria were placed on ice for 2 min. Then, 900 µl of LB medium were added and incubated for 60 min at 37 °C and 300 rpm. Between 25 and 100 µl of the solution were plated on agar plates containing the respective antibiotic and incubated at 30 °C overnight.

2.2.6.6 Bacterial cultures

To grow bacteria, 2 ml (Mini-preparation) or 25 ml (Midi-preparation) of LB-Medium containing the respective antibiotic were inoculated with a single colony from the LB agar plate and grown at 30 °C (SURE cells) or 37 °C (DH5α) overnight with gentle shaking.

2.2.6.7 Glycerol stocks

For long-term storage of transformed bacteria, 800 µl of the bacterial culture were mixed with 400 µl of glycerol. The mixture was frozen immediately in dry ice with ethanol and stored at -80 °C until further use. For inoculation of a new culture a small piece of the frozen stock was scratched with a pipette tip. Glycerol stocks were never thawed.

2.2.6.8 Plasmid extraction

Bacterial cultures were centrifuged for 10 min at 4000 xg and the supernatant was discarded.

2.2.6.8.1 Mini preparation

For the small volume plasmid extraction the GenElute HP Plasmid Midiprep Kit was used. The bacteria pellet was re-suspended in 200 µl of re-suspension buffer and subsequently 200 µl of lysis buffer were added. Samples were inverted several times and incubated for 5 min at RT. Then, 200 µl of neutralization buffer were added and the samples were again gently inverted. After 5 min of incubation on ice and inversion of the tubes a centrifugation step of 10 min at 16 000 xg followed. Subsequently, 500 µl of the supernatant were transferred into a fresh tube and 1 ml of 100% ethanol was added. Then, the samples were mixed and centrifuged for 10 min at 16 000 xg. The supernatant was discarded and the pellet was washed with 700 µl of 70% ethanol. Another centrifugation step of 2 min at 16 000 xg was conducted, the supernatant was discarded and the pellet was dried. Afterwards, it was dissolved in 25 µl of H_2O and kept at -20 °C until further use.

2.2.6.8.2 Midi preparation

To isolate larger amounts of plasmid DNA the Jetstar Plasmid Purification MIDI kit was used. Columns were equilibrated with 10 ml E4 buffer while the pellet was re-suspended in 4 ml E1 buffer. Then, 4 ml E2 buffer were added and the solution was incubated for 5 min at RT. After adding 4 ml of E3 buffer, the mixture was immediately inverted until the liquid was homogeneous. This solution was then centrifuged for 10 min at 1200 xg and the supernatant was transferred into the column. The column was washed twice with 10 ml of E5 buffer and eluted with 5 ml E6 buffer. After precipitation by adding 3.5 ml isopropanol the samples were centrifuged for 30 min at 12 000 xg and 4 °C. Subsequently, the supernatant was discarded; the pellet was washed once with 70% ethanol and centrifuged for 10 min at 12 000 xg. Again, the supernatant was discarded and the pellet was dried, dissolved in 60 µl H_2O, and stored at -20 °C until further use.

2.2.6.9 Quantification of DNA

DNA was quantified using a spectrophotometer to measure the OD at 260 nm. For quality control the OD_{260}/OD_{280} and OD_{260}/OD_{230} ratios were used.

2.2.6.10 Restriction

For validation of the inserted plasmid ~600 ng of plasmid DNA were digested with the appropriate restriction enzyme (see Table 15). Therefore, the plasmid DNA, as well as 1 µl of the respective buffer, 1 µl of the restriction enzyme, and H_2O to a final volume of 20 µl were incubated at 37 °C for 1 h. The fragments were separated in a 1.5% agarose gel using gel electrophoresis and visualized with ethidium bromide.

2.2.7 RNA techniques

2.2.7.1 RNA extraction from mouse tissue

For RNA extraction with Trizol® Reagent, half of a cerebellum (~25 mg) or a similar amount of cortex was used. The tissue was homogenized in 1 ml of Trizol® with a motor pestle and incubated for 5 min at RT. After adding 200 µl of chloroform and shaking for 15 s the samples were again incubated at RT for 2 - 3 min. Subsequently, the samples were centrifuged at 12 000 xg and 4 °C for 15 min and 500 µl of the aqueous phase were transferred into a new tube. For precipitation, 500 µl of isopropanol were added, the samples were gently mixed, incubated at RT for 10 min and centrifuged at 12 000 xg and 4 °C for 10 min. The supernatant was discarded and 1 ml of 70% ethanol was added to wash the pellet. After a final centrifugation step at 7500 xg and 4 °C for 5 min the ethanol was removed thoroughly. The pellet was dried and then dissolved in 30 µl of RNase-free water by incubation at 55 °C for 10 min. RNA samples were stored at -80 °C until further use.

2.2.7.2 RNA extraction from cells

RNA from cells was extracted using the QIAshredder™ and RNeasy® Mini Kits. Cells were harvested from the dish in 300 µl RLT buffer, transferred into the QIAshredder™ column and centrifuged for 2 min at 9300 xg. Then, 300 µl of 70% ethanol were added to the flow-through, the solution was mixed until homogeneous and transferred into the RNeasy Mini Kit column. After centrifugation for 1 min at 9300 xg, the flow-through was discarded and 700 µl RW1 buffer were added. Again, samples were centrifuged for 1 min at 9300 xg, the flow-through was discarded and 500 µl RPE buffer were added. This step was repeated, the collection tube was replaced and the samples were spun again for 1 min at 9300 xg. The RNeasy column was set onto a 1.5-ml-tube and the RNA was eluted with 30 µl of RNase-free water by centrifugation for 1 min at 9300 xg. The extracted RNA was stored at -80 °C until further use.

2.2.7.3 Quantification of RNA

Extracted RNA was quantified using a spectrophotometer to measure the OD at 260 nm. For quality control the OD_{260}/OD_{280} and OD_{260}/OD_{230} ratios were used.

2.2.8 Protein techniques

2.2.8.1 Protein isolation

2.2.8.1.1 Protein isolation for Western Blot

Protein isolation from cells and murine tissue for Western Blot was performed similarly using RIPA and SDS buffer. Cells from a 10-cm-dish (> 1 million) were lysed 48 h after transfection in 150 µl of RIPA buffer while 25 mg of cerebellar tissue were homogenized in 250 µl of RIPA buffer using a motor pestle. All samples were incubated for 15 min on ice and subsequently centrifuged for 20 min at 4 °C and 16 000 xg. The supernatant (RIPA fraction) was transferred into a new tube and the pellet was dissolved in ½ vol. 4% SDS buffer by sonification. Then, samples were centrifuged for 10 min at 9300 xg and RT and the supernatant was transferred into a new tube (SDS fraction). After quantification, the lysates were stored at -20 °C until further use.

2.2.8.1.2 Protein isolation for co-immunoprecipitation

For Co-IPs with cells and murine tissue, protein isolation was conducted similarly. Cells were lysed 48 h after transfection in 300 µl NP40 lysis buffer per 10-cm-dish. Cerebellar tissue (25 mg) was homogenized with a motor pestle in 250 µl of NP40 lysis buffer. Both sample types were then incubated on ice for 15 min and centrifuged for 20 min at 16 000 xg and 4 °C. The supernatant was transferred into a new tube while the pellet was not processed any further. Protein lysates were quantified and subsequently stored at -20 °C until further use.

2.2.8.2 Protein quantification

Proteins were quantified in a 96-well plate using a Tecan Microplate Reader and the MicroBC Assay Protein Quantification Kit. For the standard curve duplicates of 0, 0.5, 1, 1.5, 2, 3, 4, 5, 6, and 7 µl BSA each with 150 µl of 0.9% NaCl and 150 µl of the BCA reaction mix (A:B:C = 25:24:1) were utilized. The quantification of the protein lysates was performed using 2 µl for cell lysates and 1 µl for tissue lysates supplemented with the same amounts of 0.9% NaCl and BCA reaction mix. To be able to normalize the quantified proteins, the respective buffers were also measured. Therefore, the same amounts of buffers as for the lysates were used and handled similarly. The plate was subsequently incubated for 45 min at 37 °C and the absorbance was measured at 560 nm using the Microplate Reader. The standard curve was calculated with MS Excel and the protein amount of the samples was determined referring to it.

2.2.8.3 SDS-PAGE

Proteins were separated according to their molecular weight using SDS-PAGE (sodium dodecyl sulfate polyacrylamide gel electrophoresis). Therefore, 20 µg of proteins were supplemented with 2x loading buffer and boiled for 5 min at 95 °C to denature proteins and break up protein complexes. Then, samples were loaded onto the gel that consists of two components: a stacking gel and a running gel. The amount of acrylamide/bis-acrylamide in the running gel was depending on the protein size and the favored separation. Electrophoresis was conducted at 100 V for 20 min and subsequently at 150 V for 50 min.

2.2.8.4 Western Blot

For protein detection, the separated proteins were transferred onto a PVDF or Nitrocellulose membrane. Therefore, a wet blot system was applied. PVDF membranes were activated in 100% methanol for 3 min and equilibrated in transfer buffer for 1 min before use. Nitrocellulose membranes must not be activated in methanol but were equilibrated similarly. The gel and the membrane accompanied by a Whatman paper on each side were placed into the blot system and the blot was run at 50 V for 90 min. Membranes were blocked after transfer in 5% skim milk powder in PBST for 1 h on a shaker.

2.2.8.5 Detection of proteins

Membranes were incubated overnight with the first antibodies diluted in PBST according to Table 32. The next day, membranes were washed with PBST twice and incubated with the secondary antibody for 1 h (in lightproof falcons in case fluorescent antibodies were applied). Proteins were detected using the LI-COR Odyssey system with fluorescent secondary antibodies or the ECL (enhanced chemiluminescence) system with HRP-coupled (horse radish peroxidase) secondary antibodies. For LI-COR detection, the membranes were washed twice after incubation with the secondary antibody and then scanned with the LI-COR infrared imaging system. For ECL detection, blots were incubated for 5 min with 2 ml of each Signal West Pico Lumino/Enhancer Solution and Super Signal West Pico Stable Peroxidase Solution. Then, they were washed twice in PBST and exposed for an appropriate time to X-ray films. The films were then developed in a Curix60 table top processor. Quantification was performed via densitometric analysis with Image J software in both cases.

2.2.8.6 Co-immunoprecipitation

Protein A-agarose beads (20 µl) were pre-washed with 1 ml of Co-IP lysis buffer for 5 min on a rotating wheel. Then, the beads were centrifuged for 1 min at 2300 xg and the supernatant was discarded. This washing step was repeated before beads were incubated with 1 ml of blocking buffer for 1 h at RT. Meanwhile, to decrease unspecific binding of the protein of interest to the beads, 200 - 300 µg of protein extract were pre-incubated with the antibody of interest for 1 h at 4 °C on a rotating wheel. After centrifugation of the beads for 1 min at 2300 xg and removal of the supernatant, the protein-antibody mixture was added to the beads and the samples were incubated overnight at 4 °C on a rotating wheel. The next day, samples were centrifuged for 1 min at 2300 xg and the supernatant was discarded. To eliminate unspecific-bound proteins from the beads, they were washed three times with 1 ml of Co-IP lysis buffer while rotating for 5 min at 4 °C and centrifugation for 1 min at 2300 xg followed by complete removal of the supernatant. After the last washing step, 20 µl of H_2O as well as 25 µl of loading buffer were added and the samples were boiled for 5 min at 95 °C. Protein lysates were kept at -20 °C until they were used for SDS-Page.

2.2.9 Immunochemical techniques

2.2.9.1 Immunocytochemistry

All steps were performed in the dark because the applied plasmids carry a fluorescent tag that could get lost as a result of high light exposure. Cells were seeded on cover slips in 6-well plates and transfected with the appropriate plasmids. After 48 h, cells were fixed in 4% PFA for 20 min at RT. Then, cells were washed 3 x 5 min with 2 ml PBS per well and permeabilized using 2 ml 0.05% Triton-X-100 (in PBS) for 20 min at RT. Again, cells were washed 3 x 5 min in PBS before background was reduced by blocking in 2 ml 3% BSA (in PBS) for 1 h at RT. For the Hoechst staining cells were incubated for ~ 10 min in 2 ml PBS with 1:20 000 Hoechst (10 mg/ml) at RT and washed 3 x 5 min with PBS. No antibodies were used for this staining. Cover slips were mounted onto object slides, dried at RT overnight, and subsequently stored at 4 °C.

2.2.9.2 Immunohistochemistry

To use paraffin-embedded slices for staining, they need to be rehydrated by incubation in a descending alcohol series. Therefore, object slides were first incubated for 2 x 10 min in

xylenes before they went through 2 x 100%, 1 x 96% and 1 x 70% ethanol dilutions, each for 5 min. At the end, slices were washed in demineralized water and stored in Tris/HCl buffer pH 7.6. From that time point on, slices were always kept wet. Depending on the antibody different antigen retrieval methods were applied (see Table 32 and section 2.2.9.3).

After antigen retrieval, background was reduced by incubation of the slices in a mixture of 100% methanol, 30% H_2O_2 and Tris/HCl pH 7.6 in the proportion 1:1:8 for 30 min in a wet chamber. Then, slices were washed in Tris/HCl pH 7.6 and incubated with blocking solution (2.5 µl Triton-X-100, 18.2 mg DL-Lysine and 998 µl 5% Tris-BSA) for 30 min again in a wet chamber. Directly after the blocking step, slices were incubated with the first antibody in 800 µl Tris/HCl pH 7.6 and 200 µl 5% Tris-BSA overnight in a wet chamber at RT (antibody concentrations see Table 32). For fluorescence stainings, slices were kept in the dark during the remaining steps. The next day, slices were washed again in Tris/HCl pH 7.6. Then, 5 µl of the non-fluorescent or 1 µl of the fluorescent-tagged secondary antibody diluted in 800 µl Tris/HCl pH 7.6 and 200 µl 5% Tris-BSA were added and incubated for 90 min (non-fluorescent) or 6 h (fluorescent-tagged) in a wet chamber at RT. After this incubation step, slices were washed again in both cases. While slices used for fluorescence staining were then covered with slides and kept at 4 °C until further use, processing of non-fluorescent slides continued. To increase the antibody signal, the ABC-system (Avidin-Biotin complex) was applied (prepared 30 min prior to use and containing 982 µl Tris/HCl pH 7.6, 9 µl Elite A, and 9 µl Elite B). Slices were incubated for 60 min with ABC-Elite under the same conditions as before. Another washing step followed before the slices were stained using the VECTOR NovaRED Peroxidase (HRP) Substrate Kit. Finally, slices were washed in Tris/HCl pH 7.6, dehydrated in an ascending alcohol series (5 min Aqua dest, 5 min 70% ethanol, 5 min 96% ethanol, 2 x 5 min 100% ethanol, 2 x 10 min xylenes), and cover slips were mounted. These slides were kept at RT until further use.

2.2.9.3 Antigen retrieval methods

2.2.9.3.1 Citrate buffer, pH 6

Slices were placed into citrate buffer and boiled in the microwave for 3 x 10 min. Between these three steps, evaporated liquid was refilled. Afterwards, slides were cooled down by adding Aqua dest. and washed in Tris/HCl pH 7.6.

2.2.9.3.2 Formic Acid

For this treatment slices were incubated for 3 min with 98-100% formic acid and washed thoroughly in Tris/HCl pH 7.6 afterwards.

2.2.9.3.3 Decloaker

Boiling slices in an autoclave is one the most stringent methods for antigen retrieval. Therefore, the slices were set into a container filled with Bull's Eye Decloaker (1:20) in the autoclave. The following conditions were applied: 125 °C for 30 s and 90 °C for 10 s. Slides were subsequently cooled down by adding Aqua dest. and washed in Tris/HCl pH 7.6.

2.2.9.4 Microscopy

Pictures of immunocytochemical stainings were taken with the Zeiss Axiovert 200M microscope using a 100x magnification. Double fluorescence immunohistochemical stainings were studied with the Nikon confocal microscope Eclipse 90i and a 60x magnification. The Leica 090-135-001 microscope was applied for single immunohistochemical stainings with a 60x magnification. Pictures were processed with Adobe Photoshop.

2.2.10 Outsourced analyses

Several data analyses were outsourced to specialized companies with the appropriate laboratory equipment and data processing software. All outsourced analyses are described briefly here.

2.2.10.1 Sequencing

Sequencing was outsourced to Seqlab (Göttingen, Germany). Therefore, 600 - 700 ng of the plasmid together with 20 pmol primer in a final reaction volume of 7 µl were sent to the sequencing facility. Extended HotShot sequencing was applied by the company and the obtained chromatograms were analyzed with ApE and the DNA star package.

2.2.10.2 Microarray transcriptome analyses

Cerebella and liver from 3 vs. 3 *Atxn2*-KO mice at 6 and 24 weeks of age and 3 vs. 3 or 4 vs. 4 *Atxn2*-CAG42-KIN mice at 6 or 18 months of age, respectively, were sent to the

Microarray Genechip Facility (Tübingen, Germany) for analyses. RNA was extracted and quality controlled before 100 ng of total RNA were amplified, labeled, and biotinylated with the Affymetrix GeneChip HT 3′IVT Express Kit. The labeled and fragmented cRNA was then hybridized with the Affymetrix GeneChip HT Mouse Genome 430 2.0 Array Plates that detects 39 000 transcripts and variants corresponding to 34 000 mouse genes. The array plates were scanned with the Gene Chip Scanner 3000. To obtain raw data the Affymetrix AGCC 3.0 software was used as well as ECL files to store the data. Further analysis was performed with the software platform R.2.14.0 and the Bioconductor package (www.bioconductor.org) including RMA normalization. F-statistic was applied (empirical Bayes model) followed by further correction of the p-values for multiple testing ("Benjamini-Hochberg" test). Transcripts with p-values <0.05 were considered as significantly dysregulated and fold changes were added.

2.2.10.3 RNA deep sequencing

The cerebella from 3 vs. 3 6-month-old *Atxn2*-KO mice and 3 vs. 3 18-month-old *Atxn2*-CAG42-KIN mice were used for this analysis. An RNAseq analysis was outsourced to GenXPro (Frankfurt am Main, Germany), where a particular method focusing on the quantification of poly(A)-end and 3' untranslated region (MACE, massice sequencing analysis of C-terminal ends) was applied in view of the interaction of the ATXN2-PABPC1 protein complex with the 3'-end of mRNAs. This enabled us to assess alternative polyadenylation events, alternative splicing, and subtle abundance differences of mRNAs with ARE domains (AU-rich elements) in their 3'-untranslated region. Ribosomal RNA was depleted with the Ribo-Zero^{TM} rRNA Removal Kit (Epicentre) and the remaining RNA was random-fragmented. Before reverse transcription, TrueQuant adapters (GenXPro) were ligated and RNA was reverse transcribed and amplified. Sequencing was performed using an Illumina Hiseq200 machine. After quality control corresponding to the Sanger quality score, trimmed reads were aligned to the genome with the TopHat2 program (Kim et al., 2013). Quantification and splice variant detection were conducted using Cufflinks (Trapnell et al., 2010). Transcripts were normalized and differential gene expression was quantified via Cufflinks (Anders et al., 2012).

2.2.11 Statistical analyses

Data were analyzed with GraphPad Prism software version 4.03 (2005) mainly using Student's *t* test except for the genotype and gender statistic that was performed with GraphPad quickcalcs using the Chi square test. One way ANOVA with Bonferroni

correction was applied for the comparison of the four genotypes in the double mutants (use of ANOVA is always stated in the respective results section). Error bars indicate SEM. Significant *p* values (<0.05) were marked with asterisks as follows: $p<0.05$ *, $p<0.01$ **, $p<0.001$ ***. A trend (T) was noted when $0.05<p<0.1$.

3 Results

Part 1: Study of ATXN2 interaction partners

In this part of the work several putative or known interaction partners of ATXN2 were studied regarding their transcript and protein level as well as their intracellular localization and co-localization with ATXN2. A large part of the data is based on microarray transcriptome analyses and RNA deep sequencing (RNAseq) of the mouse lines *Atxn2*-CAG42-KIN and *Atxn2*-KO. Transcripts that were found to be dysregulated in these studies were independently validated and further characterized applying molecular, biochemical, and cell culture techniques. Given that the transcriptome analyses itself were not part of this work, they are only described briefly, mentioning the most important and further relevant outcome.

3.1 The role of the E3 ubiquitin-protein ligase subunit Fbxw8 in SCA2 pathology

3.1.1 *Atxn2*-CAG42-KIN microarray transcriptome profiling reveals significant cerebellar upregulation of *Fbxw8*

Attempting to gain deeper insight into the molecular alterations triggered by mutant Atxn2, Affymetrix microarray transcriptome studies were conducted in WT and *Atxn2*-CAG42-KIN mice (Damrath et al., 2012). Cerebellum, brainstem, and liver of animals at the age of 6 months (before manifestation of movement deficits, 3 WT vs. 3 *Atxn2*-CAG42-KIN) and 18 months (after manifestation of movement deficits, 4 WT vs. 4 *Atxn2*-CAG42-KIN) were applied for this genome-wide study. Here, the focus will be on cerebellar tissue since this is the strongest affected area in SCA2. At 6 months of age, 23 transcripts were significantly dysregulated in *Atxn2*-CAG42-KIN mice, with ten of them being up- and 13 being downregulated. The only transcript detected at two individual oligonucleotide spots was *Fbxw8,* a subunit of the SCF (Skp1, Cul1, F-box protein) E3 ubiquitin-protein ligase complex (Supplementary Table 1). Furthermore, *Fbxw8* exhibited the strongest

upregulation (1.89-fold and 2.40-fold) among all dysregulated mRNAs at this age. Compared to the 6-month-old animals, even less transcripts were significantly dysregulated in 18-month-old mice. At this age, ten transcripts were down- (one of them at two oligonucleotide spots) and only four were upregulated. Again, *Fbxw8* showed the strongest upregulation detected at two oligonucleotide spots (2.54-fold and 2.50-fold). Additionally, an RNAseq variant (MACE, proprietary method of the GenXPro company in Frankfurt am Main) at 18 months of age was conducted (3 WT vs. 3 *Atxn2*-CAG42-KIN mice). *Fbxw8* appeared among the 85 transcripts with significant dysregulation; detected as three different isoforms (1.48-fold, 1.69-fold, and 1.98-fold; Supplementary Table 2). Based on this outstanding dysregulation, *Fbxw8* was chosen for further validation and additional studies were conducted to define its role in the process of SCA2 pathology. For this interaction study homozygous animals were employed to reach a maximum effect.

3.1.2 Independent validation confirms upregulation of *Fbxw8*

Real-time RT-qPCR of *Fbxw8* was performed in *Atxn2*-CAG42-KIN tissue to confirm the continuous upregulation of *Fbxw8* at different ages and to test for tissue-specificity.

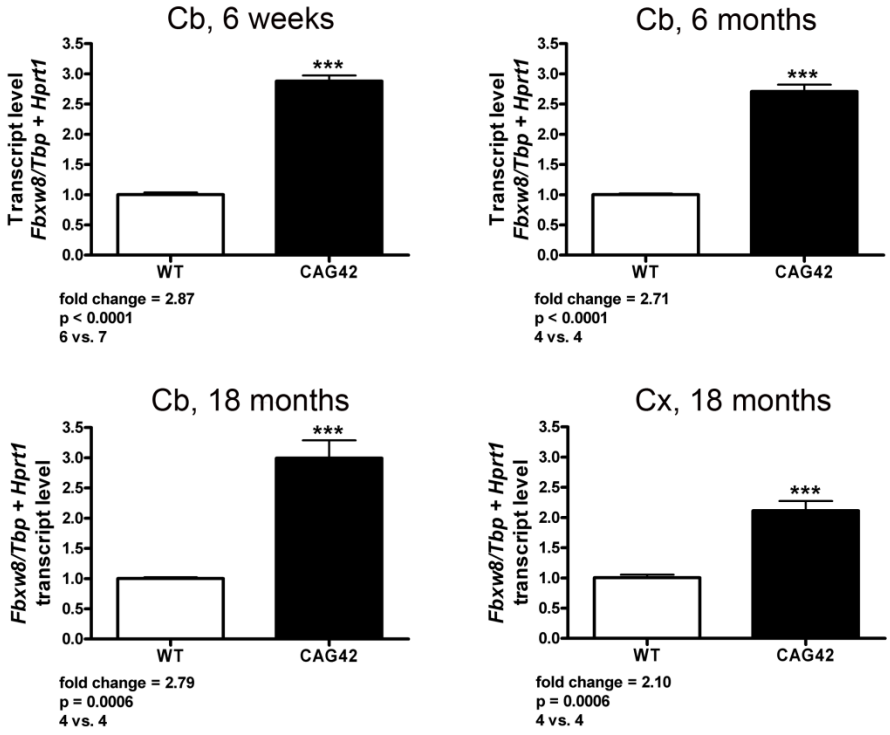

Figure 14. Fbxw8 is upregulated on transcript level in Atxn2-CAG42-KIN mice. Transcript levels were measured via RT-qPCR in cerebellum (Cb) of 6-week- and 6-month-old as well as in cerebellum and cortex (Cx) of 18-month-old WT vs. *Atxn2*-CAG42-KIN animals. *Fbxw8* always displayed significant upregulation.

Cerebellar tissue from WT and *Atxn2*-CAG42-KIN mice was used at the ages 6 weeks, 6 months, and 18 months. At all ages *Fbxw8* was strongly upregulated with fold changes between 2.71- and 2.99-fold and *p*-values between <0.0001 and 0.0005 (Figure 14). Additionally, cortical tissue from 18-month-old mice was applied showing a slightly smaller (2.10-fold) but still strongly significant ($p = 0.0006$) upregulation of *Fbxw8* in mutant animals. The results confirm that *Fbxw8* is robustly upregulated in *Atxn2*-CAG42-KIN mice independent of the age and brain region.

3.1.3 The upregulation of *Fbxw8* is a specific effect

Because Fbxw8 is part of an E3 ubiquitin-protein ligase complex that consists of additional subunits, the question raised whether these subunits are also changed in their expression in *Atxn2*-CAG42-KIN mice. Although none of the subunits turned up in the genome-wide microarray transcriptome profiling or the RNAseq, *Skp1* (S-phase kinase-associated protein 1)*, Cul1* (Cullin 1), *Cul7* (Cullin 7), and *Rbx1* (Ring-box 1) were analyzed via RT-qPCR since they could have been eliminated from the whole genome data due to multiple testing corrections. However, these transcripts did not show any upregulation in RT-qPCR either (data not shown). Nonetheless, the fact that only one of the subunits of the E3 ubiquitin-protein ligase complex is dysregulated emphasizes the importance and specificity of *Fbxw8* for SCA2 pathology.

3.1.4 Expanded ATXN2 drives FBXW8 into insolubility in cerebellum of *Atxn2*-CAG42-KIN mice

To analyze the consequences of upregulated *Fbxw8* on protein level, FBXW8 levels were determined in 18-month-old WT and *Atxn2*-CAG42-KIN mice. Therefore, protein lysates were divided into two parts: the soluble fraction lysed by RIPA buffer and containing the easily soluble proteins on the one hand and on the other hand the insoluble fraction lysed with SDS buffer where membrane-bound or aggregated proteins are solubilized. This fractionation had already been used in this mouse line to analyze protein levels of PABPC1, a known interaction partner of ATXN2 (Damrath et al., 2012). Thereby, it was shown that PABPC1 is driven into insolubility by expanded ATXN2. A similar shift was observed for FBXW8 (Figure 15). While protein levels of *Atxn2*-CAG42-KIN mice in the RIPA-soluble fraction were decreased to about half of WT levels (-1.84-fold; $p = 0.0079$), they were increased 1.57-fold ($p = 0.0321$) in the RIPA-insoluble fraction. These data

indicate that the polyQ expansion of ATXN2 renders FBXW8 less soluble and sequestrates it, like PABPC1, into relative insolubility in *Atxn2*-CAG42-KIN cerebellum.

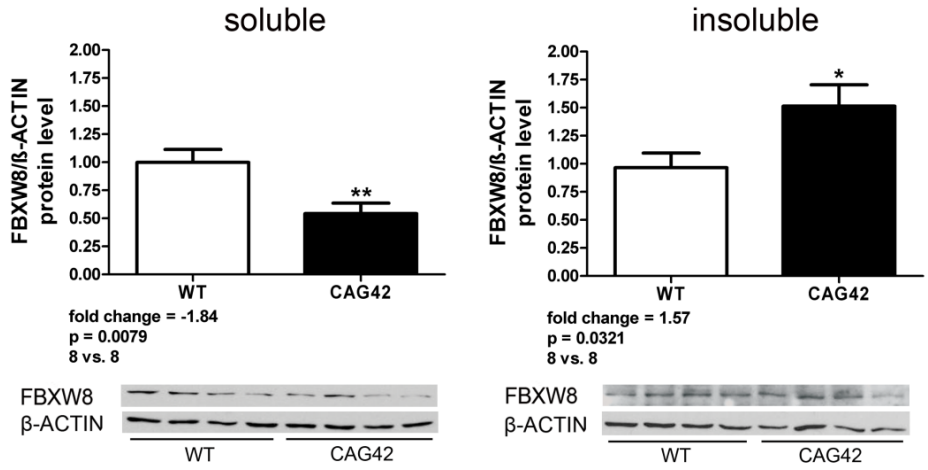

Figure 15. FBXW8 accumulates in the insoluble fraction of Atxn2-CAG42-KIN mice. Protein levels of FBXW8 were measured via quantitative immunoblots in the soluble (RIPA) and insoluble (SDS) fraction of cerebellum from WT and *Atxn2*-CAG42-KIN mice at 18 months of age. While FBXW8 was downregulated in the RIPA fraction, it accumulated in the SDS fraction.

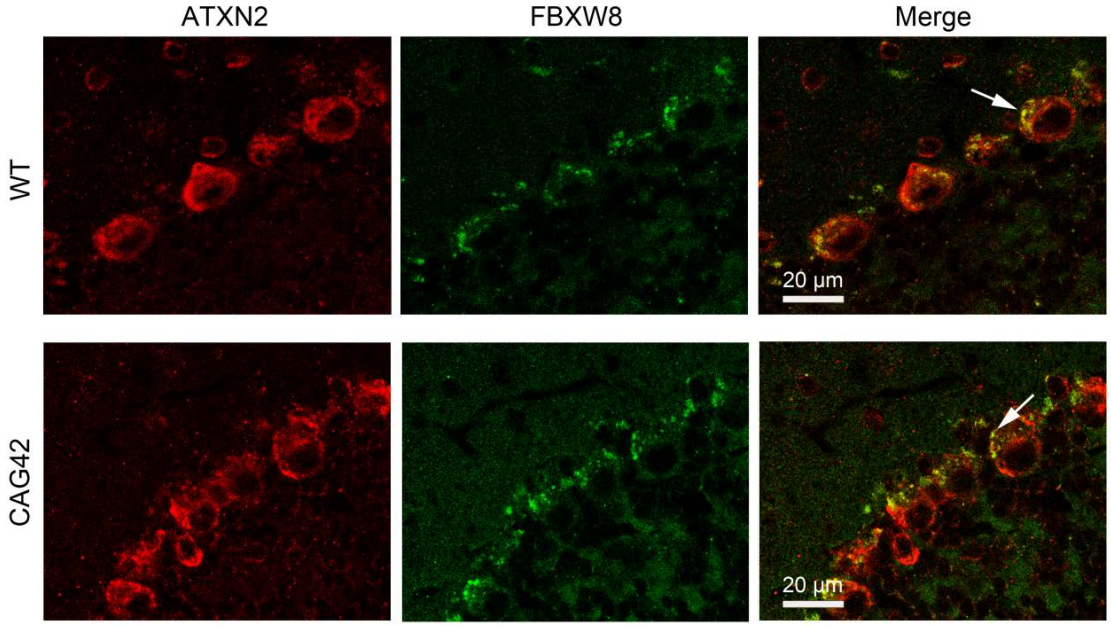

Figure 16. No visible change in FBXW8 localization between WT and Atxn2-CAG42-KIN animals. Brain slices of 24-month-old WT and *Atxn2*-CAG42-KIN animals were double stained for ATXN2 (red) and FBXW8 (green). FBXW8 did not change its localization visibly subsequent to ATXN2 aggregation.

However, a double fluorescent staining of ATXN2 and FBXW8 in WT and *Atxn2*-CAG42-KIN brain slices from 24-month-old mice did not reveal any visible differences in the co-localization of FBXW8 and ATXN2 between WT and mutant mice (Figure 16). ATXN2 (red) and FBXW8 (green) were both localized in the cytoplasm in WT and *Atxn2*-CAG42-KIN mice. While ATXN2 showed slight aggregation in the mutant mouse, FBXW8 remained scattered at the dendritic site of the Purkinje cells like in WT animals. Thus,

accumulation of FBXW8 can be seen in Western Blot but is not strong enough to be detected as aggregates in immunohistochemical stainings.

3.1.5 Expansion-independent interaction of ATXN2 and FBXW8 in cerebellum

Assuming that ATXN2 pulls FBXW8 into insolubility, these two proteins should interact with each other in cerebellar tissue. To test this hypothesis, co-immunoprecipitation (Co-IP) assays pulling either with anti-ATXN2 or anti-FBXW8 were performed in 18-month-old WT and *Atxn2*-CAG42-KIN animals. Independent of the approach, both proteins were detected in the input lanes (Figure 17 A and B) and not in the control lanes (beads incubated without antibody). For ATXN2 the band of the mutated ATXN2 is slightly higher than for WT ATXN2 due to the CAG repeat expansion. Furthermore, the immunoprecipitated proteins as well as their interacting proteins were detected in both approaches in the Co-IP lane indicating that the precipitation was successful. Thus, FBXW8 interacts with endogenous ATXN2 irrespective of the polyglutamine length in cerebellum of WT and *Atxn2*-CAG42-KIN mice.

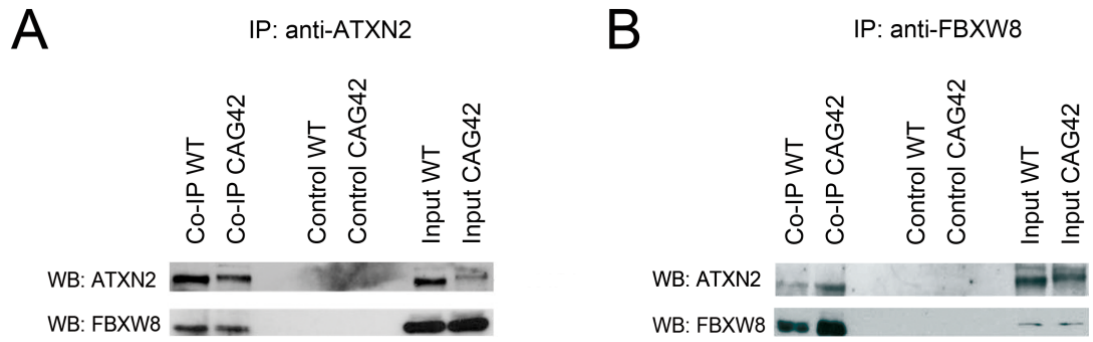

Figure 17. FBXW8 interacts with both, WT and expanded ATXN2. The interaction of FBXW8 and ATXN2 was studied in cerebellum of 18-month-old WT and *Atxn2*-CAG42-KIN mice using co-immunoprecipitation. The complex was either immunoprecipitated with anti-ATXN2 (A) or with anti-FBXW8 (B). Pulling ATXN2 enabled detection of FBXW8 and vice versa, indicating the interaction of the two proteins independent of the polyQ length.

3.1.6 ATXN2(Q22) and ATXN2(Q74) co-localize and interact with FBXW8 in a human *in vitro* model

To gain deeper insight into the role of Fbxw8 for SCA2 pathology, an *in vitro* model using HeLa cells and overexpression of the respective proteins was applied. First, the intracellular localization (via co-localization) and interaction (via Co-IP) of Q22 and Q74

ATXN2 together with FBXW8 were verified in this model. Therefore, FBXW8-Cherry (red fluorescence) and ATXN2(Q22)-GFP or ATXN2(Q74)-GFP (green fluorescence) were transiently co-transfected in HeLa cells. To facilitate the localization of the proteins in the cell, the nuclei were always stained with Hoechst (blue). Using fluorescence microscopy, their intracellular distribution was studied and compared to control transfections with plasmids containing only a Cherry- or a GFP-tag (Figure 18 A and B). Q22 and Q74 ATXN2 exhibited a granular cytoplasmic localization around the nucleus, while FBXW8 showed a scattered cytoplasmic distribution in these single transfections. The unspecific fluorescent signal in the control transfections (left panels) is clearly distinctive from the specific signal of ATNX2 and FBXW8 (middle and right panels) in these single transfections.

In a next step, ATXN2 and FBXW8 were co-expressed and appropriate control transfections were performed. The double transfection of FBXW8-Cherry together with the GFP-Control did not change the localization of the former one (Figure 18 C). Similarly, the co-expression of ATXN2(Q22)-GFP together with the Cherry-Control did not alter the localization of ATXN2 either (Figure 18 D). These control transfections prove that neither FBXW8, nor ATXN2 localization is changed due to any side effect of one of the control tags. Although the signals of the control tags are distributed throughout the cell they are weak and the signals do not specifically co-localize with those of FBXW8 or ATNX2. In contrast, the localization of FBXW8-Cherry is changed when co-expressed with either ATXN2(Q22)-GFP or ATXN2(Q74)-GFP (Figure 18 E and F). FBXW8 is no longer scattered all over the cytoplasm but located around the nucleus in a shape similar to the one of ATXN2. The fluorescent signals of the two proteins overlap and this overlap is independent of the ATXN2 polyQ length. Thus, overexpressed ATXN2(Q22) and ATXN2(Q74) alter the localization of similarly overexpressed FBXW8 in this *in vitro* model evoking their co-localization.

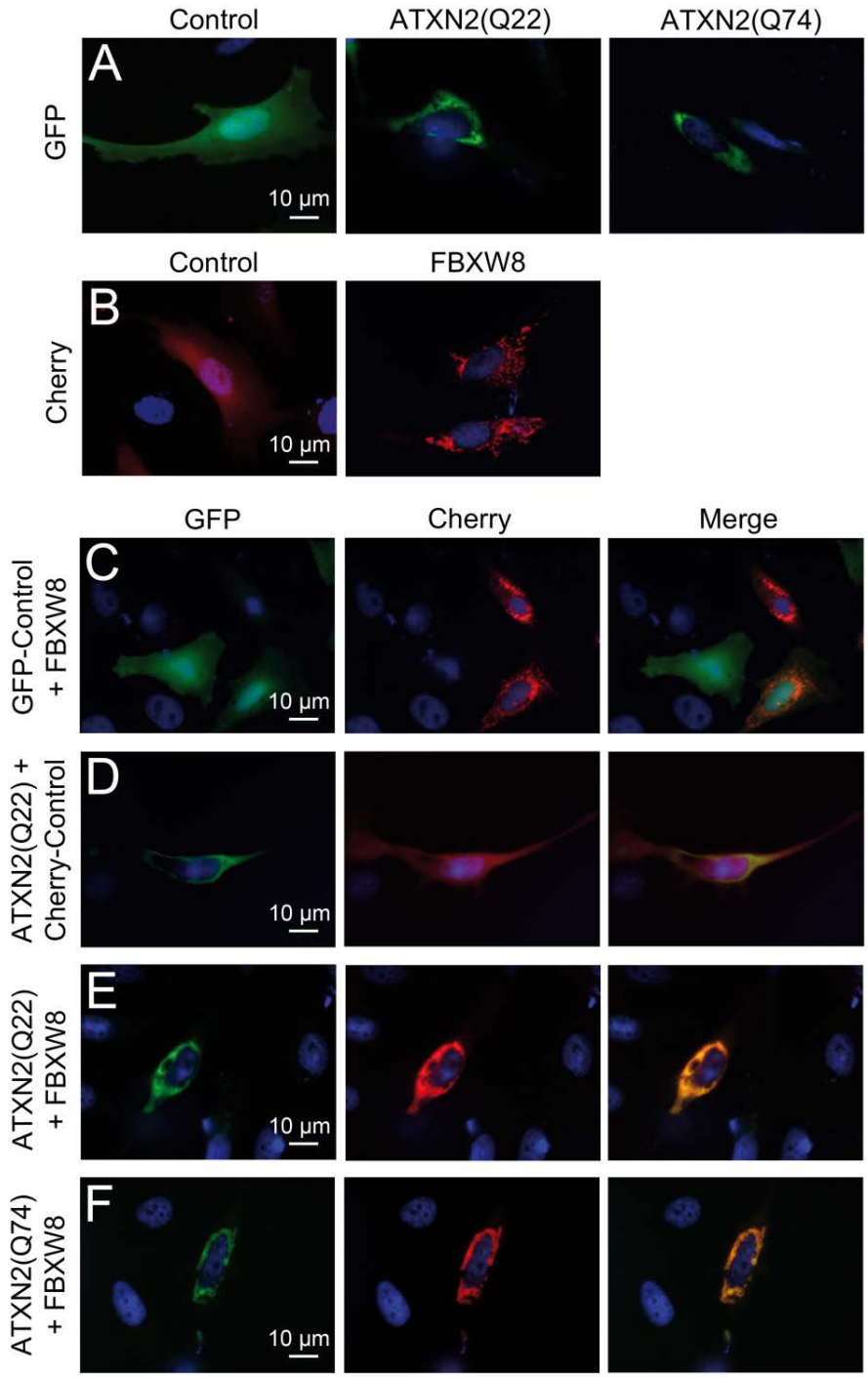

Figure 18. FBXW8 co-localizes with ATXN2 in a human in vitro model. FBXW8-Cherry and either ATXN2(Q22)-GFP or ATXN2(Q74)-GFP were transiently overexpressed in HeLa cells to study their localization. Single transfections of ATXN2(Q22)-GFP and ATXN2(Q74)-GFP revealed a granular distribution of ATXN2 around the nucleus (A) while FBXW8-Cherry exhibited a scattered cytoplasmic distribution (B). Double transfections of FBXW8-Cherry with GFP-Control did not change FBXW8 localization (C) as well as Cherry-Control did not change ATXN2(Q22)-GFP localization (D). Double transfections of either ATXN2(Q22)-GFP (E) or ATXN2(Q74)-GFP (F) with FBXW8-Cherry altered FBXW8 localization from a scattered to a granular cytoplasmic distribution around the nucleus similar to ATXN2.

In order to ensure that ATXN2 and FBXW8 not only co-localize in the *in vitro* model but also interact with each other like in the SCA2 mouse model, Co-IP experiments were performed. Therefore, ATXN2(Q22)-Myc or ATXN2(Q74)-Myc were co-expressed together with FBXW8-HA (hemagglutinin) in HeLa cells and proteins were isolated. When

immunoprecipitated either with an ATXN2 or FBXW8 antibody both proteins were detected in the input lysates of the two independent approaches (Figure 19 A and B). For ATXN2 two bands were observed representing endogenous (lower one) and overexpressed (upper one) ATXN2. In the control lanes (incubation without antibody) no bands appeared, while in the Co-IP lanes both, ATXN2 and FBXW8 were detectable independent of the pulling antibody. Consequently, the IP worked and demonstrated that in HeLa cells overexpressed FBXW8 also interacts with ATXN2 independent of the CAG repeat expansion. Additionally, the Co-IP pulling with FBXW8 also shows that this protein interacts with the endogenous as well as with the overexpressed ATXN2. In conclusion, in the *in vitro* model overexpressing Q22 or Q74 ATXN2 together with FBXW8 the two proteins co-localize and interact with each other. Therefore, this model is appropriate for further experiments regarding the effect of FBXW8 on ATXN2.

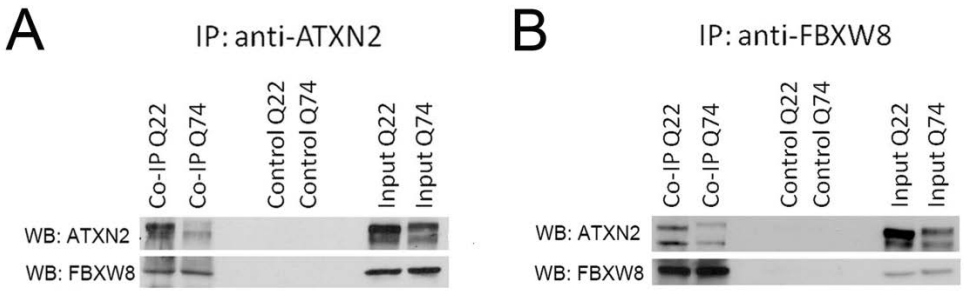

Figure 19. Interaction of FBXW8 with ATXN2 independent of the polyQ length in transiently transfected HeLa cells. ATXN2(Q22)-Myc or ATXN2(Q74)-Myc were transiently overexpressed in HeLa cells together with FBXW8-HA. For immunoprecipitation either anti-ATXN2 (A) or anti-FBXW8 (B) was used. ATXN2 showed two bands, one for endogenous and one for overexpressed ATXN2 while FBXW8 exhibited one band in both approaches. Irrespective of the pulling antibody, both proteins were detected in the lysates indicating an interaction of Q22 and Q74 ATXN2 with FBXW8 in this *in vitro* model.

3.1.7 FBXW8 reduces insoluble ATXN2(Q74) levels in the established human *in vitro* model

Given that ATXN2 and FBXW8 interact with each other, the question was raised whether FBXW8 is indeed involved in ATXN2 degradation and whether this degradation is restricted or not to pathological ATXN2. To address this issue HeLa cells were transiently single and double transfected with ATXN2(Q22)-Myc or ATXN2(Q74)-Myc and FBXW8-HA and protein levels were quantified via immunoblots.

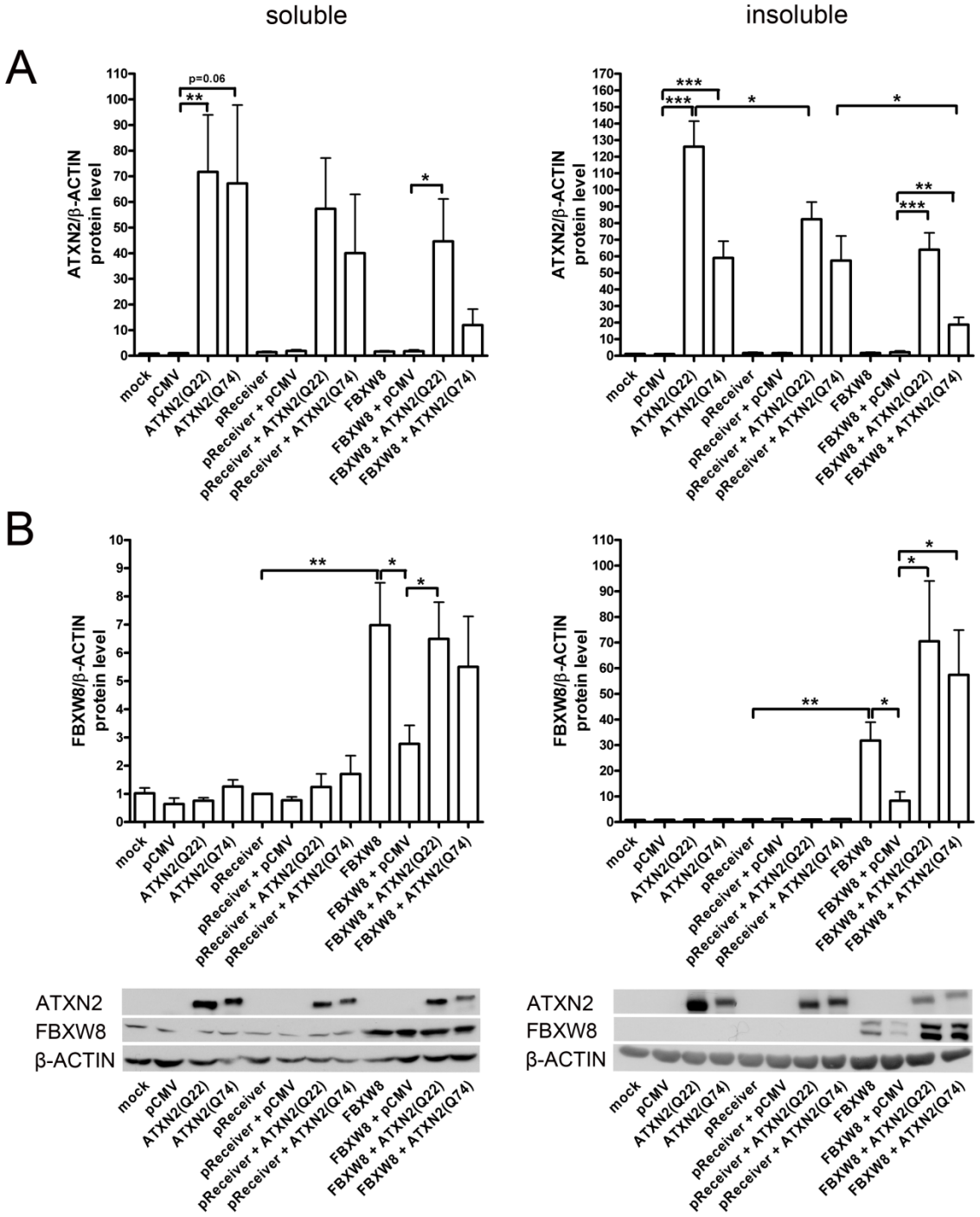

Figure 20. FBXW8 decreases proteins levels of ATXN2(Q74) in the insoluble fraction in HeLa cells. ATXN2(Q22)-Myc or ATXN2(Q74)-Myc were transiently overexpressed together with FBXW8-HA in HeLa cells. Protein levels of ATXN2 (A) and FBXW8 (B) were measured in RIPA- and SDS-soluble fraction via quantitative immunoblots. In contrast to ATXN2(Q22), ATXN2(Q74) was significantly decreased in the SDS-soluble (insoluble) fraction when co-expressed together with FBXW8 compared to co-expression with the control vector pReceiver. In the RIPA-soluble fraction, a decrease was also present but not significant due to high standard deviations. ATXN2(Q22) as well as ATXN2(Q74) both elevated FBXW8 levels in the RIPA-soluble and SDS-soluble fraction when co-expressed compared to co-expression with the control vector pCMV ($n \geq 6$).

In the RIPA-soluble fraction the single transfections of ATXN2(Q22)-Myc and ATXN2(Q74)-Myc led to an increase of ATXN2 levels by 72-fold ($p = 0.0098$) and 67-fold ($p = 0.0556$), respectively, compared to the control vector pCMV (Figure 20 A, left panel)[1]. Co-expression with the HA-Control vector pReceiver or FBXW8 did not change these levels significantly due to a high standard error of means. FBXW8 levels of the RIPA-soluble fraction were increased by 7-fold ($p = 0.0018$) compared to the control vector pReceiver (Figure 20 B, left panel) while they were significantly decreased by -2.5-fold ($p = 0.0342$) when double transfected with the pCMV control vector. Surprisingly, co-expression of FBXW8 together with ATXN2 increased FBXW8 levels significantly compared to double transfections with pCMV at least for ATXN2(Q22) (25-fold; $p = 0.0441$). In the SDS-soluble fraction (Figure 20 A, right panel), again, ATXN2 levels were increased for ATXN2(Q22) and ATXN2(Q74) compared to pCMV (126-fold; $p < 0.0001$ and 59-fold; $p < 0.0001$). In the double transfections with pReceiver, ATXN2 levels decreased for Q22 (1.5-fold; $p = 0.0361$) but not for Q74. However, comparing these levels with the double transfections of ATXN2(Q22) or ATXN2(Q74) with FBXW8 revealed a decrease only for Q74 (3-fold; $p = 0.0284$). FBXW8 levels in the SDS-soluble fraction (Figure 20 B, right panel) were similar to the RIPA-soluble fraction. FBXW8 was increased in the single transfection compared to pReceiver (32-fold; $p = 0.0011$) and decreased in the double transfection with the pCMV vector (4-fold; $p = 0.0178$). Again, double transfections with ATXN2 showed increased FBXW8 levels compared to double transfections with pCMV (30-fold; $p = 0.0002$ for Q22 and 9-fold, $p = 0.0051$ for Q74). Consequently, both Q22 and Q74 ATXN2 cause an increase of FBXW8 levels but only Q74 levels are reduced when the two proteins are co-expressed.

In an additional experiment, transcript levels of *ATXN2* and *FBXW8* were measured in the same approach to demonstrate that the observed ATXN2 reduction occurs on protein level only and not already on transcript level. Figure 21 shows that there is a significant decrease in *ATXN2*(Q22) levels between the single ATXN2 and the double control transfection (2-fold; $p = 0.0306$), but there is no alteration between these double control transfection and the double transfection with *FBXW8* ($p = 0.6045$). For *ATXN2*(Q74), there is no significant change at all between the three transfections ($p = 0.0821$ and $p = 0.7087$). *FBXW8* levels had to be measured by SYBR® Green assay since the optimized codon did not allow the utilization of a TaqMan® probe. The standard error of means for *FBXW8* levels is, therefore, quite high resulting in no significant changes although it seems that *FBXW8* levels are increased upon double transfection with *ATXN2*

[1] *For the evaluation of these two transfection studies the Student's t-test was applied since ANOVA failed to detect many of the changes due to the high number of different transfections (e.g. no significance at all for ATXN2 in the RIPA-soluble fraction).*

(p =0.5575 for single and control double; p = 0.4532 for control double and ATXN2(Q22) with FBXW8; p = 0.4791 for control double and ATXN2(Q74) with FBXW8). In summary, these data indicate that FBXW8 is involved in the selective reduction of expanded ATXN2 at least in the SDS-soluble fraction and that this effect is not mediated via the transcript levels. Furthermore, the overexpression of ATXN2 seems to increase FBXW8 levels compared to the control vector in this *in vitro* approach.

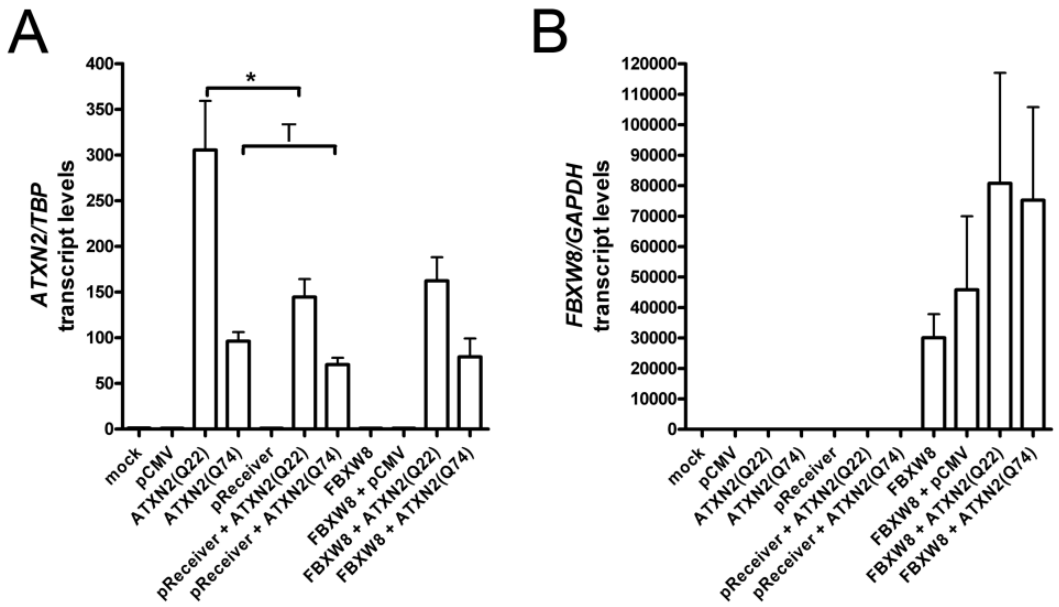

Figure 21. No significant change in ATXN2 or FBXW8 transcript levels in double transfections. HeLa cells were transiently transfected with ATXN2(Q22)-Myc or ATXN2(Q74)-Myc and FBXW8-HA and transcript levels of ATXN2 and FBXW8 were measured via real-time RT-qPCR and SYBR Green, respectively. (A) No change of ATXN2 levels was observed when overexpressed together with FBXW8 compared to overexpression with the control vector pReceiver. (B) FBXW8 levels were increased when double transfected with ATXN2 compared to double transfection with the control vector pCMV but due to the high standard deviation not significantly (n = 4).

3.1.8 PARK2, another E3 ubiquitin-protein ligase component interacts with FBXW8

The E3 ubiquitin-protein ligase PARK2 (Parkin), a Parkinson associated protein (von Coelln et al., 2004), is known to interact with ATXN2 and to be involved in ATXN2 degradation (Huynh et al., 2007). Furthermore, PARK2 was shown to interact with FBXW7, another F-box protein involved in the SCF complex (Ekholm-Reed et al., 2013; Staropoli et al., 2003). Thus, the hypothesis was proposed that PARK2 could also interact with FBXW8. An association of PARK2 with FBXW8 was first assessed *in vitro* and then *in vivo* via Co-IP. HeLa cells were transiently transfected with FBXW8-HA and PARK2-Cherry-GFP plasmids, proteins were isolated, and immunoprecipitated with an antibody against FBXW8. The double tag of the PARK2 vector was necessary to avoid an overlay

of the PARK2 band with the heavy chain of the FBXW8 antibody (both antibodies were produced in rabbit). In the input lane (Figure 22 A), FBXW8 as well as PARK2 were detected, but none of them was observed in the negative control. In the Co-IP lane, the immunoprecipitated FBXW8 as well as the interacting PARK2 were present, showing that these two proteins interact in an overexpressing *in vitro* model. To confirm this interaction *in vivo* for disease-susceptible tissue, cerebellum from 18-month-old WT and *Atxn2*-CAG42-KIN mice was applied. Again, anti-FBXW8 was used for immunoprecipitation of the complex. Figure 22 B shows that both proteins were detectable in the input lanes of WT and *Atxn2*-CAG42-KIN cerebellum with a double band for PARK2. Given that in the control lanes the upper band for PARK2 was also present, this one was considered as an unspecific signal. FBXW8 was not detectable in the control lanes but in the Co-IP lanes demonstrating the immunoprecipitation efficiency. Additionally, the lower band for PARK2 appeared in the Co-IP showing that this protein interacts with FBXW8 in WT as well as in *Atxn2*-CAG42-KIN mice. These results suggest that FBXW8 and PARK2 are located in one protein complex together with ATXN2.

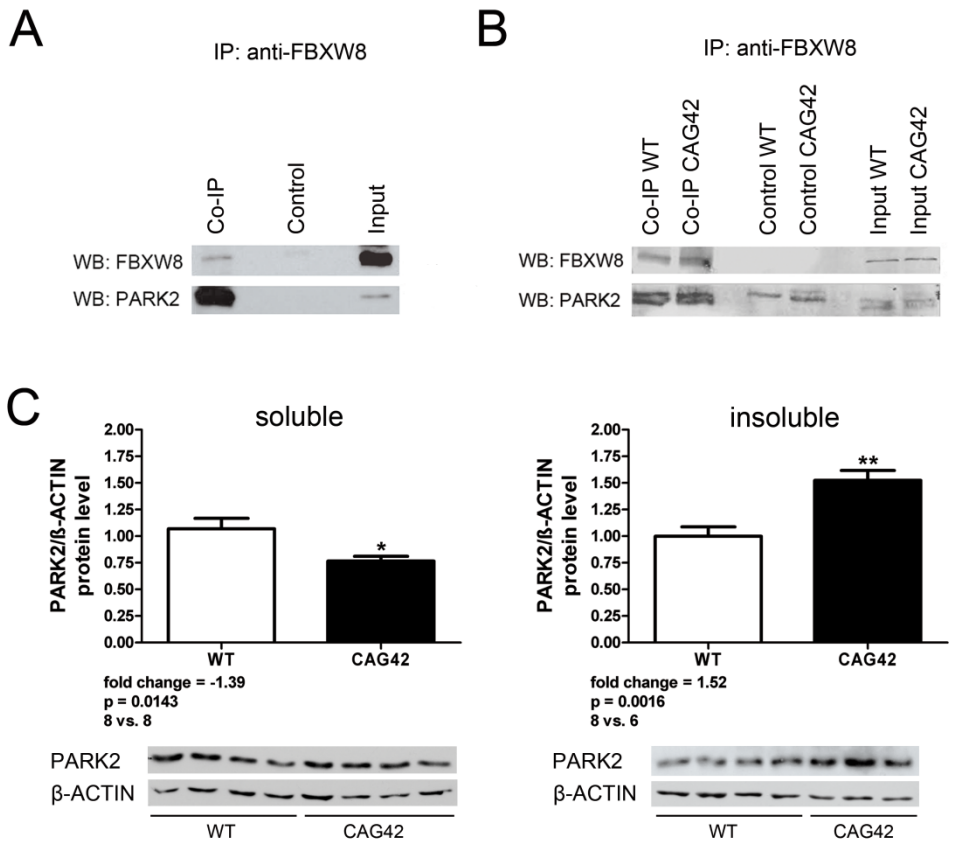

Figure 22. Interaction of PARK2 with FBXW8 and PARK2 sequestration in Atxn2-CAG42-KIN mice. In HeLa cells overexpressing FBXW8-HA and PARK2-Cherry-GFP (A) and in cerebellum of 18-month-old *Atxn2*-CAG42-KIN mice (B), immunoprecipitated FBXW8 brought down PARK2 indicating their interaction. In cerebellum, bands in the control lanes were due to an unspecific signal; lower bands represent PARK2. (C) Quantification of PARK2 protein levels in cerebellum of 18-month-old WT and *Atxn2*-CAG42-KIN mice revealed a downregulation in the RIPA-soluble fraction and an accumulation in the SDS-soluble fraction, similar to FBXW8.

To test if this interaction also affects the solubility of PARK2, protein levels were determined in WT and *Atxn2*-CAG42-KIN mice. Again, cerebellar tissue from both genotypes at the age of 18 months was used for protein detection via quantitative immunoblots in the RIPA and SDS fraction. In the RIPA-soluble fraction PARK2 levels were decreased by -1.39-fold ($p = 0.0143$), while they were increased by 1.52-fold ($p = 0.0016$) in the SDS-soluble fraction (Figure 22 C). However, determination of *Park2* transcript level in this SCA2 model did not reveal any change between WT and *Atxn2*-CAG42-KIN mice (Supplementary Figure 1 A). The presented data suggest that PARK2 is sequestered into insolubility by ATXN2 similar to FBXW8 in old *Atxn2*-CAG42-KIN mice. Furthermore, they indicate a new interaction partner of PARK2 and prove its role for SCA2 pathology.

3.1.9 *FBXW8* as a biomarker for SCA2

To investigate the role of *FBXW8* for human SCA2 pathology and to discuss its role as a biomarker for this disease, primary skin fibroblasts as well as whole blood samples from SCA2 patients and healthy controls were applied. *FBXW8* transcript levels were measured in both tissues in order to find similar upregulations as in the mouse model. Small but significant changes were detected in skin fibroblasts as well as in blood samples with fold changes of 1.16-fold ($p = 0.0357$) and 1.27-fold ($p = 0.0477$), respectively (Figure 23 A and B). *PARK2* transcript levels were also studied in SCA2 fibroblasts but like in the mouse model no regulation was observed (Supplementary Figure 1 B). Primary skin fibroblasts were preferred for protein analysis because they are easily reproducible and furthermore are not prone to strong background signals due to hemoglobin. As before, protein levels in the RIPA-soluble and SDS-soluble fraction were quantified to be able to detect a possible shift into insolubility. Indeed, FBXW8 levels in the RIPA-soluble fraction were downregulated (-1.67-fold; $p = 0.0235$), while they were upregulated (2.04-fold; $p = 0.0283$) in the SDS-soluble fraction (Figure 23 C). PARK2 levels were also analyzed in fibroblasts but the abundance was too low for quantification. In conclusion, these data confirm the sequestration of FBXW8 into insolubility by expanded ATXN2 as shown in the SCA2 mouse model. Furthermore, *FBXW8* seems to be a potential biomarker for SCA2, while *PARK2* can be definitely excluded.

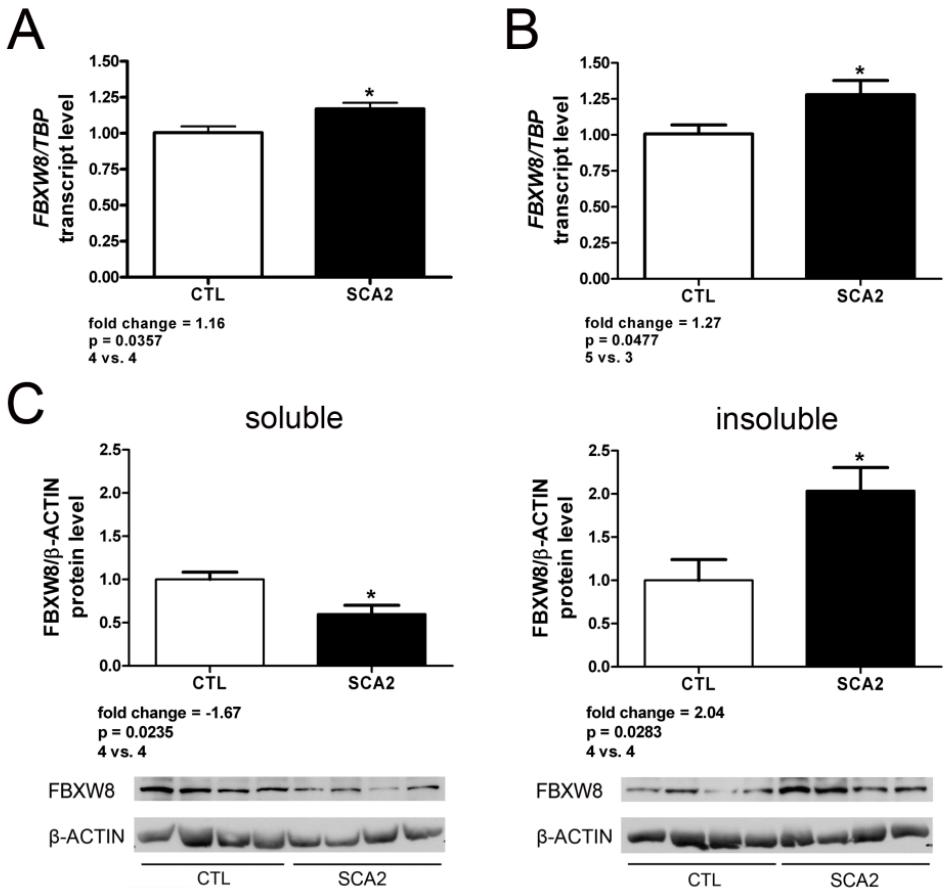

Figure 23. Transcriptional upregulation of Fbxw8 and accumulation on protein level in SCA2 patient material. Transcript levels of FBXW8 were determined via RT-qPCR in SCA2 patient tissue vs. tissue of healthy controls (CTL). FBXW8 was significantly upregulated in SCA2 primary skin fibroblasts (A) as well as in SCA2 blood samples (B). Protein quantification via immunoblots revealed a shift of FBXW8 into insolubility in SCA2 skin fibroblasts compared to controls (C).

3.2 Calcium homeostasis factors in *Atxn2*-KO and *Atxn2*-CAG42-KIN mice

3.2.1 Dysregulation of several calcium homeostasis factors in *Atxn2*-KO cerebellum detected by microarray transcriptome profiling

In order to gain deeper insight into the consequences of *Atxn2* loss, a hypothesis-free Affymetrix microarray transcriptome analysis of *Atxn2*-KO mice was performed. At 6 weeks and 6 months of age, cerebellum and liver from WT and *Atxn2*-KO mice (4 vs. 4) were used for analyses. Among the 109 transcripts consistently detected at all ages in cerebellum (some of them at two or more oligonucleotide spots), clusters for lipid dynamics, bioenergetics, RNA processing, and calcium homeostasis were found

(Fittschen et al., in press; Halbach et al., under revision). In consideration of the suggested involvement of signal transmission disturbances in neurodegeneration, those transcripts with an established role in calcium signaling at cerebellar Purkinje dendrites were preferred for further analyses. *Atp2a2* (ATPase slow twitch 2; detected at two individual oligonucleotide spots), *Inpp5a* (Inositol polyphosphate-5-phosphatase), *Itpr1* (Inositol 1,4,5-trisphosphate receptor, type 1), and *Rora* (RAR-related orphan receptor A) were significantly downregulated at all ages in cerebellum (Supplementary Table 3). While *Itpr1* and *Atp2a2* are directly involved in calcium release and re-uptake from and into the ER and *Inpp5a* dephosphorylates the *Itpr1* ligand IP3, *Rora* acts as a transcription factor for several calcium pathway genes in the nucleus. Fold changes in the microarray ranged between -1.16-fold and -1.70-fold for these four transcripts. *Itpr1* showed the highest fold change followed by *Inpp5a* and *Rora*. Furthermore, an independent RNAseq using cerebellum of 3 WT vs. 3 *Atxn2*-KO mice showed that *Inpp5a* and *Itpr1* were among the 100 most downregulated transcripts (Supplementary Figure 2). Besides, other transcripts involved in calcium signaling like *Ca8* (Carbonic anhydrase 8; an *Itpr1* interactor and mediator*)*, *Homer3* (a scaffolding protein that connects *Itpr1* with the glutamate receptor subunit *Grm1*), and *Sptbn2* (spectrin beta non-erythrocytic 2; SCA5 gene and stabilizer of the glutamate transporter *EAAT4)* were among these transcripts. The consistency of these regulations and the fact that calcium homeostasis factors have been discussed numerously in ataxic diseases were convincing so that further studies on these genes were performed.

3.2.2 Independent validation of calcium homeostasis factor downregulation in *Atxn2*-KO cerebellum

In the validation process, calcium homeostasis factor dysregulations were studied via real-time RT-qPCR. Therefore, cerebella of 6-month-old WT and *Atxn2*-KO mice were employed studying ten transcripts involved in the Ca^{2+} signaling pathway. Among them were *Atp2a2*, *Inpp5a*, *Itpr1*, and *Rora* which had been detected as downregulated at different ages in the microarray as well as *KitL* (Kit ligand; promotes cleavage of PIP_2 into IP_3 and DAG) and *Trpc3* (transient receptor potential cation channel C3; Na^+ and Ca^{2+} channel in the plasma membrane) that had been significantly dysregulated but not consistently at all ages. Additionally, *Calb1* (Calbindin 1) was chosen due to its important role in Ca^{2+} buffering and *Grm1* (Glutamate receptor metabotropic 1) because it is a glutamate receptor subunit involved in signal transmission and is connected with *Itpr1* via *Homer3*. The transcripts that appeared dysregulated in the RNAseq (*Ca8*, *Homer3*, and

Sptbn2) were also analyzed; however, *Sptbn2* did not yield any significant changes at 6 months of age and therefore was excluded from further validations. The SCA6 gene transcript *Cacna1a* was studied as well but discarded for the same reason. All of the ten transcripts depicted in Table 42 showed significant downregulation with fold changes ranging between -1.05-fold (*Itpr1*) and -1.48-fold (*KitL*). To test whether these transcript changes are cerebellum-specific, tissue from cerebral cortex, a region that is affected late in SCA2 pathology was employed. As shown in Table 42, none of the transcripts was significantly dysregulated in cortex of 6-month-old *Atxn2*-KO mice. Most of them even had a positive (but not significant) fold change. These data indicate that the downregulation of several calcium homeostasis factors in *Atxn2*-KO mice seems to be a cerebellum-specific effect.

Table 42. Transcript level changes of calcium homeostasis factors in 6-month-old Atxn2-KO animals. Transcript levels were analyzed via real-time RT-qPCR in cerebellar and cortical tissue of WT and *Atxn2*-KO animals (n = 4-11 WT vs. 3-10 HOM).

Gene symbol	WT vs. HOM Cb 6 months	WT vs. HOM Cx 6 months
Atp2a2	-1.13-fold *	+1.03-fold *n.s.*
Ca8	-1.22-fold **	+1.12-fold *n.s.*
Calb1	-1.17-fold **	+1.19-fold *n.s.*
Grm1	-1.10-fold *	+1.14-fold *n.s.*
Homer3	-1.34-fold ***	-1.08-fold *n.s.*
Inpp5a	-1.30-fold **	+1.16-fold *n.s.*
Itpr1	-1.05-fold *	-1.09-fold *n.s.*
Kitlg	-1.48-fold **	-1.01-fold *n.s.*
Rora	-1.42-fold **	+1.01-fold *n.s.*
Trpc3	-1.31-fold **	+1.20-fold *T*

3.2.3 Downregulation of calcium homeostasis factors starts early in *Atxn2*-KO cerebellum

To test if the transcription changes are not only tissue-dependent but also age- and mutation load-dependent, younger mice as well as heterozygous mice were used. Among the ten transcripts that were downregulated in the cerebellum of 6-month-old mice, only seven were already significantly downregulated in 6-week-old *Atxn2*-KO compared to WT mice (Table 43). In order to find the first transcripts that are affected in their expression by *Atxn2* loss animals at the same age but with reduced mutation load, *Atxn2*$^{+/-}$ (HET) mice were analyzed. However, the number of significantly downregulated genes did not further

decrease. Therefore, HET pups at the age of ~3 days were studied. In these animals two transcripts were already significantly downregulated (*Atp2a2* and *Inpp5a*) while three further transcripts showed a trend towards downregulation (*Grm1*, *Rora*, and *Trpc3*). *Atp2a2* and *Inpp5a* were the first transcripts dysregulated in *Atxn2*-KO mice cerebellum. In conclusion, transcript changes of calcium homeostasis factors in cerebellum start quite early during life and increase with age.

Table 43. Transcriptional changes of calcium homeostasis factors in young Atxn2-KO animals. Measurement of transcript levels via real-time RT-qPCR in cerebellum of WT vs. HOM or HET mice at the age of 6 weeks and of 3-day-old WT vs. HET animals. (n = 4-9 WT, 3-6 HET, and 4-5 HOM).

Gene symbol	WT vs. HOM Cb 6 weeks	WT vs. HET Cb 6 weeks	WT vs. HET Cb 3 days
Atp2a2	-1.24-fold *	-1.11-fold *	-1.17-fold **
Ca8	-1.19-fold ***	-1.15-fold **	+1.00-fold *n.s.*
Calb1	-1.07-fold *n.s.*	-1.04-fold *n.s.*	+1.20-fold *n.s.*
Grm1	-1.08-fold *T*	-1.15-fold **	-1.17-fold *T*
Homer3	-1.33-fold ***	-1.08-fold *n.s.*	+1.00-fold *n.s.*
Inpp5a	-1.39-fold **	-1.35-fold **	-1.19-fold **
Itpr1	-1.05-fold *n.s.*	-1.07 -fold *n.s.*	+1.04-fold *n.s.*
Kitlg	-1.52-fold **	-1.17-fold **	+1.10-fold *n.s.*
Rora	-1.11-fold **	-1.15-fold ***	-1.14-fold *T*
Trpc3	-1.21-fold *	-1.31-fold **	-1.15-fold *T*

3.2.4 Changes in calcium homeostasis factors are also present in *Atxn2*-CAG42-KIN mice

In *Atxn2*-CAG42-KIN mice, changes in calcium homeostasis factors were not detected via microarray transcriptome profiling. However, as it is possible that they were excluded due to multiple corrections and given that these changes seem to be disease relevant, the transcripts investigated before were analyzed in this SCA2 mouse model as well. Real-time RT-qPCR was applied to examine transcript levels of the ten genes in cerebellum of 18-month-old WT and *Atxn2*-CAG42-KIN mice (with manifest movement deficit). In contrast to the *Atxn2*-KO mice, only three of them (*Atp2a2*, *Itpr1*, and *Trpc3*) exhibited downregulation while one (*KitL*) was upregulated (Table 44). However, similar to the loss-of-function model, for none of the transcripts a significant dysregulation in cortical tissue of animals at the same age was documented. These findings demonstrate that expression changes in calcium homeostasis factors also occur in *Atxn2*-CAG42-KIN mice, namely in a cerebellum-specific manner but are less pronounced than in *Atxn2*-KO animals.

Table 44. Calcium homeostasis factor changes on transcript level in old Atxn2-CAG42-KIN mice. Transcript changes were analyzed via real-time RT-qPCR in cerebellum and cortex of 18-month-old WT and *Atxn2*-CAG42-KIN animals (n = 4-11 WT vs. 3-10 HOM).

Gene symbol	WT vs. HOM Cb 18 months	WT vs. HOM Cx 18 months
Atp2a2	-1.17-fold **	-1.12-fold *n.s.*
Ca8	-1.02-fold *n.s.*	-1.04-fold *n.s.*
Calb1	-1.01-fold *n.s.*	+1.02-fold *n.s.*
Grm1	-1.09-fold *n.s.*	+1.08-fold *n.s.*
Homer3	+1.05-fold *n.s.*	+1.26-fold *n.s.*
Inpp5a	+1.00-fold *n.s.*	+1.15-fold *T*
Itpr1	-1.15-fold *	-1.04-fold *n.s.*
Kitlg	+1.26-fold **	+1.03-fold *n.s.*
Rora	-1.01-fold *n.s.*	+1.09-fold *n.s.*
Trpc3	-1.21-fold **	+1.09-fold *n.s.*

3.2.5 Transcript analysis in young *Atxn2*-CAG42-KIN mice reveals *Itpr1* as the first downregulated factor

Similar to the *Atxn2*-KO mouse, the temporal dynamics of the transcriptional changes in *Atxn2*-CAG42-KIN mice were studied. Using 6-month-old WT and *Atxn2*-CAG42-KIN mice the same set of transcripts was analyzed. Table 45 indicates that at this age already three transcripts (*Atp2a2*, *Homer3,* and *Itpr1*) were significantly downregulated and one showed a trend towards downregulation (*Trpc3*). However, the downregulation of *Homer3* was not consistent in 18-month-old and also not in 6-week-old animals. At this age *Itpr1* was the only significantly downregulated transcript. The presented data indicate that *Itpr1* may have a particular role in SCA2 pathology as it was the first downregulated transcript in *Atxn2*-CAG42-KIN mice. Thus, an age-dependent transcript downregulation exists in this mouse line similar to *Atxn2*-KO mice.

Table 45. Transcript changes of calcium homeostasis factors in young Atxn2-CAG42-KIN cerebellum. Transcript levels were measured via real-time RT-qPCR in 6-month- and 6-week-old WT vs. *Atxn2*-CAG42-KIN animals (n = 4-12 WT vs. 3-9 HOM).

Gene symbol	WT vs. HOM Cb 6 months	WT vs. HOM Cb 6 weeks
Atp2a2	-1.12-fold *	-1.05-fold *n.s.*
Ca8	-1.02-fold *n.s.*	-1.01-fold *n.s.*
Calb1	-1.02-fold *n.s.*	-1.03-fold *n.s.*

Gene symbol	WT vs. HOM Cb 6 months	WT vs. HOM Cb 6 weeks
Grm1	-1.03-fold *n.s.*	-1.09-fold *n.s.*
Homer3	-1.10-fold *	-1.02-fold *n.s.*
Inpp5a	-1.05-fold *n.s.*	-1.05-fold *n.s.*
Itpr1	-1.12 -fold **	-1.12-fold *
Kitlg	-1.09-fold *n.s.*	-1.04-fold *n.s.*
Rora	+1.00-fold *n.s.*	-1.07-fold *n.s.*
Trpc3	-1.08-fold *T*	-1.12-fold *T*

3.2.6 Further calcium homeostasis factors are downregulated in KIN and KO mice

After it turned out that several calcium homeostasis transcripts were significantly dysregulated, although they had neither appeared in the microarray transcriptome study nor in the RNAseq analysis, further candidate genes implicated in this pathway were analyzed. For this purpose, cerebellum of 6-month-old *Atxn2*-KO and of 18-month-old *Atxn2*-CAG42-KIN mice was employed. Of 14 additional transcripts only four showed downregulation (trend or significant) in both mouse models (Table 46).

Table 46. Further calcium homeostasis factor changes on transcript level in Atxn2-KO and Atxn2-CAG42-KIN cerebellum. Transcript levels were analyzed in 6-month-old *Atxn2*-KO and 18-month-old *Atxn2*-CAG42-KIN mice via real-time RT-qPCR (n = 3-8 WT vs. 4-7 HOM for *Atxn2*-KO and 4 WT vs. 4 HOM for *Atxn2*-CAG42-KIN mice).

Gene symbol	*Atxn2*-KO WT vs. HOM Cb 6 months	*Atxn2*-CAG42 WT vs. HOM Cb 18 months
Atp2b2	-1.11-fold **	-1.11-fold *T*
Calm1	-1.07-fold *	-1.15-fold **
Gnaq	-1.13-fold **	-1.19-fold **
Plcb4	-1.20-fold **	-1.10-fold *T*

The transcript levels for *Calm1* (another Ca^{2+}-binding protein) and *Gnaq* (guanine nucleotide binding protein subunit that activates phospholipase C) were significantly downregulated in both, *Atxn2*-KO and *Atxn2*-CAG42-KIN mice. *Atp2b2* (equivalent of *Atp2a2* in the plasma membrane) and *Plcb4* (Phospholipase C beta 4) were only significantly downregulated in *Atxn2*-KO mice but showed a tendency towards downregulation in *Atxn2*-CAG42-KIN mice. The results suggest that a wide range of

transcripts implicated in Ca^{2+} signaling is altered in the cerebellum, when *Atxn2* is either lost or mutated.

3.2.7 Similar transcript alterations in SCA1 and SCA2 mouse models

To compare the observed transcription changes with another ataxia model and to confirm again the relevance of the chosen genes, transcript levels of calcium homeostasis factors in *Atxn1*-Q154-KIN were measured via real-time RT-qPCR. Transcriptional changes for the ten genes analyzed before were assessed using cerebellum of 10-week-old WT and *Atxn1*-Q154-KIN mice. Indeed, nine out of ten transcripts were significantly downregulated but with higher fold changes (-1.24 to -1.52-fold) compared to *Atxn2* mouse lines (Table 47). In conclusion, the effects observed in *Atxn2*-KO and *Atxn2*-CAG42-KIN mice are comparable with those in *Atxn1*-Q154-KIN mice, suggesting that there are similar pathways affected in the two diseases.

Table 47. Transcript level changes of calcium homeostasis factors in Atxn1-Q154-KIN cerebellum. Transcript levels were measured via real-time RT-qPCR in cerebellum of 10-week-old WT and *Atxn1*-Q154-KIN animals (n = 2-7 WT vs. 4-8 HOM).

Gene symbol	WT vs. HOM Cb 10 weeks
Atp2a2	-1.31-fold ***
Ca8	-1.38-fold **
Calb1	-1.44-fold **
Grm1	-1.11-fold *n.s.*
Homer3	-1.53-fold ***
Inpp5a	-1.48-fold ***
Itpr1	-1.46-fold **
Kitlg	-1.34-fold **
Rora	-1.24-fold *
Trpc3	-1.52-fold *

3.2.8 Protein levels of calcium homeostasis genes are differentially regulated in *Atxn2*-KO and *Atxn2*-CAG42-KIN mice

Transcript levels of calcium homeostasis factors have been frequently analyzed in diverse ataxia models, but in none of these studies protein levels were determined. However, protein levels could give a hint whether the transcription regulation is for example a feedback mechanism due to elevated protein levels. Furthermore, the causes for or the

consequences of transcript reduction on protein level could differ between *Atxn2*-KO and *Atxn2*-CAG-42-KIN mice. Therefore, protein levels of several calcium homeostasis factors in cerebellar tissue of 6-month-old *Atxn2*-KO and 18-month-old *Atxn2*-CAG42-KIN mice were investigated. Limited by the availability of specific antibodies, only six of the ten genes analyzed before were studied on protein level in *Atxn2*-KO mice: CA8, CALB1, GRM1, HOMER3, INPP5A, and ITPR1. All of them showed a significant downregulation in the RIPA fraction (Figure 24 A) with fold changes ranging from -1.21-fold (INPP5A) to -2.18-fold (HOMER3). In the SDS fraction only half of the analyzed proteins were significantly downregulated (Figure 24 B). CA8 (-1.31-fold; $p = 0.0439$), HOMER3 (-2.48-fold; $p = 0.0011$), and INPP5A (-1.31-fold; $p = 0.0047$) showed significantly decreased levels while CALB1, GRM1, and ITPR1 downregulation did not reach significance.

In *Atxn2*-CAG42-KIN mice, GRM1 and INPP5A protein levels were not determined since their transcript levels had not been changed significantly in this mouse line. Despite only subtle transcript level changes three of the four remaining proteins were significantly decreased in the RIPA-soluble fraction like in *Atxn2*-KO cerebellum. These proteins were CA8 (-1.96-fold; $p = 0.0061$), CALB1 (-1.20-fold; $p = 0.0252$), and ITPR1 (-1.98-fold; $p = 0.0006$) (Figure 25 A). The most pronounced downregulation in the RIPA-soluble fraction exhibited CA8 and ITPR1 with a reduction to almost half of WT levels, while HOMER3 did not show any change at all. The same number but not the same proteins showed a significant increase in the SDS-soluble fraction: HOMER3 displayed significant upregulation, while CA8 did not reach significance (Figure 25 B). Furthermore, in the SDS-soluble fraction the fold changes where smaller (1.21-fold to 1.34-fold) than in the RIPA-soluble fraction. In summary, these results indicate that proteins accumulated in the insoluble (SDS-soluble) fraction in *Atxn2*-CAG42-KIN mice, while they were downregulated (or not significantly regulated) in *Atxn2*-KO mice in both fractions. This accumulation may result from a sequestration of the proteins into insolubility by ATXN2 aggregation.

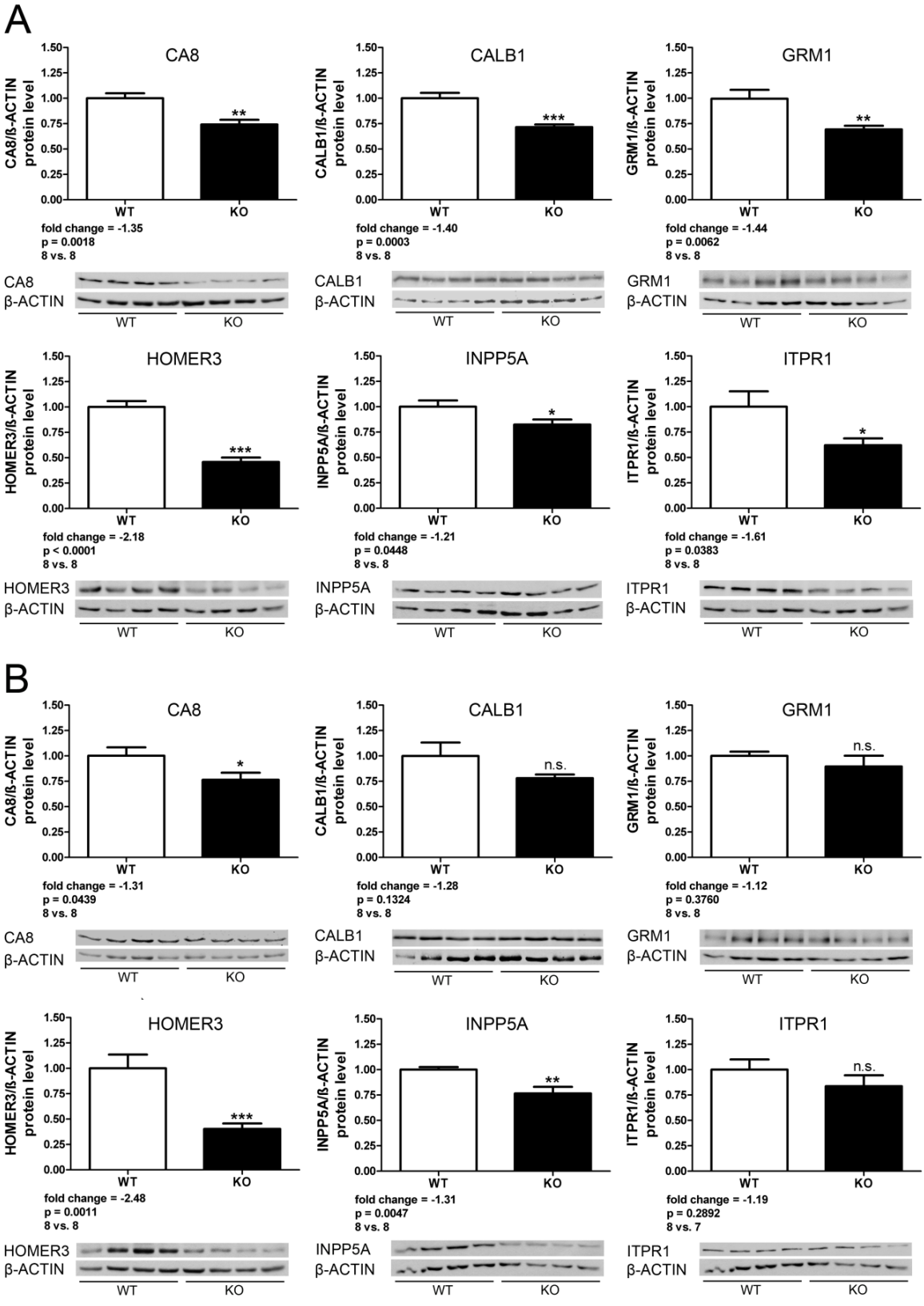

Figure 24. Downregulation of calcium homeostasis factors in Atxn2-KO mice. Protein levels of several calcium homeostasis factors were measured in cerebellum of 6-month-old WT vs. *Atxn2*-KO mice. In the RIPA-soluble fraction (A) all proteins were significantly downregulated while in the SDS-soluble fraction (B) only CA8, HOMER3, and INPP5A showed a significant decrease***.***

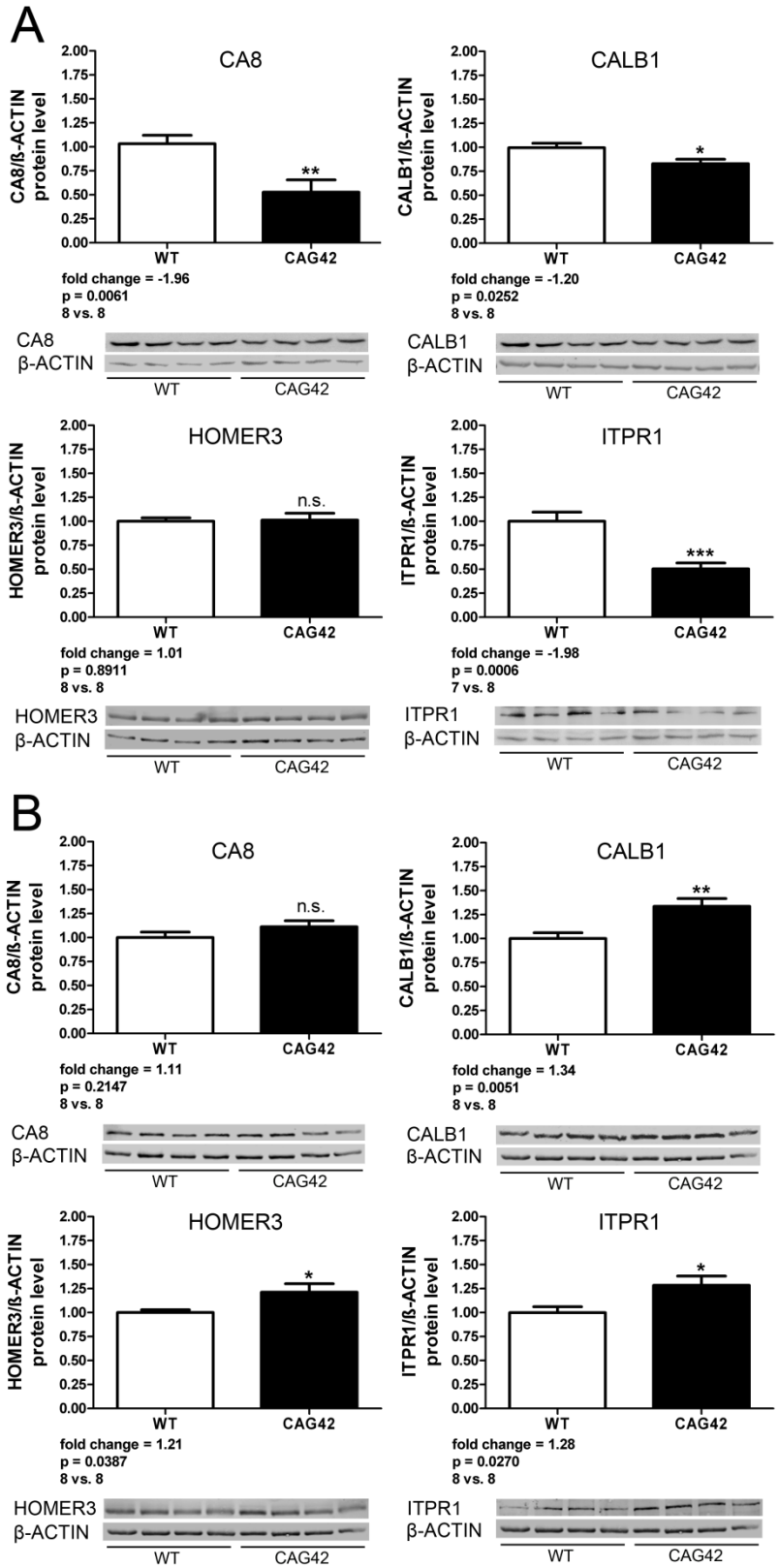

Figure 25. Calcium homeostasis factors shift into insolubility in Atxn2-CAG42-KIN mice. Protein levels in cerebellum of 18-month-old WT and *Atxn2*-CAG42-KIN were measured via quantitative immunoblots. (A) CA8, CALB1, and ITPR1 were significantly downregulated in the RIPA-soluble fraction while HOMER3 remained unchanged. (B) Significant accumulation of CALB1, HOMER3, and ITPR1 in the SDS-soluble fraction of *Atxn2*-CAG42-KIN mice.

3.2.9 ITPR1 interacts with WT and mutant ATXN2 in *Atxn2*-CAG42-KIN mice

Previously, a protein interaction between ITPR1 and expanded ATXN2 was reported in transgenic SCA2 mice to occur exclusively after polyQ expansion (Liu et al., 2009). In the *Atxn2*-CAG42-KIN mouse, ITPR1 is the first downregulated transcript and its protein seems to be sequestered into insolubility by ATXN2. Interestingly, ITPR1 abundance was changed also in the *Atxn2*-KO cerebellum in the absence of polyQ expansion. Therefore, the interaction of the two proteins was investigated further. Cerebellum of 18-month-old WT and *Atxn2*-CAG42-KIN mice was employed for Co-IP analysis. Immunoprecipitation was either conducted with anti-ATXN2 (Figure 26 A) or with anti-ITPR1 (Figure 26 B). Independent of the pulling antibody, the bait proteins were detected in the input as well as in the Co-IP lanes with a slightly higher band for expanded ATXN2. Bands for the respective interacting prey proteins appeared in both approaches independent of the ATXN2 polyQ length. In the control lanes, none of the proteins showed a band. Furthermore, when pulling with anti-ITPR1, its known interactor protein CA8 was detected in the Co-IP lane, confirming this association in WT and *Atxn2*-CAG42-KIN mice. The data demonstrate that the interaction between ITPR1 and ATXN2 does not depend on the CAG repeat length in *Atxn2*-CAG42-KIN mice and that ITPR1 relation to CA8 is not disturbed by expanded ATXN2.

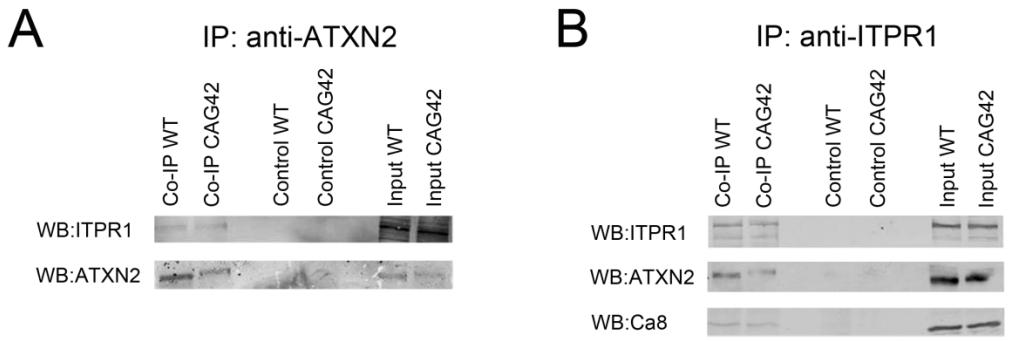

Figure 26. Immunoprecipitation of a complex including ATXN2, ITPR1, and CA8. In cerebellar tissue of 18-month-old WT and *Atxn2*-CAG42-KIN animals, pulling with anti-ATXN2 resulted in the co-immunoprecipitation of ITPR1 (A). When anti-ITPR1 was used for pulling, ATXN2 as well as the ITPR1 interactor CA8 were detected as prey proteins (B). Interaction of the proteins was independent of the ATXN2 polyQ length in both approaches.

3.2.10 ATXN2 polyQ expansion does not visibly change ITPR1 localization in Purkinje neurons

Given that the interaction of ATXN2 with ITPR1, as well as the sequestration of ITPR1 into insolubility have already been shown the question remained whether this sequestration

results in a visible change of ITPR1 localization. To study this aspect immunohistochemical stainings were performed in *Atxn2*-CAG42-KIN mice. Sagittal brain slices of 24-month-old WT and *Atxn2*-CAG42-KIN mice were stained with ATXN2 and ITPR1 antibodies in a double fluorescence approach.

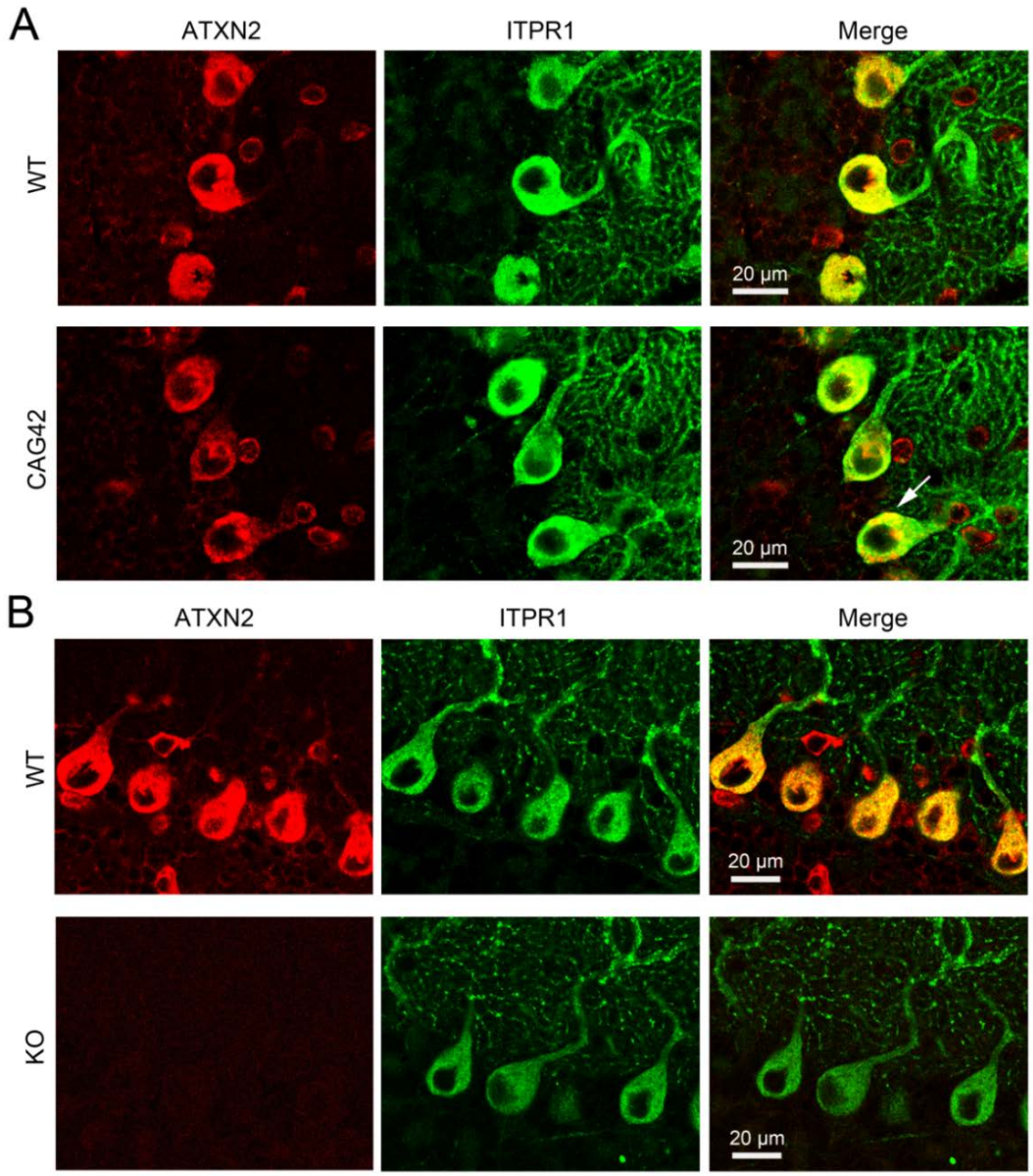

Figure 27. ATXN2 and ITPR1 co-localize in WT and Atxn2-CAG42-KIN brain slices. Paraffin-embedded brain slices from WT and *Atxn2*-CAG42-KIN mice at 24 months of age (A) or from WT and *Atxn2*-KO mice at 6 months of age (B) were double stained with ATXN2 (red) and ITPR1 (green). The two proteins co-localized in WT and mutant mice but ITPR1 localization remained unchanged in *Atxn2*-CAG42-KIN mice (where ATXN2 was aggregated) and *Atxn2*-KO mice (where no ATXN2 was detected).

Figure 27 A illustrates that ITPR1 is distributed all over the cytoplasm of the cell body and also in the dendrites in both mice while ATXN2 is mostly located in the cytoplasm of the cell body and exhibits slight aggregation in *Atxn2*-CAG42-KIN mice. The overlay reveals a co-localization of WT and expanded ATXN2 with ITPR1 as predicted. However, ITPR1 does not change visibly its localization in *Atxn2*-CAG42-KIN compared to WT mice.

Similar results were obtained when ATXN2 and ITPR1 were co-stained in *Atxn2*-KO mice: ITPR1 localization was not altered due to ATXN2 loss (Figure 27 B). Thus, ITPR1 co-localizes with WT and mutant ATXN2 but does not show visible aggregates like expanded ATXN2 or altered localization.

3.3 Loss of Atxn2 influences translation regulation

3.3.1 Microarray transcriptome profiling reveals changes in translation regulation transcripts

Translation regulation is one of the main functions ATXN2 has been implicated in. The microarray transcriptome analysis of *Atxn2*-KO mice, described in section 3.2.1, detected not only cerebellum-specific calcium homeostasis dysregulations but also tissue-independent transcriptional changes in genes involved in translation regulation. Several of these transcripts were significantly upregulated in cerebellum and liver of *Atxn2*-KO mice (Fittschen et al., in press). From 73 transcripts that showed significant upregulation in both tissues and at both analyzed ages (data not shown) 23 were involved in translation regulation (Supplementary Table 3). Among them were 17 components of the small and large ribosomal subunit (five of them detected at more than one oligonucleotide spots), a eukaryotic translation initiation and an elongation factor (*Eif2s2, Eef1g*), an interactor of the polyA binding protein (*Paip1*), a ribonucleoprotein involved in ribosome biogenesis (*Nop10*; detected at two individual oligonucleotide spots) and a G protein involved in translational repression (*Gnb2l1*). Several of the upregulated transcripts (e.g. *Rps3, Rps10, Rps15, Rpl13, Rpl23*) were also detected among the 100 most upregulated transcripts in the RNAseq (Supplementary Figure 3). The upregulation of most of these transcripts was confirmed using real-time RT-qPCR (data not shown). In conclusion, these data indicate a consistent upregulation of translation factors on transcript level induced by loss of Atxn2.

3.3.2 Translation regulation factors are increased on protein level in *Atxn2*-KO mice

To study the cause or consequences of these transcriptional upregulations protein levels of NOP10 (Nucleolar protein 10), RPS3, RPS6, RPS10, RPS18 (Ribosomal proteins 3, 6, 10, and 18), and GNB2L1/RACK1 (Guanine nucleotide binding protein; component of the 40S ribosomal subunit) were determined in liver tissue of 6-month-old animals.

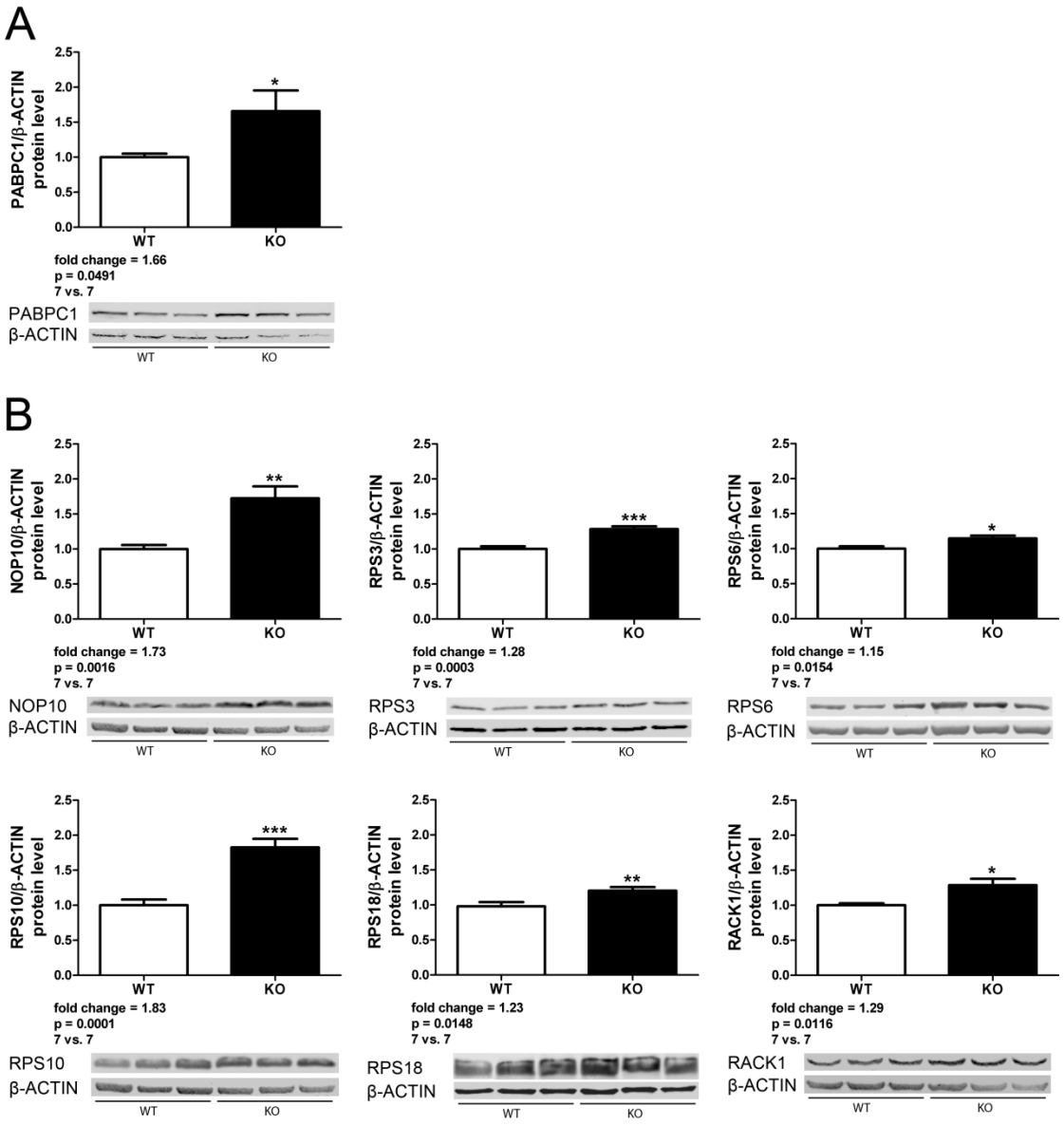

Figure 28. Proteins involved in translation regulation are increased in Atxn2-KO mice. In liver of *Atxn2*-KO mice at 6 months of age, protein levels were increased in the RIPA-soluble fraction for PABPC1 (A) and in the SDS-soluble fraction for NOP10, RPS3, RPS6, RPS10, RPS18, and RACK1 (B).

The selection of proteins was thereby depending on the availability of specific antibodies. Although the ATXN2 interactor *Pabpc1* was not found in the microarray or RNAseq, an upregulation was observed via RT-qPCR (data not shown). Moreover, a change of Pabpc1 transcript and protein level was already assessed in *Atxn2*-CAG42-KIN mice

(Damrath et al., 2012). Therefore, levels of PABPC1 were investigated as well. While a signal strong enough for quantification was only detectable in the RIPA-soluble fraction for PABPC1 in *Atxn2*-KO liver, the remaining six proteins were only measurable in the SDS-soluble fraction. All seven proteins were significantly upregulated (Figure 28). RPS10 (1.83-fold; $p = 0.0001$), NOP10 (1.73-fold; $p = 0.0016$), and PABPC1 (1.66-fold; $p = 0.0491$) showed the strongest upregulation while RPS3 (1.28-fold; $p = 0.0003$), RPS6 (1.15-fold; $p = 0.0154$), RPS18 (1.23-fold; $p = 0.0148$), and RACK1 (1.29-fold; $p = 0.0116$) exhibited a more subtle increase. The results suggest that a loss of Atxn2 increases the presence of ribosomal and translation-associated proteins mostly in the SDS-soluble fraction which contains many ER-associated ribosomes.

3.4 The role of TBC1 domain family members

3.4.1 Microarray profiling reveals dysregulation of TBC1 domain family members in *Atxn2*-KO and *Tia1*-KO mice

TBC1 (Tre-2/Bub2/Cdc16) domain family members have been shown to be affected in several mouse models of genes involved in neurodegenerative diseases and/or stress response. For example, a deletion of TDP43 decreased *Tbc1d1* levels in ES cells (Chiang et al., 2010), while overexpression of this gene increased *Tbc1d1* levels in skeletal muscle (Stallings et al., 2013). Applying Affymetrix microarray transcriptome profiling in *Tia1*-KO mice, a cluster of transcripts involved in lipid storage and membrane trafficking was revealed (Supplementary Table 4) (Heck et al., 2014). Among these transcripts was also a TBC1 domain family member named *Tbc1d24* that was upregulated (two oligonucleotide spots) in cerebellum. Furthermore, in the transcriptome data of *Atxn2*-KO mice (Supplementary Table 3), several TBC1 domain family members (*e.g. Tbc1d8b* and *Tbc1d9b*) appeared as downregulated. Due to the dysregulation of TBC1 domain family members in several mouse models whose mutated genes in interaction, a relevance of this gene family for stress response and neurodegenerative processes was postulated.

3.4.2 Slight downregulation of four TBC1 domain family members in *Atxn2*-KO brain

To validate the results of the whole-genome analysis, real-time RT-qPCR of *Tbc1d1*, *Tbc1d8b*, *Tbc1d9b,* and *Tbc1d24* was performed in cerebellum of 6-month-old WT and *Atxn2*-KO mice. *Tbc1d8b* and *Tbc1d9b* (transcripts found in *Atxn2*-KO microarray study) were significantly downregulated at this age and also in HOM animals at 6 weeks of age (Table 48). Surprisingly, *Tbc1d1* and *Tbc1d24* displayed significant downregulation in HOM and HET animals at 6 weeks of age but no regulation at any other age in cerebellum. In cortical tissue of 6-month-old animals only *Tbc1d24* was decreased while the other transcripts did not exhibit a dysregulation. In general, fold changes were rather low for all transcripts and none of the transcripts showed early downregulation in 3-day-old animals.

Given that similar transcriptional changes had been found in *Atxn2*-KO and *Atxn2*-CAG42-KIN mice before, TBC1 domain family members were also analyzed in the latter one. However, transcript analysis did not reveal any consistent changes for *Tbc1d1*, *Tbc1d8b*, and *Tbc1d9b*. Only *Tbc1d24* was significantly downregulated in cerebellum of 6-week- and 6-month-old mice but not in older animals (Supplementary Table 5). In conclusion, transcript levels of TBC1 domain family members are also dysregulated in *Atxn2* mouse models but less consistent than many other transcripts and, therefore, were not further studied.

Table 48. Transcript level changes of TBC1 domain family members in Atxn2-KO animals. Transcript levels were analyzed via real-time RT-qPCR in cerebellar and cortical tissue of 6-month-old WT and HOM animals as well as in cerebellum of 6-week-old WT vs. HET and WT vs. HOM animals and in 3-day-old WT vs. HET mice (n = 3-9 WT, 4-6 HET and 3-7 HOM mice).

Gene symbol	WT vs. HOM Cb 6 months	WT vs. HOM Cx 6 months	WT vs. HOM Cb 6 weeks	WT vs. HET Cb 6 weeks	WT vs. HET Cb 3 days
Tbc1d1	-1.06-fold *n.s.*	+1.02-fold *n.s.*	-1.05-fold *	-1.10-fold ***	-1.04-fold *n.s.*
Tbc1d8b	-1.38-fold **	-1.06-fold *n.s.*	-1.33-fold *	-1.09-fold *n.s.*	+1.03-fold *n.s.*
Tbc1d9b	-1.10-fold *	-1.09-fold *n.s.*	-1.14-fold *	-1.12-fold **	-1.06-fold *n.s.*
Tbc1d24	-1.08-fold *n.s.*	-1.26-fold *	-1.16-fold ***	-1.14-fold **	-1.04-fold *n.s.*

3.5 Ataxia genes influence each other's expression

3.5.1 Scanning of 20 ataxia genes reveals three common dysregulated transcripts in *Atxn2*-KO and *Atxn2*-CAG42-KIN mice

Given that an interaction between ATXN2 and ATXN1 (SCA1) as well as ATXN2 and ITPR1 (SCA15) has already been shown, *Atxn2*-KO and *Atxn2*-CAG42-KIN mice were investigated looking for transcriptional changes of other ataxia genes. Such changes could give a hint for new interaction partners that might influence SCA2 pathology and implicate them in a common pathway. Employing real-time RT-qPCR for 20 different ataxia genes in 6-month-old *Atxn2*-KO and 18-month-old *Atxn2*-CAG42-KIN mice, only three transcripts were found to be dysregulated in both mouse lines (Supplementary Table 6). Among them were the already known interaction partners *Atxn1* (SCA1) and *Itpr1* (SCA15) that were both downregulated in the two mouse models (Table 49). The third transcript was *Bean1* (SCA31) which was decreased in *Atxn2*-KO and increased in *Atxn2*-CAG42-KIN mice. Alterations in *Atxn3* (SCA3) were limited to *Atxn2*-KO and dysregulation of *Afg3l2* (SCA28) to *Atxn2*-CAG42-KIN cerebellum. In brief, a preliminary survey for possible ataxia gene interaction partners revealed the already known interactors *Atxn1* and *Itpr1* as well as *Bean1*.

Table 49. Transcriptional changes of ataxia genes in both Atxn2 mouse models. Transcript analysis via real-time RT-qPCR in cerebellum of 6-month-old *Atxn2*-KO and 18-month-old *Atxn2*-CAG42-KIN animals revealed only three transcripts significantly dysregulated in both mouse models (n = 8-10 WT vs. 7-8 HOM in *Atxn2*-KO and 8 WT vs. 8 HOM in *Atxn2*-CAG42-KIN animals).

Gene symbol	***Atxn2*-KO** **WT vs. HOM** **Cb 6 months**	***Atxn2*-CAG42-Kin** **WT vs. HOM** **Cb 18 months**
Atxn1 (SCA1)	↓ *	↓ *
Itpr1 (SCA15)	↓ *	↓ *
Bean1 (SCA31)	↓ *	↑ *

3.5.2 Temporal and tissue dependency of *Atxn1* and *Bean1* transcript level changes

In order to get a deeper insight into the temporal and spatial occurrence of SCA transcript level changes in Atxn2 mouse models, different ages and tissues were analyzed. Given that *Itpr1* had already been studied as a calcium homeostasis factor, only *Atxn1* and *Bean1* remained to be investigated. In cerebellar tissue of 6-month-old *Atxn2*-KO mice

Atxn1 showed a downregulation of -1.29-fold while *Bean1* was downregulated by -1.18-fold (Table 50, left part). At the same age in cortical tissue, both transcripts showed higher fold changes, however, these changes were not significant due to high standard deviations. In cerebellum from 6-week-old *Atxn2*-KO mice downregulation of *Atxn1* and *Bean1* was already detectable but not in HET pups aged ~3 days (Table 50, right part).

Table 50. Age and tissue dependency of Atxn1 and Bean1 transcript dysregulations in Atxn2-KO mice. Transcript levels were measured via real-time RT-qPCR in cerebellar and cortical tissue of 6-month-old WT vs. HOM animals, as well as in cerebellum of 6-week-old WT vs. HOM and WT vs. HET animals and in 3-day-old WT vs. HET mice (n = 4-10 WT, 3-6 HET, and 3-8 HOM animals).

Gene symbol	WT vs. HOM Cb 6 months	WT vs. HOM Cx 6 months	WT vs. HOM Cb 6 weeks	WT vs. HET Cb 6 weeks	WT vs. HET Cb 3 days
Atxn1 (SCA1)	-1.29-fold *	-1.57-fold *n.s.*	-1.02-fold *n.s.*	-1.16-fold *	+1.01-fold *n.s.*
Bean1 (SCA31)	-1.18-fold *	-1.25-fold *T*	-1.18-fold **	-1.08-fold *n.s.*	-1.03-fold *n.s.*

In the *Atxn2*-CAG42-KIN mice at 18 months of age *Atxn1* was downregulated by -1.15-fold while *Bean1* was upregulated by 1.51-fold (Table 51). In contrast to the *Atxn2*-KO mice, the dysregulation of *Bean1* persisted in cortical tissue while no regulation was measurable for *Atxn1.* In younger animals, *Atxn1* was not significantly downregulated. *Bean1* showed a downregulation at 6 weeks of age, however, no significant regulation was observed at 6 months of age. Thus, there seems to be a development in the transcript level change of *Bean1* from being decreased (6 weeks) to being increased (18 months) that was not observed in *Atxn2*-KO mice. Furthermore, *Atxn1* displayed more pronounced effects in *Atxn2*-KO mice while *Bean1* exhibited stronger dysregulation in *Atxn2*-CAG42-KIN mice. In conclusion, these results highlight a temporal dynamic in the transcript level changes of *Atxn1* and *Bean1* in both mouse models. Nevertheless, while *Bean1* transcript levels are altered similar to *Atxn1* in *Atxn2*-KO mice they change from downregulated to upregulated in *Atxn2*-CAG42-KIN animals with age. Furthermore, tissue dependency is not definite in *Atxn2*-KO for both transcripts but seems to exist at least for *Atxn1* in *Atxn2*-CAG42-KIN mice.

Table 51. Age and tissue dependency of Atxn1 and Bean1 transcript changes in Atxn2-CAG42-KIN mice. Transcript regulation was studied using real-time RT-qPCR in cerebellum of WT vs. HOM animals between 6 weeks and 18 months of age and in cortex at 18 months of age (n = 4-8 WT vs. 3-8 HOM animals).

Gene symbol	WT vs. HOM Cb 18 months	WT vs. HOM Cx 18 months	WT vs. HOM Cb 6 months	WT vs. HOM Cb 6 weeks
Atxn1 (SCA1)	-1.15-fold *	-1.03-fold *n.s.*	-1.19-fold *T*	-1.06-fold *n.s.*
Bean1 (SCA31)	+1.51-fold *	+1.16-fold *	+1.02-fold *n.s.*	-1.09-fold *

3.5.3 Accumulation of ATXN1 in the insoluble fraction of *Atxn2*-CAG42-KIN mice

In a next step, protein levels were analyzed via immunoblots as transcript levels do not give any information about the status of the proteins. BEAN1 is not a well-studied protein and it was difficult to obtain a specific antibody. Thus, only ATXN1 levels were measured in *Atxn2*-KO and *Atxn2*-CAG42-KIN mice.

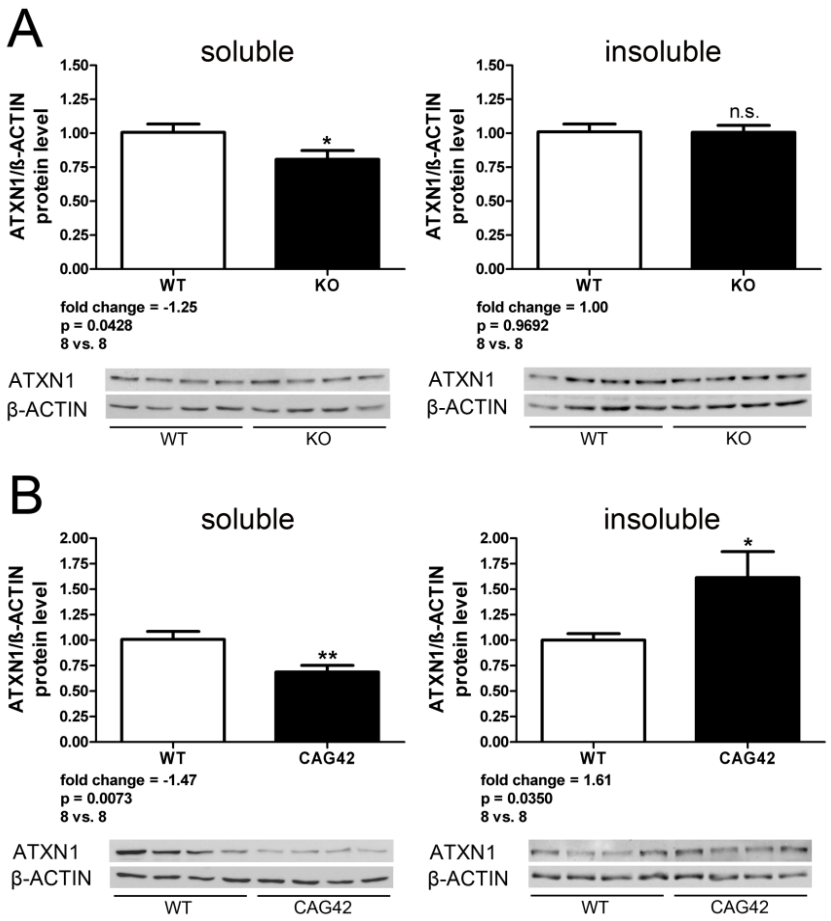

Figure 29. ATXN1 is decreased in Atxn2-KO but accumulates in Atxn2-CAG42-KIN cerebellum. Protein levels of ATXN1 were measured in cerebellum of 6-month-old WT vs. *Atxn2*-KO mice and 18-month-old WT vs. *Atxn2*-CAG42-KIN mice. (A) ATXN1 showed downregulation in the RIPA-soluble fraction of *Atxn2*-KO mice while no change was detected in the SDS-soluble fraction. (B) ATXN1 was also downregulated in the RIPA-soluble fraction of *Atxn2*-CAG42-KIN mice but accumulated in the SDS-soluble fraction.

As before, cerebellum of 6- and 18-month-old animals (*Atxn2*-KO and *Atxn2*-CAG42-KIN, respectively) was used for protein level determination in the RIPA-soluble and the SDS-soluble fraction. ATXN1 was downregulated in the RIPA-soluble fraction of *Atxn2*-KO (-1.25-fold; $p = 0.0428$) and *Atxn2*-CAG42-KIN (-1.47-fold; $p = 0.0073$) mice (Figure 29 A and B). In the SDS-soluble fraction, no change was observed in *Atxn2*-KO mice but a significant increase of 1.61-fold ($p = 0.0350$) was measurable in *Atxn2*-CAG42-KIN mice. The results suggest that similar to FBXW8 and some of the calcium homeostasis factors,

ATXN1 accumulates in the SDS-soluble fraction of *Atxn2*-CAG42-KIN mice, probably sequestered by ATXN2.

3.5.4 SCA2 skin fibroblasts exhibit similar Atxn1 expression changes as *Atxn2*-CAG42-KIN cerebellum

Given that Atxn1 is expressed in many cell types similar to Atxn2, SCA2 primary skin fibroblasts were used to assess the relevance of Atxn1 dysregulations for SCA2 pathology in humans. First, *ATXN1* transcript level was measured and revealed a reduction of -1.61-fold (p = 0.0059) in SCA2 fibroblasts (Figure 30 A). Then, protein levels of ATXN1 were determined in the RIPA-soluble and SDS-soluble fraction. As shown in Figure 30 B, ATXN1 was not significantly changed in the RIPA-soluble fraction while it was dramatically increased (3.4-fold; p = 0.0050) in the SDS-soluble fraction. In summary, Atxn1 is decreased on transcript level and accumulated in the SDS-soluble fraction on protein level in SCA2 fibroblasts; a regulation similar to that observed in *Atxn2*-CAG42-KIN mice.

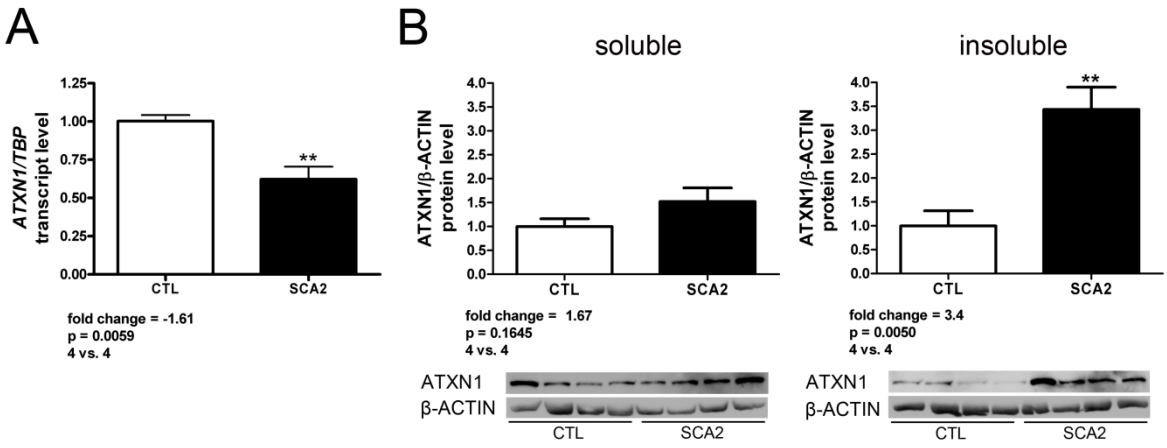

Figure 30. Atxn1 is decreased on transcript but increased on protein level in SCA2 patient fibroblasts. (A) Transcript levels of ATXN1 were measured in SCA2 patient skin fibroblasts vs. healthy controls (CTL) via RT-qPCR. ATXN1 showed a significant decrease in fibroblasts of SCA2 patients. (B) ATXN1 protein levels determined by quantitative immunoblots exhibited a small but not significant increase in the RIPA-soluble fraction as well as a significant and drastic increase in the SDS-soluble fraction of SCA2 patient fibroblasts.

3.5.5 ATXN2 accumulates in *Atxn1*-Q154-KIN mice like ATXN1 does in *Atxn2*-CAG42-KIN mice

Since an effect of Atxn2 loss and mutation on Atxn1 transcript and protein levels was observed, the question remained if this effect also exists *vice versa*. Thus, to evaluate the interaction between Atxn2 and Atxn1 from the other side, *Atxn1*-Q154-KIN mice were used to study transcript and protein level changes of Atxn2. In cerebellum of 10-week-old

Atxn1-Q154-KIN mice *Atxn2* was downregulated by -1.12-fold (Table 52). Furthermore, as in SCA2 mice, *Bean1* was analyzed and showed a downregulation (-1.48-fold) that is similar to *Atxn2*-KO but contrary to *Atxn2*-CAG42-KIN mice.

Table 52. Transcripl changes of Atxn2 and Bean1 in Atxn1-Q154-KIN cerebellum. Transcript levels were measured in 10-week-old WT vs. HOM cerebellum using real-time RT-qPCR (n = 3-7 WT vs. 4-8 HOM mice).

Gene symbol	WT vs. HOM Cb 10 weeks
Atxn2 (SCA2)	-1.12-fold **
Bean1 (SCA31)	-1.48-fold **

On protein level, ATXN2 was upregulated in both, the RIPA-soluble and SDS-soluble fraction (1.16-fold; $p = 0.0479$ and 1.53-fold; $p = 0.0037$, respectively) suggesting a sequestration of the protein by ATXN1 (Figure 31). Despite the apparent accumulation of ATXN2, no ATXN2 aggregates were detected in immunohistochemical stainings of 20-week-old *Atxn1*-Q154-KIN mice (Supplementary Figure 4). In conclusion, similar to Atxn1 in the SCA2 mouse model, Atxn2 is decreased on transcript level and accumulates on protein level in the SDS-soluble fraction in the SCA1 mouse model suggesting a mutual interaction of the two proteins in disease state.

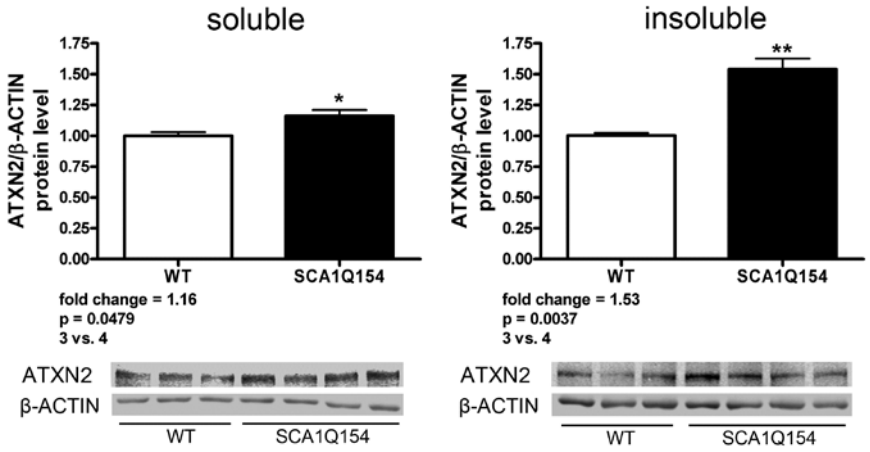

Figure 31. Accumulation of ATXN2 in Atxn1-Q154-KIN mice. Protein levels of ATXN2 were quantified via immunoblots in cerebellum of 10-week-old WT vs. *Atxn1*-Q154-KIN mice. In both, the RIPA-soluble and the SDS-soluble fraction, ATXN2 showed a significant increase suggesting a strong accumulation of this protein.

Part 2: Characterization of two new mouse models

The second part of this work is about the behavioral, molecular, and immunohistochemical characterization of two mouse models for neurodegenerative diseases. The first mouse

model is a double mutant of the formerly described *Atxn2*-CAG42-KIN and hTDP43-A315-KIN models (Damrath et al., 2012; Stribl et al., 2014). In this mouse model particularly the behavior was studied to look for a potentiation effect of the two mutations. The second mouse model, *Atxn2*-CAG100-KIN, is completely new and has not been published yet. Similar to the *Atxn2*-CAG42-KIN mouse, it harbors a CAG repeat expansion in the *Atxn2* gene but this time more than twofold longer. The enlarged repeat was expected to accelerate disease onset and intensify the symptoms facilitating the investigation of SCA2 pathology and possible therapeutics. This mouse model was studied extensively, starting with sequencing for repeat confirmation, several behavioral studies, molecular characterization, and immunohistochemical documentation with various markers.

3.6 The *Atxn2*-CAG42-KIN / hTDP43-A315T-KIN double mutant

3.6.1 Consistent weight changes in female Atxn2 single but not in double mutants

To study the effect of the two mutations on the body weight - a parameter already altered in young *Atxn2*-CAG42-KIN animals - mice were weighed at 6, 9, and 12 months of age. Female and male animals were separated due to known gender-specific differences in weight. *Atxn2*$^{+/+}$ / hTDP43$^{+/+}$ (WT/WT) were always compared to the single mutants *Atxn2*$^{+/+}$ / hTDP43$^{+/A315T}$ (WT/HET) and *Atxn2*$^{CAG42/CAG42}$ / hTDP43$^{+/+}$ (HOM/WT) as well as to *Atxn2*$^{CAG42/CAG42}$ / hTDP43$^{+/A315T}$ (HOM/HET) double mutants at the same age. Furthermore, single mutants were compared to double mutants. Weight data were analyzed via one way ANOVA with Bonferroni correction. The average weight of female animals of all four genotypes is depicted in Figure 32. Results for male mice are not shown here (Supplementary Figure 5) due to an even lower number of animals per genotype and subsequent lower statistical significance as well as lack of consistency. In contrast to former analyses (Damrath et al., 2012), *Atxn2*-CAG42-KIN single mutants showed an increased weight at 9 and 12 months of age compared to WT. The body weight of hTDP43-A315T-KIN single mutants versus WT was not changed (no statistics at 12 months of age due to low number of animals). Comparing single and double mutants no change was observed when applying an ANOVA. However, when HOM/WT and HOM/HET were compared in a separated analysis using Student's t-test, a trend was noted in 6-month-old animals and a significantly lower weight for HOM/HET mice was

detected at 9 and 12 months of age. In brief, these data indicate that while the mutation of *Atxn2* leads to a weight increase in the single mutants the additional mutation in TDP43 inhibits this weight gain in female double mutants however without reaching statistical significance compared to the single mutants when applying ANOVA.

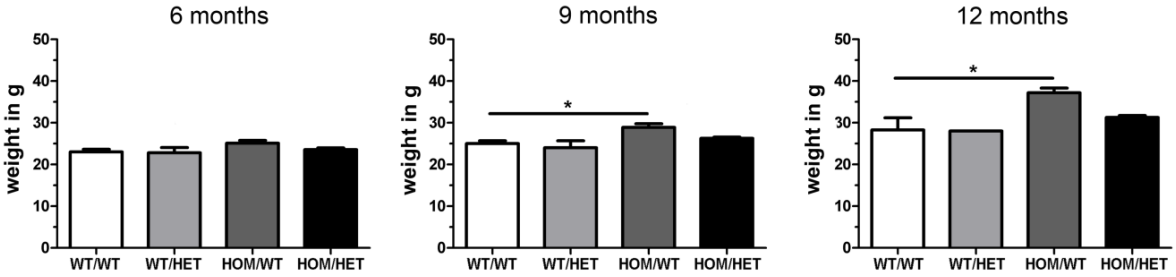

Figure 32. Body weight analyses in female Atxn2-CAG42-KIN / hTDP43-A315T-KIN mice. Body weight was measured at 6, 9, and 12 months of age in WT, single, and double mutants. At 9 and 12 months of age, *Atxn2*-CAG42-KIN single mutants were significantly heavier than WT animals, while this weight increase was rescued partially but not significantly by the additional TDP43 mutation in double mutants. WT/HET mice at 12 months of age were excluded from analyses due to the low number of animals (n (6 months) = 8 WT/WT, 5 WT/HET, 10 HOM/WT, and 19 HOM/HET; n (9 months) = 8 WT/WT, 5 WT/HET, 8 HOM/WT, and 7 HOM/HET; n (12 months) = 4 WT/WT, 1 WT/HET, 5 HOM/WT, and 4 HOM/HET animals).

3.6.2 No impairment of rotarod performance in double mutants

Given that motor impairment is a typical feature in SCA2 and ALS, the motor performance of the double mutants was assessed via rotarod analysis. For this study 6-, 9-, and 12-month-old male and female mice of all four genotypes were employed. The latency to fall was measured and mean values are shown in Figure 33, analyzed via one way ANOVA with Bonferroni correction. At 6 months of age, the rotarod performance of *Atxn2*-CAG42-KIN mice was significantly decreased while double mutants performed similar to WT animals. Changes in 9- and 12-month-old *Atxn2*-CAG42-KIN animals did not reach significance despite the high number of animals used at 9 months of age ($p = 0.1531$ for 9 months and $p = 0.1001$ for 12 months). In conclusion, no potentiation of the two mutations was detected regarding rotarod performance. In contrast, at 6 months of age double mutants even performed slightly, but not significantly, better than Atxn2 single mutants (a trend was noted when analyzed separately via Student's t-test).

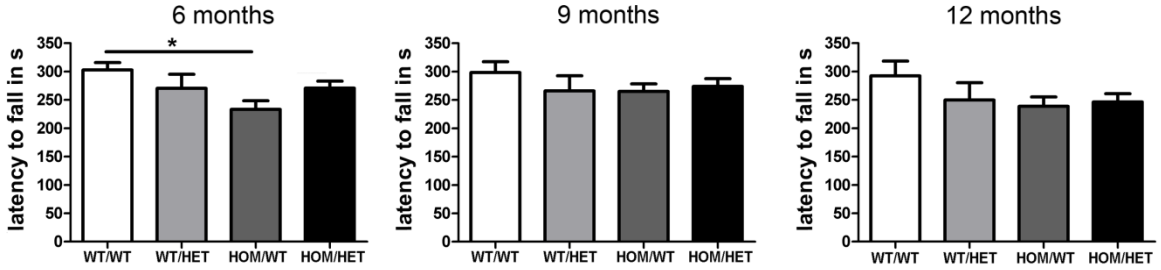

Figure 33. Rotarod performance of double mutants is not changed compared to WT animals. Latency to fall was determined in 6-, 9-, and 12-month-old animals of all genotypes. Significant changes were only documented at 6 months of age where *Atxn2*-CAG42-KIN mice performed worse while the performance of double mutants remained unchanged compared to WT (n (6 months) = 7 WT/WT, 6 WT/HET, 16 HOM/WT, and 15 HOM/HET; n (9 months) = 10WT/WT, 9 WT/HET, 18 HOM/WT, and 17 HOM/HET; n (12 months) = 5 WT/WT, 4 WT/HET, 11 HOM/WT, and 10 HOM/HET animals).

3.6.3 Reduced general locomotor activity in double mutants

The overall activity of double mutants was assessed using an open field apparatus to investigate the locomotor behavior of the mice. Animals of the same ages as before were employed and their activity was measured regarding 21 parameters. The data were analyzed via one way ANOVA with Bonferroni correction. Those parameters that were showing significant differences between the genotypes in 6-month-old animals are illustrated in Figure 34. At this age, no differences were observed between WT and TDP43 single mutants. In contrast, movement and rest time, the total distance mice travelled, vertical activity, vertical movement number, vertical time, and horizontal movement number were significantly altered when comparing WT to Atxn2 single mutants. Only the vertical parameters were significantly reduced in the double mutants compared to WT animals but a slight – even though not significant – decrease was observed for almost all depicted parameters. Regarding alterations between single and double mutants only one significant effect was observed when TDP43 mutation was added to Atxn2 mutation (Atxn2 single versus double mutants): a rescue of the horizontal movement number. However, it should be noted that most parameters showed a slight but not significant rescue effect of TDP43 mutation as well. In contrast, a deterioration of movement time, rest time, total distance travelled, vertical activity, and vertical movement number was noted when TDP43 single and double mutants were compared.

The similar task was conducted employing 9-month-old animals of all genotypes. As depicted in Figure 35, only vertical parameters were significantly altered at this age. Still, no difference was detected between WT and TDP43 single mutants. Atxn2 single as well as double mutants exhibited reduced vertical activity, vertical movement number, and vertical time compared to WT animals. It should be noted that for the remaining parameters, Atxn2 single and double mutants also displayed slightly but not statistically significant reduced activity. The activity of double mutants for all displayed parameters was either similar or slightly above that of Atxn2 single mutants. No rescue effect was detected (Atxn2 single vs. double mutants) and also no deterioration (TDP43 single vs. double mutants).

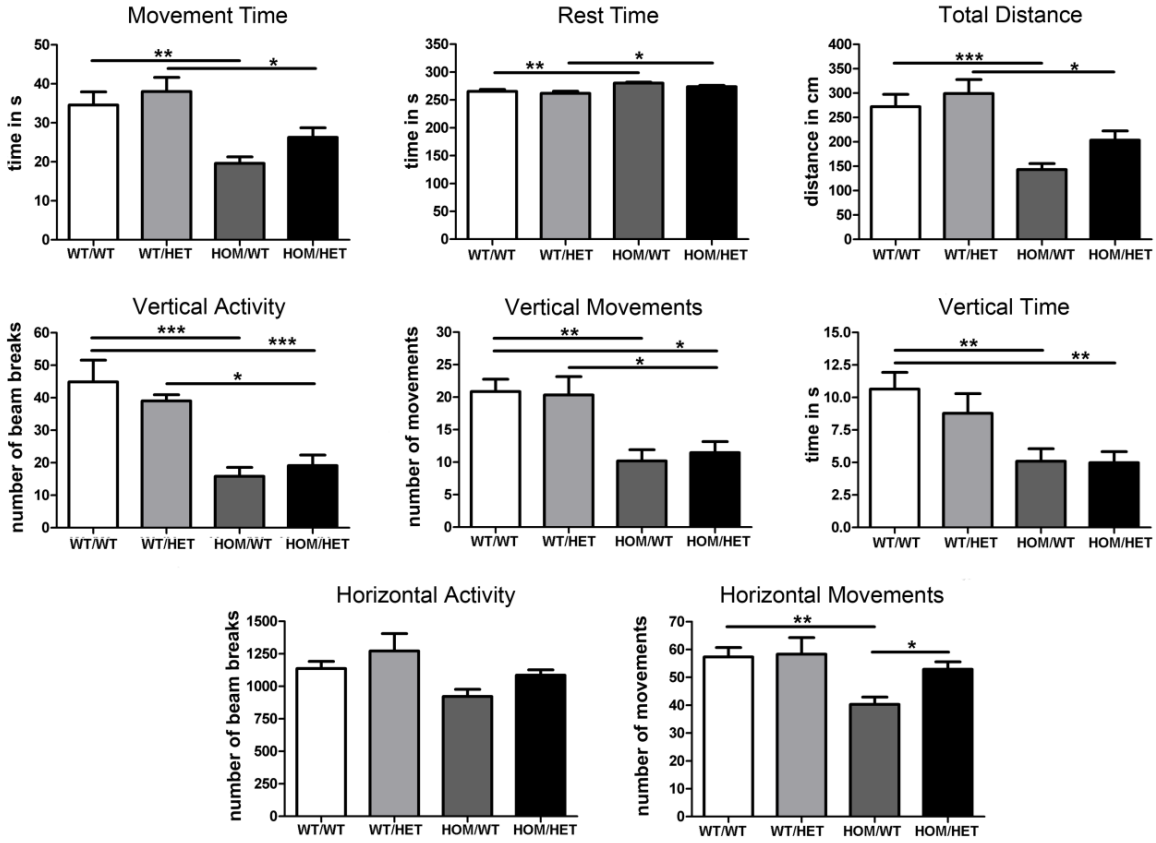

Figure 34. Open field analysis of 6-month-old double mutants indicates a slight rescue effect for TDP43 mutation. Open field performance of WT/WT, WT/HET, HOM/WT, and HOM/HET animals was assessed at 6 months of age. TDP43 single mutants did not differ from WT animals, while almost all movement parameters were significantly decreased in Atxn2 single mutants. Double mutants only showed decreased vertical parameters (n = 7 WT/WT, 6 WT/HET, 16 HOM/WT, and 15 HOM/HET animals).

At 12 months of age, again, several significant changes were detected between the four genotypes (Figure 36). Most striking is the significantly decreased activity of the double mutants displayed in all parameters when compared to WT animals. Between WT and Atxn2 single mutants, significance was observed for six out of the eight parameters: total distance the mice travelled, vertical activity, vertical movement number, vertical time, and horizontal movement number. As before, TDP43 single mutants did not differ from WT mice. However, comparing TDP43 single to double mutants, a reduced activity was observed for vertical parameters as well as for horizontal activity in double mutants. Double mutants were also slightly but not significantly less active than Atxn2 single mutants for most parameters.

Looking at the same parameter in each genotype at the three different ages, a slight decrease of the total distance travelled and a pronounced reduction of all vertical parameters as well as of horizontal movements was observed. This effect was independent of the genotype and may therefore be age related.

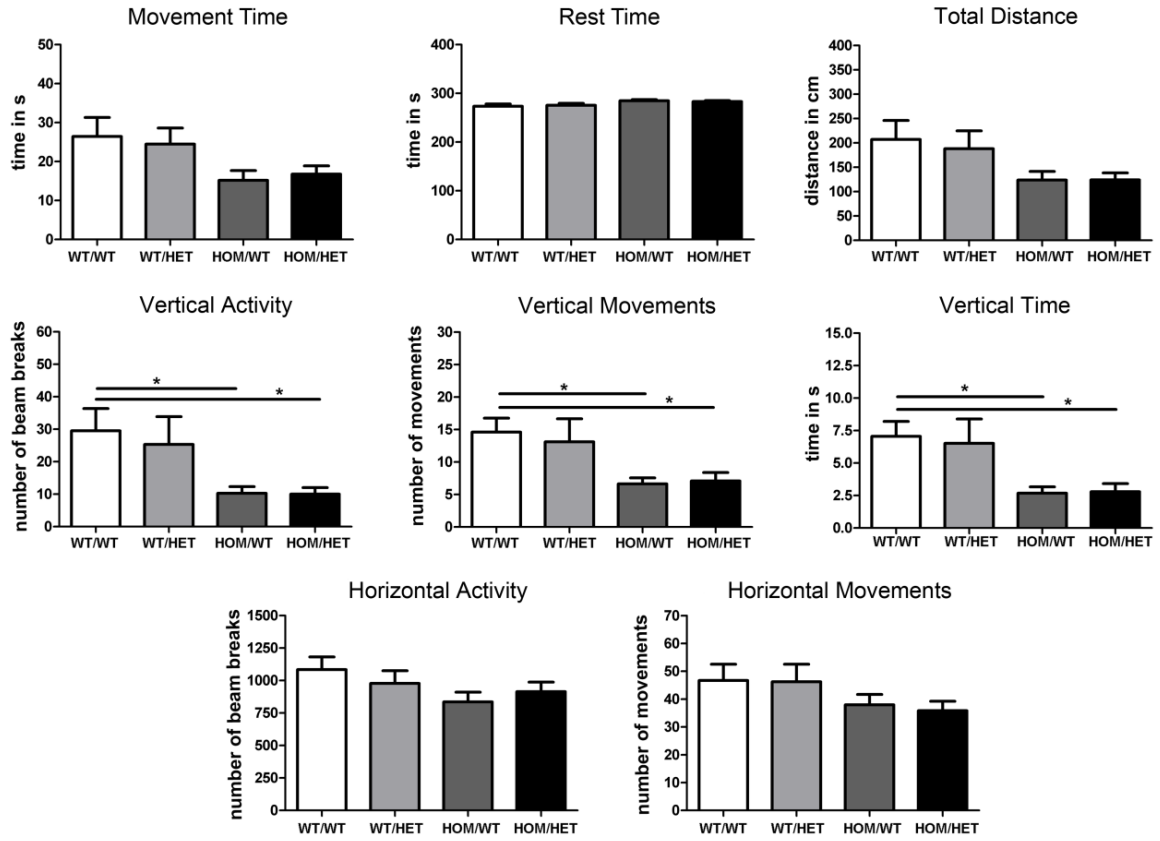

Figure 35. Open field analysis of 9-month-old double mutants only detects alterations in vertical parameters. Open field performance of WT/WT, WT/HET, HOM/WT, and HOM/HET animals at 9 months of age revealed only little significant changes. Vertical parameters were reduced for Atxn2 single and double mutants. None of the other parameters showed significant changes although there was a decrease of activity for Atxn2 single and double mutants in most of the remaining parameters (n = 10 WT/WT, 9 WT/HET, 14 HOM/WT, and 13 HOM/HET animals).

In summary, these data indicate that at 6, 9, and 12 months of age Atxn2 single and double mutants were less active than WT or TDP43 single mutants although this change was not always significant. TDP43 single mutants never differed from WT animals, while Atxn2 single mutants were always less active. In general, vertical parameters showed the most pronounced effects. At 6 months of age a slight rescue effect or a deterioration of the locomotor behavior was detected between double mutants and Atxn2 or TDP43 single mutants, respectively. This rescue effect was no longer present at later ages. Instead, the overall activity of double mutants decreased. Thus, Atxn2 mutation deteriorates the TDP43 single locomotor behavior at all ages, while TDP43 mutation seems to have a slight rescue effect at young but not at later ages referring to the Atxn2 single locomotor behavior.

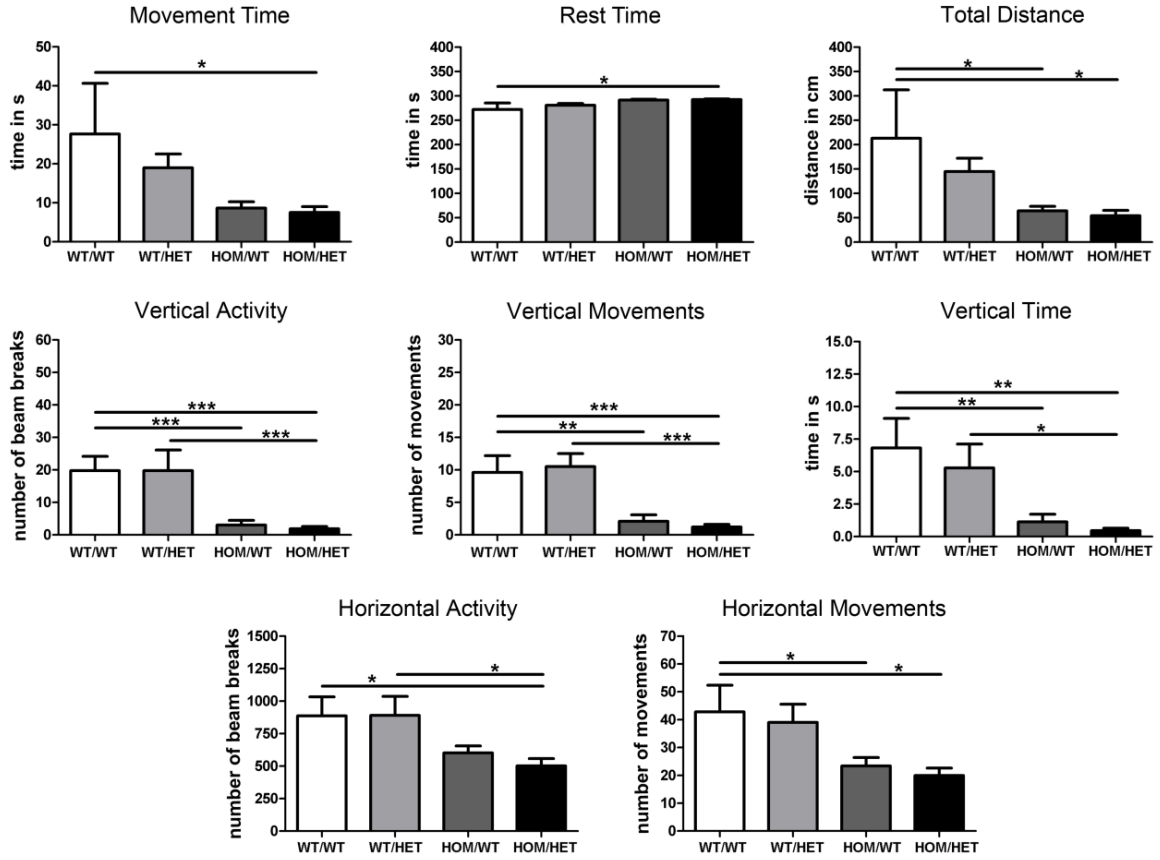

Figure 36. Open field analysis of 12-month-old double mutants displays strongly reduced overall activity of double mutants. Open field performance of WT/WT, WT/HET, HOM/WT, and HOM/HET animals was assessed at 12 months of age. TDP43 single mutants did not differ from WT animals. Atxn2 single and double mutants showed decreased activity for six and eight parameters, respectively. No difference was detected between these two genotypes (n = 5 WT/WT, 4 WT/HET, 11 HOM/WT, and 10 HOM/HET animals).

3.7 The *Atxn2*-CAG100-KIN mouse

3.7.1 Sequencing confirms CAG repeat expansion of *Atxn2*-CAG100-KIN mice

To genotype the founder animals and their offspring and for sequencing, DNA was extracted from tail biopsies. A PCR with primers flanking the Neo-excised *Atxn2* locus was applied for genotyping. This PCR resulted in a band of 793 bp for the WT (CAG1) and 948 bp for the KIN (CAG100) allele (Figure 37 A). In a second PCR, CAG repeat flanking primers were used to confirm the expanded CAG repeat resulting in a band of 94 bp for CAG1 and 400 bp for CAG100 (Figure 37 B). A sample from a heterozygous *Atxn2*-

CAG42-KIN mouse (CAG1/CAG42) was included in the study to compare the repeat lengths (217 bp for CAG42).

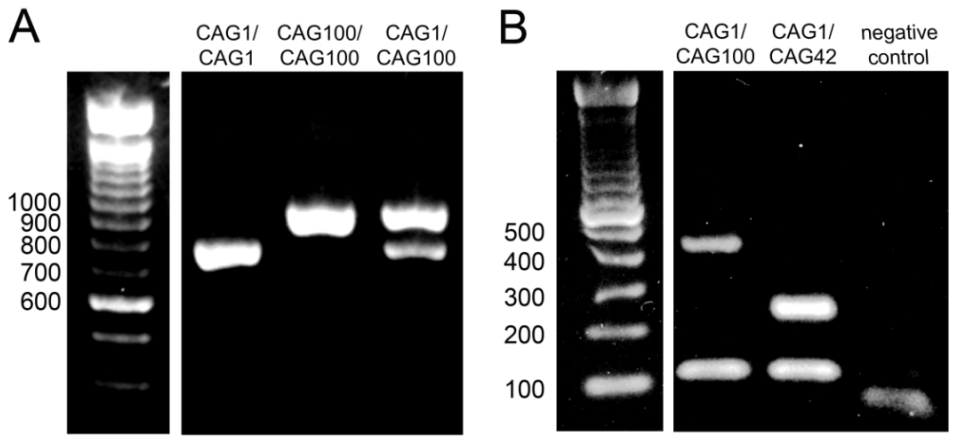

Figure 37. Genotyping and CAG repeat PCR in Atxn2-CAG100-KIN mice. PCRs were conducted with DNA isolated from tail biopsies. (A) A PCR with primers flanking the Neo-excised *Atxn2* locus was used for genotyping of *Atxn2*-CAG100-KIN mice. CAG1/CAG1 animals showed a band at 793 bp, CAG100/CAG100 at 948 bp and CAG1/CAG100 mice displayed both bands. (B) CAG repeat flanking primers were applied to amplify this section for subsequent sequencing. CAG1/CAG100 mice showed a PCR product with 94 bp (WT allele) and with 400 bp (KIN allele) while the product of the KIN allele of *Atxn2*-CAG42-KIN mice has only 217 bp.

The CAG100 PCR product was then ligated into a vector and sent to the company Seqlab for sequencing. Because long GC-rich sequences are not easy to clone and to sequence, several clones were sequenced. Figure 38 depicts the aligned sequence (A) and a section of the chromatogram (B) from forward sequencing of clone 22.1. The nucleotide transition in the forward primer was inserted during generation of the original vector for ES cell transfection. The CAG repeat shows no nucleotide exchanges or deletions. However, there is one nucleotide missing in the reverse primer sequence. Sequencing of another clone from the same animal did not show this missing nucleotide but had a nucleotide transition in the forward primer instead indicating that these changes were caused during the sequencing process. All together, the sequencing data confirm the expansion and correct sequence in *Atxn2*-CAG42-KIN founder mice.

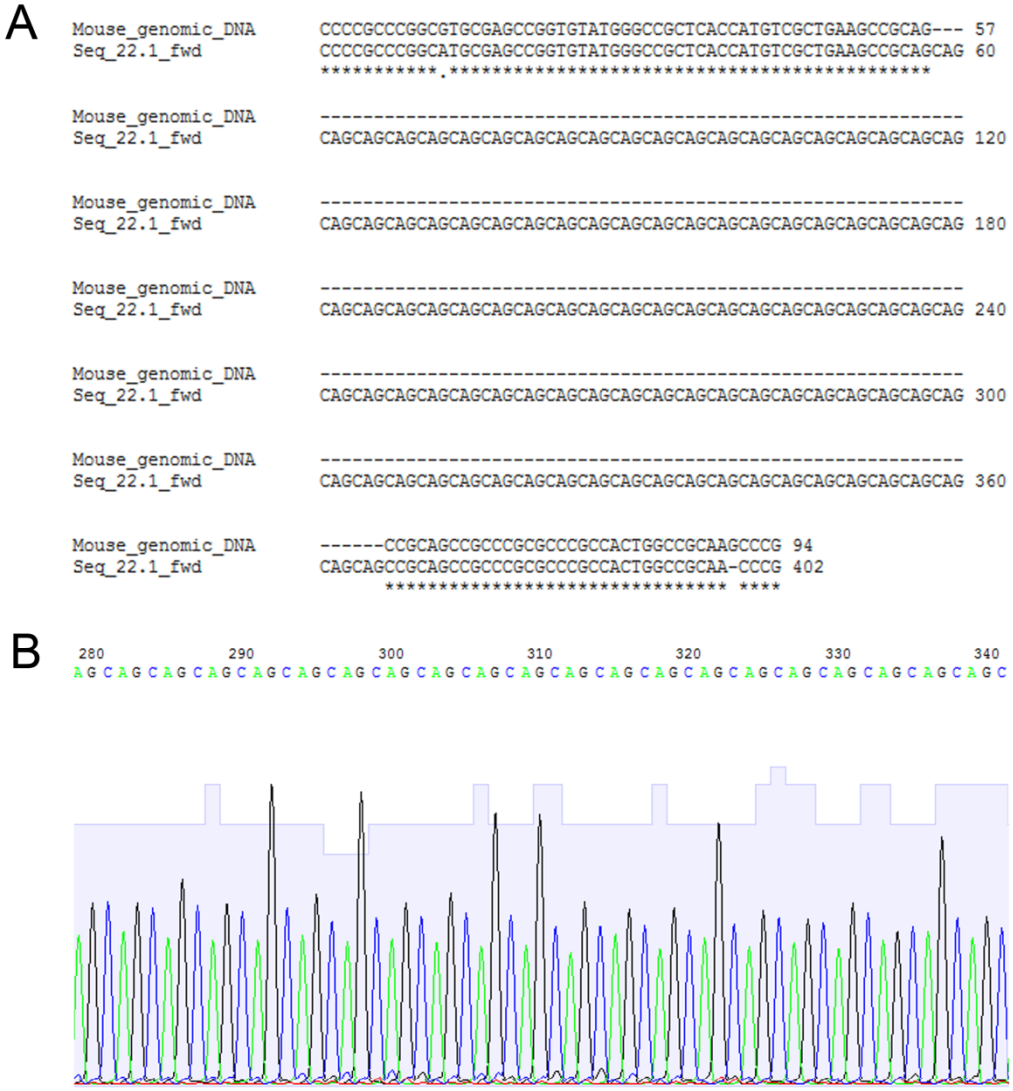

Figure 38. Sequencing confirms correct insertion of the CAG repeat in Atxn2-CAG100-KIN mice. (A) Forward sequencing of the PCR amplification product from clone 22.1 revealed correct insertion of the CAG repeat. The nucleotide transition in the forward primer sequence was included during the generation of the original vector. The second transition in the reverse primer sequence is a sequencing artifact and did not appear in another clone of the same founder animal. (B) Section of the chromatogram from clone 22.1 sequencing.

3.7.2 *Atxn2*-CAG100-KIN offspring shows expected genotype distribution but more male than female pups

To examine the breeding outcome of *Atxn2*-CAG100-KIN mice, 166 pups were analyzed regarding their genotype and sex using Chi Square Test. The mean number of pups per litter (heterozygous matings) was around nine. Table 53 shows that from 166 pups 39 were *Atxn2*$^{+/+}$ (WT), 89 *Atxn2*$^{CAG1/CAG100}$ (HET), and 38 *Atxn2*$^{CAG100/CAG100}$ (HOM) which is consistent with a normal Mendelian frequency of 1:2:1 (p = 0.6442; Chi Square test). In contrast, an equal amount of male and female animals was anticipated but with 96 male and 70 female pups (Table 53) there were significantly more male than female animals

born (p = 0.0436; Chi Square test). In brief, these analyses suggest that *Atxn2*-CAG100-KIN mice show normal breeding behavior except for a slight tendency towards more male pups.

Table 53. Genotype distribution among Atxn2-CAG100-KIN pups. The offspring of the four heterozygous founder breeding pairs was genotyped and the distribution of the genotypes was assessed via Chi Square test. Chi squared equaled 0.880 with 2 degrees of freedom and p = 0.6442 (n = 166).

Genotype	Counted No.	Expected No.	Expected %
CAG1/CAG1 (WT)	39	41.5	25
CAG1/CAG100 (HET)	89	83	50
CAG100/CAG100 (HOM)	38	41.5	25

Table 54. Gender distribution among Atxn2-CAG100-KIN pups. Sex of the founder breeding pairs' offspring was determined and expected distribution was analyzed. Chi squared equaled 4.072 with 1 degree of freedom and p = 0.0436 (n = 166).

Gender	Counted No.	Expected No	Expected %
Male	96	83	50
Female	70	83	50

3.7.3 *Atxn2*-CAG100-KIN mice have a reduced life span and significantly less weight

Since mutations in genes often reduce the lifetime of the respective animals, a survival curve for up to 20-week-old *Atxn2*-CAG100-KIN animals was generated. Therefore, 29 WT, 15 HET, and 28 HOM animals were studied regarding the occurrence of sudden cases of death. The analysis revealed that while none of the WT and only one HET animal died, 9 HOM mice passed way during the first 20 weeks (Figure 39). The results indicate that *Atxn2*-CAG100-KIN mice have a decreased life span with sudden fatal casualties occurring significantly more often in HOM than in WT animals.

Reduction of body weight due to loss of subcutaneous fat is quite prominent in SCA2 and has also been observed early in *Atxn2*-CAG42-KIN animals although these mice did not show any behavioral symptoms before 18 months of age. Therefore, a weight curve for *Atxn2*-CAG100-KIN mice was drafted. Male and female animals were separated for this analysis due to strong gender-specific differences (Figure 40 A and B).

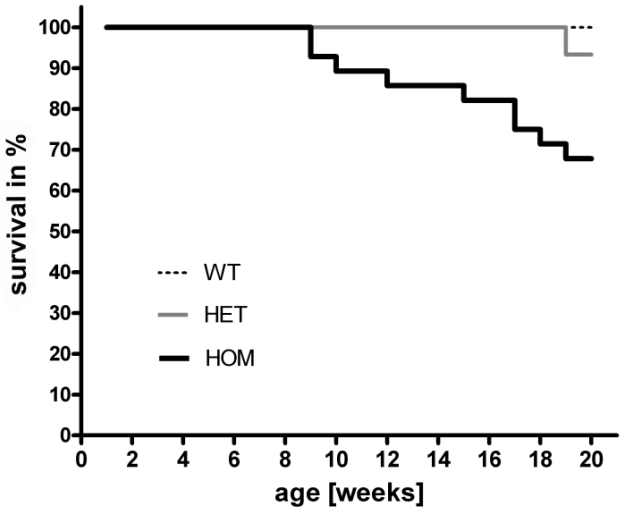

Figure 39. Survival curve of Atxn2-CAG100-KIN mice. For a time span of 20 weeks starting at birth WT, HET, and HOM animals were monitored regarding the occurrence of sudden death cases. In this time frame 0% of the WT, ~7% of the HET, and ~32% of the HOM animals died (n = 29 WT, 15 HET, and 28 HOM animals).

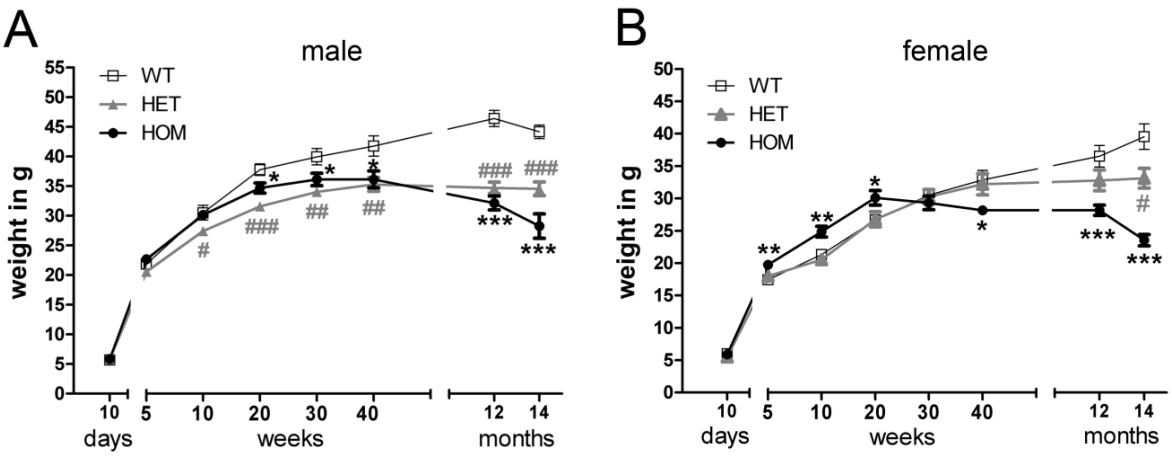

Figure 40. Decreased weight in Atxn2-CAG100-KIN mice. (A) Male HET animals showed a decreased body weight at 10 weeks of age, HOM males at 20 weeks of age; both persist until 14 months of age. (B) Female HET mice did not exhibit significantly decreased weight until age 14 months, while HOM animals displayed significantly increased weight from 5 to 20 weeks of age and significantly decreased weight starting at age 40 weeks and lasting till 14 months (n[male] = 7-17 for animals aged 10 days to 12 months and 4-11 for animals aged 14 months; n[female] = 8-19 for animals of all ages).

At 10 days and 5 weeks of age WT, HET, and HOM animals of both sexes did not significantly differ in their weight. Later, at 10 weeks of age, male HET mice and finally at 20 weeks of age also male HOM mice exhibited a significantly reduced body weight which persisted until 14 months of age. The weight of male HOM mice at 14 months of age was even reduced compared to 30-week-old males, for example. Contrarily, female HOM animals were significantly heavier than WT animals at the beginning, then showed no difference at 30 weeks of age and finally exhibited decreased weight starting at 40 weeks until 14 months of age. Female HET mice did not display decreased weight until

14 months of age. In summary, these data show a significantly reduced weight for both male and female *Atxn2*-CAG100-KIN animals at older ages.

3.7.4 Reduced motor performance in *Atxn2*-CAG100-KIN mice

To monitor the behavioral deficits in motor performance, *Atxn2*-CAG100-KIN mice were tested on the rotarod at different ages. For 10-week-old animals no significant differences were detected between WT and HET or HOM animals (Figure 41). From 10 to 20 weeks of age the rotarod performance of HOM animals drastically decreased so that they showed a significantly reduced latency to fall at 20 weeks. This reduced performance persisted until 14 months of age although WT animals also performed worse with increasing age. HET animals did not show significant differences at any age when compared to WT animals. Thus, homozygous *Atxn2*-CAG100-KIN mice have a reduced rotarod performance starting at age 20 weeks that indicates motor impairment and movement incoordination in these animals.

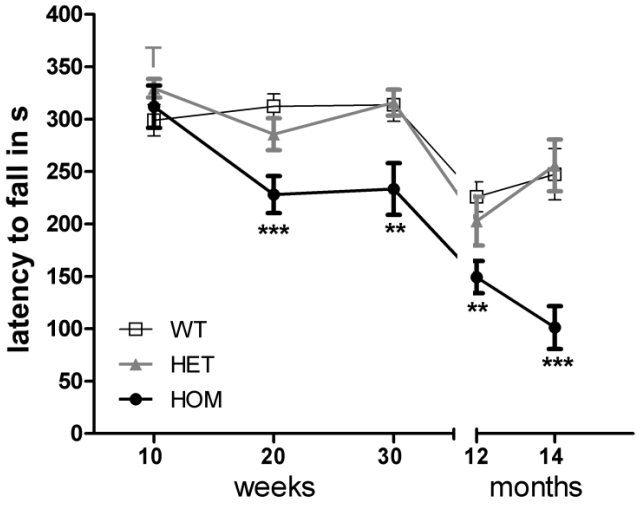

Figure 41. Reduced rotarod performance of Atxn2-CAG100-KIN mice. Latency to fall was assessed at different ages using male and female mice together. At 20 weeks of age, HOM animals showed a decreased latency to fall that was continuously observed at all later ages. HET animals did not show any significant changes compared to WT (n = 9-22 WT, 8-17 HET, and 8-16 HOM animals per age).

3.7.5 *Atxn2*-CAG100-KIN mice show increased horizontal but reduced vertical activity

The aim of the open field analysis was to assess the overall activity of *Atxn2*-CAG100-KIN animals. Mice aged 10, 20, and 30 weeks, as well as 12 and 14 months and of all three

genotypes were used for this study. From 21 open field parameters, those 10 with the highest change and the most consistent significance were chosen (Figure 42). HET animals are not depicted in the figure because they did not show consistent regulations over the selected time span (Supplementary Table 7).

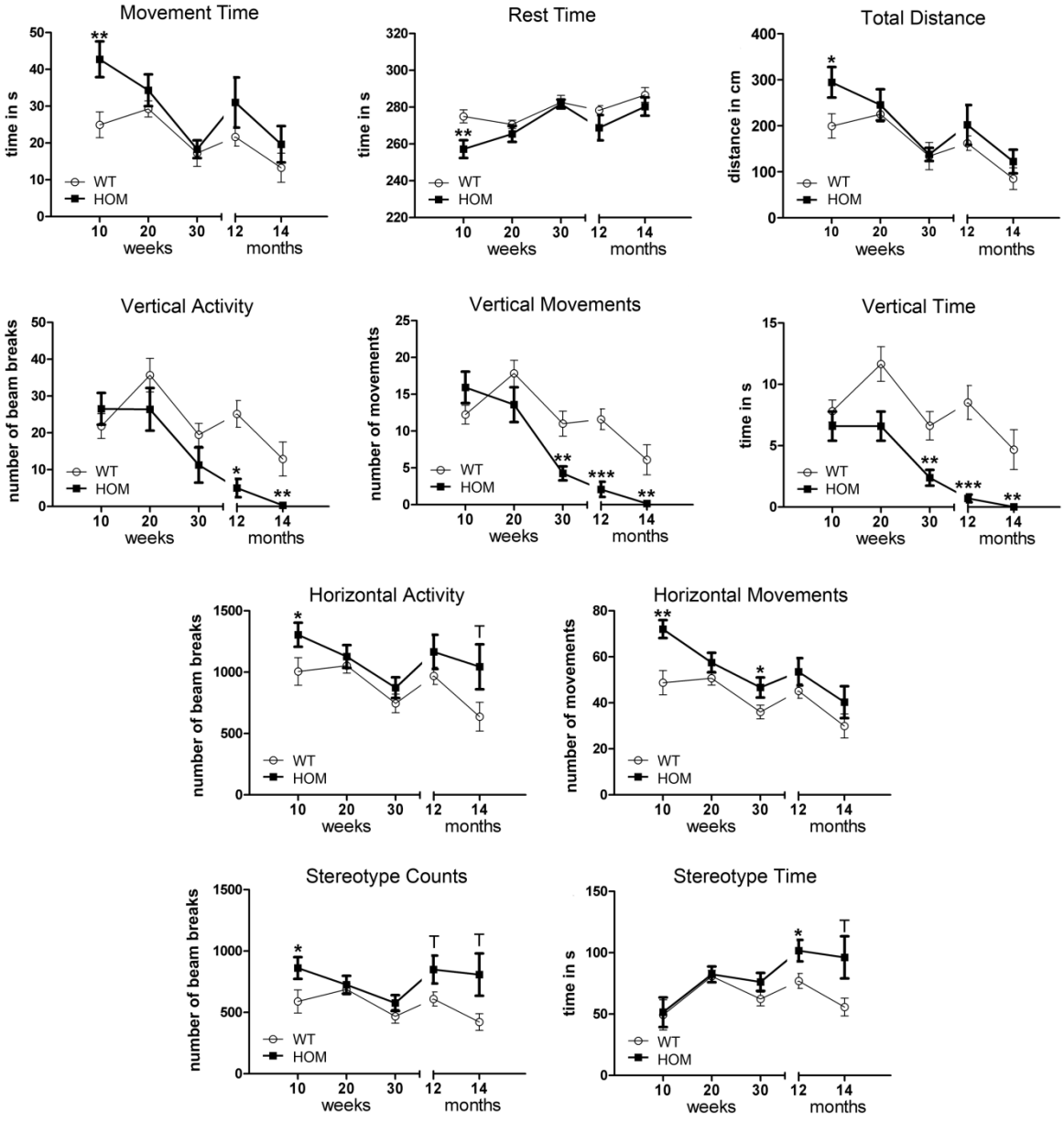

Figure 42. Increased horizontal but decreased vertical activity in Atxn2-CAG100-KIN mice. Several parameters of locomotor activity were measured at five different ages in WT and HOM animals. In 10-week-old HOM animals, significantly more horizontal and overall but not vertical activity was observed. Vertical parameters started to be significantly decreased at 30 weeks of age and this decrease lasted until 14 months of age. Stereotypic behavior was elevated at later ages (n = 11-21 WT and 12-22 HOM animals per age).

Horizontal and overall behaviors were increased while rest time was decreased at all ages in *Atxn2*-CAG100-KIN mice but only significantly at 10 weeks of age. In contrast to horizontal behaviors, all parameters for vertical behavior were similar in WT and HOM animals at age 10 weeks. However, starting at 30 weeks of age a decrease in vertical

parameters (activity, movement number, and movement time) was observed for HOM mice that lasted until 14 months of age. Additionally, *Atxn2*-CAG100-KIN mice exhibited increased stereotypic behavior, especially at later ages (12 and 14 months). In conclusion, the open field data reveal a hyperactivity regarding horizontal movements but a strongly decreased vertical activity in *Atxn2*-CAG100-KIN mice.

3.7.6 Video analysis depicts clasping behavior and flattened body posture of *Atxn2*-CAG100-KIN mice

At 40 weeks of age, *Atxn2*-CAG100-KIN mice started to show visible movement alterations including subtle shaking especially of the head. To compare these changes, 14-month-old WT and HOM animals were videotaped and fixed-images of these videos were taken. Figure 43 illustrates the behavior of WT (A) and HOM (B) mice when suspended by their tails.

Figure 43. Clasping behavior of old Atxn2-CAG100-KIN mice. WT and HOM animals at the age of 14 months were suspended by their tails and the behavior of the mice was documented via video taping. Fixed-images of these videos are depicted here. (A) WT animals spread their legs and tried to get up laterally. (B) HOM animals first cramped their toes, then put their hind legs together and finally clasped their fore legs (bat-like posture).

WT animals spread their legs and tried to get up. In contrast, HOM mice first started to cramp their toes then pressed their hind legs against each other and finally clasped them with their forelegs (bat-like posture). Several HOM mice also did a grooming-like behavior with their forelegs at the beginning but none of them tried to get up laterally as WT

animals did. Some HET animals also showed this altered behavior but at later ages and mostly not as pronounced as HOM mice.

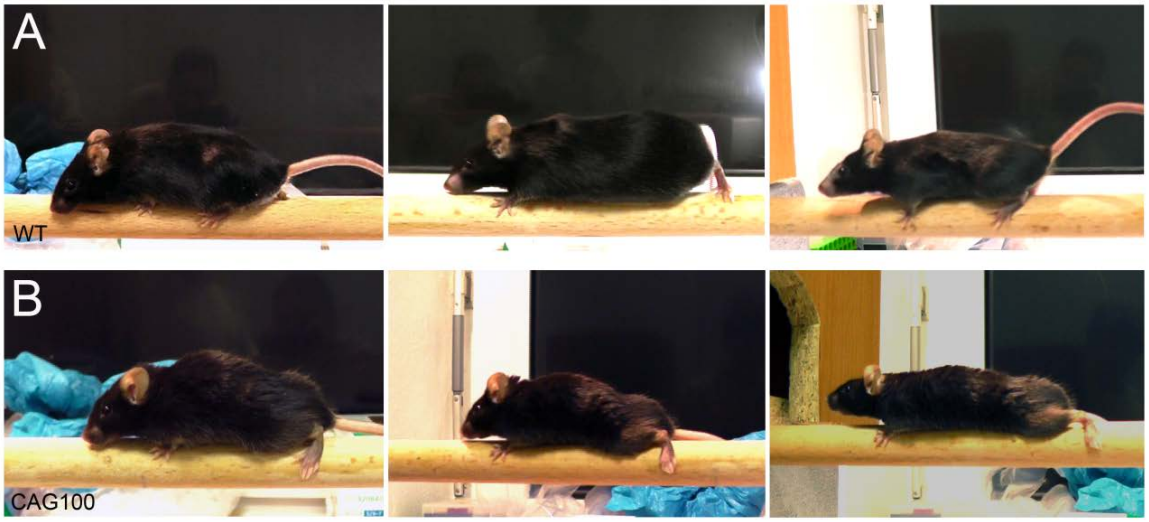

Figure 44. Altered beam walking performance of old Atxn2-CAG100-KIN animals. While walking on an 18-mm-diameter beam HOM animals performed as well as WT animals although their body and tail posture was altered. HOM mice used less their tails to balance on the beam and their bodies were flattened except for the curved spine (kyphosis).

When *Atxn2*-CAG100-KIN mice were walking on a flat ground, their body seemed flattened and their walking behavior looked different. To illustrate this abnormal posture, 14-month-old WT and HOM animals were put on a horizontal beam where they were intended to walk until they reach a darkened box. While WT mice were not willing to move when put onto the beam, most HOM mice started immediately to walk along the beam although they had a visible tremor and trouble with locomotion. WT animals that walked along the beam used their tail for balancing (Figure 44 A). In contrast, the tail of HOM animals was hanging down while walking (Figure 44 B). Their forelegs were much more ahead of the rest of their body, while their hind legs were turned in a 90° ankle and mostly far behind their body. This foot position resulted in a flattened body posture with the curved spine (kyphosis) being the only towering part. Furthermore, when HOM mice were walking on a flat ground (Figure 45), the difference in their walking behavior was hearable as they were pushing their hind legs to the back thereby scratching the ground with their claws. Again, the extreme position of their hind legs was visible and the animals rested from time to time lying on the ground with their hind legs far behind their body. In conclusion, *Atxn2*-CAG100-KIN mice showed a drastically changed walking behavior as well as clasping of their hind legs together with a subtle tremor.

Figure 45. Flattened body posture and altered feet position of Atxn2-CAG100-KIN mice. At 14 months of age, a flattened body posture and extreme differences in walking behavior were observed in HOM animals. Hind legs of the animals were no longer underneath their body while walking but were pushed extremely backwards**.**

3.7.7 Strongly decreased brain size and weight of old *Atxn2*-CAG100-KIN mice

Dissection of *Atxn2*-CAG100-KIN mice revealed a strongly decreased overall brain size (Figure 46 A). Even after shrinkage due to dehydration and paraffination, there was an evident size difference apparent in the sagittal view (Figure 46 B).

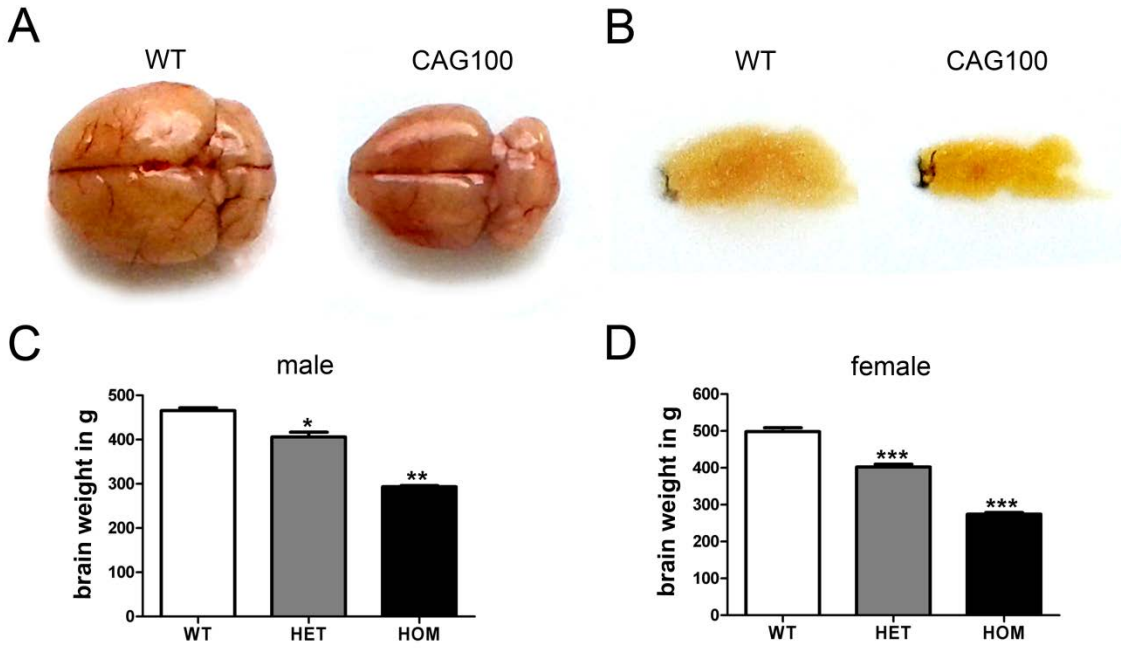

Figure 46. Decreased brain size and weight of 14-month-old Atxn2-CAG100-KIN animals. Photos of WT and HOM brains were taken directly after dissection (A) and after dehydration and embedding in paraffin in sagittal view (B). Brain weight of WT, HET, and HOM animals was compared for male (C) and female (D) animals (n[male] = 2 WT vs. 7 HET vs. 2 HOM; n[female] = 7 WT vs. 7 HET vs. 6 HOM).

Due to this obvious decreased size, brains were weighed after dissection and removal of the olfactory bulb. Brains from HOM but also from HET mice showed significantly decreased brain weight in male and female animals (Figure 46 C and D). For female mice, brain weight was decreased -1.24-fold ($p < 0.0001$) in HET and -1.82-fold ($p < 0.0001$) in

HOM animals. Regarding male mice, only 2 WT and 2 HOM male animals at 14 months of age were dissected making a statistical interpretation difficult. However, a strong decrease of brain weight in HET and HOM animals can already be assumed from the two sample data. Consequently, atrophy in *Atxn2*-CAG100-KIN animals seems to result in strongly decreased brain size and weight of HET and HOM animals that is not restricted to the cerebellum but includes all parts of the brain.

3.7.8 Aggregation of ATXN2 in diverse regions of *Atxn2*-CAG100-KIN central nervous system

To document pathology in *Atxn2*-CAG100-KIN brain and spinal cord immunohistochemical stainings with ATXN2 and the polyQ-binding 1C2 antibody were performed. For this purpose, paraffin-embedded slices of 14-month-old WT and HOM animals were used. Several typically affected regions in SCA2 were scanned for aggregates of ATXN2. In Figure 47, microscopic pictures of cerebellum, inferior olive, pontine nuclei, cerebral cortex, hippocampus, and spinal cord stained for ATXN2 are shown. In all regions ATXN2 aggregates were clearly detectable in *Atxn2*-CAG100-KIN tissue while an evenly cytoplasmic distribution was observed in WT animals. In cerebellar Purkinje neurons the ATXN2 aggregates were mostly punctuate and larger distinct accumulations were not seen. In all other regions punctuate and dense but also larger and less dense aggregates were detected.

The 1C2 antibody binds polyQ expansions of at least 38 glutamines. Thus, almost no staining was expected and also observed in WT animals. In HOM animals, only little Purkinje neurons and neurons of the brainstem were stained with 1C2 while more neurons in the cerebral cortex displayed polyQ-containing aggregates (Figure 48). Overall, 1C2 stained less neurons than ATXN2. In conclusion, a strong aggregation of ATXN2 emerged in several regions of the brain as well as in spinal cord neurons in *Atxn2*-CAG100-KIN mice. The 1C2 staining revealed less aggregates but definitely confirmed their occurrence. All aggregates showed cytoplasmic localization with many of them located at the plasma membrane.

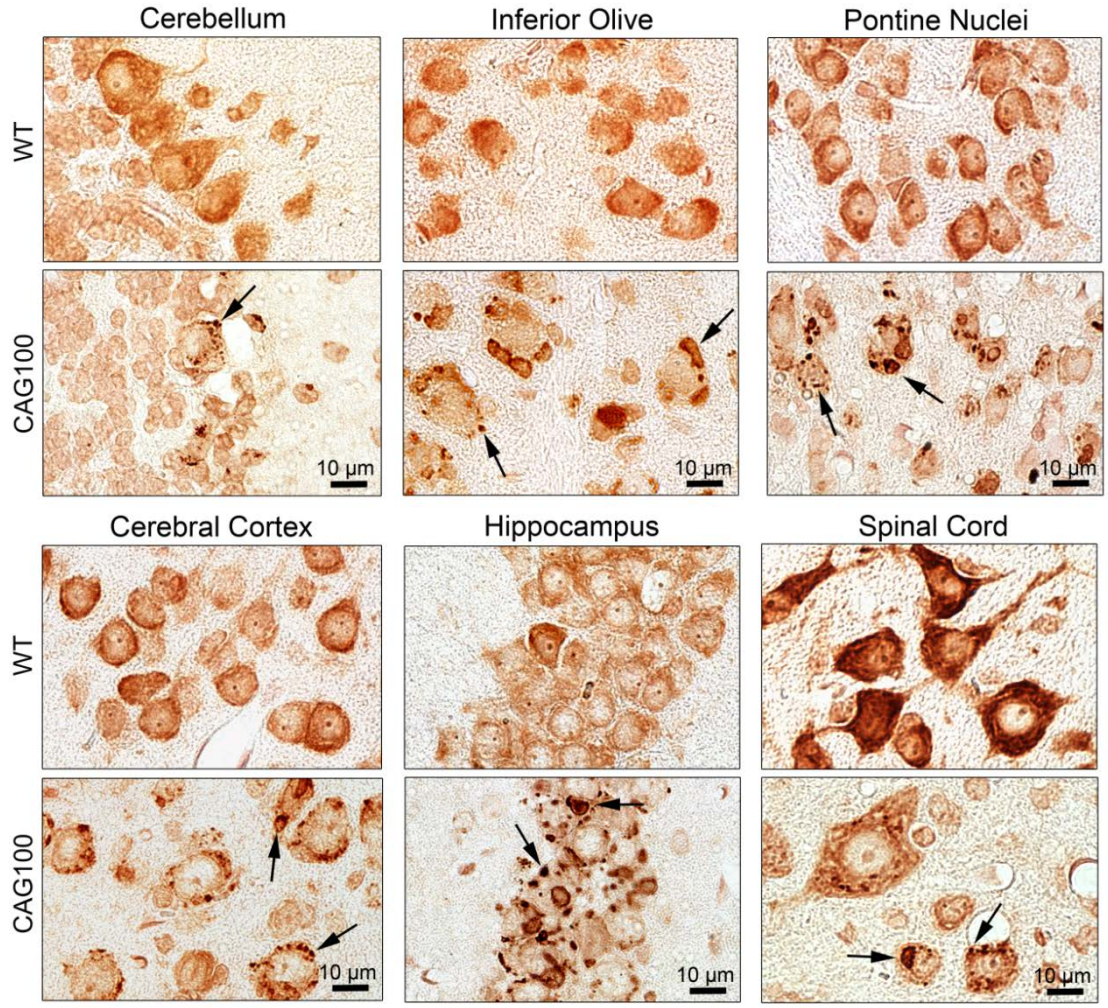

Figure 47. Strong aggregation of ATXN2 in the central nervous system of old Atxn2-CAG100-KIN animals. Paraffin-embedded slices of 14 month-old WT and HOM animals were stained for ATXN2. Microscopic pictures of cerebellum, inferior olive, pontine nuclei, cerebral cortex, hippocampus, and spinal cord were taken. HOM animals showed strong aggregation of ATXN2 either in punctuate and dense aggregates or in larger and less dense accumulations.

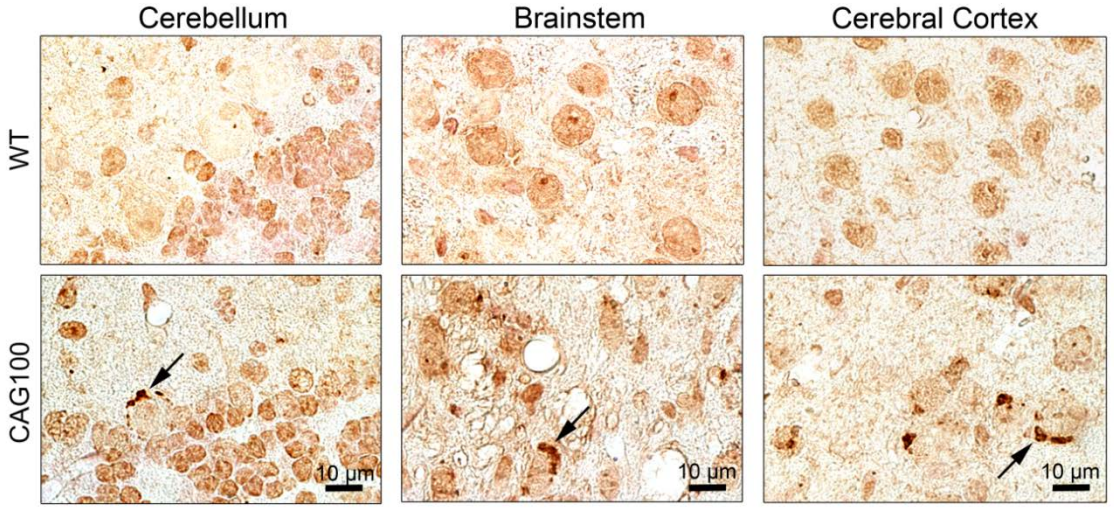

Figure 48. 1C2 staining detects aggregation of polyQ domains in Atxn2-CAG100-KIN mice. The 1C2 antibody detects polyQ repeats of at least 38 glutamines. WT and HOM brains of 14-month-old animals were stained with 1C2 and aggregates were observed in similar regions as for ATXN2 but less often. Cerebellum, brainstem, and cerebral cortex aggregates are depicted.

3.7.9 Expanded ATXN2 co-localizes with the inclusion markers p62 and ubiquitin

When misfolded or mutant proteins shall be degraded, they are tagged with ubiquitin (UBQ) to mark them for proteasomal or autophagosomal degradation. Therefore, UBQ is a common component of protein aggregates in many neurodegenerative diseases (Ansorge et al., 2004; Koyano et al., 1999; Lowe et al., 1988; Rub et al., 2014; Schiffer et al., 1991). In order to identify if UBQ is also part of ATXN2 aggregates in *Atxn2*-CAG100-KIN mice, a double staining for ATXN2 and UBQ was conducted. Paraffin-embedded slices of 14-month-old WT and HOM mice were employed. Neurons of the cerebellum, brainstem, and spinal cord are shown in Figure 49 with ATXN2 stained in red and UBQ in green. While UBQ showed stronger presence in the nucleus than in the cytoplasm in all regions in WT slices, it was strongly aggregated in the cytoplasm in *Atxn2*-CAG100-KIN slices (Figure 49). Only some of the Purkinje neurons showed aggregates including UBQ (A) but many UBQ positive aggregates were detected in brainstem (B) and spinal cord (C). Nevertheless, in all cells in which UBQ aggregation was detected, concurrently a co-localization with ATXN2 was observed.

Sqstm1/p62 is a protein that binds ubiquitinated proteins and is involved in their aggregation and degradation via autophagy or proteasomes. Like UBQ, it has been shown to be part of inclusions in several neurodegenerative diseases (Alves et al., 2014; Kuusisto et al., 2001; Rue et al., 2013; Seidel et al., 2010). To explore if p62 also present in ATXN2 aggregates, a double staining similar to UBQ was performed. In cerebellum and brainstem of WT mice only a diffuse / background staining for p62 was detectable in the WT, while in the *Atxn2*-CAG100-KIN some neurons displayed aggregated p62. In these aggregates p62 and ATXN2 co-localized (Figure 50 A and B). Neurons of the spinal cord (Figure 50 C) already exhibited a stronger (cytoplasmic and nuclear) signal for p62 in WT compared to cerebellum and brainstem with a slight co-localization of the two proteins. However, in the *Atxn2*-CAG100-KIN tissue the two proteins showed much stronger co-localization in dense cytoplasmic aggregates. Furthermore, similar to UBQ, much more neurons displayed co-localization of the two proteins in brainstem and spinal cord than in cerebellum. These data indicate that p62 is sequestered into ATXN2 aggregates probably due to previous ubiquitination of the protein. In conclusion, the double stainings demonstrate that UBQ and p62, two proteins involved in protein degradation and important inclusion markers of neurodegenerative diseases, form also part of the ATXN2 aggregates in *Atxn2*-CAG100-KIN mice.

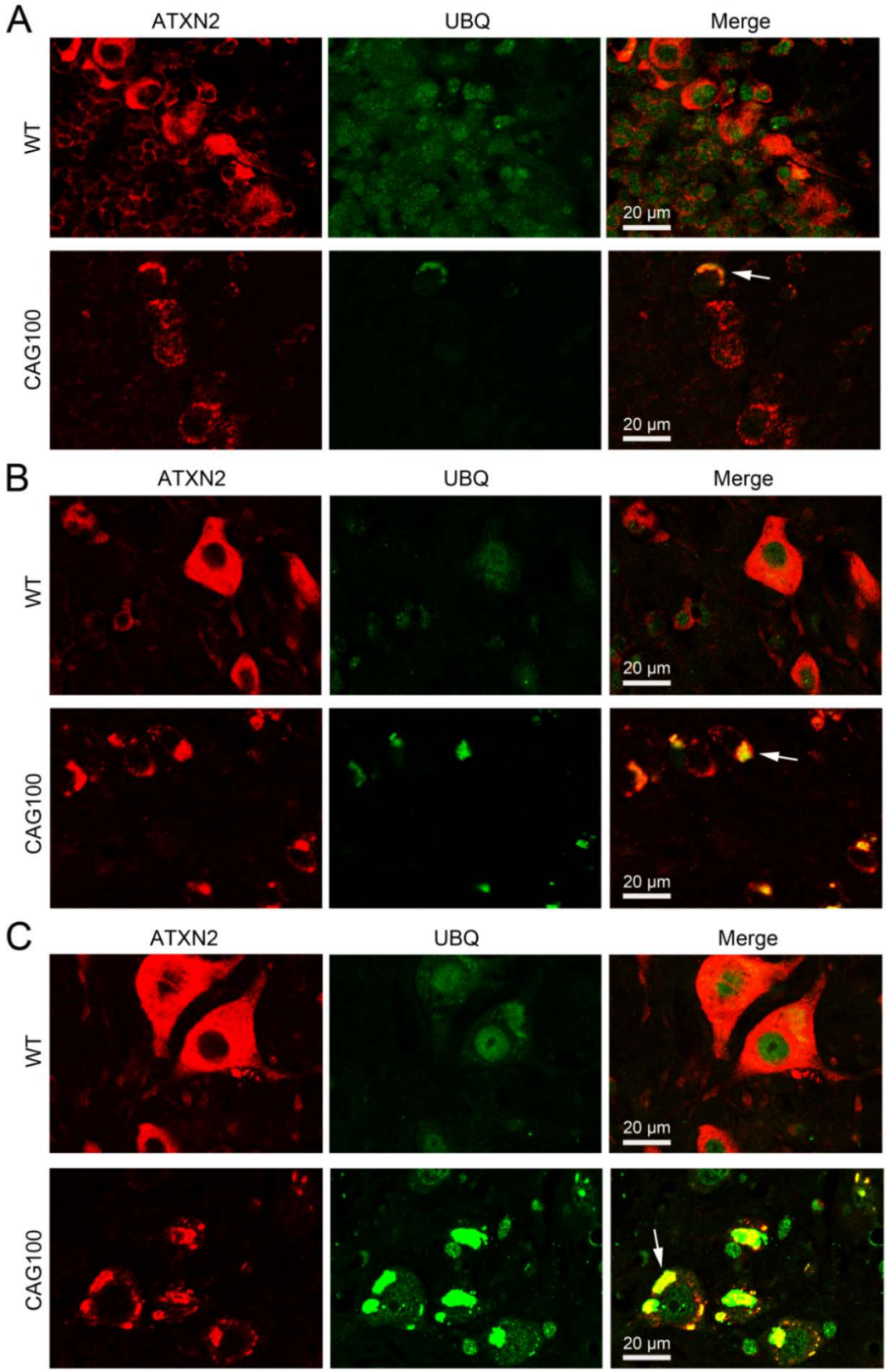

Figure 49. Co-localization of ATXN2 and UBQ in aggregates of old Atxn2-CAG100-KIN mice. Brain and spinal cord slices of 14-month-old WT and HOM animals were double stained for ATXN2 (red) and UBQ (green). UBQ staining in WT animals was cytoplasmic and nuclear while in HOM animals a strong cytoplasmic aggregation was observed. In cerebellum (A) only some neurons showed co-localization of the two proteins in aggregates. In brainstem (B) and spinal cord (C) more and larger joint aggregates were detected.

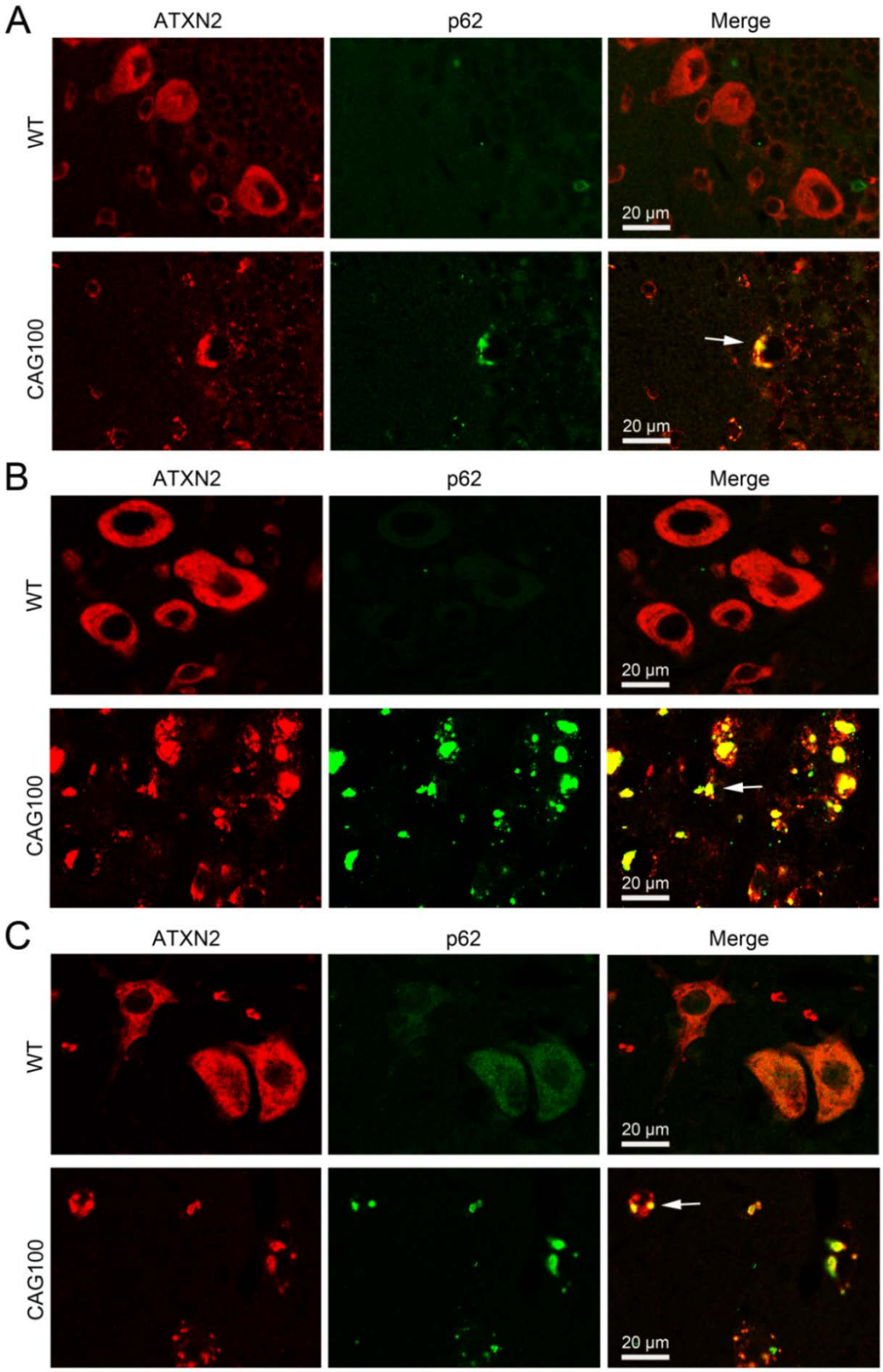

Figure 50. ATXN2 and p62 co-localize in cytoplasmic aggregates of old Atxn2-CAG100-KIN animals. Brain and spinal cord slices of 14-month-old WT and HOM animals were double stained for ATXN2 (red) and p62 (green). In WT animals, p62 was either not or only slightly stained in the cytoplasm while a strong staining was detected in HOM animals. (A) Cerebellar Purkinje cells showed rarely aggregation of both, ATXN2 and p62, in HOM mice. In brainstem (B) as well as in spinal cord (C) many neurons exhibited a co-localization of the two proteins in the cytoplasm.

3.7.10 Transcript level changes in *Atxn2*-CAG100-KIN cerebellum

Given that consistent changes of calcium homeostasis factors had been found in *Atxn2*-KO and *Atxn2*-CAG42-KIN mice, these genes were also studied in the new mouse line to see if this feature of pathology is represented as well. Therefore, transcript levels in cerebellum from WT and *Atxn2*-CAG100-KIN mice at 10 weeks, 20 weeks, and 14 months of age were analyzed. Significant changes in nine out of ten analyzed genes were already detectable in the youngest animals with fold changes of -1.13-fold to -1.33-fold (Table 55). In 20-week-old animals, again nine transcripts showed downregulation but this time with higher fold changes (-1.21-fold to -1.39-fold). At the latest analyzed time point, 14 months, where the animals already exhibit drastic behavioral pathology all transcripts were downregulated between -1.32-fold and -1.94-fold. Thus, changes of close to 2-fold were observed in these animals. Besides, in 10-week-old animals some more genes implicated in this pathway and found as dysregulated in other polyQ mouse models were studied to see if they are similarly affected. *Atp2b2*, *Gria3* (Glutamate receptor ionotropic AMPA 4), *Grid2* (Glutamate receptor ionotropic delta 2), *Grm4* (Glutamate receptor metabotropic 4), *Pcp4* (Purkinje cell protein 4), *Plcb4*, *Plcg1* (Phospholipase C gamma 1), and *Pvalb* (Parvalbumin) also showed decreased expression in HOM mice (Table 56). In conclusion, these results suggest that calcium homeostasis factors play an important role in the pathology of SCA2 because they were strongly downregulated in the *Atxn2*-CAG100-KIN mouse model and their downregulation increased with the progression of the pathology. Probably, there is also an effect on protein level similar to *Atxn2*-CAG42-KIN mice.

Table 55. Transcript changes of calcium homeostasis factors in cerebellum of Atxn2-CAG100-KIN mice. Transcript levels of WT and HOM cerebellar tissue at 10 and 20 weeks as well as 14 months of age were assessed via real-time RT-qPCR (n = 4-8 WT vs. 3-8 HOM animals).

Gene symbol	WT vs. HOM Cb 10 weeks	WT vs. HOM Cb 20 weeks	WT vs. HOM Cb 14 months
Atp2a2	-1.19-fold **	-1.09-fold *n.s.*	-1.57-fold **
Ca8	-1.33-fold **	-1.39-fold **	-1.82-fold **
Calb1	-1.13-fold *	-1.21-fold **	-1.58-fold **
Grm1	-1.13-fold *	-1.29-fold *	-1.32-fold **
Homer3	-1.22-fold ***	-1.36-fold **	-1.75-fold ***
Inpp5a	-1.25-fold **	-1.37-fold **	-1.69-fold **
Itpr1	-1.17-fold *	-1.36-fold **	-1.81-fold **
Kitlg	-1.33-fold **	-1.34-fold *	-1.94-fold **
Rora	-1.18-fold ***	-1.35-fold ***	-1.32-fold **
Trpc3	-1.16-fold *T*	-1.21-fold *	-1.86-fold **

Table 56. Additional calcium homeostasis transcripts downregulated in Atxn2-CAG100-KIN cerebellum. Several more genes involved in calcium homeostasis were studied via real-time RT-qPCR for transcript level changes between 10-week-old WT and *Atxn2*-CAG100-KIN mice (n = 4-8 WT vs. 4-8 HOM animals).

Gene symbol	WT vs. HOM Cb 10 weeks
Atp2b2	-1.16-fold **
Gria3	-1.36-fold **
Grid2	-1.13-fold **
Grm4	-1.17-fold *
Pcp4	-1.24-fold ***
Plcb4	-1.22-fold **
Plcg1	-1.52-fold *

Furthermore, the SCA genes that had been dysregulated in *Atxn2*-KO and *Atxn2*-CAG42-KIN mice were also analyzed in *Atxn2*-CAG100-KIN mice to prove their relevance. Using animals of the same age as for calcium homeostasis factors, no transcript changes were observed for *Atxn1* (Table 57). In contrast to that, a significant dysregulation of *Bean1* was found in 20-week- and 14-month-old animals. Similar to *Atxn2*-KO and *Atxn1*-Q154-KIN mice but converse to *Atxn2*-CAG42-KIN mice, *Bean1* was downregulated in *Atxn2*-CAG100-KIN cerebellum reaching -1.87-fold at 14 months of age. Additionally, *Atxn2* mRNA was dysregulated as well in this mouse line, showing a downregulation of -1.12-fold in young and -1.31-fold in old animals indicating that the aggregation is not caused by an overexpression of the protein.

Table 57. Transcript level changes of SCA genes in Atxn2-CAG100-KIN cerebellum. In cerebellum of 10-week-, 20-week-, and 14-month-old WT and HOM animals, transcript levels for three selected SCA genes were determined using real-time RT-qPCR (n = 4-8 WT vs. 3-8 HOM animals).

Gene symbol	WT vs. HOM Cb 10 weeks	WT vs. HOM Cb 20 weeks	WT vs. HOM Cb 14 months
Atxn1 (SCA1)	+1.07-fold *n.s.*	+1.10-fold *n.s.*	-1.11-fold *n.s.*
Atxn2 (SCA2)	-1.12-fold *	-1.15-fold *T*	-1.31-fold *
Bean1 (SCA31)	+1.02-fold *n.s.*	-1.23-fold *	-1.87-fold **

Several more transcripts that either showed already dysregulation in *Atxn2*-KO or *Atxn2*-CAG42-KIN mice or in other SCA mouse models were analyzed in *Atxn2*-CAG100-KIN cerebellum, too (Table 58). Interestingly, *Fbxw8* that was strongly upregulated in *Atxn2*-CAG42-KIN did not show any significant and consistent changes in *Atxn2*-CAG100-KIN mice (similar to *Atxn1*-Q154-KIN mice, data not shown). Contrarily, *Pabpc1*, upregulated in *Atxn2*-KO and *Atxn2*-CAG42-KIN mice also exhibited increased levels in *Atxn2*-CAG100-KIN mice. Furthermore, strong downregulations were observed for the transcripts of *Icmt (isoprenylcysteine carboxyl methyltransferase)*, *TH (tyrosine*

hydroxylase), and *Mbp (myelin basic protein),* while *Syne1 (spectrin repeat containing, nuclear envelope 1)* and *EP300 (E1A binding protein p300)* were significantly upregulated. *Icmt*, *Syne1*, and *Mbp* have already shown pronounced effects in *Atxn2*-KO mice and *TH* additionally in *Atxn2*-CAG42-KIN mice (data not shown). To assess the causes and consequences of these transcript dysregulations was beyond the scope of this thesis. Overall, the *Atxn2*-CAG100-KIN mouse model shows similar but more pronounced dysregulations of diverse transcripts which seem to be involved in SCA2 pathology and give a hint for new interaction partners.

Table 58. Additional transcripts with significant dysregulation in Atxn2-CAG100-KIN cerebellum. Several genes of interest were analyzed in 10-week-old WT and *Atxn2*-CAG100-KIN mice via real-time RT-qPCR (n = 4-8 WT vs. 3-8 HOM animals).

Gene symbol	**WT vs. HOM Cb 10 weeks**
Fbxw8	-1.07-fold *n.s.*
EP300	+1.16-fold *
Icmt	-1.57-fold ***
Mbp	-1.43-fold *
Pabpc1	+1.16-fold *
Syne1	+1.13-fold *
TH	-2.72-fold ***

4 Discussion

Since the discovery of the first hereditary ataxias in the middle of the 19th century numerous researchers have investigated the pathomechanism of these diseases. Nowadays, there are almost 40 known Spinocerebellar ataxias and their number is steadily increasing. For most of them the causative gene has already been identified. Nevertheless, the pathological mechanisms that underlie these diseases remain unsolved. To gain a better understanding of the pathology of one of the most common SCAs, SCA2, several putative and known interaction partners of its causative gene, ATXN2, as well as two new mouse models were studied in this thesis.

4.1 The role of ATXN2 interaction partners

4.1.1 The E3 ubiquitin-protein ligase component Fbxw8 is relevant for degradation of moderately expanded Atxn2 and could serve as a biomarker for SCA2

The polyQ diseases and also other neurodegenerative disorders have in common that their causative proteins aggregate in affected neurons. This conjoint feature raised the hypothesis that the so called proteinopathies also share a common pathomechanism (Scherzinger et al., 1997). Interestingly, several components of the UPS machinery are sequestered into these protein aggregates. Ubiquitin and its adaptor protein p62/SQSTM1 are two of the main proteins that were found to be recruited into protein aggregates in different neurodegenerative diseases (Alves et al., 2014; Koyano et al., 1999; Kuusisto et al., 2001; Pikkarainen et al., 2008; Rue et al., 2013; Seidel et al., 2010; Sieradzan et al., 1999; Yang et al., 2014b). Given that the UPS is a critical regulator of protein homeostasis by degrading short-lived, misfolded, and damaged proteins it was suggested that the UPS may be involved in the pathomechanism of polyQ and other neurodegenerative diseases. Moreover, the sequestration of p62 indicates that not only the UPS but also the autophagic system is somehow involved in the pathological process of these disorders.
In *Atxn2*-CAG42-KIN mouse cerebellum, however, no accumulation of p62 (Damrath, 2012) or UBQ (data not shown) was observed. This fact may result from the relatively

small repeat expansion (for a mouse model) and the subsequent late and only moderate aggregation of ATXN2. Instead, an induction of the E3 ubiquitin-protein ligase component *Fbxw8* was observed on transcript level in a microarray transcriptome study of 6- and 18-month-old animals (Supplementary Table 1) (Damrath et al., 2012).

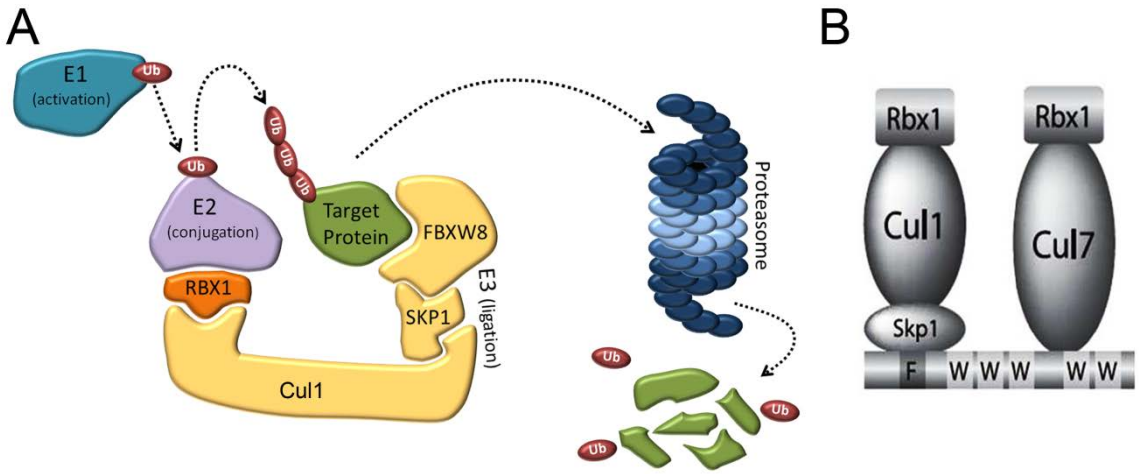

Figure 51. FBXW8 in the ubiquitin-proteasome system. (A) Ubiquitin is first activated by the E1 enzyme and then via the E2 transferred to the target protein which is bound by the E3 ligase. Here the E3 ligase is a SCF complex composed of SKP1, CUL1, and the F-box-protein and target recognizing subunit FBXW8. Ubiquitinated proteins are subsequently degraded by the proteasome. (B) Binding positions of CUL1 and CUL7 to FBXW8. CUL1 binding is mediated through SKP1 and targets the F-box domain while CUL7 binds directly to the WD-repeat domain (Tsunematsu et al., 2006).

FBXW8 belongs to the group of F-box proteins that constitute the target specificity in several multi-subunit RING finger E3 ligases. As indicated by their name, these multi-subunit RING finger E3 ligases, in contrast to all other E3 ligases (HECT domain, U-box domain, and single RING-finger domain E3 ligases), consist of several components and not only of one. The involved subunits are an E2-binding protein with the RING-finger domain (RBX1 or RBX2), one of the cullins (e.g. CUL1 or CUL7), an adaptor protein (e.g. SKP1; not mandatory) and as mentioned before the target recognizing subunit (F-box protein or others). One of these multi-subunit RING finger E3 ligases is the SCF complex consisting of the three subunits it is named after (SKP1, CUL1, F-box protein) as well as an RBX1 subunit (Figure 51 A). FBXW8 forms part of this complex but can also participate in the CUL7 complex which is similar to the SCF complex apart from the cullin isoform (Tsunematsu et al., 2006). However, in the CUL7 complex, FBXW8 is the only possible F-box protein known yet (Dias et al., 2002; Litterman et al., 2011). While the interaction with the SCF complex is mediated via the F-box domain of FBXW8, the interaction with the CUL7 complex - which occurs more frequently - is probably established via the WD40 repeat domain and SKP1 is not absolutely necessary (Figure 51 B) (Tsunematsu et al., 2006). Consequently, FBXW8 can form part of both complexes

at the same time maybe acting in concert to ubiquitinate the substrate (Ponyeam and Hagen, 2012).

Several substrates of FBXW8 have already been identified including cyclin D1 (CCND1; CUL1 or CUL7 complex), the hematopoietic progenitor kinase 1 (HPK1; CUL7 complex), and the Golgi reassembly and stacking protein GRASP65/GORASP1 (CUL7 complex) (Litterman et al., 2011; Okabe et al., 2006; Wang et al., 2014). In the GRASP65 substrate study, the authors furthermore show CUL7/FBXW8 complex localization at the Golgi and elucidate a role in Golgi morphogenesis and dendrite elaboration (Litterman et al., 2011). Besides, the insulin receptor substrate 1 (IRS1) as well as TBC1D3 which is indirectly involved in the degradation of the IRS1 are substrates of the CUL7/FBXW8 complex indicating a role for this complex in insulin signaling and glucose homeostasis (Kong et al., 2012; Scheufele et al., 2014; Xu et al., 2008).

Regarding polyQ diseases, FBXW8 was recently found to be a modifier of HTT (Huntingtin) toxicity. In an *in vitro* approach using shRNA Fbxw8 was suppressed and this suppression resulted in increased HTT aggregation without affecting HTT expression (Yamanaka et al., 2014). Additionally, the expression of the SCF complex subunits SKP1 and CUL1 were altered in HD mice, suggesting a role for this E3 ubiquitin-protein ligase in polyQ diseases (Bhutani et al., 2012). Interestingly, another E3 ligase, named MGRN1 (Mahogunin ring finger 1), was recently determined to influence mutant HTT and ATXN3 proteins with a depletion of MGRN1 increasing and an overexpression decreasing aggregate formation (Chhangani et al., 2014).

In *Atxn2*-CAG42-KIN mice, *Fbxw8* showed significant transcript upregulation at all ages and in all tissues when independently analyzed by RT-qPCR (Figure 14). Similar to p62 and UBQ, no aggregation was observed in immunohistochemical stainings of cerebellar slices (Figure 16). However, an accumulation of FBXW8 in the SDS-soluble fraction was detected in quantitative immunoblots (Figure 15). This accumulation is probably caused by a sequestration through expanded ATXN2 for which a similar shift had been observed before (Damrath, 2012). Furthermore, the accumulation gave a first hint that there could be an interaction between ATXN2 and FBXW8. This interaction was subsequently proven pulling either with an anti-ATXN2 or an anti-FBXW8 antibody (Figure 17).

In contrast to *Fbxw8*, none of the other known E3 ligase components and FBXW8 interactors was significantly dysregulated on transcript level in *Atxn2*-CAG42-KIN cerebellum. The reason for this specific upregulation may be the target specificity of FBXW8. As mentioned before, FBXW8 is able to participate in different E3 complexes. Therefore, it is possible that the scaffold for FBXW8 is interchangeable and consequently not upregulated on transcript level. Moreover, there are only 16 subtypes of E1 and 53 subtypes of E2, but there are 527 known subtypes of E3 ligases today (Ortega and

Lucas, 2014). Thus, while different E1 and E2 enzymes may be involved in ATXN2 degradation and also different other subunits of the E3 complex; FBXW8 is the only specific component resulting in a strong upregulation of its transcript.

According to the observation that there is no UPS impairment in polyQ diseases, a significant decrease of ATXN2(Q74) levels was observed in the SDS-soluble fraction in an *in vitro* model overexpressing ATXN2 and FBXW8 (Figure 20). These data indicate that FBXW8 accumulates together with ATXN2 but does not lose its activity and helps to degrade ATXN2. In contrast to that, no significantly decreased ATXN2(Q74) levels were observed in the RIPA-soluble fraction. Besides, no change in *ATXN2* transcript levels was detected (Figure 21) suggesting that the effect is indeed degradation-dependent. FBXW8 showed significantly increased protein levels but also slightly, but not significantly, increased transcript levels (similar to the mouse model) in response to overexpression together with ATXN2. This upregulation was independent of the polyQ length or the solubility and may be the reaction to the increased ATXN2 levels. It is furthermore of interest that although FBXW8 is able to interact with WT and expanded ATXN2 *in vivo* and *in vitro* a significant degradation was only detected for the latter one. Possibly, FBXW8 prefers to bind expanded ATXN2 due to its misfolding but detailed studies about ATXN2 degradation by FBXW8 need to be performed.

The ATXN2 protein was already shown to interact and to be degraded by the help of another E3 ligase: PARK2, a Parkinson-associated protein that is normally a single RING-finger type E3 (Huynh et al., 2007). PARK2 furthermore interacts with another protein causative for familial Parkinson's disease, PINK1 (PARK2 induced kinase 1), at the mitochondrial membrane. Recently an association between PINK1 and the translation complex including PABP was demonstrated for selected mRNAs (Gehrke et al., 2015). These data indicate that ATXN2 could be implicated in the functional consequences of this interaction and mutated ATXN2 could disturb this process similar to a mutation of PARK2 or PINK1. Possibly, this association is the reason for the Parkinsonian features some SCA2 patients develop.

Interestingly, PARK2 was found to interact with an F-box protein named FBXW7 (Staropoli et al., 2003). The consequences of FBXW7/PARK2 interaction are still under debate. First, it was suggested that they act together with CUL1 to degrade other targets (Staropoli et al., 2003) but later on this effect could not be confirmed. Instead, it was proposed that PARK2 is a higher order E3 ligase and FBXW7 is a target of PARK2 activity (Ekholm-Reed et al., 2013). Regarding these results it is of interest that loss of FBXW7 was found to inhibit PARK2 translocation and mitophagy (Ivatt et al., 2014) challenging the hypothesis of FBXW7 as a pure target of PARK2. Despite the PARK2 involvement in ATXN2 degradation, PARK2 did not show significant transcript upregulation in *Atxn2-*

CAG42-KIN mice. However, it accumulated together with ATXN2 and FBXW8 in the SDS-soluble fraction of murine cerebellar tissue. Similar to FBXW7, an interaction of FBXW8 with PARK2 was observed *in vivo* and *in vitro* (Figure 22). The results suggest that PARK2 either interacts with FBXW8 to degrade proteins by providing a scaffold similar to the SCF and Cul7 complex or it acts as a higher order E3 ligase involved in the degradation of FBXW8. However, given that both proteins are involved in ATXN2 degradation it is likely that they act in concert at the same level. The fact that only *Fbxw8* but not *Park2* or any other complex subunit is upregulated on transcript level also favors this hypothesis.

To study the relevance of Fbxw8 for disease, SCA2 patient material was employed. Similar Fbxw8 dysregulations as in the mouse model were detected. However, *FBXW8* showed only a slight induction on transcript level in skin fibroblasts as well as in blood samples. In contrast, the depletion of FBXW8 in the RIPA-soluble fraction and its accumulation in the SDS-soluble protein fraction of SCA2 patient skin fibroblasts resembled quite well the effects observed in murine tissue (Figure 23). In conclusion, FBXW8 could serve as a biomarker for SCA2 in contrast to PARK2, which was not regulated on transcript level in SCA2 fibroblasts. Still, it should be considered that due to the low fold change false positive or false negative results are likely to happen. Nevertheless, the fact that FBXW8 showed a dysregulation in SCA2 patient material proves that its upregulation is not just an unspecific effect observed in a mouse model but indeed is relevant for human disease.

In summary, the data implicate FBXW8 in the degradation of expanded ATXN2. Furthermore, new interactions between ATXN2, FBXW8, and PARK2 were observed suggesting the involvement of different E3 ligases in the degradation of ATXN2. FBXW8 seems to be more specific for ATXN2 than PARK2 as shown by the exclusive transcript upregulation in the mouse model and in human tissue. However, on the basis of the present data no definite mechanism can be proposed how these proteins act together.

4.1.2 Loss and mutation of ATXN2 probably cause cerebellar calcium homeostasis defects differently

Calcium signaling plays a key role in neuronal function, for example in synaptic plasticity, excitability and neurotransmitter release (Kitamura and Kano, 2013). Intracellular calcium levels are controlled by various mechanisms including different types of receptors, channels, exchangers, Ca^{2+} -binding proteins, and intracellular Ca^{2+} stores. It is of interest that several of the causative polyQ or SCA proteins in general have an already approved

function in calcium signaling like SPTBN2 (SCA5), CACNA1A (SCA6), PRKCG (SCA14), or ITPR1 (SCA15/16/29). In addition, a downregulation of several transcripts implicated in calcium homeostasis was found in SCA1 (Crespo-Barreto et al., 2010; Lin et al., 2000; Serra et al., 2004), SCA2 (Hansen et al., 2013), SCA3 (Chou et al., 2008), SCA7 (Friedrich et al., 2012; Gatchel et al., 2008), HD (Friedrich et al., 2012; Luthi-Carter et al., 2002a), and DRPLA (Luthi-Carter et al., 2002b) mouse models. In *Atxn2*-KO mice, data from microarray transcriptome studies and RNAseq gave a first hint for reduced calcium homeostasis transcripts (Halbach et al., under revision). These data were further confirmed via RT-qPCR in cerebellum of mice at the same age and younger (Table 42 and Table 43) revealing a progressive development of these changes. Additional relevant transcripts were chosen and were detected to be downregulated, also suggesting a strong affection of calcium signaling. Most of the analyzed genes have a known association with each other as depicted in Figure 52. Transcriptional downregulations were already detected as early as 3 days of age in heterozygous *Atxn2*-KO mice (Table 43). These early affected genes were *Atp2a2* and *Inpp5a*. In contrast to *Atp2a2* (the gene that is responsible for Ca^{2+} uptake into the ER), *Itpr1* (the gene that mediates Ca^{2+} release from the ER) was only affected at later stages in *Atxn2*-KO mice. This is of interest when comparing the data to those of *Atxn2*-CAG42-KIN mice in which *Itpr1* was the earliest transcript that showed downregulation (Table 45). Possibly, although similar genes are affected in KO and KIN mice there is a difference in the effect strength. Nevertheless, both mouse models had in common that only the cerebellum but not the cortex was affected. The reason for this difference may originate from the fact that excitation is differently organized in cerebellar and cortical neurons and the role of Ca^{2+} may differ between these two brain regions. It is therefore possible that in the cortex (where aggregation of the mutant protein and neurodegeneration occur as well) other signaling pathways are more affected or that cortical neurons are more successful in balancing these alterations. Furthermore, transcript level changes in general increased with age, reflecting the progressive development of these disturbances.

It is of interest that *Calb1*, one of the main Ca^{2+} buffering proteins that has been shown to be severely depleted for example in HD and SCA1 mice (Dougherty et al., 2013; Serra et al., 2004) only exhibited small fold changes in *Atxn2*-KO and *Atxn2*-CAG42-KIN mice. In the KIN mice, this result may be explained by the moderate repeat expansion. In a HD mouse model with a polyQ expansion of 100Q also no effect was detected for *Calb1* while in HTT-Q200 mice it was significantly reduced. Similarly, in *Atxn2*-CAG100-KIN mice a stronger downregulation of *Calb1* was observed than in *Atxn2*-CAG42-KIN animals. In general, expression changes in the *Atxn2*-CAG100-KIN mice were much stronger (up to 2-fold; Table 55) than in *Atxn2*-KO or *Atxn2*-CAG42-KIN animals. They were comparable

to those noted in *Atxn1*-Q154-KIN mice (Table 47) due to the longer polyQ domain and the subsequent stronger pathological phenotype. Nevertheless, in all four mouse models a similar set of transcripts was affected pointing to a common mechanism.

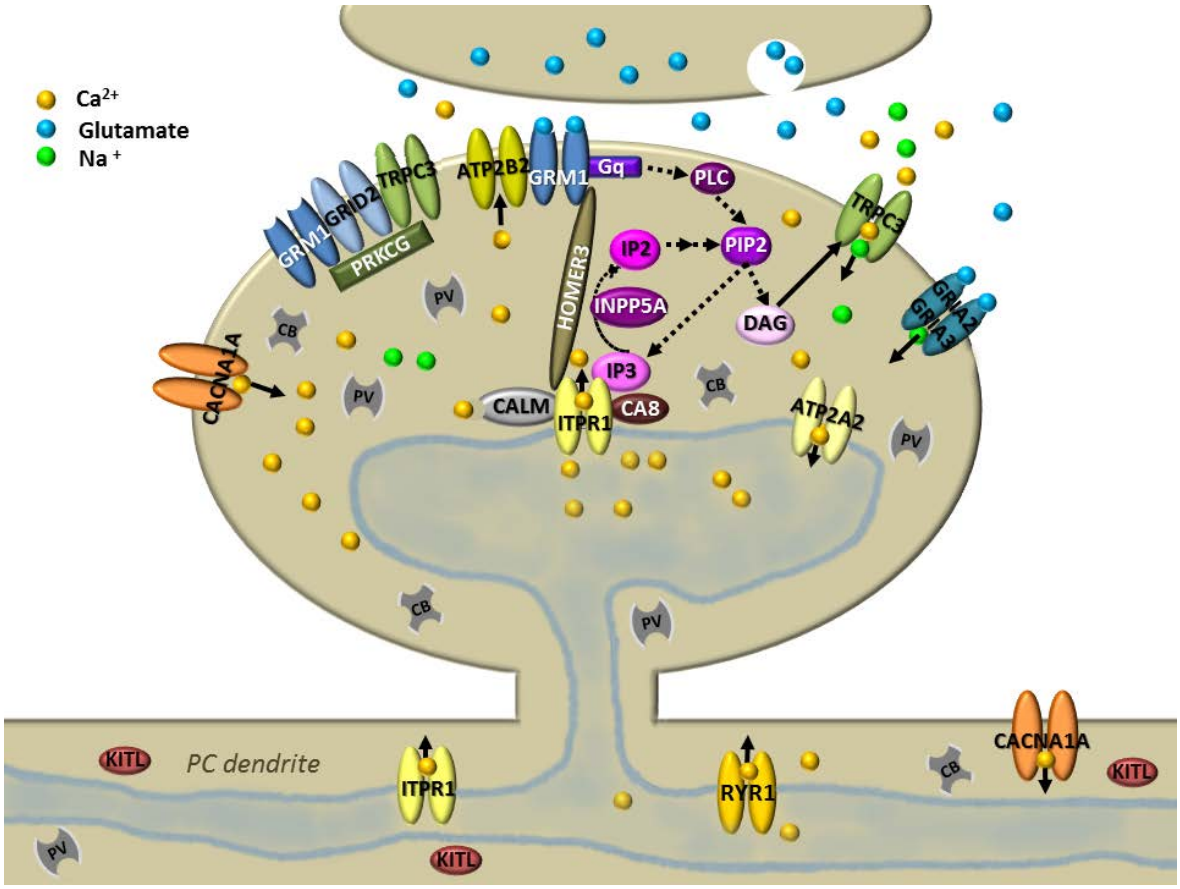

Figure 52. Calcium signaling in the Purkinje cell dendrite. Glutamate binding to the glutamate receptor (e.g. subunit GRM1) leads to activation of the G-protein subunit Gq and subsequent activation of PLC. PLC hydrolyzes PIP2 into DAG and IP3. IP3 can activate ITPR1 which in turn releases Ca^{2+} from the ER. CA8 and CALM1 are modifiers of ITPR1 activity. ITPR1 is linked to GRM1 via the scaffolding protein HOMER3. ATP2A2 pumps Ca^{2+} back into the ER while ATP2B2 pumps Ca^{2+} out of the cell. RYR1 is another receptor in the ER that releases Ca^{2+}. TRPC3 is a Ca^{2+} and Na^{+} channel that is regulated by DAG. There are also other glutamate receptors in the plasma membrane with subunits like GRIA2, GRIA3, or GRID2 for example. GRID2, TRPC3, and GRM1 are linked via PRKCG. CACNA1A is a calcium channel subunit and CB and PV are calcium buffering proteins. KITL is the ligand of the c-KIT receptor involved in cell survival and proliferation. ATP2A2 = ATPase, slow twitch 2; ATP2B2 = ATPase, plasma membrane 2; CA8 = Carbonic anhydrase 8, CACNA1A = Calcium channel, voltage-dependent, P/Q type, alpha 1A subunit; CALM = Calmodulin; CB = Calbindin; DAG = Diacylglycerol; GRIA2 =Glutamate receptor, ionotropic, AMPA 2; GRIA3 = Glutamate receptor, ionotropic, AMPA 3; GRID2 = Glutamate receptor, ionotropic, delta 2; GRM1 = Glutamate receptor, metabotropic 1; Gq = Guanine nucleotide binding protein (G protein), q polypeptide; INPP5A = Inositol polyphosphate-5-Phosphatase; IP2 = Inositol diphosphate; IP3 = Inositol triphosphate; ITPR1 = Inositol triphosphate receptor 1; KITL = c-Kit ligand; PIP2 = Phosphatidylinositol 4,5-bisphosphate, PRKCG = Protein kinase C, gamma; PLC = Phospholipase C; PV = Parvalbumin; RYR1 = Ryanodine receptor 1; TRPC3 = Transient receptor potential cation channel, subfamily C, member 3.

While transcript expression of calcium homeostasis factors was sufficiently analyzed in various polyQ mouse models, protein levels were not even studied once. Therefore, protein levels in *Atxn2*-KO and *Atxn2*-CAG42-KIN cerebellum were quantified in the RIPA (soluble) and in the SDS (insoluble) fraction. In general, protein levels of selected proteins were downregulated in the RIPA-soluble fraction in both mouse lines, while the proteins

accumulated in the SDS-soluble fraction in *Atxn2*-CAG42-KIN mice. In contrast, in the SDS-soluble fraction of *Atxn2*-KO mice, proteins were either downregulated as in the RIPA-soluble fraction or were not altered. Interestingly, ITPR1 showed moderate downregulation in the RIPA-soluble fraction of *Atxn2*-KO mice and no significant regulation in the SDS-soluble fraction (Figure 24), while it was drastically downregulated in the RIPA-soluble fraction of *Atxn2*-CAG42-KIN mice and upregulated in the SDS-soluble fraction (Figure 25). Comparison of ATP2A2 protein levels in the two mouse lines would have been of interest since *Atp2a2* showed the strongest dysregulation in *Atxn2*-KO mice and is the antagonist of ITPR1 but due to the lack of an appropriate antibody ATP2A2 was not quantified. The analysis of protein levels reveals that there are differences on protein level for calcium homeostasis factors, which parallel similar changes on transcript level. The data suggest that in *Atxn2*-KO mice the lack of ATXN2 leads to an overall decrease in protein levels while in *Atxn2*-CAG42-KIN mice proteins accumulate in the SDS-soluble fraction due to the CAG repeat expansion. It remains to be elucidated if overall protein levels are also altered in the *Atxn2*-CAG42-KIN mouse or if there is only a shift in solubility.

For SCA1, a mechanism how calcium homeostasis could be impaired has already been suggested: ATXN1 may affect the expression of several genes through its interaction with the transcription factor RORA and its co-activator TIP60 (Gehrking et al., 2011; Serra et al., 2006). Rora itself leads to ataxia when it is lost (“staggerer” mouse) and controls the transcript levels of several other components involved in the calcium pathway. A partial loss of TIP60 was demonstrated to slow down SCA1 progression in a mouse model by influencing RORA and thereby RORA-dependent transcripts (Gehrking et al., 2011).

Although *Rora* is downregulated in SCA2 and SCA3 (Konno et al., 2014) models as well the previous focus in these polyQ disorders was on a protein localized at the ER, ITPR1. This IP3 (Inositol triphosphate) receptor is an important mediator of calcium release from the ER. Liu et al. reported that the ITPR subtype 1 interacts with polyQ-expanded but not with WT ATXN2 *in vitro* and *in vivo* and that mutant ATXN2 facilitates ITPR1-mediated Ca^{2+} release in cultured Purkinje cells causing increased calcium content in the cytoplasm (Liu et al., 2009). Similar results were observed for mutant ATXN3 and HTT (Chen et al., 2008; Tang et al., 2003). Furthermore, in SCA2 transgenic mice altering Ca^{2+} signaling by use of a stabilizer or by suppression rescued motor incoordination (Kasumu et al., 2012). ITPR1 is specifically expressed in Purkinje cells of the cerebellum and exists as homo- and heterotetramer (together with ITPR2 and ITPR3). By binding of glutamate to the glutamate receptor (with GRM1 being one of the subunits that is linked to ITPR1 via HOMER3), the G protein subunit G_q (GNAQ) activates the phospholipase C (PLC; e.g. subunit PLCB4) that in turn hydrolyzes PIP2 (Phosphatidylinositol 4,5-bisphosphate) into

DAG (Diacylglycerol) and IP3 (Figure 52). This molecule then induces the release of Ca^{2+} from the ER by binding to ITPR1 while the ATPases *Atp2a2* and *Atp2b2* are responsible for Ca^{2+} transport back into the ER and out of the cell, respectively. IP3 can be dephosphorylated by INPP5A resulting in IP2 which is subsequently converted into PIP2 again. The activity of ITPR1 is furthermore regulated by its interactor protein CA8 as well as by the Ca^{2+} binding protein CALM1 (Adkins et al., 2000; Hirota et al., 2003; Kasri et al., 2004; Michikawa et al., 1999; Sun and Taylor, 2008).

In contrast to the data presented in Liu et al., an interaction of ITPR1 with both, WT and expanded ATXN2 was observed in *Atxn2*-CAG42-KIN cerebellum (Liu et al., 2009). Furthermore, CA8 was found to form part of this complex (Figure 26). Combining the data from *Atxn2*-KO and *Atxn2*-CAG42-KIN mice, one possible model is that ATXN2 and ITPR1 can interact at the ER membrane and in the cytoplasm. Due to a low stringency of the Co-IP lysis buffer used in this work it is possible that the observed interaction for WT and KIN only occurs in the RIPA-soluble fraction. Contrarily, in the SDS-soluble fraction the interaction may be limited to mutant ATXN2 as suggested by Liu and colleagues. This interaction then induces the accumulation of ITPR1 together with ATXN2 and leads to an increased activity of the receptor. However, according to the model proposed by Liu et al., ITPR1 activity should not be altered in *Atxn2*-KO animals as there is no mutated ATXN2. Thus, if ITPR1 activity is unchanged in *Atxn2*-KO mice the question rises how the observed changes are caused in this mouse model. Therefore, a second possible explanation is that the conditions applied in the earlier approach lead to a disruption of the interaction between WT ATXN2 and ITPR1, while the interaction between mutant ATXN2 and ITPR1 is stronger and therefore was not affected by these conditions. Consequently, in *Atxn2*-CAG42-KIN mice ITPR1 activity could be increased due to accumulation of ATXN2, while it could be decreased due to loss of ATXN2 in *Atxn2*-KO cerebellum. In *Atxn2*-Q58 transgenic mice it was observed that overexpression of INPP5A (which hydrolyzes IP3 thereby decreasing its amount and the possibility of ITPR1 activation) leads to an improvement of the rotarod and beam walk performance of the mice (Kasumu et al., 2012). Conversely, an overexpression of INPP5A in WT mice resulted in a slightly decreased performance. Thus, these data would fit to the second model indicating that too little (*Atxn2*-KO) as well as too much (*Atxn2*-KIN) ITPR1 activity is harmful. The length of the CAG repeat may thereby affect the strength of the interaction and the subsequent ITPR1 activity resulting in a stronger phenotype in *Atxn2*-CAG100-KIN animals.

If protein levels of calcium homeostasis factors are altered by loss or accumulation of ATXN2 the question remains through which mechanism transcript levels of these factors are changed. In *Atxn2*-CAG42-KIN mice, these changes could result from the accumulation of the protein and a subsequent feedback mechanism, but in *Atxn2*-KO

mice there is no accumulation that could cause a feedback mechanism. It is therefore possible that expression changes - and maybe also protein changes - are caused by a loss of ATXN2 function that affects transcript levels. Through its interaction with AREs (AU rich elements in the 3' untranslated region) in specific mRNAs (Figure 53) ATXN2 was shown to be responsible for their stabilization resulting in appropriate protein levels (Yokoshi et al., 2014). If ATXN2 is lost or mutated the efficiency of the stabilization is reduced and less mRNA is translated into protein. Transcripts of calcium homeostasis factors could be targets of ATXN2 resulting in decreased mRNA stability and presence. Consequently, there are various possible mechanisms that could disturb Ca^{2+} signaling and it remains unclear if ATXN2 affects transcript levels of the calcium homeostasis factors or protein levels or maybe both.

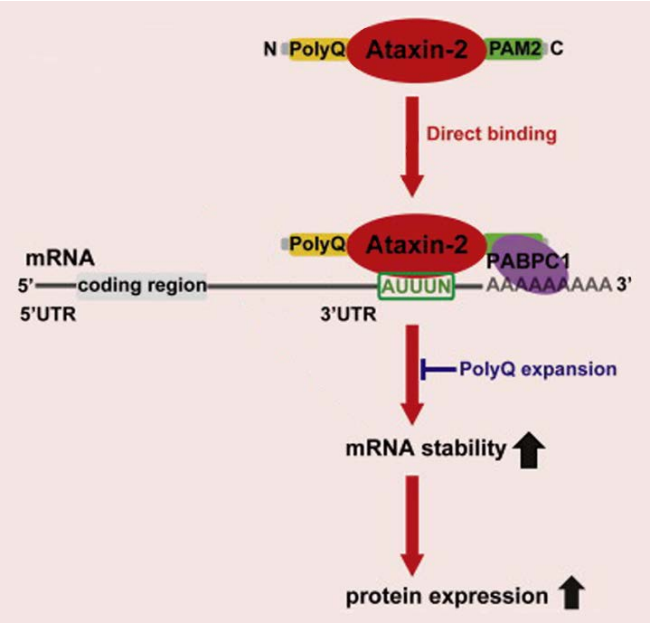

Figure 53. Influence of ATXN2 on mRNA stability. ATXN2 binds to AU-rich sequences (AREs) in the 3'UTR of target mRNAs thereby increasing mRNA stability and protein expression. PolyQ expanded ATXN2 has a decreased ability to stabilize target mRNAs (adapted from (Yokoshi et al., 2014)).

Independent of the mechanism that triggers downregulation, it is also possible that ATXN2 does not directly regulate the levels of all affected genes but only of specific ones. These specific genes may then influence other mRNAs or proteins of calcium homeostasis factors leading to an overall downregulation. The snowball hypothesis is indeed quite probable since a mutation or KO of other calcium homeostasis factors not involved in polyQ disorders like *Grm1*, *Ca8*, *Atp2b2*, and *Rora* also result in an ataxic phenotype and show similar transcript dysregulations (Guergueltcheva et al., 2012; Matsumoto et al., 1996; Rossi et al., 2010; Street et al., 1998; Turkmen et al., 2009). Motor incoordination on the rotarod has furthermore been observed in mouse models with abnormalities in the genes *Gnaq*, *Grid2*, and *Plcb4* (Ito, 2000). It is unlikely that each of these genes affect

every of the other genes. Probably, always one factor of the complex network is mutated or lost disturbing the signaling and subsequently all other factors are similarly affected.

Mitochondrial dysfunction should also be considered when discussing calcium signaling defects given that a depletion of ATP can cause ATPase dysfunctions and mitochondria also take up and release Ca^{2+}. Recently, it was found that the mitochondrial membrane protein PINK1 associates with mRNAs and translation initiation factors recruiting PABP to mitochondria (Hart et al., 2013). Therefore, it is possible that the PABP interactor ATXN2 also affects mitochondrial Ca^{2+} signaling. Furthermore, in a Purkinje cell model for SCA28 a defect in mitochondrial Ca^{2+} signaling was observed. Reduction of the Ca^{2+} influx by partial silencing of *Grm1* or the administration of an antibiotic that promotes synaptic glutamate clearance improved ataxic symptoms in this SCA28 model (Maltecca et al., 2015).

Interestingly, not only polyQ disorders exhibit altered calcium homeostasis but also other neurodegenerative diseases like AD (Bezprozvanny, 2010; Emilsson et al., 2006; Sepulveda-Falla et al., 2014), PD (Bezprozvanny, 2010; Melachroinou et al., 2013; Schapira, 2013), and ALS (Bezprozvanny, 2010; Grosskreutz et al., 2010; Lautenschlaeger et al., 2012; Mutihac et al., 2015) manifest with disturbed calcium signaling. Furthermore, it is known that calcium signaling in general is altered in the aging brain with an increase in cytoplasmic calcium concentration (Foster et al., 2001; Khachaturian, 1989; Verkhratsky and Toescu, 1998). It is therefore possible that the normal changes in calcium homeostasis are somehow aggravated by the loss or mutation of diverse proteins. Given that similar results were found in KO and KIN mice of Atxn1 and Atxn2 it is probable that a combination of both, gain- and loss-of-function causes the pathology observed in SCA1 and SCA2 (Zoghbi and Orr, 2009). Each mutant protein may influence calcium homeostasis in its own way for example by being directly involved in the calcium pathway or by means of transcription or translation regulation but the pathological features converge in the end.

4.1.3 ATXN2 loss strongly affects expression of ribosomal factors

A first clue for ATXN2 involvement in translation regulation came from interaction studies in *S. cerevisiae* showing that the ATXN2 homolog, PBP1, interacts with the RNA-binding proteins A2BP1 and PABP (Mangus et al., 1998; Shibata et al., 2000). Later on, ATXN2 was implicated in translation regulation in the germline of *C. elegans* and exhibited physical association with polyribosomes in *D. melanogaster* and in human cells *in vitro* (Ciosk et al., 2004; Satterfield and Pallanck, 2006). Furthermore, a co-localization of

ATXN2 with rough ER markers like calreticulin, calnexin, and GFP-ER was shown (van de Loo et al., 2009). More recently, *D. melanogaster* ATXN2, dATX2, was implicated in the translation regulation of a circadian clock gene (Lim and Allada, 2013; Zhang et al., 2013). Finally, as mentioned before, in 2014, Yokoshi et al. revealed ATXN2 binding to AU-rich elements in the 3'UTR of mRNAs mediating mRNA stability and protein expression (Yokoshi et al., 2014).

In the microarray transcriptome study of *Atxn2*-KO mice (Fittschen et al., in press), 17 ribosomal transcripts of the small and large ribosomal subunit were upregulated in cerebellum and liver. Fold changes of the transcript upregulations were small but very consistent and furthermore confirmed via RT-qPCR. In liver tissue of *Atxn2*-KO mice, several of the investigated factors selected by the availability of an appropriate antibody showed also strong upregulation on protein level (Figure 28). While PABPC1 was only measurable in the RIPA fraction, all other proteins were quantified in the SDS fraction. The reason for this difference may be that PABPC1 is more associated with the mRNA poly(A)-tail which is not necessarily located at the ER. Contrarily, many of the ribosomal proteins are localized at the rough ER and may be therefore less soluble than cytoplasmic ones. Fold changes for PABPC1, NOP10, and RPS10 were relatively high while minor alterations were detected for RPS3, RPS6, RPS18, and RACK1. The upregulation of PABPC1 in *Atxn2*-KO mice is an interesting observation because this protein also demonstrated increased transcript levels as well as a shift into insolubility on protein level in *Atxn2*-CAG42-KIN mice. Furthermore, an interaction of ATXN2 and PABPC1 was observed in these mice (Damrath et al., 2012). The similar regulation of Pabpc1 in the two mouse models suggests that loss and mutation of ATXN2 have similar consequences regarding translation regulation.

Assuming that ATXN2 is necessary for mRNA stability and protein expression and a depletion of ATXN2 leads to decreased protein expression at first glance it seems illogical that there is a protein increase in *Atxn2*-KO mice. Though, this upregulation may be an indirect effect of ATXN2 loss. Many other proteins, for example some of the calcium homeostasis factors may be downregulated due to the missing ATXN2. In turn, proteins involved in mRNA translation are upregulated to compensate for this decreased protein expression. Consequently, the global increase in transcript and protein expression of the translation machinery may not be a direct effect of ATXN2 loss but some kind of secondary compensating mechanism.

4.1.4 TBC1 domain family transcripts play a minor role in SCA2

TBC domain family members are a group of more than 40 different proteins with GTPase activity. For most of them their specificity has not been determined yet, but Rab proteins are a frequent target (Fukuda, 2011). TBC1 domain proteins proved to play a role in several mouse or cell culture models of neurodegenerative diseases. Tbc1d1, for example, was differentially regulated when the ALS gene TDP43 was deleted or overexpressed (Chiang 2010, Stallings 2013). Furthermore, in a KO mouse model of the stress granule marker *Tia1*, *Tbc1d24* was significantly upregulated. Unfortunately, knowledge about the TBC1 domain family members is limited.

In the microarray transcriptome data of *Atxn2*-KO mice, *Tbc1d8b* and *Tbc1d9b* appeared downregulated. The study of these two TBC1 domain family members as well as *Tbc1d1* and *Tbc1d24* in cerebellum and cortex of *Atxn2*-KO mice via RT-qPCR revealed subtle but not strikingly convincing downregulations (Table 48). Significant *Tbc1d1* and *Tbc1d24* downregulations were only detectable in cerebellum of 6-week-old animals. Tbc1d1 is the founding member of the TBC1 domain family and the only well-studied among the four mentioned genes. Its major impact is the insulin-mediated glucose transport via GLUT4 in skeletal muscle (Chadt et al., 2014; Chavez et al., 2008; Dokas et al., 2013; Roach et al., 2007). Besides, it has been associated with obesity and mutations in this gene are accompanied with leanness observed in the *lean* mouse (Chadt et al., 2008; Stone et al., 2006). In conclusion, dysregulations in *Tbc1d1* could have been involved in the development of the obese phenotype of *Atxn2*-KO but the observed expression changes do not seem convincing enough. These data, however, do not exclude the possibility that Tbc1d1 is somehow dysregulated on protein level. In contrast to *Tbc1d1*, *Tbc1d24* was additionally downregulated in cortex but not in cerebellum of 6-month-old *Atxn2*-KO mice. A slight downregulation was furthermore detected in young but not in old *Atxn2*-CAG42-KIN mice. The *Tbc1d24* gene has been associated with various brain disorders like epilepsy, cognitive impairment, cerebro-cerebellar malformation as well as with deafness (Afawi et al., 2013; Azaiez et al., 2014; Falace et al., 2010; Rehman et al., 2014). Therefore, it could have been involved in the brain pathology of SCA mice but again fold changes were low and not consistent. *Tbc1d8b* and *Tbc1d9b* showed decreased expression in cerebellum (but not in cortex) at 6 weeks and 6 months with a relatively high fold change for *Tbc1d8b*. Literature for Tbc1d8b is rare and for Tbc1d9b it is only known that it is a GTPase for *Rab11a* and that it regulates transcytosis in polarized canine kidney cells (Gallo et al., 2014). In conclusion, downregulation of these four transcripts is not strong and consistent enough (at least on transcript level) to trigger any credible effect. The overall effect size of TBC1 domain family member dysregulations in *Atxn2* mice was rather small. In *Atxn2*-CAG42-KIN mice no consistent expression changes at all were

observed. Thus, transcript data of TBC1 domain family genes do not indicate a major role for these genes in SCA2. Fold changes in the *Tia1*-KO, for example, were much more pronounced. However, these genes might be good candidates to be studied in the Atxn2 + TDP43 double mutant.

4.1.5 ATXN1 is relevant for human SCA2 pathology and BEAN1 is a potential candidate

The SCA genes are a heterogeneous group although their mutations all result in ataxia accompanied with varying other symptoms. An interaction between these genes or an implication in a common pathway could explain their similar phenotype. Some interactions and effects on each other's pathology have already been observed. For example, ATXN2 has been shown to interact with ATXN1 (SCA1) and ITPR1 (SCA15/16/29). The interplay of ATXN2 and ATXN1 was studied *in vitro* as well as in *D. melanogaster* models and an influence of ATXN2 on SCA1 pathology was observed (Al-Ramahi et al., 2007). A similar effect of ATXN2 was observed for SCA3 (Lessing and Bonini, 2008). Therefore, SCA transcript levels were studied in three Atxn2 mouse models in search for modulators of SCA2 pathology.

Only three out of ~ 20 SCA genes exhibited dysregulation in *Atxn2*-KO and *Atxn2*-CAG42-KIN mice: *Atxn1* and *Itpr1* for both of which an protein interaction with ATXN2 had already been shown and *Bean1*, an interactor of the ubiquitin-protein ligase NEDD4. *Atxn1* was similarly reduced on transcript level in cerebellar tissue of both mouse models (Table 50, Table 51). Fold changes were small but the alterations were consistent. *Bean1* was downregulated in *Atxn2*-KO mice similar to *Atxn1* but changed from being decreased in young to being strongly increased in old *Atxn2*-CAG42-KIN mice.

Protein data of *Atxn2*-KO, *Atxn2*-CAG42-KIN, and SCA2 patient fibroblasts are convincing in that Atxn1 is indeed somehow involved in SCA2 pathology. In general, the main outcome was the same in *Atxn2*-CAG42-KIN mice and SCA2 patient fibroblasts: a decreased transcript level and an accumulation of the protein in the SDS-soluble fraction. It is of interest that in *Atxn1*-Q154-KIN mice Atxn2 was downregulated on transcript level comparable to Atxn1 in Atxn2 mice and accumulated on protein level in both fractions (Figure 31). Nevertheless, no visible accumulation of ATXN2 was observed in immunohistochemical slices of *Atxn1*-Q154-KIN brains. Regarding immunohistochemical stainings it should be mentioned here that none of the commercially available antibodies for ATXN1 was able to detect a specific signal in the nucleus. Stainings with different antibodies and different antigen retrieval techniques always revealed either no or only a

cytoplasmic signal. Consequently, ATXN1 staining in *Atxn2*-CAG42-KIN mice was not shown here.

Atxn1 and Atxn2 both display a similar regulation in the respective other mouse model indicating that there is a mutual influence. Although Atxn1 is not dysregulated on transcript level in *Atxn2*-CAG100-KIN mice which show a strong SCA2 pathology it seems to be of clinical relevance as it is also altered in SCA2 patient material. Possibly, the length of the CAG repeat does not only influence effect strength but also the pool of affected genes. Thus, Atxn1 could be involved in the pathology of moderate Atxn2 expansion while another SCA gene is more affected in longer Atxn2 expansions. SCA6, 11, and 13, for example, are significantly altered in *Atxn2*-CAG100-KIN mice and could be modifiers of SCA2 pathology resulting from long repeat expansions. Furthermore, Bean1 probably would have been a quite good candidate for these studies as well since it showed even higher fold changes than Atxn1 in all mouse models but the literature about Bean1 is scarce and antibody availability limited. Thus, studies about Bean1 look promising and may be continued at a later point in time.

4.2 Evaluation of two new mouse lines for ALS and SCA2

Usually, when a new mouse model of disease is being generated, it is gratifying to observe an early and strong phenotype. At the same time, the mouse line should model the disease adequately with characteristics similar to human disease. The use of a transgenic mouse model with overexpression of the respective gene can hasten the pathological progression, whereas a knock-in model resembles more the natural expression pattern of the mutant gene and the natural history of the disease. The aim of the study is thereby decisive for the type of the mouse model that shall be generated.

In this thesis two new mouse lines were characterized: a double KIN mutant consisting of two formerly studied mouse lines for SCA2 and ALS and a completely new SCA2 KIN mouse model. Both mouse models were generated in an attempt to get a better insight into the general (not cerebellum-specific) function of Atxn2 and its interaction with the ALS gene *Tardbp*.

4.2.1 ATXN2 and TDP43 might affect each other's pathology

SCA2 and ALS are two neurodegenerative diseases that at first sight do not seem to possess many common features. SCA2 is exclusively inherited while ALS mostly occurs sporadically (Sreedharan and Brown, 2013). The age of onset in ALS is usually later than in SCA2 but ALS shows a much faster progression than SCA2 does (Cleveland and Rothstein, 2001). Furthermore, SCA2 is caused by one specific gene and mainly affects the cerebellum while several different genes account for the various ALS subtypes and impinge on the spinal cord (Arai et al., 2006; DeJesus-Hernandez et al., 2011; Kwiatkowski et al., 2009; Neumann et al., 2006; Renton et al., 2011; Rosen et al., 1993; Sreedharan and Brown, 2013; Synofzik et al., 2012; Vance et al., 2009). Nonetheless, an association of ATXN2 with ALS risk (Elden et al., 2010) and an involvement of ALS genes in SCA2 pathology (Toyoshima et al., 2011) have been observed. Moreover, ATXN2 and the ALS causing protein TDP43 were shown to interact in *S. cerevisiae* and *D. melanogaster* and ATXN2 was demonstrated to be a modifier of TDP43 toxicity (Elden et al., 2010; Kim et al., 2014). TDP43 is special in that it is not only implicated in ALS when it is mutated but also when other genes are the main causative factors (Neumann et al., 2006; Tollervey et al., 2011). To study the mutual effect of ATXN2 and TDP43 in mice, two mouse models with mutations in these genes were combined to receive a double KIN mutant. This double mutant was subsequently characterized on behavioral level together with the single mutants and WT animals to look for a possible potentiation effect.

4.2.1.1 Behavioral observations in double mutants differ from expectations

In both, SCA2 and ALS, weight loss is frequently observed and - at least for ALS - associated with shorter survival (Abdel-Aleem and Zaki, 2008; Korner et al., 2013). Furthermore, in formerly *Atxn2*-CAG42-KIN (starting at 10 weeks of age) and hTDP43-A315T-KIN (starting at 15 months of age) single mutants a reduction in body weight was observed (Damrath et al., 2012; Stribl et al., 2014). Therefore, double mutants were supposed to exhibit an even stronger decrease in body weight compared to single mutants. Strikingly, no reduction in weight was noted in the new single or double mutants compared to WT until 12 months of age (Figure 32 and Supplementary Figure 5). In female mice, Atxn2 single mutants even showed an increase in weight at 9 and 12 months. The only difference between the single mutants in this study and in the former ones is a slight change in background. Both single mutants were not completely backcrossed (> eight times) from 129Sv/Pas (ATXN2) and Rosa26Cre (TDP43) to C57BL/6 when their body weight was assessed in earlier studies (Damrath et al., 2012; Stribl et al., 2014). For the generation of the double mutants, mice that were crossed back

at least eight times into C57BL/6 were used. However, there was again a slight difference as C57BL/6J mice were used for *Atxn2*-CAG42-KIN mice and C57BL/6N for hTDP43-A315T-KIN mice. The final double mutants were not further backcrossed acting on the assumption that the differences between these two substrains are insignificant. However, there seem to be differences either due to a change in background caused by backcrossing or due to a mixed J+N background in the new breeding colony including double mutants, single mutants, and WT animals. Irrespective of the fact that there were alterations between former and new single mutants, there was no significant change between the new single and double mutants which were all in the same mixed background.

The assessment of impaired cerebellar coordination movement tasks in mouse models is traditionally done via rotarod analysis. With the help of this rotating rod the ability of the animals to walk and to balance on a moving ground is assessed. In the course of a trial the rotarod can accelerate thereby increasing the difficulty of the task. Animals with impaired movement coordination have a lower latency to fall than WT animals. *Atxn2*-CAG42-KIN animals were supposed to show a rotarod phenotype at 18 months of age. In the study together with the double mutants, Atxn2 single mutants performed worse at 6 month of age but not at 9 or 12 months of age. This is in contrast to what would be expected from a progressive mouse model. Given that there was only a small number of animals available, the ones used for the trials at 6 and 9 months of age were partly the same. Therefore, it is likely that some of the 9-month-old animals learnt and became used to the testing procedure, consequently performing better than they would normally do. At 12 months of age the fold change is again higher between Atxn2 single mutants and WT animals but due to a low number of animals the standard deviation is too high for significance to be reached. Given the reduced (although not significant) latency to fall of Atxn2 single mutants at 9 and 12 months of age it is quite probable that these mice show again a decreased rotarod performance at later ages (> 15 months) or when the number of animals is increased at 12 months of age. TDP43 single mutants did not show a decreased rotarod performance at the analyzed ages, an observation similar to that in earlier studies of these mice. Double mutants also did not differ from WT animals and only at 6 months of age performed slightly but not significantly better than Atxn2 single mutants. Nevertheless, given that at 12 months of age all mutants seem to have a slightly decreased (but not significant) rotarod performance compared to WT animals it is possible that they will exhibit a motor impairment on the rotarod at 15 months of age or later. Regarding the background changes, it should be mentioned that there is an approved difference in this motor task between C57BL/6J and C57BL/6N mice with the latter ones exhibiting a significantly lower latency to fall (Bryant et al., 2008). Thus, the rotarod

performance of the new mutants could differ from former observations and, therefore, it is definitely worth to study older animals on the rotarod.

The spontaneous locomotor behavior of the double mutants was assessed in the open field, a test paradigm that reveals pathology of basal ganglia, cortex, and spinal cord. In a glass box of 20 x 20 cm, every movement of the mouse is tracked via laser beams. This study revealed the most pronounced changes of all behavioral tests. Still, TDP43 single mutants did not show any deviation from WT mice, but Atxn2 single mutants exhibited significantly decreased activity at 6, 9, and 12 months of age. This is in contrast to the formerly studied single mutants that did not show consistent changes in the open field (Damrath et al., 2012). Furthermore, the open field study was the only analysis in which changes between WT and double mutants and even between single and double mutants were detectable. While Atxn2 single mutants displayed a reduced activity at all ages, the additional TDP43 mutation increased the activity of the double mutants (rescue) at 6 months of age (Figure 34). Interestingly, this increase was limited to horizontal parameters; vertical parameters were similarly decreased in Atxn2 single and double mutants. However, this rescue effect was no longer seen in 9- and 12-month-old animals. At 12 months of age, double mutants were even slightly but not significantly less active than Atxn2 single mutants (Figure 36). Comparing TDP43 single and double mutants, alterations remained stable throughout the ages. Deterioration due to the additional Atxn2 mutation was already detectable at 6 months of age and again at 12 months of age. The fact that at 9 months of age significances were only detected for vertical parameters may result from the repeated usage of the same animals as explained above. In conclusion, the effect of TDP43 mutation on the activity of Atxn2 single mutants varies with the age while Atxn2 mutation continuously decreases the activity of TDP43 single mutants. Generally, vertical parameters were most affected and may result from problems with upright positioning and balancing.

4.2.1.2 Possible potentiation effect of ATXN2 and TDP43 mutation in old animals

The double mutants were generated to study a possible potentiation effect of ATXN2 and TDP43 since a strong impact of ATXN2 on TDP43 toxicity was observed in *S. cerevisiae* and *D. melanogaster* models (Elden et al., 2010; Kim et al., 2014). Given that formerly both single mutants showed a decrease in body weight an effect on this parameter was most probable. The fact that there was no alteration was astonishing but may be explained by changes of the genetic background in the mouse lines. Neither for the rotarod performance nor for the locomotor activity measured in the open field paradigm a potentiation effect was consistently observed either, although there seems to be a

progression of motor deficits. Transcript levels of ATXN2 and TDP43 (murine or human) also remained unchanged between single and double mutants (data not shown). This fact is again surprising as it was shown that TDP43 is one of the targets of ATXN2 regarding the regulation of mRNA stability and protein expression via binding to the 3'UTR (Yokoshi et al., 2014). Consequently, the mutation of ATXN2 should decrease TDP43 transcript levels. Possibly, this effect is diminished by the strong overexpression of human TDP43 which cannot be regulated due to a missing 3'UTR. Overall, in none of the analyzed parameters a potentiation effect of ATXN2 and TDP43 was determined. However, the data look very promising to obtain this effect at older ages (>15 months or later) given that the rescue effect of TDP43 disappeared at older ages and the activity of double mutants slightly decreased compared to Atxn2 single mutants. Furthermore, the results emphasize the relevance of the genetic background as a possible covariate to explain phenotypes in double mutants.

4.2.2 The *Atxn2*-CAG100-KIN mouse manifests several features of SCA2 pathology

The *Atxn2*-CAG42-KIN mouse was the first SCA2 mouse model that expressed mutated Atxn2 under the murine Atxn2 promoter without overexpression but with natural temporal and spatial expression. Nevertheless, the usefulness of this mouse model was limited since the first behavioral symptoms appeared late (18 months of age). To age mice for such a long period is time-consuming and expensive and the lead time for a new experiment is quite long. Besides, the effects observed in *Atxn2*-CAG42-KIN mice were minor compared with those in transgenic mice or with human SCA2 pathology. Therefore, a second KIN mouse line was generated with an expanded repeat of 100 CAGs. Regarding the fact that a longer CAG repeat has been associated with a stronger disease phenotype this mouse model was expected to exhibit an earlier and more severe pathology (Almaguer-Mederos et al., 2013). To study the usefulness of this model it was characterized on behavioral, immunohistochemical and molecular level.

4.2.2.1 Shortened lifetime as a feature of SCA2 pathology

While in some other SCAs life expectancy of the patients is not affected (e.g. SCA6), a decreased survival rate was observed in SCA1, SCA2, SCA4, and SCA7 (Tezenas du Montcel et al., 2012). In a study of Cuban SCA2 patients, ~4% of the individuals in the sex- and age-matched healthy control group passed away compared to ~29% in the SCA2 patient group. Furthermore, the survival of the patients was dependent on the CAG

repeat length (Almaguer-Mederos et al., 2013). No alteration in the survival was observed in the moderate expansion *Atxn2*-CAG42-KIN mouse model (Damrath, 2012). In contrast, decreased survival was determined for homozygous *Atxn2*-CAG100-KIN (HOM) mice. About 32% of the HOM mice died suddenly without any obvious pathological indication, while none of the WT animals died within the first 20 weeks of age (Figure 39). Interestingly, a decreased survival has also been reported for SCA1, HD, and SBMA mice indicating that this is a frequent feature in polyQ mouse models (Adachi et al., 2001; Hurlbert et al., 1999; Watase et al., 2002). Thus, *Atxn2*-CAG100-KIN mice displayed similar shortening of survival rates as SCA2 patients although there was no visible health impairment at young ages.

4.2.2.2 Indication for a role of fatty acid metabolism in SCA2 pathology

A sign that was already observed in *Atxn2*-CAG42-KIN mice and that is one of the most obvious changes in late stage SCA2 patients is weight loss (Damrath et al., 2012). In humans it is associated with the loss of subcutaneous fat preceded by an increased appetite and moderate obesity in the mid-course of disease (Abdel-Aleem and Zaki, 2008; Auburger, 2012). A drastic stagnation in weight gain and at later stages also a weight loss was observed in male and female *Atxn2*-CAG100-KIN mice. However, there was a difference in the development of this leanness between male and female animals: male mice showed an earlier affection than female mice and HET animals were also affected, while this was not the case in young female animals (Figure 40). These data indicate that there are gender-specific differences in the strength of pathology. Regarding this aspect it is of interest that mean age at onset can vary between male and female SCA2 patients with an earlier occurrence in male patients. Furthermore, CAG repeat instability is more pronounced in paternal than in maternal transmission (Giuffrida et al., 1999). It is therefore possible that the *Atxn2*-CAG100-KIN mouse reflects gender-specific differences of SCA2. Generally, alterations in weight have also been associated with other polyQ disorders like SCA1 (Mahler et al., 2014), SCA3 (Saute et al., 2012), SCA17 (Kelp et al., 2013), HD (Aziz et al., 2008; Hamilton et al., 2004), and SBMA (Adachi et al., 2001) but also with other neurodegenerative diseases like AD and PD (Sergi et al., 2013; Sharma and Vassallo, 2014). Furthermore, in SCA17 mice, a later weight loss was observed in female compared to male mice like in *Atxn2*-CAG100-KIN animals (Kelp et al., 2013).

Possibly, weight loss in SCAs is associated with glucose metabolism and fatty acid availability. In SCA34 and SCA38, for example, an involvement of fatty acid metabolism has already been observed since the causative proteins ELOVL4 and ELOVL5 are fatty acid elongases (Di Gregorio et al., 2014). Furthermore, *Atxn2*-KO mice show an obese phenotype, deranged insulin signaling, and disturbed lipid metabolism in the cerebellum

(Lastres-Becker et al., 2008a). Thus, it is quite possible that ATXN2 is also involved in this pathway. Macroscopically, the amount of subcutaneous fat seemed decreased in *Atxn2*-CAG100-KIN mice but was not statistically evaluated. In fact, a deranged fatty acid metabolism could not only explain changes in fat deposition and weight loss but could also affect the brain function. Lipids are essential for neuronal signaling and for example the myelin sheath around the dendrites is mainly composed of fat. Intracellular signaling is based on lipids as well because they serve as precursors for various second messengers (Adibhatla and Hatcher, 2007). Consequently, an altered lipid metabolism may not only account for the weight loss but could also be involved in neuronal degeneration.

4.2.2.3 Early and pronounced impairment of cerebellar motor coordination in *Atxn2*-CAG100-KIN mice may result from defects in glutamate and calcium signaling

Movement incoordination manifesting as progressive ataxia is the joint feature of all SCAs. A reduced rotarod performance was already observed in SCA1 (Watase et al., 2002), SCA2 (Hansen et al., 2013), SCA3 (Switonski et al., 2015), SCA6 (Watase et al., 2008), SCA7 (Yoo et al., 2003), HD (Carter et al., 1999), and SBMA (Adachi et al., 2001) mouse models. In *Atxn2*-CAG42-KIN mice, a rotarod phenotype was not detected before the age of 18 months. Young heterozygous mice of this mouse line even performed better than WT animals (Damrath et al., 2012). Regarding *Atxn2*-CAG100-KIN mice, WT, HET, and HOM animals exhibited a similar latency to fall off the rotarod at 10 weeks of age. Deficits in motor performance started at 20 weeks of age for HOM (but not HET) mice (Figure 41). The ability to walk and balance on the accelerating rotarod further decreased in these mice until 14 months of age. During the four trials of one experimental day the motor performance of all, WT, HET, and HOM mice, was increasing from trial to trial irrespective of the age (data not shown). Consequently, their ability to learn was not decreased. This effect was also observed in *Atxn2*-CAG42-KIN mice (Damrath, 2012). The data indicate that while the motor coordination of homozygous *Atxn2*-CAG100-KIN mice is impaired, they are still able to learn and to improve their coordination. Besides, *Atxn1*-Q154-KIN mice show a similar ability to learn on the rotarod and when these mice were trained for four consecutive weeks on the rotarod their lifespan was significantly extended (Fryer et al., 2011; Watase et al., 2002). Indeed, studies in Spinocerebellar ataxia patients demonstrate that physiotherapy and coordination exercises improve motor performance and ataxia in children and adults (Ilg et al., 2012; Ilg et al., 2009; Synofzik and Ilg, 2014).

In contrast to the rotarod which mainly measures movement coordination and balance, the open field apparatus assesses the overall activity of the mice. Open field analysis is less

frequently used in polyQ mouse models but is of specific interest in regard of the overall locomotor and exploration behavior of the animals. In *Atxn2*-CAG42-KIN mice no consistent alterations were detected in this behavioral test (Damrath et al., 2012). Contrarily, HOM *Atxn2*-CAG100-KIN mice exhibited hyperactivity on horizontal level at younger ages but decreased vertical parameters at older ages (Figure 42). The horizontal parameters indicate that the exploration behavior of the mice is increased and the mice are less anxious travelling around most of the time. The decreased vertical activity suggests that the animals avoid upright positions maybe due to balancing problems. Interestingly, in a study employing rats the use of different NMDA and AMPA receptor antagonists lead to an increased horizontal but decreased vertical activity in the open field test (Danysz et al., 1994) like in *Atxn2*-CAG100-KIN animals. Additionally, ataxia and stereotypic behavior occurred in these animals. It is possible that the effects observed in the open field in *Atxn2*-CAG100-KIN mice are derived from the deranged glutamate and calcium signaling in these animals. Consequently, modulating this pathway could potentially improve the locomotor deficits of these mice.

4.2.2.4 Clasping, altered gait, and tremor prove severe pathology in old *Atxn2*-CAG100-KIN mice

Although there are gait disturbances in SCA mouse models, a real ataxic gait is barely observed since this feature is much less evident in quadripedal rodents (Yang et al., 2014a). Similarly, in *Atxn2*-CAG100-KIN mice, a typical ataxic gait was not visible in the examined time frame (14 months of age). However, disturbances in walking behavior and limb coordination were detected in old HOM animals. Via video analyses, clasping and walking behavior were compared between old WT and HOM animals. While WT animals spread their limbs when suspended by their tails HOM animals clasped their hind and sometimes also their fore legs (bat-like posture) (Figure 43). A similar behavior was observed in SCA3 (Boy et al., 2009; Cemal et al., 2002), SCA6 (Alonso et al., 2008; Takahashi et al., 2009; Takahashi et al., 2010), SCA7 (Chou et al., 2010; Garden et al., 2002), SCA14 (Zhang et al., 2009a), HD (Heng et al., 2007; Mangiarini et al., 1996; Reddy et al., 1998), and SBMA (McManamny et al., 2002) mouse models. Interestingly, a clasping phenotype was also documented in the “staggerer” mouse (loss of *Rora*) (Lalonde, 1987; Zhang et al., 2009a). Given that most of these genes cause cerebellar damage it is possible that the clasping phenotype in these mice is caused by deficits in this brain structure. Nevertheless, HD is not a typical cerebellar disease but mouse models of HD show the clasping phenotype as well as mouse models of AD (Lalonde et al., 2005). Thus, clasping may not only be associated with cerebellar deficits but may

comprise cerebello-cortico-reticular and cortico-striato-pallido-reticular pathways (Lalonde and Strazielle, 2011).

When walking on a beam or on a flat ground, HOM animals showed an abnormal hind leg and a flattened body position. WT mice walking on the beam used their tails for balancing (Figure 44) an attitude that was less pronounced in HOM mice and suggests decreased balancing capability. Besides, HOM mice showed a stretching behavior pushing their feet far behind their body. When walking, the altered gait of the HOM mice was hearable as their claws scratched on the ground when they pushed them backwards. A visible tremor especially of the head (titubation) and when suspended by the tail adds to these pathological observations. Tremor is a quite common symptom in SCA2. In particular tremor of the postural and intention type but also titubation have been observed (Estrada et al., 1999; Jhunjhunwala et al., 2014; Schols et al., 1997). These additional observations suggest a profound behavioral phenotype in *Atxn2*-CAG100-KIN mice with a strong affection of voluntary movement coordination.

4.2.2.5 Brain abnormalities in old *Atxn2*-CAG100-KIN mice

Neurodegeneration can be either observed microscopically in brain slices by counting the cell number or macroscopically by measuring the weight of the brain as neuronal loss is associated with brain weight loss. In old *Atxn2*-CAG100-KIN mice, neurodegeneration was already observable by eye since HOM brains showed a dramatic shrinkage in size (Figure 46). Interestingly, not only the cerebellum showed massive neurodegeneration but the whole brain exhibited a decrease in size. In SCA2, atrophy is most often observed in the cerebellum, especially the Purkinje cells but also in the pontine nuclei, inferior olive, and substantia nigra of the brainstem, in the cerebral cortex, and in the anterior horn of the spinal cord. The affection of the different brain areas varies from patient to patient and may also include other regions like thalamus, red nucleus, locus coerulus, and the posterior column of the spinal cord (Brenneis et al., 2003; Huynh et al., 2007; Ishida et al., 2011). Overall, there is a shrinkage of the brain in SCA2 associated with a marked reduction in brain weight (<1000 g) (Prayson, 2005) as modeled in *Atxn2*-CAG100-KIN mice. The normal brain weight is about 1336 g in male and 1198 g in female adults (Hartmann et al., 1994). Thus, the estimated average brain weight of an adult human is about 1267 g. Assuming a brain weight of 999 g for SCA2 patients this would already imply a decrease of more than 20%. In 14-month-old female HOM mice the average brain weight loss was about 45% weight loss (Figure 46). Similar effects were reported in HD patients and HD mouse models. Brain weight reduction in HD patients was observed to be ~30% (de la Monte et al., 1988) and 20% in a transgenic HD mouse model with ~125 CAGs (Mangiarini et al., 1996).

Another common hallmark of neurodegenerative disorders is the formation of cytoplasmic or nuclear aggregates / inclusion bodies. Most of the polyQ disorders show mainly nuclear inclusion bodies like SCA1 (Cummings et al., 1999), SCA3 (Paulson et al., 1997; Switonski et al., 2015), SCA7 (Holmberg et al., 1998), SCA17 (Rolfs et al., 2003), and HD (Davies et al., 1997). Contrarily, in SCA2, the cytoplasmic ATXN2 protein forms aggregates primarily in the cytoplasm and less in the nucleus (Huynh et al., 2007; Ishida et al., 2011).

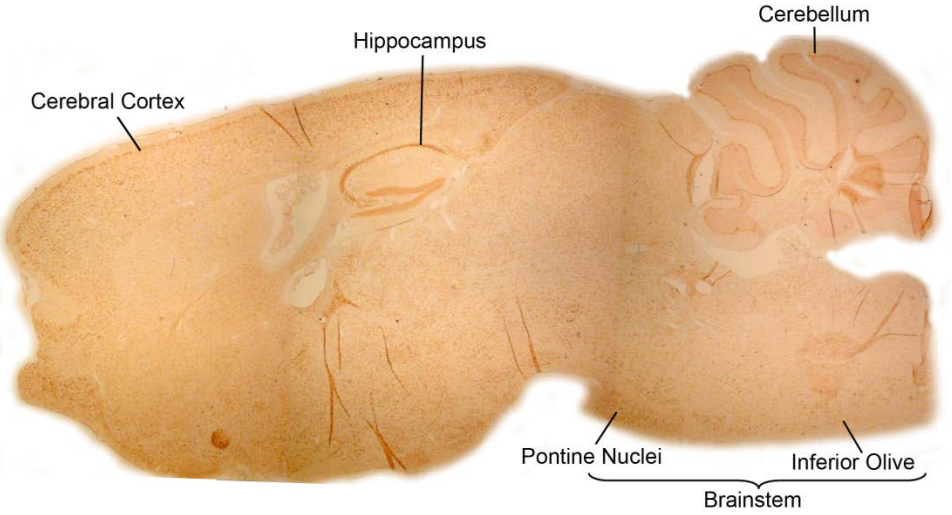

Figure 54. Brain regions in Atxn2-CAG100-KIN mice with pronounced ATXN2 aggregation. Sagittal slice of a 14-month-old *Atxn2*-CAG100-KIN brain stained with anti-ATXN2. The brain regions in which ATXN2 aggregates and aggregates with ATXN2+p62 or ATXN2+UBQ were displayed in Figure 47, Figure 50, and Figure 49 are depicted. Aggregates were also detected in basal forebrain.

In brain slices of old HOM *Atxn2*-CAG100-KIN mice aggregation of ATXN2 was detected in various brain regions similar to human pathology (Figure 54). Cytoplasmic aggregates were found in the Purkinje cells, the inferior olive, pontine nuclei, cerebral cortex, hippocampus, the spinal cord (Figure 47 and Figure 54) and other brain regions not depicted here. Nuclear inclusions were not observed. Usage of an antibody specific for long polyQ tracts confirmed the aggregation of ATXN2 in these brain regions (Figure ***48***). Already at an age of 30 weeks strong aggregation of ATXN2 was found in several brain regions (data not shown). It would be of interest at which age accumulation can be noticed for the first time and if this time point is prior to the start of the behavioral deficits. In *Atxn2*-CAG42-KIN mice aggregates of ATXN2 were detected starting at 14 months of age while rotarod deficits were observed not before 18 months of age (Damrath et al., 2012). In contrast, in many other polyQ mouse models, behavioral deficits precede detectable aggregation of the mutant protein which may therefore not account for the behavioral deficits (Boy et al., 2009; Chou et al., 2008; Clark et al., 1997). In SCA1 and SCA7 mice, inclusion body formation has even been proven to be helpful for survival (Bowman et al., 2005; Watase et al., 2002; Yoo et al., 2003). Furthermore, a recent publication

demonstrates that short Q-rich prion-like proteins can prevent the cytotoxicity of aggregates by altering their physical properties (Ripaud et al., 2014). Thus, it remains elusive whether aggregate formation in general is helpful for the neurons or not and if it contributes to the behavioral deficits.

It has furthermore to be elucidated what is the role of the sequestrated proteins in these inclusions. Ubiquitin and p62, representatives of the cellular degradation machinery, are frequently found in aggregates of polyQ and other neurodegenerative diseases indicating that this is a general mechanism occurring when mutant, aggregation-prone proteins are present (Alves et al., 2014; Koyano et al., 1999; Kuusisto et al., 2001; Pikkarainen et al., 2008; Rue et al., 2013; Seidel et al., 2010; Sieradzan et al., 1999; Yang et al., 2014b). Concerning this matter, it is of interest that p62 and UBQ were not found in ATXN2 aggregates of *Atxn2*-CAG42-KIN mice although these mice show several signs of pathology (Damrath, 2012). Possibly, due to the moderate repeat expansion and only slight ATXN2 aggregation (compared to *Atxn2*-CAG100-KIN mice) sequestration of these factors occurs at very late stages but as it is hard to age mice more than 24 months older animals have not been studied, yet. This observation suggests that p62 and UBQ sequestration are not necessarily part of the protein aggregates and consequently their impairment may not cause the observed pathology. Unfortunately, it does not help to answer the question if protein sequestration is for the sake or for the fate of the cell. Regarding this aspect, different roles have been proposed for p62. In an HD mouse model depletion of p62 ameliorated pathology (Kurosawa et al., 2015). Contrarily, it exacerbated the motor phenotype in SBMA mice, while overexpression of p62 helped against AR toxicity (Doi et al., 2013). In an *in vitro* model for SCA3, p62 was necessary for aggresome formation and helped against ATXN3-induced cell death (Kurosawa et al., 2015; Zhou et al., 2014). Moreover, a *D. melanogaster* model for SCA3 showed that a knockdown of p62 delayed the degradation of the mutant ATXN3 protein and exacerbated eye degeneration (Saitoh et al., 2015). Thus, the role of p62 in protein aggregates is still up for debate.

Interestingly, in *Atxn2*-CAG100-KIN mice a difference in the frequency of p62 and UBQ aggregation was observed in the examined brain regions. In brainstem and spinal cord several neurons showed co-localization of ATXN2 and UBQ or p62 in cytoplasmic aggregates. Co-localization did not occur throughout all aggregates but in the main parts. In Purkinje cells, inclusion formation of these two proteins was rarely detected. While ATXN2 was aggregated in nearly all Purkinje cells, UBQ or p62 showed accumulation in only some of these cells resulting in few neurons with co-localization. This is an interesting observation given that the main SCA2 pathology is caused by cerebellar deficits. Maybe there are other markers that are specifically sequestrated in Purkinje cells and that have not been examined yet (e.g. chaperones) or are still unknown. Alternatively, assuming that

p62 and UBQ are helpful for decreasing mutant protein levels and pathology, Purkinje cells may be more vulnerable as they barely include these markers. The shape and size of the aggregates may also be associated with these differences since co-localization was most often seen in larger and more granular aggregates that were not observed in Purkinje cells. In summary, a strong affection of the brain with aggregation of the mutant protein as well as other markers and obvious atrophy in *Atxn2*-CAG100-KIN represents SCA2 pathology appropriately.

4.2.2.6 The *Atxn2*-CAG100-KIN mouse is a useful and valuable model for SCA2

Atxn2-CAG100-KIN mice mimic several features of SCA2 pathology like decreased survival, weight loss, and impaired motor performance. All these features were already observed in young mice and further increased with age indicating a progressive disease development. Especially motor coordination on the rotarod is a parameter that is regularly used to study motor impairment before and after therapeutic treatments. In this regard, the early appearance of the rotarod phenotype renders this mouse an appropriate model for therapeutic trials. Furthermore, these mice show an early and strong pathology with aggregation of the mutant protein including sequestration of common inclusion markers like ubiquitin and p62. The appearance of an early phenotype is also important for electrophysiological studies. Previous studies in *Atxn2*-KO mice regarding calcium signaling were not successful because the phenotype in young mice was not strong enough (data not shown) and old mice cannot be used for electrophysiological studies. In contrast, the phenotype of young *Atxn2*-CAG100-KIN should be sufficient to detect Ca^{2+} disturbances.

Generally, the *Atxn2*-CAG100-KIN mouse should be employed for several more experimental studies to gain a deeper understanding of ATXN2 function. Profound and consistent changes in transcription levels of genes like *Icmt*, *TH, Syne1, Mbp, and EP300* (Table 57) indicate that there are more potential interaction partners or interacting pathways that have not been examined, yet.

The great advantage of KIN mice over transgenic ones is the ubiquitous expression of the mutant protein that is regulated via the endogenous promoter. The natural expression pattern in *Atxn2*-CAG100-KIN mice allows the study of mutant ATXN2 effects also in non-cerebellar tissue. Data received from these tissues can help to unravel the function of ATXN2. Furthermore, neuronal and non-neuronal data can be compared to elucidate why only neuronal tissue is affected. It is possible that neurons are simply more fragile and more sensitive to polyQ-dependent expression changes and more vulnerable to stress (Mohan et al., 2014). Given that they are not able to proliferate like non-neuronal cells every cell is essential for neuronal integrity and cannot just be replaced by a new one.

Due to the KIN approach, *Atxn2* is not overexpressed in *Atxn2*-CAG100-KIN mice but even slightly reduced on transcript level. This reduction may result from accumulation of ATXN2 protein and a subsequent feedback mechanism. Unfortunately, ATXN2 protein levels could not be studied on protein level since the protein was not dissolvable in any of the used lysis buffers ranging from low (RIPA) to high (SDS + Urea + autoclave) stringency. However, ATXN2 protein was detectable in immunohistochemical stainings and there is no doubt that it is mutated because it shows profound aggregation.

In conclusion, *Atxn2*-CAG100-KIN mice have been proven to be a valuable model for SCA2 with an early strong and progressive phenotype mimicking several features of human disease. In contrast to transgenic mouse models that also show a strong phenotype the ubiquitous expression of ATXN2 with a natural distribution pattern in these mice permits research on ATXN2 function in non-cerebellar or non-neuronal tissue, an approach that will be helpful to understand SCA2 pathology.

5 Perspectives

In the present thesis the focus of the first part was on the identification and preliminary characterization of ATXN2 interaction partners. In a next step the mechanisms behind the interaction should be clarified in more detail.

For the interaction of ATXN2 with FBXW8 this means a detailed analysis of their interaction and the subsequent consequences. To elucidate if ATXN2 is indeed ubiquitinated by the help of FBXW8 *in vitro* assays should be conducted. Overexpressing ATXN2 together with ubiquitin should lead to an ubiquitination of ATXN2 (studied via co-immunoprecipitation) in the presence but not in the absence (knock-down) of FBXW8. Further *in vitro* studies measuring the levels of FBXW8 with or without overexpressed PARK2 could give an answer to the question whether or not PARK2 degrades FBXW8. Interaction studies with deletion constructs of ATXN2 and FBXW8 could elucidate which domains of the two proteins are necessary for their interaction. A similar analysis is suggested for FBXW8 and PARK2. Furthermore, FBXW8 should be taken into account for neuroprotective therapies against ATXN2 accumulation in SCA2 patients with a repeat length of around 40 CAGs.

Regarding the effects of ATXN2 on calcium homeostasis, the data in *Atxn2*-CAG100-KIN mice look more promising than in *Atxn2*-CAG42-KIN animals. Thus, these mice should be used for further studies in this field. It is definitely necessary to do electrophysiological and Ca^{2+}-imaging studies in these mice which were impossible in the other two mouse lines due to the mild phenotype in young mice. Calcium release in Purkinje cells as well as Purkinje cell firing should be analyzed to clarify defects in this pathway. Furthermore, the c-Kit receptor ligand, KitL, exhibited the most pronounced changes in all mouse models and was also observed to be downregulated in other polyQ models. However, none of the studies focused on this protein. In the present work, KitL was not analyzed on protein level or in immunohistochemical stainings due to unavailability of an appropriate antibody. If there is an appropriate antibody, more efforts should be put into the study of this protein since it seems to play an important role for pathology. Generally, given that several transcript levels were decreased in these mice and ATXN2 was shown to be involved in mRNA stability it would be of interest to investigate the mechanism of ATXN2-RNA interactions.

In the second part of the thesis the focus was on the characterization of two new mouse models. This basic characterization was necessary to be able to judge the value of these mouse models and how they could be used to study ATXN2 function.

The *Atxn2*-CAG42-KIN/hTDP43-A315T-KIN double mutant is still in the stage of initial characterization. Until the age of 12 months only slight behavioral differences between double mutants and WT animals and no changes between double and Atxn2 single mutants were observed. However, the obtained results look promising that there could be a potentiation effect in double mutants at some time point in the future. Therefore, behavioral characterization should be continued. Additionally, these mice should be studied on immunohistochemical level since both single mutants formerly showed aggregation of the mutant protein. It would be of interest to know whether the two proteins aggregate in the same neurons and whether they co-localize in these aggregates. Given that TDP43 is one of the proposed targets of ATXN2 for 3'UTR binding, mRNA stabilization, and protein expression, protein levels of the two proteins should be investigated to see if there is an effect of ATXN2 mutation on TDP43 abundance. Certainly, this study will become difficult due to the fact that hTDP43-A315T-KIN mice are heterozygous expressing murine as well as human TDP43 (without 3'UTR) but it is worth a try.

In contrast to the double mutants, the *Atxn2*-CAG100-KIN mouse model is already well characterized on behavioral and immunohistochemical level. It shows an early strong and progressive phenotype. Further studies in this mouse model should be dedicated to the investigation of the whole transcriptome, proteome, and metabolome. The combination of these data will give a clear impression of the affected pathways in SCA2 and will facilitate the placement of ATXN2 within these pathways. Besides, non-cerebellar tissue especially spinal cord as another strongly affected CNS region should be subject of further investigations. With regard to the missing ATXN2 detection in immunoblots a filter-trap assay with protein lysates of *Atxn2*-CAG100-KIN mice could help to detect aggregated ATXN2. Besides, as many data point to a role for ATXN2 in lipid metabolism studies on energy consumption and fat deposition should be conducted in these mice.

6 Summary

INTRODUCTION

The Spinocerebellar ataxias (SCAs) are a group of autosomal dominantly inherited neurodegenerative diseases. Nowadays, almost 40 different SCAs are known named by the order of their discovery SCA1 to SCA40. With few exceptions, all SCAs are caused by variable mutations in different genes. The expansion of a CAG repeat encoding glutamine, is causative for six out of the ~40 SCAs (SCA1, 2, 3, 6, 7, and 17). This group is therefore known as the poly glutamine (polyQ) disorders. Furthermore, Huntington's disease (HD), Spinal and bulbar muscular atrophy (SBMA), and Dentatorubral pallidoluysian atrophy (DRPLA) also form part of this group but are not SCAs. Frequently in polyQ diseases, larger CAG repeats are associated with an earlier disease onset and a stronger disease progression (Cancel et al., 1997; Sasaki et al., 1998; Schols et al., 1997; Velazquez-Perez et al., 2004). Compared to Alzheimer's (AD) or Parkinson's disease (PD) SCAs are rather rare diseases. However, for many SCA types there are founder regions with a high prevalence of the disease, for example, a region on Cuba called Holguín for SCA2.

In 1971, SCA2 was one of the first SCAs that was described (Wadia and Swami, 1971). It stands out among the other SCAs due to the pronounced affection of saccadic eye movement (Velazquez-Perez et al., 2011). Clinical symptoms of SCA2 are gait, stance, trunk, and limb ataxia but also tremor, dysmetria, dysarthria, hyporeflexia, and dysdiadochokynesia (Estrada et al., 1999; Gierga et al., 2005; Velazquez-Perez et al., 2011). The impairment of movement coordination refers to a strong affection of the cerebellum with neurodegeneration. Neuronal loss is also observed in the pons, medulla oblongata, frontal lobe, cranial nerves, and substantia nigra (Estrada et al., 1999; Gierga et al., 2005). In contrast to other SCAs, SCA2 shows barely nuclear inclusions while cytoplasmic aggregates are common (Huynh et al., 2000; Koyano et al., 2002; Koyano et al., 2014; Pang et al., 2002).

Ataxin-2 (*ATXN2*) has been described as the causative gene for SCA2 (Imbert et al., 1996; Pulst et al., 1996; Sanpei et al., 1996). It is widely expressed in the central nervous system (CNS), for example in cerebellum, cerebral cortex, and spinal cord but also in non-neuronal tissue (Huynh et al., 1999; Nechiporuk et al., 1998). Apart from the polyQ domain, ATXN2 harbors a PABP interacting motif (PAM2) motif through which it binds the poly(A) binding protein (PABP) and therefore has been associated with translation regulation (Albrecht et al., 2004; Damrath et al., 2012). Furthermore, there are two Lsm (like Sm) domains that mediate RNA binding (Albrecht et al., 2004). Four proline-rich domains connect ATXN2 with SH3 (Src homology 3) domains of various other proteins

(Nonis et al., 2008). The implication of ATXN2 in translation regulation via PABP has been proven in studies using *Saccharomyces cerevisiae* and *Drosophila melanogaster* homologues of the two proteins (Mangus et al., 1998; Satterfield and Pallanck, 2006). Moreover, recently, ATXN2 was found to regulate mRNA stability and protein expression through binding to AU-rich (AREs) sequences in the 3'UTR of mRNAs (Yokoshi et al., 2014). PABP contributed to these effects but was not essential. An expansion of ATXN2 also only slightly interfered with this function, while a deletion of ATXN2 had a more pronounced effect on mRNA stability and protein expression. However, both, mutation and loss resulted in a decreased stabilization.

ATXN2 is not only the causative gene for SCA2 but has also turned out to be a risk factor for other neurodegenerative diseases like Amyotrophic lateral sclerosis (ALS) (Elden et al., 2010; Gispert et al., 2012), Frontotemporal dementia (FTD) (Lattante et al., 2014; van Blitterswijk et al., 2014), and Levodopa-responsive idiopathic Parkinson's disease (PD) (Charles et al., 2007; Gwinn-Hardy et al., 2000; Kim et al., 2007; Yamashita et al., 2014). In particular the interaction between ATXN2 and the ALS causing gene TDP43 (Tardbp; transactive response DNA binding protein 43 kDa) has been studied given that aggregates of ATXN2 were observed in spinal cord motor neurons of ALS patients and TDP43 aggregates in SCA2 neurons (Elden et al., 2010; Toyoshima et al., 2011). Moreover, ATXN2 and TDP43 have been shown to interact in an RNA dependent manner and the ATXN2 homologs from *S. cerevisiae* and *D. melanogaster* are dose-sensitive modifiers of TDP43 toxicity in these models (Elden et al., 2010). These two proteins have furthermore in common that they (together with PABP) re-localize to small cytoplasmic foci called stress granules during stress response. In these foci mRNAs, translation initiation factors, ribosomal subunits, and other mRNA stabilizing and de-stabilizing proteins are stalled under stress conditions (Kedersha et al., 2000).

In general, the mechanisms leading to SCA2 or ALS pathology have not been clarified, yet. For SCA2, a (partial) loss-of-function as well as a (toxic) gain-of-function hypothesis have been proposed. The loss-of-function theory refers to a loss of ATXN2 function due to the expansion and probably a changed conformation of the protein. Although, knock-out (KO) models of diverse SCA genes do not show a typical SCA phenotype there are similarities between knock-in (KIN) and KO models. In *Atxn1*-KO and *Atxn1*-Q154-KIN mice similar transcript expression changes (including several calcium homeostasis factors) were observed (Crespo-Barreto et al., 2010). Furthermore, *Atxn2*-KO mice, like *Atxn2*-Q58 transgenic and *Atxn2*-CAG42-KIN animals, show a significantly altered rotarod performance (Damrath et al., 2012; Huynh et al., 2000; Kiehl et al., 2006). In contrast, the (toxic) gain-of-function theory mainly results from the fact that the mutant proteins aggregate and these aggregates or inclusions may provoke cellular disturbances resulting

in neuronal loss. However, there are discussions ongoing about the role of aggregates given that studies in SCA1 and SCA7 mouse models revealed that inclusion bodies help the cells to survive longer (Bowman et al., 2005; Watase et al., 2002; Yoo et al., 2003). Thus, if the aggregates are for the sake or for the fate of the cells remains elusive, but it is known that several other proteins are sequestered into these aggregates what might have consequences for the cellular integrity. In the end, it is possible that a combination of both, gain- and loss-of-function is responsible for the resulting disease phenotype.

AIM OF THE THESIS

The aim of this thesis was on the one hand to find novel interaction partners of ATXN2 and to investigate them with reference to ATXN2 function or malfunction using already established ATXN2 mouse models. On the other hand, two new mouse models for SCA2 and SCA2/ALS should be characterized on behavioral, immunohistochemical and molecular level to prove their relevance for further studies of SCA2 and ALS pathology.

RESULTS AND DISCUSSION:

PART 1

For the first part of this work several potential or known interaction partners of ATXN2 were studied. Revealed by a microarray transcriptome study in *Atxn2*-CAG42-KIN mice as being modified by ATXN2 mutation, the E3 ubiquitin-protein ligase component *Fbxw8* (F-box and WD repeat domain containing 8) was investigated. RT-qPCR confirmed the strong upregulation of *Fbxw8* on transcript level at different ages and in different brain regions of *Atxn2*-CAG42-KIN mice. E3 ubiquitin-protein ligases are involved in the last enzymatic step of protein ubiquitination. While the E1 enzyme activates ubiquitin and the E2 enzyme conjugates the ubiquitin, the E3 enzyme binds the target protein and the E2 enzyme enabling the ubiquitination and providing target specificity. The upregulation of *Fbxw8* in *Atxn2*-CAG42-KIN mice was of interest especially in view of its exclusive regulation. E3 enzymes can either consist of one or of multiple subunits. FBXW8 forms part of such a multiple subunit complex, however, no other component of the known FBXW8 including complexes showed a dysregulation as well. On protein level, a shift of FBXW8 into insolubility was observed in cerebellum similar to ATXN2 and PABPC1 in these mice (Damrath et al., 2012). Interaction studies *in vivo* and *in vitro* revealed an interaction of ATXN2 and FBXW8 independent of the polyQ length. Further *in vitro* studies using overexpression of the participating proteins demonstrated an effect of FBXW8 on ATXN2 protein level in the SDS-soluble fraction that was limited to expanded ATXN2. These experiments suggest that FBXW8 interacts with both WT and expanded ATXN2 but predominantly degrades the latter one when accumulated. Consequently, *Fbxw8*

upregulation in *Atxn2*-CAG42-KIN mice indeed seems to rely on its involvement in protein degradation. In view of the variable E3 complexes FBXW8 participates in it is possible that only the subunit with the target specificity is upregulated, while the other subunits are interchangeable and therefore not regulated.

FBXW8 is not the only E3 ligase component that is involved in ATXN2 degradation. Formerly, PARK2 (Parkin), a PD related protein, was proven to degrade ATNX2 (Huynh et al., 2007). Furthermore, this protein was shown to interact with an F-box protein called FBXW7 (Ekholm-Reed et al., 2013; Staropoli et al., 2003). Therefore, an interaction between PARK2 and FBXW8 was proposed and subsequently confirmed: PARK2 and FBXW8 were observed to interact *in vitro* and *in vivo*. *Park2* transcript levels remained unchanged in *Atxn2*-CAG42-KIN mice but protein levels exhibited a similar shift into insolubility like FBXW8. It remains elusive if PARK2 and FBXW8 act together to degrade ATXN2 or if PARK2 is a higher order E3 ligase that degrades FBXW8.

To prove the relevance of Fbxw8 for SCA2 pathology, *FBXW8* levels were measured in SCA2 patient skin fibroblasts and blood samples. *FBXW8* was slightly increased on transcript level in both patient materials. On protein level a similar shift into insolubility as in the mouse model was observed in skin fibroblasts. Hence, Fbxw8 is not just any E3 ubiquitin-protein ligase component that is upregulated in an SCA2 mouse model but it has also relevance for human pathology. Additional *in vitro* experiments should be performed to prove that ATXN2 is indeed ubiquitinated via FBXW8 and subsequently degraded, to study the hierarchy of FBXW8 and PARK2 and the relevance of FBXW8 for therapies in SCA2 patients with small (~40) CAG repeat expansions.

Besides the microarray study, an RNA sequencing revealed several calcium homeostasis factors to be among the 100 most downregulated transcripts in *Atxn2*-KO cerebellum. Given that expression changes of transcripts involved in this pathway were already observed in SCA1 (Crespo-Barreto et al., 2010; Lin et al., 2000; Serra et al., 2004), SCA2 (Hansen et al., 2013), SCA3 (Chou et al., 2008), SCA7 (Friedrich et al., 2012; Gatchel et al., 2008), HD (Friedrich et al., 2012; Luthi-Carter et al., 2002a), and DRPLA (Luthi-Carter et al., 2002b) mouse models their age and tissue dependency was subsequently studied in *Atxn2*-KO and *Atxn2*-CAG42-KIN mice. Both mouse models showed downregulation of several factors that started early in life and were limited to the cerebellum. Similar but even more pronounced expression changes were observed in *Atxn2*-CAG100-KIN mice (characterized in the second part of this thesis). Protein quantification demonstrated a downregulation of selected calcium homeostasis factors in the RIPA-soluble fraction of *Atxn2*-KO and *Atxn2*-CAG42-KIN mice. Interestingly, in the SDS-soluble fraction there were differences between these two mouse lines: while in KO mice several factors were also downregulated like in the RIPA-soluble fraction, an accumulation was observed in

KIN mice. These data suggest that mutant ATXN2 leads to a shift of proteins into insolubility for at least some of these factors. Still, it is of interest that in immunohistochemical stainings of ATXN2 and ITPR1 no alterations in the localization of ITPR1 due to ATXN2 mutation or loss were detected. A subsequent co-immunoprecipitation study of the already known ATXN2 interaction partner ITPR1 (Inositol 1,4,5-trisphosphate receptor type 1) in *Atxn2*-CAG42-KIN mice indicated a polyQ-independent complex including the ITPR1 modulator CA8. Contrarily, a polyQ-dependent interaction was observed in former reports (Liu et al., 2009). The reason for these varying observations may be the use of lysis buffers with different stringency. Possibly, ATXN2 and ITPR1 normally only interact in the more soluble fraction. In mutant mice the additional interaction at the ER (SDS-soluble fraction) and the subsequent accumulation could lead to the proposed increase in Ca^{2+} release (Liu et al., 2009). Alternatively, the harsh conditions applied by Liu and co-workers destroyed the interaction of ITPR1 and WT ATXN2 while the interaction with mutant ATXN2 was stronger and therefore detectable. The sequestration of various proteins may furthermore provoke a feedback mechanism resulting in decreased transcript expression. However, the decrease in transcript levels needs to have some additional cause as there is no accumulation in the KO mice but still reduced transcript levels. It is possible that the recently demonstrated involvement of ATXN2 in the regulation of mRNA stability and protein expression is causative for these changes (Yokoshi et al., 2014). In conclusion, the results suggest profound changes of calcium signaling in ATXN2 mouse models similar to other SCA models. Electrophysiological studies in *Atxn2*-CAG100-KIN mice (strongest phenotype) could give a more detailed insight into calcium signaling disturbances and could reveal if ITPR1 is in fact the key player in SCA2 or if other calcium homeostasis factors are similarly involved.

A role for ATXN2 in translation, lipid metabolism, and its implication in other SCAs has already been suggested (Lastres-Becker et al., 2008a; Lessing and Bonini, 2008; Lim et al., 2006; Mangus et al., 1998; Yokoshi et al., 2014). Several ribosomal proteins and translation initiation factors were upregulated in a microarray transcriptome study of *Atxn2*-KO mice. Subsequently, a similar dysregulation was observed on protein level for specific ribosomal translation proteins in liver tissue. These upregulations may be a secondary response to decreased protein levels of other proteins. If ATXN2 regulates protein expression via mRNA stability the levels of the respective proteins should be decreased when ATXN2 is lost. In order to compensate for these decreased protein levels the translation machinery is accelerated by an increased expression of its components.
Another group of possible ATXN2 interactors were the TBC1 domain family proteins that are involved in lipid metabolism, but their downregulation detected via microarray was not

clearly confirmed using RT-qPCR. Consequently, lipid metabolism may be influenced by ATXN2, but the investigated TBC1 domain family members seem to play a minor role in this process.

Furthermore, there is a known influence of ATXN2 on SCA1 and SCA3 pathology in *D. melanogaster* models (Al-Ramahi et al., 2007; Lessing and Bonini, 2008). In the SCA1 model a decrease of dAtx2 ameliorated the SCA1 phenotype while overexpression exacerbated it (Al-Ramahi et al., 2007). Analyzing more than 20 SCA genes only SCA1, SCA15, and SCA31 showed consistent dysregulation in *Atxn2*-KO and *Atxn2*-CAG42-KIN mice. An interaction of ATXN1 (SCA1) and ATXN2 was already demonstrated (Al-Ramahi et al., 2007; Lim et al., 2006). Therefore, Atxn1 levels were studied in ATXN2 mouse models and vice versa to investigate the mutual influence of these two genes. Transcript levels were always decreased, while protein levels shifted into insolubility in the disease (but not the KO) models. Similar results were obtained for Atxn1 in SCA2 patient skin fibroblasts. These data indicate that ATXN1 and ATXN2 could indeed be modifiers of each other's diseases. Consequently, the interaction of ATXN1 and ATXN2 may influence SCA1 and SCA2 pathology. Though, it should be mentioned that no difference in *Atxn1* transcript level was observed in *Atxn2*-CAG100-KIN mice.

PART 2

In the second part of this thesis the characterization of two new mouse models for SCA2 and ALS is described. The double mutant of *Atxn2*-CAG42-KIN and hTDP43-A315T-KIN mice was generated to test the hypothesis of a potentiation effect of mutated ATXN2 and TDP43. In contrast to the formerly described single mutants no significant weight loss was observed in the new single or in the double mutants. This altered phenotype in the single mutants may result from changes in the background of the mice. Rotarod analysis also revealed no significantly decreased motor performance for single or double mutants. Because impaired rotarod performance in ATXN2 single mutants was formerly not observed before 18 months of age and no rotarod phenotype was detected in TDP43 single mutants it may be necessary to study older animals. In the open field analysis ATXN2 single mutants and double mutants were significantly less active regarding horizontal and vertical parameters. TDP43 single mutants did not alter from WT animals and consequently there was a significant difference between TDP43 single and double mutants but not between ATXN2 single and double mutants. The additional Atxn2 mutation always deteriorated the activity of TDP43 mutants. In summary, until 12 months of age no potentiation effect was found in double mutants but studies should be continued with older animals as it is likely that such a phenotype will develop. Furthermore, immunohistochemical analyses should be conducted because aggregation of the mutant

protein has been observed in both single mutants and is probable to occur in the double mutants as well.

The second mouse line, the *Atxn2*-CAG100-KIN mouse, was generated after the moderate repeat expansion in *Atxn2*-CAG42-KIN animals did only yield a mild and late-onset phenotype. The longer repeat was expected to provoke a stronger and earlier phenotype that would allow further promising experiments in these mice. *Atxn2*-CAG100-KIN mice showed a reduced weight in old animals and a decreased survival rate. Motor impairment on the rotarod was detected starting at 20 weeks of age for homozygous *Atxn2*-CAG100-KIN (HOM) mice and progressed until 14 month of age (the last analyzed time point). In the open field analysis, young HOM animals showed horizontal hyperactivity, while vertical activity decreased with age and was significantly reduced starting at 30 weeks of age. Further behavioral testing revealed a clasping phenotype and walking disturbances with an altered hind leg position and back-pushing of the hind legs while walking. A tremor, especially of the head, was observed as well. Marked neuronal atrophy was noted affecting the whole brain accompanied by a visible shrinkage of the brain and dramatic brain weight loss in old HOM animals. In immunohistochemical stainings, ATXN2 aggregates were detected in the cerebellum, inferior olive, pontine nuclei (brainstem in general), cerebral cortex, hippocampus, and spinal cord. Double immunofluorescent stainings showed a co-localization of ATXN2 with the typical inclusion markers ubiquitin and p62/Sequestosome1. In conclusion, the *Atxn2*-CAG100-KIN mouse manifests with an early strong behavioral phenotype, including marked atrophy and typical aggregation of the mutant protein together with other inclusion markers. Thus, several features of human disease like decreased weight and survival, motor impairment, protein aggregation, and neurodegeneration are mimicked in this mouse model. Moreover, it shows a progressive phenotype which is also observed in SCA2 patients. In contrast to transgenic SCA2 mouse models it has the advantage that *Atxn2* is not overexpressed (even slightly decreased probably due to protein aggregation) and its expression is controlled by the endogenous promoter in a natural temporal a spatial distribution. Therefore, studies on ATXN2 function are not limited to the cerebellum but can be conducted in every tissue. This is of specific interest since SCA2 is not a pure cerebellar diseases and Purkinje cell specific expression neglects the effect of the mutant protein in other parts of the CNS. In the end, the *Atxn2*-CAG100-KIN mouse proved to be a useful and valuable model for SCA2.

Summing up, this thesis shows the significance of the E3 ubiquitin-protein ligase component FBXW8 for moderately expanded ATXN2 using murine and human tissue. It reveals that alterations in calcium homeostasis factors are not limited to mutant ATXN2

but also occur in case of ATXN2 loss and that they are age- and tissue-dependent. Besides, it shows a preliminary description of a combined ATXN2/TDP43 and finally a thorough characterization of a new and highly valuable SCA2 mouse model.

7 Zusammenfassung

EINLEITUNG

Die Spinozerebellären Ataxien (SCAs) sind eine Gruppe von autosomal dominant vererbten neurodegenerativen Erkrankungen. Inzwischen sind fast 40 unterschiedliche SCAs bekannt, welche nach der Reihenfolge ihrer Entdeckung SCA1 bis SCA40 benannt wurden. Mit wenigen Ausnahmen werden alle SCAs durch unterschiedliche Mutation in verschiedenen Genen hervorgerufen. Die Expansion eines Trinukleotids (CAG), welches für die Aminosäure Glutamin kodiert ist ursächlich für sechs dieser ~40 SCAs. Diese Gruppe (SCA1, 2, 3, 6, 7 und 17) bezeichnet man daher auch als Polyglutaminerkrankungen. Zu den Polyglutaminerkrankungen zählen außerdem die Huntington-Krankheit (HD), die Spinobulbäre Muskelatrophie (SBMA) und die Dentatorubrale pallidoluysische Atrophie (DRPLA). Die Länge der Expansion ist bei Polyglutaminerkrankungen häufig mit dem Zeitpunkt des Krankheitsausbruchs assoziiert (Cancel et al., 1997; Sasaki et al., 1998; Schols et al., 1997; Velazquez-Perez et al., 2004). Verglichen mit der Alzheimer- (AD) oder Parkinson-Krankheit (PD) zählen SCAs zu den eher seltenen neurodegenerativen Erkrankungen. Jedoch gibt es für viele SCA-Subtypen sogenannte Gründerregionen mit einer hohen Prävalenz. Die Region Holguín auf Kuba zum Beispiel ist solch eine Gründerregion für den SCA-Subtyp 2 (SCA2).

SCA2 wurde 1971 als eine der ersten SCAs beschrieben (Wadia and Swami, 1971) und sticht unter den anderen SCAs aufgrund der hohen Anfälligkeit der sakkadischen Augenbewegungen heraus (Velazquez-Perez et al., 2011). Weitere klinische Symptome von SCA2 sind Ataxie, Tremor, Dysmetrie, Dysarthrie, Hyporeflexie und Dysdiadochokinese (Estrada et al., 1999; Gierga et al., 2005; Velazquez-Perez et al., 2011). Die mangelnde Koordination der Bewegungen geht auf eine starke Anfälligkeit und Neurodegeneration des Kleinhirns zurück. Der Verlust von Neuronen wurde auch im Pons, in der Medulla oblongata, dem Frontallappen, den Kranialnerven und der Substantia nigra beobachtet (Estrada et al., 1999; Gierga et al., 2005). Im Gegensatz zu anderen SCAs finden sich bei SCA2 nur wenige nukleäre Einschlusskörperchen, wohingegen cytoplasmatische Aggregate häufig vorkommen (Huynh et al., 2000; Koyano et al., 2002; Koyano et al., 2014; Pang et al., 2002).

Das Gen, welches SCA2 verursacht heißt Ataxin-2 (*ATXN2*) und wurde 1996 von drei unterschiedlichen Arbeitsgruppen unabhängig beschrieben (Imbert et al., 1996; Pulst et al., 1996; Sanpei et al., 1996). ATXN2 wird in weiten Teilen des Zentralnervensystems, aber auch in vielen nicht-neuronalen Geweben exprimiert (Huynh et al., 1999; Nechiporuk et al., 1998). Abgesehen von der Polyglutamin-Domäne besitzt ATXN2 noch ein PAM2-

Motiv (PABP interacting motif), über welches es PABP (poly(A) binding protein) bindet und in die Translationsregulierung involviert ist (Albrecht et al., 2004; Damrath et al., 2012). Außerdem gibt es zwei Lsm-Domänen (like Sm), welche die RNA-Bindung vermitteln (Albrecht et al., 2004). Vier Prolin-reiche Domänen sind für die Interaktion mit anderen Proteinen über deren SH3-Domäne (src homology 3) zuständig (Nonis et al., 2008). Vor kurzem wurde eine Regulierung der mRNA-Stabilität und der Proteinexpression durch die Bindung von ATXN2 an AU-reiche Sequenzen (AREs) im 3'UTR von mRNAs beschrieben (Yokoshi et al., 2014). Eine Expansion von ATXN2 hatte nur einen kleinen Einfluss, während ein Verlust von ATXN2 einen starken Effekt auf die mRNA-Stabilität und die folgende Proteinexpression hatte. In beiden Fällen kam es jedoch zu einer Reduktion der Stabilität.

Ataxin-2 ist nicht nur ursächlich für SCA2, sondern auch ein Risikofaktor für andere neurodegenerative Krankheiten wie Amyotrophe Lateralsklerose (ALS) (Elden et al., 2010; Gispert et al., 2012), Frontotemporale Demenz (FTD) (Lattante et al., 2014; van Blitterswijk et al., 2014) und Levodopa-responsives idiopatisches Parkinson (PD) (Charles et al., 2007; Gwinn-Hardy et al., 2000; Kim et al., 2007; Yamashita et al., 2014). Insbesondere die Interaktion zwischen ATXN2 und dem ALS verursachenden TDP43 (Tardbp; transactive response DNA interacting protein 43 kDa) wurde zahlreich untersucht, da Aggregate von ATXN2 in Motoneuronen des Rückenmarks von ALS-Patienten und aggregiertes TDP43 in SCA2-Neuronen beobachtet wurden (Elden et al., 2010; Toyoshima et al., 2011). Eine Interaktion von ATXN2 und TDP43 wurde bereits gezeigt und erfolgt indirekt über die RNA (Elden et al., 2010). Die ATNX2 Homologe in *Saccharomyces cerevisiae* und *Drosophila melanogaster* sind außerdem dosisabhängige Modifikatoren der TDP43-Toxizität in diesen Krankheitsmodellen (Elden et al., 2010). ATXN2 und TDP43 haben gemeinsam, dass sie bei zellulärem Stress in Stressgranula relokalisieren. Dabei handelt es sich um kleine cytoplasmatische Ansammlungen in denen unter Stressbedingungen mRNAs, ribosomale Untereinheiten, Translationsinitiationsfaktoren und andere mRNA stabilisierende und destabilisierende Proteine gelagert werden (Kedersha et al., 2000).

Generell sind die Mechanismen, die zur Pathologie von SCA2 und ALS führen, noch weitgehend unklar. Für SCA2 wurde sowohl ein partieller Funktionsverlust (*loss-of-function)* als auch ein toxischer Funktionsgewinn (*gain-of-function)* als ursächlich vorgeschlagen. Die *loss-of-function* Theorie bezieht sich auf den Funktionsverlust von ATXN2 aufgrund der Expansion und den damit verbundenen Konformationsänderungen des Proteins. Obwohl Knock-Out-Modelle (KO-Modelle) diverser SCA-Gene nicht den typischen SCA Phänotyp zeigen, gibt es Ähnlichkeiten zwischen KO- und Knock-In-Modellen (KIN-Modellen). In *Atxn1*-KO- und *Atxn1*-Q154-KIN-Mäusen wurden ähnliche

Veränderungen der Transkriptspiegel (auch in Bezug auf Kalziumhomöostasefaktoren) festgestellt (Crespo-Barreto et al., 2010). Zudem zeigen *Atxn2*-KO-Mäuse ähnliche Defizite in der Rotarod-Performance wie transgene *Atxn2*-Q58- und *Atxn2*-CAG42-KIN-Mäuse (Damrath et al., 2012; Huynh et al., 2000; Kiehl et al., 2006). Im Gegensatz dazu beruht die *gain-of-function* Theorie ursprünglich auf der Tatsache, dass die mutierten Proteine aggregieren und diese Aggregate oder Einschlusskörperchen zelluläre Veränderungen hervorrufen, die in einem neuronalen Verlust resultieren. Über die Rolle der Aggregate herrscht jedoch Uneinigkeit, da Studien in SCA1- und SCA7-Mausmodellen gezeigt haben, dass Einschlusskörperchen den Zellen sogar beim Überleben hilfreich sein können (Bowman et al., 2005; Watase et al., 2002; Yoo et al., 2003). Es bleibt daher zu klären, ob Aggregate den Zellen schaden oder helfen. Es ist jedoch bekannt, dass weitere Proteine in diese Aggregate sequestriert werden was wiederum Konsequenzen für die Integrität der Zelle haben könnte. Letztendlich ist es wahrscheinlich, dass eine Kombination aus *gain-* und *loss-of-function* für den resultieren Phänotyp verantwortlich ist.

ZIEL DER ARBEIT

Das Ziel dieser Doktorarbeit war einerseits neue Interaktionspartner von ATXN2 zu finden und diese in Bezug auf die Funktion von ATXN2 mit Hilfe von bereits etablierten Atxn2-Mausmodellen zu untersuchen. Andererseits sollten zwei neue Mausmodelle für SCA2 und SCA2/ALS auf Verhaltensebene, immunhistologisch und molekular charakterisiert werden, um ihre Relevanz für weitere Studien an der Pathologie von SCA2 und ALS zu demonstrieren.

ERGEBNISSE UND DISKUSSION

TEIL 1

Für den ersten Teil der Arbeit wurden mehrere potenzielle oder bekannte Interaktionspartner von ATXN2 untersucht. Eine Transkriptomstudie in *Atxn2*-CAG42-KIN-Mäusen zeigte eine starke Expressionsänderung der E3-Ubiquitin-Protein-Ligasekomponente *Fbxw8*. Die Hochregulierung dieses Transkripts wurde per RT-qPCR in unterschiedlich alten Tieren und verschiedenen Gehirnregionen bestätigt. E3-Ubiquitin-Protein-Ligasen sind am letzten Schritt des Ubiquitinierungsprozesses von Proteinen beteiligt. Während die E1-Enzyme Ubiquitin aktivieren und die E2-Enzyme Ubiquitin konjugieren, binden die E3-Ligasen das Protein sowie das E2-Enzym und stellen die Substratspezifität her. Von besonderem Interesse war die Hochregulation von *Fbxw8* in *Atxn2*-CAG42-KIN-Mäusen aufgrund ihrer Exklusivität. FBXW8 ist eine Komponente verschiedener E3-Ligasekomplexe, allerdings konnte für keine der anderen Komponenten

eine ähnliche Dysregulation festgestellt werden. Auf Proteinebene wurde eine Verschiebung von FBXW8 in die unlösliche Fraktion beobachtet ähnlich wie zuvor bei ATXN2 und PABPC1 (Damrath et al., 2012). Interaktionsstudien *in vivo* und *in vitro* zeigten außerdem eine expansionsunabhängige Wechselbeziehung von ATXN2 und FBXW8. In weiteren *in vitro* Studien ließ sich ein Effekt von FBXW8 auf expandiertes ATXN2 in der unlöslichen Fraktion erkennen. Diese Ergebnisse lassen vermuten, dass FBXW8 zwar mit WT und expandiertem ATXN2 interagiert, aber hauptsächlich das mutierte, akkumulierte ATXN2 degradiert. In Anbetracht der unterschiedlichen E3-Komplexe in die FBXW8 involviert ist, ist es möglich, dass nur die Untereinheit mit der Substratspezifität hochreguliert ist, während die anderen Untereinheiten austauschbar und daher nicht reguliert sind.

FBXW8 ist nicht die einzige E3-Ligasekomponente, die in die Degradierung von ATXN2 involviert ist. PARK2 (Parkin), ein PD assoziiertes Protein, wurde bereits als E3-Ligase, die ATXN2 für den Abbau markiert, identifiziert (Huynh et al., 2007). Des Weiteren wurde eine Interaktion von PARK2 mit einem anderen F-Box-Protein namens FBXW7 dokumentiert (Ekholm-Reed et al., 2013; Staropoli et al., 2003). Daher wurde eine Interaktion von PARK2 und FBXW8 vermutet und schließlich *in vitro* und *in vivo* bewiesen. Es bleibt zu klären, ob PARK2 und FBXW8 zusammenarbeiten, um ATXN2 abzubauen oder ob PARK2 eine übergeordnete E3-Ligase ist, die FBXW8 degradiert.

Um die Relevanz von Fbxw8 für die SCA2-Pathologie zu demonstrieren, wurden *FBXW8*-Spiegel in SCA2-Patientenfibroblasten aus der Haut sowie Blutproben analysiert und ebenfalls eine Hochregulation festgestellt. Auf Proteinebene wurde eine ähnliche Verschiebung in die Unlöslichkeit beobachtet wie im Mausmodell. Damit ist Fbxw8 keine beliebige E3-Ligasekomponente, deren Hochregulation in einem SCA2-Mausmodell beobachtet wurde, sondern hat auch Relevanz für die humane Pathologie. Weitere *in vitro* Experimente zur Klärung, ob ATXN2 tatsächlich von FBXW8 ubiquitiniert wird und zur Hierarchie von FBXW8 und PARK2 sollten daher als Ergänzung durchgeführt werden. Außerdem sollte die Relevanz von FBXW8 für neuroprotektive Therapien in SCA2-Patienten mit ~40 CAGs getestet werden.

Mithilfe einer RNA-Sequenzierung wurden mehrere Kalziumhomöostasefaktoren unter den 100 am stärksten herunterregulierten Transkripten in *Atxn2*-KO-Mäusen identifiziert. Da bereits in Mausmodellen für SCA1 (Crespo-Barreto et al., 2010; Lin et al., 2000; Serra et al., 2004), SCA2 (Hansen et al., 2013), SCA3 (Chou et al., 2008), SCA7 (Friedrich et al., 2012; Gatchel et al., 2008), HD (Friedrich et al., 2012; Luthi-Carter et al., 2002a) und DRPLA (Luthi-Carter et al., 2002b) eine Beteiligung dieses Signalwegs an der Pathologie gezeigt werden konnte, wurde die zeitliche und lokale Abhängigkeit der Expressionsveränderungen in *Atxn2*-KO- und *Atxn2*-CAG42-KIN-Mäusen untersucht.

Beide Mausmodelle zeigten eine Herunterregulierung mehrerer Faktoren, die in frühem Alter begann und spezifisch im Cerebellum auftrat. Ähnliche, aber stärkere Expressionsveränderungen wurden im *Atxn2*-CAG100-KIN-Mausmodell festgestellt (im zweiten Teil dieser Arbeit charakterisiert). Proteinquantifizierungen zeigten eine Verminderung der Spiegel von ausgewählten Faktoren in der löslichen Fraktion von *Atxn2*-KO- und *Atxn2*-CAG42-KIN-Mäusen. Interessanterweise traten in der unlöslichen (SDS-) Fraktion Unterschiede in der Regulierung auf: Während in KO-Mäusen diverse Faktoren ebenfalls verminderte Spiegel aufwiesen, wurde in den KIN-Mäusen eine Hochregulation mehrerer Proteine festgestellt. Die Ergebnisse lassen vermuten, dass expandiertes ATXN2 zu einer Verschiebung der Löslichkeit von zumindest einigen dieser Faktoren führt. Eine anschließende Co-Immunopräzipitationsstudie des bereits bekannten ATXN2-Interaktors ITPR1 (Inositol 1,4,5-trisphosphate receptor type 1) in *Atxn2*-CAG42-KIN-Mäusen zeigte eine expansionsunabhängige Interaktion der beiden Proteine in einem Komplex zusammen mit dem ITPR1-Modulator CA8. Im Gegensatz dazu wurde in früheren Untersuchungen eine expansionsabhängige Interaktion beobachtet (Liu et al., 2009). Der Grund für diese unterschiedlichen Ergebnisse könnte die Stärke der jeweils verwendeten Lysepuffer sein. Möglicherweise interagieren ATXN2 und ITPR1 normalerweise nur in der löslichen Fraktion. In mutierten Mäusen könnte die zusätzliche Interaktion am ER (unlösliche Fraktion) und die darauffolgende Akkumulation zum Anstieg der Ca^{2+}-Freisetzung führen (Liu et al., 2009). Alternativ führte die Verwendung eines stärkeren Lysepuffers bei der früheren Studie zu einem Aufbrechen der Interaktion von ITPR1 und WT ATXN2 während die Interaktion mit mutiertem ATXN2 stabiler und daher nachweisbar war. Die Sequestrierung der verschiedenen Proteine könnte außerdem einen Feedback-Mechanismus auslösen, der zu einer verminderten Expression der mRNA führt. Dieser Mechanismus ist allerdings nicht auf *Atxn2*-KO-Mäuse, welche eine ähnliche Herunterregulierung aufweisen, anwendbar, da hier keine Sequestrierung stattfindet. Es muss daher andere/weitere Gründe für die verminderten Transkriptspiegel geben. Möglicherweise spielt die erst kürzlich gezeigte Beteiligung von ATXN2 an der Regulation der mRNA-Stabilität dabei eine Rolle (Yokoshi et al., 2014). Zusammengefasst weisen die Daten auf eine starke Veränderung des Kalziumsignalwegs in Atxn2-Mausmodellen hin, ähnlich wie in anderen SCA-Modellen. Elektrophysiologische Studien in *Atxn2*-CAG100-KIN-Mäusen (stärkster Phänotyp) könnten einen tieferen Einblick in die Störungen der Kalziumsignalkaskade geben und zeigen, ob ITPR1 tatsächlich der Hauptakteur im Fall von SCA2 ist oder ob andere Kalziumhomöostasefaktoren ähnlich involviert sind.

Für ATXN2 wurde bereits eine Rolle in der Translation, dem Lipidmetabolismus und in der Pathologie anderer SCAs dokumentiert (Lastres-Becker et al., 2008a; Lessing and Bonini,

2008; Lim et al., 2006; Mangus et al., 1998; Yokoshi et al., 2014). Mehrere ribosomale Proteine und Translationsinitiationsfaktoren zeigten in der Transkriptomstudie der *Atxn2*-KO-Mäuse eine Hochregulation. Anschließend wurde eine ähnliche Hochregulierung auch auf Proteinebene in Lebergewebe beobachtet. Diese Hochregulation könnte eine indirekte Antwort auf die verminderten Spiegel anderer Proteine sein. Wenn ATXN2 die Proteinexpression über die mRNA-Stabilität reguliert, sollten die entsprechenden Proteinspiegel im Falle eines Verlusts von ATXN2 reduziert sein. Um diese verminderten Spiegel zu kompensieren wird vermutlich die Translationsmachinerie verstärkt, indem die Zahl der beteiligten Proteine erhöht wird.

Eine weitere Gruppe von möglichen ATXN2-Interaktoren sind einige Mitglieder der TBC1-Domänen-Familie, welche mit dem Lipidmetabolismus assoziiert sind. Die Herunterregulierung der Transkripte konnte allerdings auf RT-qPCR Ebene nicht eindeutig bestätigt werden. Daher mag der Lipidmetabolismus in SCA2 zwar verändert sein, die untersuchten Mitglieder der TBC1-Domänen-Familie scheinen dabei aber eher eine untergeordnete Rolle zu spielen.

Ein Einfluss von ATXN2 auf die Pathologie von SCA1 und SCA3 wurde bereits in *D. melanogaster*-Modellen gezeigt (Al-Ramahi et al., 2007; Lessing and Bonini, 2008). Dabei verbesserte eine Verminderung von dAtx2 den SCA1-Phänotyp, während eine Überexpression von dAtx2 diesen verschlechterte (Al-Ramahi et al., 2007). Bei der Analyse von mehr als 20 SCA Genen zeigten in *Atxn2*-KO- und *Atxn2*-CAG42-KIN-Tieren lediglich SCA1, SCA15 und SCA31 eine konsistente Dysregulation. Die Interaktion von ATXN1 (SCA1) und ATXN2 wurde bereits gezeigt (Al-Ramahi et al., 2007; Lim et al., 2006). Deshalb wurden Atxn1-Spiegel in Atxn2-Mausmodellen untersucht und umgekehrt, um den gegenseitigen Einfluss dieser beiden Gene zu untersuchen. Die Ergebnisse zeigten jeweils verminderte Transkriptspiegel, während die Proteinspiegel in den SCA1- und SCA2-Mausmodellen eine Verschiebung des jeweils anderen Proteins in die Unlöslichkeit darlegten. Ähnliche Ergebnisse wurden bei der Untersuchung von Atxn1 in SCA2-Patientenfibroblasten erzielt. Es ist daher sehr wahrscheinlich, dass die Interaktion von ATXN1 und ATXN2 die Pathologie von SCA1 und SCA2 beeinflusst. In dieser Hinsicht sollte jedoch erwähnt werden, dass in *Atxn2*-CAG100-KIN-Mäusen keine Veränderung der Atxn1-Transkriptspiegel festgestellt werden konnte.

TEIL 2

Im zweiten Teil dieser Doktorarbeit wird die Charakterisierung von zwei neuen Mausmodellen beschrieben. Die Doppelmutante aus *Atxn2*-CAG42-KIN- und hTDP43-A315T-KIN-Mäusen wurde generiert, um die Hypothese zu testen, dass mutiertes ATXN2 und TDP43 sich in ihrer Wirkung gegenseitig verstärken. Im Gegensatz zu dem in den

früheren beiden Einzelmutanten beschriebenen Gewichtsverlust konnte in den neuen Einzelmutanten mit gemischtem Hintergrund keine signifikante Veränderung des Gewichts innerhalb der ersten 12 Monate bemerkt werden. Studien am Rotarod zeigten außerdem keine vom WT signifikant abweichenden motorischen Fähigkeiten der Einzel- oder Doppelmutante. Da die ATXN2-Einzelmutanten allerdings bereits zuvor erst mit 18 Monaten einen Rotarod Phänotyp entwickelt haben und TDP43-Einzelmutanten während der Zeit der Verhaltensuntersuchungen keine derartigen Defizite aufwiesen, ist es wahrscheinlich, dass ein solcher Phänotyp erst in höherem Alter (>15 Monate) auftritt. In der *Open Field* Analyse zeigten Atxn2-Einzelmutanten und Doppelmutanten deutlich weniger horizontale und vertikale Aktivität. TDP43-Einzelmutanten unterschieden sich nicht von den WT-Tieren, was wiederum in einem signifikanten Unterschied zwischen TDP43-Einzelmutanten und Doppelmutanten resultierte. In allen drei untersuchten Altersstufen verminderte die zusätzliche ATXN2 Mutation in den TDP43-Mutanten die Aktivität der Tiere. Atxn2-Einzelmutanten hingegen unterschieden sich nicht von Doppelmutanten, lediglich eine kleine, jedoch nicht signifikante Verbesserung der Aktivität war im Alter von 6 Monaten zu erkennen. Zusammengefasst zeigte sich keine Verstärkung der pathologischen Effekte von ATXN2 und TDP43 in den Doppelmutanten bis zu einem Alter von 12 Monaten. Die bisherigen Daten lassen allerdings vermuten, dass dieser Effekt in höherem Alter eintreten könnte. Die Verhaltensstudien sollten daher fortgeführt werden. Außerdem sollten die Gehirne der Tiere immunhistologisch untersucht werden, da beide bisherigen Einzelmutanten Aggregate der jeweiligen Proteine zeigten und diese wahrscheinlich auch in der Doppelmutante auftreten.

Die zweite Mauslinie, die *Atxn2*-CAG100-KIN-Maus, wurde generiert, um im Vergleich zur *Atxn2*-CAG42-KIN-Maus mit moderater Expansion einen stärkeren und früher feststellbaren Phänotyp zu erreichen, der weitere vielversprechende Experimente in dieser Mauslinie ermöglicht. *Atxn2*-CAG100-KIN-Mäuse zeigten einen Gewichtsverlust und eine verminderte Überlebensrate. Motorische Störungen wurden zum ersten Mal im Alter von 20 Wochen für homozygote (HOM) Tiere am Rotarod festgestellt und waren progressiv. In der *Open Field* Analyse waren junge HOM-Mäuse hyperaktiv in Bezug auf horizontale Parameter. Vertikale Parameter zeigten anfangs keine Unterschiede, ließen aber mit zunehmendem Alter stärker werdende Defizite bei den HOM-Mäusen erkennen. In weiteren Verhaltensuntersuchungen fielen die HOM-Tiere durch einen *Clasping* Phänotyp, Gangstörungen sowie einen Tremor auf. Eine neuronale Atrophie und daraus folgend ein Größen- und Gewichtsverlust des Hirns waren in alten HOM-Mäusen offensichtlich. Immunhistochemische Färbungen offenbarten cytoplasmatische ATXN2-Aggregate im Cerebellum, dem Hirnstamm, dem cerebralen Cortex, dem Hippocampus und im Rückenmark. Zudem wurden die typischen Aggregatmarker p62/Sequestosom1

und Ubiquitin gemeinsam mit ATXN2 in Aggregaten gefunden. Folglich manifestiert die *Atxn2*-CAG100-KIN-Maus einen frühen und starken Phänotyp auf Verhaltensebene, mit auffälliger Atrophie und typischer Aggregation des mutierten Proteins sowie weiterer Markerproteine. Damit werden mehrere Charakteristika der humanen Pathologie wie Gewichtsverlust, verminderte Überlebensrate, motorische Störungen, Proteinaggregation und Neurodegeneration in diesem Mausmodell nachempfunden. Zudem wird die Progression der Pathologie dargestellt. Im Gegensatz zu transgenen SCA2-Mausmodellen hat das *Atxn2*-CAG100-KIN-Mausmodell den Vorteil, dass es Atxn2 nicht überexprimiert (sogar leicht reduzierte Transkriptspiegel vermutlich aufgrund der Proteinaggregation) und die Expression durch den endogenen Promotor kontrolliert wird. Daher sind Funktionsstudien zu ATXN2 nicht auf das Cerebellum beschränkt. Dies ist wichtig, da ATXN2 nicht eine rein cerebelläre Erkrankung ist und eine purkinjezellspezifische Expression von *Atxn2* diesen Aspekt außer Acht lässt. Somit ist die *Atxn2*-CAG100-KIN-Maus ein hilfreiches und sehr wertvolles Modell für SCA2.

Zusammengefasst zeigt diese Arbeit die Bedeutung des ATXN2-Interaktors FBXW8 im SCA2-Mausmodell als auch im Patientenmaterial. Sie betont die Relevanz des *Atxn2*-KO-Modells in Bezug auf Störungen der Kalziumhomöostase und dokumentiert die Alters- und Gewebespezifität dieser Veränderungen. Außerdem beinhaltet sie die vorläufige Beschreibung eines kombinierten Atxn2/TDP43-Mausmodells und schließlich die ausführliche Charakterisierung eines vollkommen neuen und äußerst wertvollen SCA2-Mausmodells.

8 References

Abdel-Aleem, A., Zaki, M. S., 2008. Spinocerebellar ataxia type 2 (SCA2) in an Egyptian family presenting with polyphagia and marked CAG expansion in infancy. Journal of neurology. 255**,** 413-9.

Abele, M., Burk, K., Laccone, F., et al., 2001. Restless legs syndrome in spinocerebellar ataxia types 1, 2, and 3. Journal of neurology. 248**,** 311-4.

Adachi, H., Kume, A., Li, M., et al., 2001. Transgenic mice with an expanded CAG repeat controlled by the human AR promoter show polyglutamine nuclear inclusions and neuronal dysfunction without neuronal cell death. Human molecular genetics. 10**,** 1039-48.

Adibhatla, R. M., Hatcher, J. F., 2007. Role of Lipids in Brain Injury and Diseases. Future lipidology. 2**,** 403-422.

Adkins, C. E., Morris, S. A., De Smedt, H., et al., 2000. Ca2+-calmodulin inhibits Ca2+ release mediated by type-1, -2 and -3 inositol trisphosphate receptors. The Biochemical journal. 345 Pt 2**,** 357-63.

Afawi, Z., Mandelstam, S., Korczyn, A. D., et al., 2013. TBC1D24 mutation associated with focal epilepsy, cognitive impairment and a distinctive cerebro-cerebellar malformation. Epilepsy research. 105**,** 240-4.

Affaitati, A., de Cristofaro, T., Feliciello, A., et al., 2001. Identification of alternative splicing of spinocerebellar ataxia type 2 gene. Gene. 267**,** 89-93.

Agan, K., Kutlu, D., Basak, N., et al., 2006. Spinocerebellar ataxia type 2 in a turkish family. Marmara Medical Journal. 19**,** 4.

Al-Ramahi, I., Perez, A. M., Lim, J., et al., 2007. dAtaxin-2 mediates expanded Ataxin-1-induced neurodegeneration in a Drosophila model of SCA1. PLoS genetics. 3**,** e234.

Albrecht, M., Golatta, M., Wullner, U., et al., 2004. Structural and functional analysis of ataxin-2 and ataxin-3. European journal of biochemistry / FEBS. 271**,** 3155-70.

Almaguer-Mederos, L. E., Aguilera Rodriguez, R., Gonzalez Zaldivar, Y., et al., 2013. Estimation of survival in spinocerebellar ataxia type 2 Cuban patients. Clinical genetics. 83**,** 293-4.

Almeida, B., Fernandes, S., Abreu, I. A., et al., 2013. Trinucleotide repeats: a structural perspective. Frontiers in neurology. 4**,** 76.

Alonso, I., Marques, J. M., Sousa, N., et al., 2008. Motor and cognitive deficits in the heterozygous leaner mouse, a Cav2.1 voltage-gated Ca2+ channel mutant. Neurobiology of aging. 29**,** 1733-43.

Alves, S., Cormier-Dequaire, F., Marinello, M., et al., 2014. The autophagy/lysosome pathway is impaired in SCA7 patients and SCA7 knock-in mice. Acta neuropathologica. 128**,** 705-22.

Amador-Ortiz, C., Lin, W. L., Ahmed, Z., et al., 2007. TDP-43 immunoreactivity in hippocampal sclerosis and Alzheimer's disease. Annals of neurology. 61**,** 435-45.

Anders, S., Reyes, A., Huber, W., 2012. Detecting differential usage of exons from RNA-seq data. Genome research. 22**,** 2008-17.

Anderson, P., Kedersha, N., 2002. Visibly stressed: the role of eIF2, TIA-1, and stress granules in protein translation. Cell stress & chaperones. 7**,** 213-21.

Anderson, P., Kedersha, N., 2006. RNA granules. The Journal of cell biology. 172**,** 803-8.

Andrei, M. A., Ingelfinger, D., Heintzmann, R., et al., 2005. A role for eIF4E and eIF4E-transporter in targeting mRNPs to mammalian processing bodies. RNA. 11**,** 717-27.

Ansorge, O., Giunti, P., Michalik, A., et al., 2004. Ataxin-7 aggregation and ubiquitination in infantile SCA7 with 180 CAG repeats. Annals of neurology. 56**,** 448-52.

Apps, R., Garwicz, M., 2005. Anatomical and physiological foundations of cerebellar information processing. Nature reviews. Neuroscience. 6**,** 297-311.

Arai, T., Hasegawa, M., Akiyama, H., et al., 2006. TDP-43 is a component of ubiquitin-positive tau-negative inclusions in frontotemporal lobar degeneration and amyotrophic lateral sclerosis. Biochemical and biophysical research communications. 351**,** 602-11.

Arai, T., Mackenzie, I. R., Hasegawa, M., et al., 2009. Phosphorylated TDP-43 in Alzheimer's disease and dementia with Lewy bodies. Acta neuropathologica. 117**,** 125-36.

Arnold, E. S., Ling, S. C., Huelga, S. C., et al., 2013. ALS-linked TDP-43 mutations produce aberrant RNA splicing and adult-onset motor neuron disease without aggregation or loss of nuclear TDP-43. Proceedings of the National Academy of Sciences of the United States of America. 110**,** E736-45.

Auburger, G., Gispert, S., Lahut, S., et al., 2014. 12q24 locus association with type 1 diabetes: SH2B3 or ATXN2? World journal of diabetes. 5**,** 316-27.

Auburger, G. W., 2012. Spinocerebellar ataxia type 2. Handbook of clinical neurology. 103**,** 423-36.

Ayala, Y. M., De Conti, L., Avendano-Vazquez, S. E., et al., 2011. TDP-43 regulates its mRNA levels through a negative feedback loop. The EMBO journal. 30**,** 277-88.

Azaiez, H., Booth, K. T., Bu, F., et al., 2014. TBC1D24 mutation causes autosomal-dominant nonsyndromic hearing loss. Human mutation. 35**,** 819-23.

Aziz, N. A., van der Burg, J. M., Landwehrmeyer, G. B., et al., 2008. Weight loss in Huntington disease increases with higher CAG repeat number. Neurology. 71**,** 1506-13.

Barmada, S. J., Skibinski, G., Korb, E., et al., 2010. Cytoplasmic mislocalization of TDP-43 is toxic to neurons and enhanced by a mutation associated with familial amyotrophic lateral sclerosis. The Journal of neuroscience : the official journal of the Society for Neuroscience. 30**,** 639-49.

Barreau, C., Paillard, L., Osborne, H. B., 2005. AU-rich elements and associated factors: are there unifying principles? Nucleic acids research. 33**,** 7138-50.

Baumer, D., East, S. Z., Tseu, B., et al., 2014. FTLD-ALS of TDP-43 type and SCA2 in a family with a full ataxin-2 polyglutamine expansion. Acta neuropathologica. 128**,** 597-604.

Bear, M. F. C., B.W.; Paradiso, M.A., 2001. Neuroscience: exploring the brain. Lippincott Williams & Wilkins.

Beau, I., Esclatine, A., Codogno, P., 2008. Lost to translation: when autophagy targets mature ribosomes. Trends in cell biology. 18**,** 311-4.

Belal, S., Cancel, G., Stevanin, G., et al., 1994. Clinical and genetic analysis of a Tunisian family with autosomal dominant cerebellar ataxia type 1 linked to the SCA2 locus. Neurology. 44**,** 1423-6.

Bettencourt, C., Ryten, M., Forabosco, P., et al., 2014. Insights from cerebellar transcriptomic analysis into the pathogenesis of ataxia. JAMA neurology. 71**,** 831-9.

Bezprozvanny, I. B., 2010. Calcium signaling and neurodegeneration. Acta naturae. 2**,** 72-82.

Bhanpuri, N. H., Okamura, A. M., Bastian, A. J., 2012. Active force perception depends on cerebellar function. Journal of neurophysiology. 107**,** 1612-20.

Bhutani, S., Das, A., Maheshwari, M., et al., 2012. Dysregulation of core components of SCF complex in poly-glutamine disorders. Cell death & disease. 3**,** e428.

Bjorkoy, G., Lamark, T., Brech, A., et al., 2005. p62/SQSTM1 forms protein aggregates degraded by autophagy and has a protective effect on huntingtin-induced cell death. The Journal of cell biology. 171**,** 603-14.

Bjorkoy, G., Lamark, T., Johansen, T., 2006. p62/SQSTM1: a missing link between protein aggregates and the autophagy machinery. Autophagy. 2**,** 138-9.

Bonini, N. M., Gitler, A. D., 2011. Model organisms reveal insight into human neurodegenerative disease: ataxin-2 intermediate-length polyglutamine expansions are a risk factor for ALS. Journal of molecular neuroscience : MN. 45**,** 676-83.

Bowman, A. B., Yoo, S. Y., Dantuma, N. P., et al., 2005. Neuronal dysfunction in a polyglutamine disease model occurs in the absence of ubiquitin-proteasome system impairment and inversely correlates with the degree of nuclear inclusion formation. Human molecular genetics. 14**,** 679-91.

Boy, J., Schmidt, T., Wolburg, H., et al., 2009. Reversibility of symptoms in a conditional mouse model of spinocerebellar ataxia type 3. Human molecular genetics. 18**,** 4282-95.

Brenneis, C., Bosch, S. M., Schocke, M., et al., 2003. Atrophy pattern in SCA2 determined by voxel-based morphometry. Neuroreport. 14**,** 1799-802.

Bryant, C. D., Zhang, N. N., Sokoloff, G., et al., 2008. Behavioral differences among C57BL/6 substrains: implications for transgenic and knockout studies. Journal of neurogenetics. 22**,** 315-31.

Buratti, E., Baralle, F. E., 2008. Multiple roles of TDP-43 in gene expression, splicing regulation, and human disease. Frontiers in bioscience : a journal and virtual library. 13**,** 867-78.

Bushara, K., Bower, M., What is Ataxia? Ataxia Ireland, Dublin, 2008.

Cadieux-Dion, M., Turcotte-Gauthier, M., Noreau, A., et al., 2014. Expanding the clinical phenotype associated with ELOVL4 mutation: study of a large French-Canadian family with autosomal dominant spinocerebellar ataxia and erythrokeratodermia. JAMA neurology. 71**,** 470-5.

Campuzano, V., Montermini, L., Molto, M. D., et al., 1996. Friedreich's ataxia: autosomal recessive disease caused by an intronic GAA triplet repeat expansion. Science. 271**,** 1423-7.

Cancel, G., Durr, A., Didierjean, O., et al., 1997. Molecular and clinical correlations in spinocerebellar ataxia 2: a study of 32 families. Human molecular genetics. 6**,** 709-15.

Carlson, K. M., Andresen, J. M., Orr, H. T., 2009. Emerging pathogenic pathways in the spinocerebellar ataxias. Current opinion in genetics & development. 19**,** 247-53.

Carter, R. J., Lione, L. A., Humby, T., et al., 1999. Characterization of progressive motor deficits in mice transgenic for the human Huntington's disease mutation. The Journal of neuroscience : the official journal of the Society for Neuroscience. 19**,** 3248-57.

Cemal, C. K., Carroll, C. J., Lawrence, L., et al., 2002. YAC transgenic mice carrying pathological alleles of the MJD1 locus exhibit a mild and slowly progressive cerebellar deficit. Human molecular genetics. 11**,** 1075-94.

Chadt, A., Immisch, A., de Wendt, C., et al., 2014. Deletion of Both Rab-GTPase-Activating Proteins TBC1D1 and TBC1D4 in Mice Eliminates Insulin- and AICAR-Stimulated Glucose Transport. Diabetes.

Chadt, A., Leicht, K., Deshmukh, A., et al., 2008. Tbc1d1 mutation in lean mouse strain confers leanness and protects from diet-induced obesity. Nature genetics. 40**,** 1354-9.

Chai, Y., Koppenhafer, S. L., Shoesmith, S. J., et al., 1999. Evidence for proteasome involvement in polyglutamine disease: localization to nuclear inclusions in SCA3/MJD and suppression of polyglutamine aggregation in vitro. Human molecular genetics. 8**,** 673-82.

Charles, P., Camuzat, A., Benammar, N., et al., 2007. Are interrupted SCA2 CAG repeat expansions responsible for parkinsonism? Neurology. 69**,** 1970-5.

Chavez, J. A., Roach, W. G., Keller, S. R., et al., 2008. Inhibition of GLUT4 translocation by Tbc1d1, a Rab GTPase-activating protein abundant in skeletal muscle, is partially relieved by AMP-activated protein kinase activation. The Journal of biological chemistry. 283**,** 9187-95.

Chen, X., Tang, T. S., Tu, H., et al., 2008. Deranged calcium signaling and neurodegeneration in spinocerebellar ataxia type 3. The Journal of neuroscience : the official journal of the Society for Neuroscience. 28**,** 12713-24.

Chhangani, D., Nukina, N., Kurosawa, M., et al., 2014. Mahogunin ring finger 1 suppresses misfolded polyglutamine aggregation and cytotoxicity. Biochimica et biophysica acta. 1842**,** 1472-84.

Chiang, P. M., Ling, J., Jeong, Y. H., et al., 2010. Deletion of TDP-43 down-regulates Tbc1d1, a gene linked to obesity, and alters body fat metabolism. Proceedings of the National Academy of Sciences of the United States of America. 107**,** 16320-4.

Chio, A., Calvo, A., Moglia, C., et al., 2014. ATXN2 polyQ intermediate repeats are a modifier of ALS survival. Neurology.

Chou, A. H., Chen, C. Y., Chen, S. Y., et al., 2010. Polyglutamine-expanded ataxin-7 causes cerebellar dysfunction by inducing transcriptional dysregulation. Neurochemistry international. 56**,** 329-39.

Chou, A. H., Yeh, T. H., Kuo, Y. L., et al., 2006. Polyglutamine-expanded ataxin-3 activates mitochondrial apoptotic pathway by upregulating Bax and downregulating Bcl-xL. Neurobiology of disease. 21**,** 333-45.

Chou, A. H., Yeh, T. H., Ouyang, P., et al., 2008. Polyglutamine-expanded ataxin-3 causes cerebellar dysfunction of SCA3 transgenic mice by inducing transcriptional dysregulation. Neurobiology of disease. 31**,** 89-101.

Choudhry, S., Mukerji, M., Srivastava, A. K., et al., 2001. CAG repeat instability at SCA2 locus: anchoring CAA interruptions and linked single nucleotide polymorphisms. Human molecular genetics. 10**,** 2437-46.

Ciechanover, A., Brundin, P., 2003. The ubiquitin proteasome system in neurodegenerative diseases: sometimes the chicken, sometimes the egg. Neuron. 40**,** 427-46.

Ciosk, R., DePalma, M., Priess, J. R., 2004. ATX-2, the C. elegans ortholog of ataxin 2, functions in translational regulation in the germline. Development. 131**,** 4831-41.

Clark, H. B., Burright, E. N., Yunis, W. S., et al., 1997. Purkinje cell expression of a mutant allele of SCA1 in transgenic mice leads to disparate effects on motor behaviors, followed by a progressive cerebellar dysfunction and histological alterations. The Journal of neuroscience : the official journal of the Society for Neuroscience. 17**,** 7385-95.

Cleveland, D. W., Rothstein, J. D., 2001. From Charcot to Lou Gehrig: deciphering selective motor neuron death in ALS. Nature reviews. Neuroscience. 2**,** 806-19.

Crespo-Barreto, J., Fryer, J. D., Shaw, C. A., et al., 2010. Partial loss of ataxin-1 function contributes to transcriptional dysregulation in spinocerebellar ataxia type 1 pathogenesis. PLoS genetics. 6**,** e1001021.

Cummings, C. J., Orr, H. T., Zoghbi, H. Y., 1999. Progress in pathogenesis studies of spinocerebellar ataxia type 1. Philosophical transactions of the Royal Society of London. Series B, Biological sciences. 354**,** 1079-81.

D'Angelo, E., Casali, S., 2012. Seeking a unified framework for cerebellar function and dysfunction: from circuit operations to cognition. Frontiers in neural circuits. 6**,** 116.

Damrath, E., The characterization of the Atxn2-CAG42-knock-in mouse as a model for Spinocerebellar Ataxia Type 2. Vol. PhD. Johannes Gutenberg University, Mainz, 2012.

Damrath, E., Heck, M. V., Gispert, S., et al., 2012. ATXN2-CAG42 sequesters PABPC1 into insolubility and induces FBXW8 in cerebellum of old ataxic knock-in mice. PLoS genetics. 8**,** e1002920.

Dantuma, N. P., Bott, L. C., 2014. The ubiquitin-proteasome system in neurodegenerative diseases: precipitating factor, yet part of the solution. Frontiers in molecular neuroscience. 7**,** 70.

Danysz, W., Essmann, U., Bresink, I., et al., 1994. Glutamate antagonists have different effects on spontaneous locomotor activity in rats. Pharmacology, biochemistry, and behavior. 48**,** 111-8.

Davies, S. W., Turmaine, M., Cozens, B. A., et al., 1997. Formation of neuronal intranuclear inclusions underlies the neurological dysfunction in mice transgenic for the HD mutation. Cell. 90**,** 537-48.

de Chiara, C., Menon, R. P., Strom, M., et al., 2009. Phosphorylation of S776 and 14-3-3 binding modulate ataxin-1 interaction with splicing factors. PloS one. 4**,** e8372.

de la Monte, S. M., Vonsattel, J. P., Richardson, E. P., Jr., 1988. Morphometric demonstration of atrophic changes in the cerebral cortex, white matter, and neostriatum in Huntington's disease. Journal of neuropathology and experimental neurology. 47**,** 516-25.

DeJesus-Hernandez, M., Mackenzie, I. R., Boeve, B. F., et al., 2011. Expanded GGGGCC hexanucleotide repeat in noncoding region of C9ORF72 causes chromosome 9p-linked FTD and ALS. Neuron. 72**,** 245-56.

Delplanque, J., Devos, D., Huin, V., et al., 2014. TMEM240 mutations cause spinocerebellar ataxia 21 with mental retardation and severe cognitive impairment. Brain : a journal of neurology. 137**,** 2657-63.

Dewey, C. M., Cenik, B., Sephton, C. F., et al., 2012. TDP-43 aggregation in neurodegeneration: are stress granules the key? Brain research. 1462**,** 16-25.

Di Gregorio, E., Borroni, B., Giorgio, E., et al., 2014. ELOVL5 mutations cause spinocerebellar ataxia 38. American journal of human genetics. 95**,** 209-17.

Di Prospero, N. A., Fischbeck, K. H., 2005. Therapeutics development for triplet repeat expansion diseases. Nature reviews. Genetics. 6**,** 756-65.

Dias, D. C., Dolios, G., Wang, R., et al., 2002. CUL7: A DOC domain-containing cullin selectively binds Skp1.Fbx29 to form an SCF-like complex. Proceedings of the National Academy of Sciences of the United States of America. 99**,** 16601-6.

Doi, H., Adachi, H., Katsuno, M., et al., 2013. p62/SQSTM1 differentially removes the toxic mutant androgen receptor via autophagy and inclusion formation in a spinal and bulbar muscular atrophy mouse model. The Journal of neuroscience : the official journal of the Society for Neuroscience. 33**,** 7710-27.

Dokas, J., Chadt, A., Nolden, T., et al., 2013. Conventional knockout of Tbc1d1 in mice impairs insulin- and AICAR-stimulated glucose uptake in skeletal muscle. Endocrinology. 154**,** 3502-14.
Dorsman, J. C., Bremmer-Bout, M., Pepers, B., et al., 2002. Interruption of perfect CAG repeats by CAA triplets improves the stability of glutamine-encoding repeat sequences. BioTechniques. 33**,** 976-8.
Dougherty, S. E., Reeves, J. L., Lesort, M., et al., 2013. Purkinje cell dysfunction and loss in a knock-in mouse model of Huntington disease. Experimental neurology. 240**,** 96-102.
Dumitrescu, L., Popescu, B. O., 2015. MicroRNAs in CAG Trinucleotide Repeat Expansion Disorders: an Integrated Review of the Literature. CNS & neurological disorders drug targets.
Ekholm-Reed, S., Goldberg, M. S., Schlossmacher, M. G., et al., 2013. Parkin-dependent degradation of the F-box protein Fbw7beta promotes neuronal survival in response to oxidative stress by stabilizing Mcl-1. Molecular and cellular biology. 33**,** 3627-43.
Elden, A. C., Kim, H. J., Hart, M. P., et al., 2010. Ataxin-2 intermediate-length polyglutamine expansions are associated with increased risk for ALS. Nature. 466**,** 1069-75.
Ellerby, L. M., Hackam, A. S., Propp, S. S., et al., 1999. Kennedy's disease: caspase cleavage of the androgen receptor is a crucial event in cytotoxicity. Journal of neurochemistry. 72**,** 185-95.
Emilsson, L., Saetre, P., Jazin, E., 2006. Alzheimer's disease: mRNA expression profiles of multiple patients show alterations of genes involved with calcium signaling. Neurobiology of disease. 21**,** 618-25.
Estrada, R., Galarraga, J., Orozco, G., et al., 1999. Spinocerebellar ataxia 2 (SCA2): morphometric analyses in 11 autopsies. Acta neuropathologica. 97**,** 306-10.
Falace, A., Filipello, F., La Padula, V., et al., 2010. TBC1D24, an ARF6-interacting protein, is mutated in familial infantile myoclonic epilepsy. American journal of human genetics. 87**,** 365-70.
Farg, M. A., Soo, K. Y., Warraich, S. T., et al., 2013. Ataxin-2 interacts with FUS and intermediate-length polyglutamine expansions enhance FUS-related pathology in amyotrophic lateral sclerosis. Human molecular genetics. 22**,** 717-28.
Farrar, A. M., Murphy, C. A., Paterson, N. E., et al., 2014. Cognitive deficits in transgenic and knock-in HTT mice parallel those in Huntington's disease. Journal of Huntington's disease. 3**,** 145-58.
Figueroa, K. P., Farooqi, S., Harrup, K., et al., 2009. Genetic variance in the spinocerebellar ataxia type 2 (ATXN2) gene in children with severe early onset obesity. PloS one. 4**,** e8280.
Finsterer, J., 2009a. Ataxias with autosomal, X-chromosomal or maternal inheritance. The Canadian journal of neurological sciences. Le journal canadien des sciences neurologiques. 36**,** 409-28.
Finsterer, J., 2009b. Mitochondrial ataxias. The Canadian journal of neurological sciences. Le journal canadien des sciences neurologiques. 36**,** 543-53.
Finsterer, J., Handbook of the Cerebellum and Cerebellar Disorders. In: M. Manto, et al., Eds.). Springer, 2013.
Fittschen, M., Lastres-Becker, I., Halbach, M. V., et al., in press. Genetic ablation of ataxin-2 increases several global translation factors in their transcript abundance, but decreases translation rate. Neurogenetics.
Foster, T. C., Sharrow, K. M., Masse, J. R., et al., 2001. Calcineurin links Ca2+ dysregulation with brain aging. The Journal of neuroscience : the official journal of the Society for Neuroscience. 21**,** 4066-73.
Freund, H. J., Barnikol, U. B., Nolte, D., et al., 2007. Subthalamic-thalamic DBS in a case with spinocerebellar ataxia type 2 and severe tremor-A unusual clinical benefit. Movement disorders : official journal of the Movement Disorder Society. 22**,** 732-5.
Friedrich, B., Euler, P., Ziegler, R., et al., 2012. Comparative analyses of Purkinje cell gene expression profiles reveal shared molecular abnormalities in models of different polyglutamine diseases. Brain research. 1481**,** 37-48.
Fryer, J. D., Yu, P., Kang, H., et al., 2011. Exercise and genetic rescue of SCA1 via the transcriptional repressor Capicua. Science. 334**,** 690-3.
Fujioka, S., Sundal, C., Wszolek, Z. K., 2013. Autosomal dominant cerebellar ataxia type III: a review of the phenotypic and genotypic characteristics. Orphanet journal of rare diseases. 8**,** 14.
Fukuda, M., 2011. TBC proteins: GAPs for mammalian small GTPase Rab? Bioscience reports. 31**,** 159-68.
Gallo, L. I., Liao, Y., Ruiz, W. G., et al., 2014. TBC1D9B functions as a GTPase-activating protein for Rab11a in polarized MDCK cells. Molecular biology of the cell. 25**,** 3779-97.
Garden, G. A., Libby, R. T., Fu, Y. H., et al., 2002. Polyglutamine-expanded ataxin-7 promotes non-cell-autonomous purkinje cell degeneration and displays proteolytic cleavage in ataxic transgenic mice. The Journal of neuroscience : the official journal of the Society for Neuroscience. 22**,** 4897-905.
Gatchel, J. R., Watase, K., Thaller, C., et al., 2008. The insulin-like growth factor pathway is altered in spinocerebellar ataxia type 1 and type 7. Proceedings of the National Academy of Sciences of the United States of America. 105**,** 1291-6.
Gatchel, J. R., Zoghbi, H. Y., 2005. Diseases of unstable repeat expansion: mechanisms and common principles. Nature reviews. Genetics. 6**,** 743-55.
Gehrke, S., Wu, Z., Klinkenberg, M., et al., 2015. PINK1 and Parkin Control Localized Translation of Respiratory Chain Component mRNAs on Mitochondria Outer Membrane. Cell metabolism. 21**,** 95-108.
Gehrking, K. M., Andresen, J. M., Duvick, L., et al., 2011. Partial loss of Tip60 slows mid-stage neurodegeneration in a spinocerebellar ataxia type 1 (SCA1) mouse model. Human molecular genetics. 20**,** 2204-12.
Gellera, C., Ticozzi, N., Pensato, V., et al., 2012. ATAXIN2 CAG-repeat length in Italian patients with amyotrophic lateral sclerosis: risk factor or variant phenotype? Implication for genetic testing and counseling. Neurobiology of aging. 33**,** 1847 e15-21.

Giachino, C., Lantelme, E., Lanzetti, L., et al., 1997. A novel SH3-containing human gene family preferentially expressed in the central nervous system. Genomics. 41**,** 427-34.
Gierga, K., Burk, K., Bauer, M., et al., 2005. Involvement of the cranial nerves and their nuclei in spinocerebellar ataxia type 2 (SCA2). Acta neuropathologica. 109**,** 617-31.
Gispert, S., Kurz, A., Waibel, S., et al., 2012. The modulation of Amyotrophic Lateral Sclerosis risk by ataxin-2 intermediate polyglutamine expansions is a specific effect. Neurobiology of disease. 45**,** 356-61.
Gispert, S., Lunkes, A., Santos, N., et al., 1995. Localization of the candidate gene D-amino acid oxidase outside the refined I-cM region of spinocerebellar ataxia 2. American journal of human genetics. 57**,** 972-5.
Giuffrida, S., Lanza, S., Restivo, D. A., et al., 1999. Clinical and molecular analysis of 11 Sicilian SCA2 families: influence of gender on age at onset. European journal of neurology : the official journal of the European Federation of Neurological Societies. 6**,** 301-7.
Gold, D. A., Baek, S. H., Schork, N. J., et al., 2003. RORalpha coordinates reciprocal signaling in cerebellar development through sonic hedgehog and calcium-dependent pathways. Neuron. 40**,** 1119-31.
Gold, D. A., Gent, P. M., Hamilton, B. A., 2007. ROR alpha in genetic control of cerebellum development: 50 staggering years. Brain research. 1140**,** 19-25.
Grosskreutz, J., Van Den Bosch, L., Keller, B. U., 2010. Calcium dysregulation in amyotrophic lateral sclerosis. Cell calcium. 47**,** 165-74.
Gudbjartsson, D. F., Bjornsdottir, U. S., Halapi, E., et al., 2009. Sequence variants affecting eosinophil numbers associate with asthma and myocardial infarction. Nature genetics. 41**,** 342-7.
Guergueltcheva, V., Azmanov, D. N., Angelicheva, D., et al., 2012. Autosomal-recessive congenital cerebellar ataxia is caused by mutations in metabotropic glutamate receptor 1. American journal of human genetics. 91**,** 553-64.
Gunawardena, S., Goldstein, L. S., 2005. Polyglutamine diseases and transport problems: deadly traffic jams on neuronal highways. Archives of neurology. 62**,** 46-51.
Gunawardena, S., Her, L. S., Brusch, R. G., et al., 2003. Disruption of axonal transport by loss of huntingtin or expression of pathogenic polyQ proteins in Drosophila. Neuron. 40**,** 25-40.
Gwinn-Hardy, K., Chen, J. Y., Liu, H. C., et al., 2000. Spinocerebellar ataxia type 2 with parkinsonism in ethnic Chinese. Neurology. 55**,** 800-5.
Haacke, A., Broadley, S. A., Boteva, R., et al., 2006. Proteolytic cleavage of polyglutamine-expanded ataxin-3 is critical for aggregation and sequestration of non-expanded ataxin-3. Human molecular genetics. 15**,** 555-68.
Halbach, M. V., Stehning, T., Damrath, E., et al., under revision. Atxn2 knock-out and CAG42-knock-in cerebellum shows similarly dysregulated expression of calcium homeostasis factors.
Hamilton, B. A., Frankel, W. N., Kerrebrock, A. W., et al., 1996. Disruption of the nuclear hormone receptor RORalpha in staggerer mice. Nature. 379**,** 736-9.
Hamilton, J. M., Wolfson, T., Peavy, G. M., et al., 2004. Rate and correlates of weight change in Huntington's disease. Journal of neurology, neurosurgery, and psychiatry. 75**,** 209-12.
Hansen, S. T., Meera, P., Otis, T. S., et al., 2013. Changes in Purkinje cell firing and gene expression precede behavioral pathology in a mouse model of SCA2. Human molecular genetics. 22**,** 271-83.
Harding, A. E., 1993. Clinical features and classification of inherited ataxias. Advances in neurology. 61**,** 1-14.
Hart, M. L., Neumayer, K. M., Vaegler, M., et al., 2013. Cell-based therapy for the deficient urinary sphincter. Current urology reports. 14**,** 476-87.
Hart, M. P., Brettschneider, J., Lee, V. M., et al., 2012. Distinct TDP-43 pathology in ALS patients with ataxin 2 intermediate-length polyQ expansions. Acta neuropathologica. 124**,** 221-30.
Hart, M. P., Gitler, A. D., 2012. ALS-associated ataxin 2 polyQ expansions enhance stress-induced caspase 3 activation and increase TDP-43 pathological modifications. The Journal of neuroscience : the official journal of the Society for Neuroscience. 32**,** 9133-42.
Hartmann, P., Ramseier, A., Gudat, F., et al., 1994. [Normal weight of the brain in adults in relation to age, sex, body height and weight]. Der Pathologe. 15**,** 165-70.
Heck, M. V., Azizov, M., Stehning, T., et al., 2014. Dysregulated expression of lipid storage and membrane dynamics factors in Tia1 knockout mouse nervous tissue. Neurogenetics. 15**,** 135-44.
Heng, M. Y., Tallaksen-Greene, S. J., Detloff, P. J., et al., 2007. Longitudinal evaluation of the Hdh(CAG)150 knock-in murine model of Huntington's disease. The Journal of neuroscience : the official journal of the Society for Neuroscience. 27**,** 8989-98.
Hernandez, A., Magarino, C., Gispert, S., et al., 1995. Genetic mapping of the spinocerebellar ataxia 2 (SCA2) locus on chromosome 12q23-q24.1. Genomics. 25**,** 433-5.
Herrup, K., Kuemerle, B., 1997. The compartmentalization of the cerebellum. Annual review of neuroscience. 20**,** 61-90.
Higashi, S., Iseki, E., Yamamoto, R., et al., 2007. Concurrence of TDP-43, tau and alpha-synuclein pathology in brains of Alzheimer's disease and dementia with Lewy bodies. Brain research. 1184**,** 284-94.
Highley, J. R., Kirby, J., Jansweijer, J. A., et al., 2014. Loss of nuclear TDP-43 in amyotrophic lateral sclerosis (ALS) causes altered expression of splicing machinery and widespread dysregulation of RNA splicing in motor neurones. Neuropathology and applied neurobiology. 40**,** 670-85.
Hirota, J., Ando, H., Hamada, K., et al., 2003. Carbonic anhydrase-related protein is a novel binding protein for inositol 1,4,5-trisphosphate receptor type 1. The Biochemical journal. 372**,** 435-41.
Hoffmann, G. F., Zschocke, J., Nyhan, W. L., Inherited metbolic diseases: A clinical approach. Springer Heidelberg, 2010.

Holmberg, M., Duyckaerts, C., Durr, A., et al., 1998. Spinocerebellar ataxia type 7 (SCA7): a neurodegenerative disorder with neuronal intranuclear inclusions. Human molecular genetics. 7**,** 913-8.

Huang, F., Zhang, L., Long, Z., et al., 2014. miR-25 alleviates polyQ-mediated cytotoxicity by silencing ATXN3. FEBS letters. 588**,** 4791-8.

Hurlbert, M. S., Zhou, W., Wasmeier, C., et al., 1999. Mice transgenic for an expanded CAG repeat in the Huntington's disease gene develop diabetes. Diabetes. 48**,** 649-51.

Huynh, D. P., Del Bigio, M. R., Ho, D. H., et al., 1999. Expression of ataxin-2 in brains from normal individuals and patients with Alzheimer's disease and spinocerebellar ataxia 2. Annals of neurology. 45**,** 232-41.

Huynh, D. P., Figueroa, K., Hoang, N., et al., 2000. Nuclear localization or inclusion body formation of ataxin-2 are not necessary for SCA2 pathogenesis in mouse or human. Nature genetics. 26**,** 44-50.

Huynh, D. P., Nguyen, D. T., Pulst-Korenberg, J. B., et al., 2007. Parkin is an E3 ubiquitin-ligase for normal and mutant ataxin-2 and prevents ataxin-2-induced cell death. Experimental neurology. 203**,** 531-41.

Igaz, L. M., Kwong, L. K., Xu, Y., et al., 2008. Enrichment of C-terminal fragments in TAR DNA-binding protein-43 cytoplasmic inclusions in brain but not in spinal cord of frontotemporal lobar degeneration and amyotrophic lateral sclerosis. The American journal of pathology. 173**,** 182-94.

Ikram, M. K., Sim, X., Jensen, R. A., et al., 2010. Four novel Loci (19q13, 6q24, 12q24, and 5q14) influence the microcirculation in vivo. PLoS genetics. 6**,** e1001184.

Ilg, W., Schatton, C., Schicks, J., et al., 2012. Video game-based coordinative training improves ataxia in children with degenerative ataxia. Neurology. 79**,** 2056-60.

Ilg, W., Synofzik, M., Brotz, D., et al., 2009. Intensive coordinative training improves motor performance in degenerative cerebellar disease. Neurology. 73**,** 1823-30.

Imbert, G., Saudou, F., Yvert, G., et al., 1996. Cloning of the gene for spinocerebellar ataxia 2 reveals a locus with high sensitivity to expanded CAG/glutamine repeats. Nature genetics. 14**,** 285-91.

Iranzo, A., Comella, C. L., Santamaria, J., et al., 2007. Restless legs syndrome in Parkinson's disease and other neurodegenerative diseases of the central nervous system. Movement disorders : official journal of the Movement Disorder Society. 22 Suppl 18**,** S424-30.

Ishida, C., Komai, K., Yonezawa, K., et al., 2011. An autopsy case of an aged patient with spinocerebellar ataxia type 2. Neuropathology : official journal of the Japanese Society of Neuropathology. 31**,** 510-8.

Ito, M., 2000. Mechanisms of motor learning in the cerebellum. Brain research. 886**,** 237-245.

Ivatt, R. M., Sanchez-Martinez, A., Godena, V. K., et al., 2014. Genome-wide RNAi screen identifies the Parkinson disease GWAS risk locus SREBF1 as a regulator of mitophagy. Proceedings of the National Academy of Sciences of the United States of America. 111**,** 8494-9.

Jayadev, S., Bird, T. D., 2013. Hereditary ataxias: overview. Genetics in medicine : official journal of the American College of Medical Genetics. 15**,** 673-83.

Jen, J. C., Graves, T. D., Hess, E. J., et al., 2007. Primary episodic ataxias: diagnosis, pathogenesis and treatment. Brain : a journal of neurology. 130**,** 2484-93.

Jhunjhunwala, K., Netravathi, M., Purushottam, M., et al., 2014. Profile of extrapyramidal manifestations in 85 patients with spinocerebellar ataxia type 1, 2 and 3. Journal of clinical neuroscience : official journal of the Neurosurgical Society of Australasia. 21**,** 1002-6.

Jin, Y., Suzuki, H., Maegawa, S., et al., 2003. A vertebrate RNA-binding protein Fox-1 regulates tissue-specific splicing via the pentanucleotide GCAUG. The EMBO journal. 22**,** 905-12.

Johnson, J. O., Mandrioli, J., Benatar, M., et al., 2010. Exome sequencing reveals VCP mutations as a cause of familial ALS. Neuron. 68**,** 857-64.

Johnson, R., Zuccato, C., Belyaev, N. D., et al., 2008. A microRNA-based gene dysregulation pathway in Huntington's disease. Neurobiology of disease. 29**,** 438-45.

Kandel, E. R., Schwartz, J. H., Jessel, T. M. Eds.), 2000. Principles of Neural Sciences.

Kasri, N. N., Bultynck, G., Smyth, J., et al., 2004. The N-terminal Ca2+-independent calmodulin-binding site on the inositol 1,4,5-trisphosphate receptor is responsible for calmodulin inhibition, even though this inhibition requires Ca2+. Molecular pharmacology. 66**,** 276-84.

Kasumu, A. W., Liang, X., Egorova, P., et al., 2012. Chronic suppression of inositol 1,4,5-triphosphate receptor-mediated calcium signaling in cerebellar purkinje cells alleviates pathological phenotype in spinocerebellar ataxia 2 mice. The Journal of neuroscience : the official journal of the Society for Neuroscience. 32**,** 12786-96.

Kedersha, N., Anderson, P., 2002. Stress granules: sites of mRNA triage that regulate mRNA stability and translatability. Biochemical Society transactions. 30**,** 963-9.

Kedersha, N., Cho, M. R., Li, W., et al., 2000. Dynamic shuttling of TIA-1 accompanies the recruitment of mRNA to mammalian stress granules. The Journal of cell biology. 151**,** 1257-68.

Kedersha, N., Stoecklin, G., Ayodele, M., et al., 2005. Stress granules and processing bodies are dynamically linked sites of mRNP remodeling. The Journal of cell biology. 169**,** 871-84.

Kelp, A., Koeppen, A. H., Petrasch-Parwez, E., et al., 2013. A novel transgenic rat model for spinocerebellar ataxia type 17 recapitulates neuropathological changes and supplies in vivo imaging biomarkers. The Journal of neuroscience : the official journal of the Society for Neuroscience. 33**,** 9068-81.

Kerber, K. A., Jen, J. C., Lee, H., et al., 2007. A new episodic ataxia syndrome with linkage to chromosome 19q13. Archives of neurology. 64**,** 749-52.

Khachaturian, Z. S., 1989. The role of calcium regulation in brain aging: reexamination of a hypothesis. Aging. 1**,** 17-34.

Kiehl, T. R., Nechiporuk, A., Figueroa, K. P., et al., 2006. Generation and characterization of Sca2 (ataxin-2) knockout mice. Biochemical and biophysical research communications. 339**,** 17-24.

Kim, D., Pertea, G., Trapnell, C., et al., 2013. TopHat2: accurate alignment of transcriptomes in the presence of insertions, deletions and gene fusions. Genome biology. 14**,** R36.
Kim, H. J., Raphael, A. R., LaDow, E. S., et al., 2014. Therapeutic modulation of eIF2alpha phosphorylation rescues TDP-43 toxicity in amyotrophic lateral sclerosis disease models. Nature genetics. 46**,** 152-60.
Kim, J. M., Hong, S., Kim, G. P., et al., 2007. Importance of low-range CAG expansion and CAA interruption in SCA2 Parkinsonism. Archives of neurology. 64**,** 1510-8.
Kim, V. N., Han, J., Siomi, M. C., 2009. Biogenesis of small RNAs in animals. Nature reviews. Molecular cell biology. 10**,** 126-39.
Kitamura, K., Kano, M., 2013. Dendritic calcium signaling in cerebellar Purkinje cell. Neural networks : the official journal of the International Neural Network Society. 47**,** 11-7.
Kong, C., Samovski, D., Srikanth, P., et al., 2012. Ubiquitination and degradation of the hominoid-specific oncoprotein TBC1D3 is mediated by CUL7 E3 ligase. PloS one. 7**,** e46485.
Konno, A., Shuvaev, A. N., Miyake, N., et al., 2014. Mutant ataxin-3 with an abnormally expanded polyglutamine chain disrupts dendritic development and metabotropic glutamate receptor signaling in mouse cerebellar Purkinje cells. Cerebellum. 13**,** 29-41.
Koppers, M., van Blitterswijk, M. M., Vlam, L., et al., 2012. VCP mutations in familial and sporadic amyotrophic lateral sclerosis. Neurobiology of aging. 33**,** 837 e7-13.
Korner, S., Hendricks, M., Kollewe, K., et al., 2013. Weight loss, dysphagia and supplement intake in patients with amyotrophic lateral sclerosis (ALS): impact on quality of life and therapeutic options. BMC neurology. 13**,** 84.
Koshy, B. T., Zoghbi, H. Y., 1997. The CAG/polyglutamine tract diseases: gene products and molecular pathogenesis. Brain pathology. 7**,** 927-42.
Kottgen, A., 2010. Genome-wide association studies in nephrology research. American journal of kidney diseases : the official journal of the National Kidney Foundation. 56**,** 743-58.
Koyano, S., Iwabuchi, K., Yagishita, S., et al., 2002. Paradoxical absence of nuclear inclusion in cerebellar Purkinje cells of hereditary ataxias linked to CAG expansion. Journal of neurology, neurosurgery, and psychiatry. 73**,** 450-2.
Koyano, S., Uchihara, T., Fujigasaki, H., et al., 1999. Neuronal intranuclear inclusions in spinocerebellar ataxia type 2: triple-labeling immunofluorescent study. Neuroscience letters. 273**,** 117-20.
Koyano, S., Yagishita, S., Kuroiwa, Y., et al., 2014. Neuropathological Staging of Spinocerebellar Ataxia Type 2 by Semiquantitative 1C2-Positive Neuron Typing. Nuclear Translocation of Cytoplasmic 1C2 Underlies Disease Progression of Spinocerebellar Ataxia Type 2. Brain pathology. 24**,** 599-606.
Kozlowska, E., Krzyzosiak, W. J., Koscianska, E., 2013. Regulation of huntingtin gene expression by miRNA-137, -214, -148a, and their respective isomiRs. International journal of molecular sciences. 14**,** 16999-7016.
Kraemer, B. C., Schuck, T., Wheeler, J. M., et al., 2010. Loss of murine TDP-43 disrupts motor function and plays an essential role in embryogenesis. Acta neuropathologica. 119**,** 409-19.
Kubodera, T., Yokota, T., Ohwada, K., et al., 2003. Proteolytic cleavage and cellular toxicity of the human alpha1A calcium channel in spinocerebellar ataxia type 6. Neuroscience letters. 341**,** 74-8.
Kurosawa, M., Matsumoto, G., Kino, Y., et al., 2015. Depletion of p62 reduces nuclear inclusions and paradoxically ameliorates disease phenotypes in Huntington's model mice. Human molecular genetics. 24**,** 1092-1105.
Kuusisto, E., Salminen, A., Alafuzoff, I., 2001. Ubiquitin-binding protein p62 is present in neuronal and glial inclusions in human tauopathies and synucleinopathies. Neuroreport. 12**,** 2085-90.
Kwiatkowski, T. J., Jr., Bosco, D. A., Leclerc, A. L., et al., 2009. Mutations in the FUS/TLS gene on chromosome 16 cause familial amyotrophic lateral sclerosis. Science. 323**,** 1205-8.
Laco, M. N., Oliveira, C. R., Paulson, H. L., et al., 2012. Compromised mitochondrial complex II in models of Machado-Joseph disease. Biochimica et biophysica acta. 1822**,** 139-49.
Lagier-Tourenne, C., Polymenidou, M., Cleveland, D. W., 2010. TDP-43 and FUS/TLS: emerging roles in RNA processing and neurodegeneration. Human molecular genetics. 19**,** R46-64.
Lahut, S., Omur, O., Uyan, O., et al., 2012. ATXN2 and its neighbouring gene SH2B3 are associated with increased ALS risk in the Turkish population. PloS one. 7**,** e42956.
Lalonde, R., 1987. Motor abnormalities in staggerer mutant mice. Experimental brain research. 68**,** 417-20.
Lalonde, R., Dumont, M., Staufenbiel, M., et al., 2005. Neurobehavioral characterization of APP23 transgenic mice with the SHIRPA primary screen. Behavioural brain research. 157**,** 91-8.
Lalonde, R., Strazielle, C., 2011. Brain regions and genes affecting limb-clasping responses. Brain research reviews. 67**,** 252-9.
Lam, Y. C., Bowman, A. B., Jafar-Nejad, P., et al., 2006. ATAXIN-1 interacts with the repressor Capicua in its native complex to cause SCA1 neuropathology. Cell. 127**,** 1335-47.
Lastres-Becker, I., Brodesser, S., Lutjohann, D., et al., 2008a. Insulin receptor and lipid metabolism pathology in ataxin-2 knock-out mice. Human molecular genetics. 17**,** 1465-81.
Lastres-Becker, I., Rub, U., Auburger, G., 2008b. Spinocerebellar ataxia 2 (SCA2). Cerebellum. 7**,** 115-24.
Lattante, S., Millecamps, S., Stevanin, G., et al., 2014. Contribution of ATXN2 intermediary polyQ expansions in a spectrum of neurodegenerative disorders. Neurology. 83**,** 990-5.
Lautenschlaeger, J., Prell, T., Grosskreutz, J., 2012. Endoplasmic reticulum stress and the ER mitochondrial calcium cycle in amyotrophic lateral sclerosis. Amyotrophic lateral sclerosis : official publication of the World Federation of Neurology Research Group on Motor Neuron Diseases. 13**,** 166-77.

Lee, T., Li, Y. R., Ingre, C., et al., 2011. Ataxin-2 intermediate-length polyglutamine expansions in European ALS patients. Human molecular genetics. 20**,** 1697-700.
Lee, Y., Samaco, R. C., Gatchel, J. R., et al., 2008. miR-19, miR-101 and miR-130 co-regulate ATXN1 levels to potentially modulate SCA1 pathogenesis. Nature neuroscience. 11**,** 1137-9.
Lessing, D., Bonini, N. M., 2008. Polyglutamine genes interact to modulate the severity and progression of neurodegeneration in Drosophila. PLoS biology. 6**,** e29.
Li, Y. R., King, O. D., Shorter, J., et al., 2013. Stress granules as crucibles of ALS pathogenesis. The Journal of cell biology. 201**,** 361-72.
Lieberman, A. P., Harmison, G., Strand, A. D., et al., 2002. Altered transcriptional regulation in cells expressing the expanded polyglutamine androgen receptor. Human molecular genetics. 11**,** 1967-76.
Lilienbaum, A., 2013. Relationship between the proteasomal system and autophagy. International journal of biochemistry and molecular biology. 4**,** 1-26.
Lim, C., Allada, R., 2013. ATAXIN-2 activates PERIOD translation to sustain circadian rhythms in Drosophila. Science. 340**,** 875-9.
Lim, J., Crespo-Barreto, J., Jafar-Nejad, P., et al., 2008. Opposing effects of polyglutamine expansion on native protein complexes contribute to SCA1. Nature. 452**,** 713-8.
Lim, J., Hao, T., Shaw, C., et al., 2006. A protein-protein interaction network for human inherited ataxias and disorders of Purkinje cell degeneration. Cell. 125**,** 801-14.
Lin, X., Antalffy, B., Kang, D., et al., 2000. Polyglutamine expansion down-regulates specific neuronal genes before pathologic changes in SCA1. Nature neuroscience. 3**,** 157-63.
Litterman, N., Ikeuchi, Y., Gallardo, G., et al., 2011. An OBSL1-Cul7Fbxw8 ubiquitin ligase signaling mechanism regulates Golgi morphology and dendrite patterning. PLoS biology. 9**,** e1001060.
Liu, C. T., Garnaas, M. K., Tin, A., et al., 2011. Genetic association for renal traits among participants of African ancestry reveals new loci for renal function. PLoS genetics. 7**,** e1002264.
Liu, J., Tang, T. S., Tu, H., et al., 2009. Deranged calcium signaling and neurodegeneration in spinocerebellar ataxia type 2. The Journal of neuroscience : the official journal of the Society for Neuroscience. 29**,** 9148-62.
Liu, X., Lu, M., Tang, L., et al., 2013. ATXN2 CAG repeat expansions increase the risk for Chinese patients with amyotrophic lateral sclerosis. Neurobiology of aging. 34**,** 2236 e5-8.
Livak, K. J., Schmittgen, T. D., 2001. Analysis of relative gene expression data using real-time quantitative PCR and the 2(-Delta Delta C(T)) Method. Methods. 25**,** 402-8.
Lopez-Lastra, M., Rivas, A., Barria, M. I., 2005. Protein synthesis in eukaryotes: the growing biological relevance of cap-independent translation initiation. Biological research. 38**,** 121-46.
Lorenzetti, D., Watase, K., Xu, B., et al., 2000. Repeat instability and motor incoordination in mice with a targeted expanded CAG repeat in the Sca1 locus. Human molecular genetics. 9**,** 779-85.
Lowe, J., Blanchard, A., Morrell, K., et al., 1988. Ubiquitin is a common factor in intermediate filament inclusion bodies of diverse type in man, including those of Parkinson's disease, Pick's disease, and Alzheimer's disease, as well as Rosenthal fibres in cerebellar astrocytomas, cytoplasmic bodies in muscle, and mallory bodies in alcoholic liver disease. The Journal of pathology. 155**,** 9-15.
Luthi-Carter, R., Hanson, S. A., Strand, A. D., et al., 2002a. Dysregulation of gene expression in the R6/2 model of polyglutamine disease: parallel changes in muscle and brain. Human molecular genetics. 11**,** 1911-26.
Luthi-Carter, R., Strand, A. D., Hanson, S. A., et al., 2002b. Polyglutamine and transcription: gene expression changes shared by DRPLA and Huntington's disease mouse models reveal context-independent effects. Human molecular genetics. 11**,** 1927-37.
Mahler, A., Steiniger, J., Endres, M., et al., 2014. Increased catabolic state in spinocerebellar ataxia type 1 patients. Cerebellum. 13**,** 440-6.
Maltecca, F., Baseggio, E., Consolato, F., et al., 2015. Purkinje neuron Ca2+ influx reduction rescues ataxia in SCA28 model. The Journal of clinical investigation. 125**,** 263-274.
Mangiarini, L., Sathasivam, K., Seller, M., et al., 1996. Exon 1 of the HD gene with an expanded CAG repeat is sufficient to cause a progressive neurological phenotype in transgenic mice. Cell. 87**,** 493-506.
Mangus, D. A., Amrani, N., Jacobson, A., 1998. Pbp1p, a factor interacting with Saccharomyces cerevisiae poly(A)-binding protein, regulates polyadenylation. Molecular and cellular biology. 18**,** 7383-96.
Martin, S., Zekri, L., Metz, A., et al., 2013. Deficiency of G3BP1, the stress granules assembly factor, results in abnormal synaptic plasticity and calcium homeostasis in neurons. Journal of neurochemistry. 125**,** 175-184.
Matilla-Duenas, A., Sanchez, I., Corral-Juan, M., et al., 2010. Cellular and molecular pathways triggering neurodegeneration in the spinocerebellar ataxias. Cerebellum. 9**,** 148-66.
Matilla, A., Koshy, B. T., Cummings, C. J., et al., 1997. The cerebellar leucine-rich acidic nuclear protein interacts with ataxin-1. Nature. 389**,** 974-8.
Matilla, A., Roberson, E. D., Banfi, S., et al., 1998. Mice lacking ataxin-1 display learning deficits and decreased hippocampal paired-pulse facilitation. The Journal of neuroscience : the official journal of the Society for Neuroscience. 18**,** 5508-16.
Matsumoto, M., Nakagawa, T., Inoue, T., et al., 1996. Ataxia and epileptic seizures in mice lacking type 1 inositol 1,4,5-trisphosphate receptor. Nature. 379**,** 168-71.
Maynard, C. J., Bottcher, C., Ortega, Z., et al., 2009. Accumulation of ubiquitin conjugates in a polyglutamine disease model occurs without global ubiquitin/proteasome system impairment. Proceedings of the National Academy of Sciences of the United States of America. 106**,** 13986-91.

McCann, C., Holohan, E. E., Das, S., et al., 2011. The Ataxin-2 protein is required for microRNA function and synapse-specific long-term olfactory habituation. Proceedings of the National Academy of Sciences of the United States of America. 108**,** E655-62.

McDonald, K. K., Aulas, A., Destroismaisons, L., et al., 2011. TAR DNA-binding protein 43 (TDP-43) regulates stress granule dynamics via differential regulation of G3BP and TIA-1. Human molecular genetics. 20**,** 1400-10.

McManamny, P., Chy, H. S., Finkelstein, D. I., et al., 2002. A mouse model of spinal and bulbar muscular atrophy. Human molecular genetics. 11**,** 2103-11.

Melachroinou, K., Xilouri, M., Emmanouilidou, E., et al., 2013. Deregulation of calcium homeostasis mediates secreted alpha-synuclein-induced neurotoxicity. Neurobiology of aging. 34**,** 2853-65.

Mendoza, J. F., AL., 2008. Clinical Neuroanatomy: A Neurobehavioral Approach.

Menon, R. P., Nethisinghe, S., Faggiano, S., et al., 2013. The role of interruptions in polyQ in the pathology of SCA1. PLoS genetics. 9**,** e1003648.

Michalik, A., Van Broeckhoven, C., 2003. Pathogenesis of polyglutamine disorders: aggregation revisited. Human molecular genetics. 12 Spec No 2**,** R173-86.

Michikawa, T., Hirota, J., Kawano, S., et al., 1999. Calmodulin mediates calcium-dependent inactivation of the cerebellar type 1 inositol 1,4,5-trisphosphate receptor. Neuron. 23**,** 799-808.

Mizutani, A., Wang, L., Rajan, H., et al., 2005. Boat, an AXH domain protein, suppresses the cytotoxicity of mutant ataxin-1. The EMBO journal. 24**,** 3339-51.

Mohan, R. D., Abmayr, S. M., Workman, J. L., 2014. The expanding role for chromatin and transcription in polyglutamine disease. Current opinion in genetics & development. 26C**,** 96-104.

Mutihac, R., Alegre-Abarrategui, J., Gordon, D., et al., 2015. TARDBP pathogenic mutations increase cytoplasmic translocation of TDP-43 and cause reduction of endoplasmic reticulum Ca signaling in motor neurons. Neurobiology of disease. 75**,** 64-77.

Nechiporuk, T., Huynh, D. P., Figueroa, K., et al., 1998. The mouse SCA2 gene: cDNA sequence, alternative splicing and protein expression. Human molecular genetics. 7**,** 1301-9.

Neuenschwander, A. G., Thai, K. K., Figueroa, K. P., et al., 2014. Amyotrophic Lateral Sclerosis Risk for Spinocerebellar Ataxia Type 2 ATXN2 CAG Repeat Alleles: A Meta-analysis. JAMA neurology. 71**,** 1529-1534.

Neumann, M., Sampathu, D. M., Kwong, L. K., et al., 2006. Ubiquitinated TDP-43 in frontotemporal lobar degeneration and amyotrophic lateral sclerosis. Science. 314**,** 130-3.

Nihei, Y., Ito, D., Suzuki, N., 2012. Roles of ataxin-2 in pathological cascades mediated by TAR DNA-binding protein 43 (TDP-43) and Fused in Sarcoma (FUS). The Journal of biological chemistry. 287**,** 41310-23.

Nonhoff, U., Ralser, M., Welzel, F., et al., 2007. Ataxin-2 interacts with the DEAD/H-box RNA helicase DDX6 and interferes with P-bodies and stress granules. Molecular biology of the cell. 18**,** 1385-96.

Nonis, D., Schmidt, M. H., van de Loo, S., et al., 2008. Ataxin-2 associates with the endocytosis complex and affects EGF receptor trafficking. Cellular signalling. 20**,** 1725-39.

Nucifora, F. C., Jr., Ellerby, L. M., Wellington, C. L., et al., 2003. Nuclear localization of a non-caspase truncation product of atrophin-1, with an expanded polyglutamine repeat, increases cellular toxicity. The Journal of biological chemistry. 278**,** 13047-55.

Okabe, H., Lee, S. H., Phuchareon, J., et al., 2006. A critical role for FBXW8 and MAPK in cyclin D1 degradation and cancer cell proliferation. PloS one. 1**,** e128.

Orozco Diaz, G., Nodarse Fleites, A., Cordoves Sagaz, R., et al., 1990. Autosomal dominant cerebellar ataxia: clinical analysis of 263 patients from a homogeneous population in Holguin, Cuba. Neurology. 40**,** 1369-75.

Orr, H. T., Zoghbi, H. Y., 2007. Trinucleotide repeat disorders. Annual review of neuroscience. 30**,** 575-621.

Ortega, Z., Diaz-Hernandez, M., Maynard, C. J., et al., 2010. Acute polyglutamine expression in inducible mouse model unravels ubiquitin/proteasome system impairment and permanent recovery attributable to aggregate formation. The Journal of neuroscience : the official journal of the Society for Neuroscience. 30**,** 3675-88.

Ortega, Z., Lucas, J. J., 2014. Ubiquitin-proteasome system involvement in Huntington's disease. Frontiers in molecular neuroscience. 7**,** 77.

Oyama, G., Thompson, A., Foote, K. D., et al., 2014. Deep brain stimulation for tremor associated with underlying ataxia syndromes: a case series and discussion of issues. Tremor and other hyperkinetic movements. 4**,** 228.

Packer, A. N., Xing, Y., Harper, S. Q., et al., 2008. The bifunctional microRNA miR-9/miR-9* regulates REST and CoREST and is downregulated in Huntington's disease. The Journal of neuroscience : the official journal of the Society for Neuroscience. 28**,** 14341-6.

Pang, J. T., Giunti, P., Chamberlain, S., et al., 2002. Neuronal intranuclear inclusions in SCA2: a genetic, morphological and immunohistochemical study of two cases. Brain : a journal of neurology. 125**,** 656-63.

Pankiv, S., Clausen, T. H., Lamark, T., et al., 2007. p62/SQSTM1 binds directly to Atg8/LC3 to facilitate degradation of ubiquitinated protein aggregates by autophagy. The Journal of biological chemistry. 282**,** 24131-45.

Panov, A. V., Gutekunst, C. A., Leavitt, B. R., et al., 2002. Early mitochondrial calcium defects in Huntington's disease are a direct effect of polyglutamines. Nature neuroscience. 5**,** 731-6.

Parker, C. C., Evans, O. B., 2003. Metabolic disorders causing childhood ataxia. Seminars in pediatric neurology. 10**,** 193-9.

Paulson, H. L., Perez, M. K., Trottier, Y., et al., 1997. Intranuclear inclusions of expanded polyglutamine protein in spinocerebellar ataxia type 3. Neuron. 19**,** 333-44.

Persengiev, S., Kondova, I., Otting, N., et al., 2011. Genome-wide analysis of miRNA expression reveals a potential role for miR-144 in brain aging and spinocerebellar ataxia pathogenesis. Neurobiology of aging. 32**,** 2316 e17-27.

Pikkarainen, M., Hartikainen, P., Alafuzoff, I., 2008. Neuropathologic features of frontotemporal lobar degeneration with ubiquitin-positive inclusions visualized with ubiquitin-binding protein p62 immunohistochemistry. Journal of neuropathology and experimental neurology. 67**,** 280-98.

Ponyeam, W., Hagen, T., 2012. Characterization of the Cullin7 E3 ubiquitin ligase--heterodimerization of cullin substrate receptors as a novel mechanism to regulate cullin E3 ligase activity. Cellular signalling. 24**,** 290-5.

Prayson, R. A. (Ed.) 2005. Neuropathology. Saunders.

Pujana, M. A., Corral, J., Gratacos, M., et al., 1999. Spinocerebellar ataxias in Spanish patients: genetic analysis of familial and sporadic cases. The Ataxia Study Group. Human genetics. 104**,** 516-22.

Pulst, S. M., Nechiporuk, A., Nechiporuk, T., et al., 1996. Moderate expansion of a normally biallelic trinucleotide repeat in spinocerebellar ataxia type 2. Nature genetics. 14**,** 269-76.

Pulst, S. M., Santos, N., Wang, D., et al., 2005. Spinocerebellar ataxia type 2: polyQ repeat variation in the CACNA1A calcium channel modifies age of onset. Brain : a journal of neurology. 128**,** 2297-303.

Purves, D., Augustine, G. J., Fitzpatrick, D., et al., 2001. Neuroscience. Sinauer Associates, Sunderland.

Ralser, M., Albrecht, M., Nonhoff, U., et al., 2005a. An integrative approach to gain insights into the cellular function of human ataxin-2. Journal of molecular biology. 346**,** 203-14.

Ralser, M., Nonhoff, U., Albrecht, M., et al., 2005b. Ataxin-2 and huntingtin interact with endophilin-A complexes to function in plastin-associated pathways. Human molecular genetics. 14**,** 2893-909.

Ramani, B., Harris, G. M., Huang, R., et al., 2015. A knockin mouse model of spinocerebellar ataxia type 3 exhibits prominent aggregate pathology and aberrant splicing of the disease gene transcript. Human molecular genetics. 24**,** 1211-1224.

Reddy, P. H., Shirendeb, U. P., 2012. Mutant huntingtin, abnormal mitochondrial dynamics, defective axonal transport of mitochondria, and selective synaptic degeneration in Huntington's disease. Biochimica et biophysica acta. 1822**,** 101-10.

Reddy, P. H., Williams, M., Charles, V., et al., 1998. Behavioural abnormalities and selective neuronal loss in HD transgenic mice expressing mutated full-length HD cDNA. Nature genetics. 20**,** 198-202.

Reeber, S. L., Otis, T. S., Sillitoe, R. V., 2013. New roles for the cerebellum in health and disease. Frontiers in systems neuroscience. 7**,** 83.

Rehman, A. U., Santos-Cortez, R. L., Morell, R. J., et al., 2014. Mutations in TBC1D24, a gene associated with epilepsy, also cause nonsyndromic deafness DFNB86. American journal of human genetics. 94**,** 144-52.

Renton, A. E., Majounie, E., Waite, A., et al., 2011. A hexanucleotide repeat expansion in C9ORF72 is the cause of chromosome 9p21-linked ALS-FTD. Neuron. 72**,** 257-68.

Riley, B. E., Kaiser, S. E., Shaler, T. A., et al., 2010. Ubiquitin accumulation in autophagy-deficient mice is dependent on the Nrf2-mediated stress response pathway: a potential role for protein aggregation in autophagic substrate selection. The Journal of cell biology. 191**,** 537-52.

Ripaud, L., Chumakova, V., Antonin, M., et al., 2014. Overexpression of Q-rich prion-like proteins suppresses polyQ cytotoxicity and alters the polyQ interactome. Proceedings of the National Academy of Sciences of the United States of America. 111**,** 18219-24.

Ristori, G., Romano, S., Visconti, A., et al., 2010. Riluzole in cerebellar ataxia: a randomized, double-blind, placebo-controlled pilot trial. Neurology. 74**,** 839-45.

Roach, W. G., Chavez, J. A., Miinea, C. P., et al., 2007. Substrate specificity and effect on GLUT4 translocation of the Rab GTPase-activating protein Tbc1d1. The Biochemical journal. 403**,** 353-8.

Rodriguez-Lebron, E., Liu, G., Keiser, M., et al., 2013. Altered Purkinje cell miRNA expression and SCA1 pathogenesis. Neurobiology of disease. 54**,** 456-63.

Rolfs, A., Koeppen, A. H., Bauer, I., et al., 2003. Clinical features and neuropathology of autosomal dominant spinocerebellar ataxia (SCA17). Annals of neurology. 54**,** 367-75.

Rosen, D. R., Siddique, T., Patterson, D., et al., 1993. Mutations in Cu/Zn superoxide dismutase gene are associated with familial amyotrophic lateral sclerosis. Nature. 362**,** 59-62.

Ross, O. A., Rutherford, N. J., Baker, M., et al., 2011. Ataxin-2 repeat-length variation and neurodegeneration. Human molecular genetics. 20**,** 3207-12.

Rossi, P. I., Vaccari, C. M., Terracciano, A., et al., 2010. The metabotropic glutamate receptor 1, GRM1: evaluation as a candidate gene for inherited forms of cerebellar ataxia. Journal of neurology. 257**,** 598-602.

Rub, U., Brunt, E. R., Petrasch-Parwez, E., et al., 2006. Degeneration of ingestion-related brainstem nuclei in spinocerebellar ataxia type 2, 3, 6 and 7. Neuropathology and applied neurobiology. 32**,** 635-49.

Rub, U., Del Turco, D., Burk, K., et al., 2005. Extended pathoanatomical studies point to a consistent affection of the thalamus in spinocerebellar ataxia type 2. Neuropathology and applied neurobiology. 31**,** 127-40.

Rub, U., Hentschel, M., Stratmann, K., et al., 2014. Huntington's disease (HD): degeneration of select nuclei, widespread occurrence of neuronal nuclear and axonal inclusions in the brainstem. Brain pathology. 24**,** 247-60.

Rub, U., Schols, L., Paulson, H., et al., 2013. Clinical features, neurogenetics and neuropathology of the polyglutamine spinocerebellar ataxias type 1, 2, 3, 6 and 7. Progress in neurobiology. 104**,** 38-66.

Rue, L., Lopez-Soop, G., Gelpi, E., et al., 2013. Brain region- and age-dependent dysregulation of p62 and NBR1 in a mouse model of Huntington's disease. Neurobiology of disease. 52**,** 219-28.
Sahba, S., Nechiporuk, A., Figueroa, K. P., et al., 1998. Genomic structure of the human gene for spinocerebellar ataxia type 2 (SCA2) on chromosome 12q24.1. Genomics. 47**,** 359-64.
Saitoh, Y., Fujikake, N., Okamoto, Y., et al., 2015. P62 Plays a Protective Role in the Autophagic Degradation of Polyglutamine Protein Oligomers in Polyglutamine Disease Model Flies. The Journal of biological chemistry. 290**,** 1442-1453.
Sanchez, I., Xu, C. J., Juo, P., et al., 1999. Caspase-8 is required for cell death induced by expanded polyglutamine repeats. Neuron. 22**,** 623-33.
Sanpei, K., Takano, H., Igarashi, S., et al., 1996. Identification of the spinocerebellar ataxia type 2 gene using a direct identification of repeat expansion and cloning technique, DIRECT. Nature genetics. 14**,** 277-84.
Sasaki, H., Wakisaka, A., Sanpei, K., et al., 1998. Phenotype variation correlates with CAG repeat length in SCA2--a study of 28 Japanese patients. Journal of the neurological sciences. 159**,** 202-8.
Sathasivam, K., Hobbs, C., Mangiarini, L., et al., 1999. Transgenic models of Huntington's disease. Philosophical transactions of the Royal Society of London. Series B, Biological sciences. 354**,** 963-9.
Sathasivam, K., Neueder, A., Gipson, T. A., et al., 2013. Aberrant splicing of HTT generates the pathogenic exon 1 protein in Huntington disease. Proceedings of the National Academy of Sciences of the United States of America. 110**,** 2366-70.
Satterfield, T. F., Pallanck, L. J., 2006. Ataxin-2 and its Drosophila homolog, ATX2, physically assemble with polyribosomes. Human molecular genetics. 15**,** 2523-32.
Saute, J. A., Silva, A. C., Souza, G. N., et al., 2012. Body mass index is inversely correlated with the expanded CAG repeat length in SCA3/MJD patients. Cerebellum. 11**,** 771-4.
Schaefer, A., O'Carroll, D., Tan, C. L., et al., 2007. Cerebellar neurodegeneration in the absence of microRNAs. The Journal of experimental medicine. 204**,** 1553-8.
Schapira, A. H., 2013. Calcium dysregulation in Parkinson's disease. Brain : a journal of neurology. 136**,** 2015-6.
Scherzinger, E., Lurz, R., Turmaine, M., et al., 1997. Huntingtin-encoded polyglutamine expansions form amyloid-like protein aggregates in vitro and in vivo. Cell. 90**,** 549-58.
Scheufele, F., Wolf, B., Kruse, M., et al., 2014. Evidence for a regulatory role of Cullin-RING E3 ubiquitin ligase 7 in insulin signaling. Cellular signalling. 26**,** 233-9.
Schiffer, D., Autilio-Gambetti, L., Chio, A., et al., 1991. Ubiquitin in motor neuron disease: study at the light and electron microscope. Journal of neuropathology and experimental neurology. 50**,** 463-73.
Schipper-Krom, S., Juenemann, K., Jansen, A. H., et al., 2014. Dynamic recruitment of active proteasomes into polyglutamine initiated inclusion bodies. FEBS letters. 588**,** 151-9.
Schliwa, M., Woehlke, G., 2003. Molecular motors. Nature. 422**,** 759-65.
Schmahmann, J. D., 2010. The role of the cerebellum in cognition and emotion: personal reflections since 1982 on the dysmetria of thought hypothesis, and its historical evolution from theory to therapy. Neuropsychology review. 20**,** 236-60.
Schmidt, A., Wolde, M., Thiele, C., et al., 1999. Endophilin I mediates synaptic vesicle formation by transfer of arachidonate to lysophosphatidic acid. Nature. 401**,** 133-41.
Schmidt, T., Lindenberg, K. S., Krebs, A., et al., 2002. Protein surveillance machinery in brains with spinocerebellar ataxia type 3: redistribution and differential recruitment of 26S proteasome subunits and chaperones to neuronal intranuclear inclusions. Annals of neurology. 51**,** 302-10.
Schols, L., Bauer, P., Schmidt, T., et al., 2004. Autosomal dominant cerebellar ataxias: clinical features, genetics, and pathogenesis. The Lancet. Neurology. 3**,** 291-304.
Schols, L., Gispert, S., Vorgerd, M., et al., 1997. Spinocerebellar ataxia type 2. Genotype and phenotype in German kindreds. Archives of neurology. 54**,** 1073-80.
Schwab, C., Arai, T., Hasegawa, M., et al., 2008. Colocalization of transactivation-responsive DNA-binding protein 43 and huntingtin in inclusions of Huntington disease. Journal of neuropathology and experimental neurology. 67**,** 1159-65.
Scoles, D. R., Pflieger, L. T., Thai, K. K., et al., 2012. ETS1 regulates the expression of ATXN2. Human molecular genetics. 21**,** 5048-65.
Seidel, K., den Dunnen, W. F., Schultz, C., et al., 2010. Axonal inclusions in spinocerebellar ataxia type 3. Acta neuropathologica. 120**,** 449-60.
Sephton, C. F., Good, S. K., Atkin, S., et al., 2010. TDP-43 is a developmentally regulated protein essential for early embryonic development. The Journal of biological chemistry. 285**,** 6826-34.
Sepulveda-Falla, D., Barrera-Ocampo, A., Hagel, C., et al., 2014. Familial Alzheimer's disease-associated presenilin-1 alters cerebellar activity and calcium homeostasis. The Journal of clinical investigation. 124**,** 1552-67.
Sergi, G., De Rui, M., Coin, A., et al., 2013. Weight loss and Alzheimer's disease: temporal and aetiologic connections. The Proceedings of the Nutrition Society. 72**,** 160-5.
Serra, H. G., Byam, C. E., Lande, J. D., et al., 2004. Gene profiling links SCA1 pathophysiology to glutamate signaling in Purkinje cells of transgenic mice. Human molecular genetics. 13**,** 2535-43.
Serra, H. G., Duvick, L., Zu, T., et al., 2006. RORalpha-mediated Purkinje cell development determines disease severity in adult SCA1 mice. Cell. 127**,** 697-708.
Serrano-Munuera, C., Corral-Juan, M., Stevanin, G., et al., 2013. New subtype of spinocerebellar ataxia with altered vertical eye movements mapping to chromosome 1p32. JAMA neurology. 70**,** 764-71.

Sharma, J. C., Vassallo, M., 2014. Prognostic significance of weight changes in Parkinson's disease: the Park-weight phenotype. Neurodegenerative disease management. 4**,** 309-16.
Shibata, H., Huynh, D. P., Pulst, S. M., 2000. A novel protein with RNA-binding motifs interacts with ataxin-2. Human molecular genetics. 9**,** 1303-13.
Sieradzan, K. A., Mechan, A. O., Jones, L., et al., 1999. Huntington's disease intranuclear inclusions contain truncated, ubiquitinated huntingtin protein. Experimental neurology. 156**,** 92-9.
Simon, D. K., Zheng, K., Velazquez, L., et al., 2007. Mitochondrial complex I gene variant associated with early age at onset in spinocerebellar ataxia type 2. Archives of neurology. 64**,** 1042-4.
Sinha, M., Ghose, J., Bhattarcharyya, N. P., 2011. Micro RNA -214,-150,-146a and-125b target Huntingtin gene. RNA biology. 8**,** 1005-21.
Slow, E. J., Graham, R. K., Osmand, A. P., et al., 2005. Absence of behavioral abnormalities and neurodegeneration in vivo despite widespread neuronal huntingtin inclusions. Proceedings of the National Academy of Sciences of the United States of America. 102**,** 11402-7.
Sobczak, K., Krzyzosiak, W. J., 2005. CAG repeats containing CAA interruptions form branched hairpin structures in spinocerebellar ataxia type 2 transcripts. The Journal of biological chemistry. 280**,** 3898-910.
Sreedharan, J., Blair, I. P., Tripathi, V. B., et al., 2008. TDP-43 mutations in familial and sporadic amyotrophic lateral sclerosis. Science. 319**,** 1668-72.
Sreedharan, J., Brown, R. H., Jr., 2013. Amyotrophic lateral sclerosis: Problems and prospects. Annals of neurology. 74**,** 309-16.
Stallings, N. R., Puttaparthi, K., Dowling, K. J., et al., 2013. TDP-43, an ALS linked protein, regulates fat deposition and glucose homeostasis. PloS one. 8**,** e71793.
Stallings, N. R., Puttaparthi, K., Luther, C. M., et al., 2010. Progressive motor weakness in transgenic mice expressing human TDP-43. Neurobiology of disease. 40**,** 404-14.
Staropoli, J. F., McDermott, C., Martinat, C., et al., 2003. Parkin is a component of an SCF-like ubiquitin ligase complex and protects postmitotic neurons from kainate excitotoxicity. Neuron. 37**,** 735-49.
Stenoien, D. L., Mielke, M., Mancini, M. A., 2002. Intranuclear ataxin1 inclusions contain both fast- and slow-exchanging components. Nature cell biology. 4**,** 806-10.
Stone, S., Abkevich, V., Russell, D. L., et al., 2006. TBC1D1 is a candidate for a severe obesity gene and evidence for a gene/gene interaction in obesity predisposition. Human molecular genetics. 15**,** 2709-20.
Storey, E., 2014. Genetic cerebellar ataxias. Seminars in neurology. 34**,** 280-92.
Street, V. A., McKee-Johnson, J. W., Fonseca, R. C., et al., 1998. Mutations in a plasma membrane Ca2+-ATPase gene cause deafness in deafwaddler mice. Nature genetics. 19**,** 390-4.
Stribl, C., Samara, A., Trumbach, D., et al., 2014. Mitochondrial dysfunction and decrease in body weight of a transgenic knock-in mouse model for TDP-43. The Journal of biological chemistry. 289**,** 10769-84.
Sun, Y., Taylor, C. W., 2008. A calmodulin antagonist reveals a calmodulin-independent interdomain interaction essential for activation of inositol 1,4,5-trisphosphate receptors. The Biochemical journal. 416**,** 243-53.
Swarup, V., Phaneuf, D., Bareil, C., et al., 2011. Pathological hallmarks of amyotrophic lateral sclerosis/frontotemporal lobar degeneration in transgenic mice produced with TDP-43 genomic fragments. Brain : a journal of neurology. 134**,** 2610-26.
Switonski, P. M., Szlachcic, W. J., Krzyzosiak, W. J., et al., 2015. A new humanized ataxin-3 knock-in mouse model combines the genetic features, pathogenesis of neurons and glia and late disease onset of SCA3/MJD. Neurobiology of disease. 73**,** 174-88.
Synofzik, M., Ilg, W., 2014. Motor training in degenerative spinocerebellar disease: ataxia-specific improvements by intensive physiotherapy and exergames. BioMed research international. 2014**,** 583507.
Synofzik, M., Ronchi, D., Keskin, I., et al., 2012. Mutant superoxide dismutase-1 indistinguishable from wild-type causes ALS. Human molecular genetics. 21**,** 3568-74.
Takahashi, E., Niimi, K., Itakura, C., 2009. Motor coordination impairment in aged heterozygous rolling Nagoya, Cav2.1 mutant mice. Brain research. 1279**,** 50-7.
Takahashi, E., Niimi, K., Itakura, C., 2010. Neonatal motor functions in Cacna1a-mutant rolling Nagoya mice. Behavioural brain research. 207**,** 273-9.
Takao, M., Aoyama, M., Ishikawa, K., et al., 2011. Spinocerebellar ataxia type 2 is associated with Parkinsonism and Lewy body pathology. BMJ case reports. 2011.
Tang, T. S., Tu, H., Chan, E. Y., et al., 2003. Huntingtin and huntingtin-associated protein 1 influence neuronal calcium signaling mediated by inositol-(1,4,5) triphosphate receptor type 1. Neuron. 39**,** 227-39.
Tarun, S. Z., Jr., Sachs, A. B., 1996. Association of the yeast poly(A) tail binding protein with translation initiation factor eIF-4G. The EMBO journal. 15**,** 7168-77.
Tazen, S., Figueroa, K., Kwan, J. Y., et al., 2013. Amyotrophic lateral sclerosis and spinocerebellar ataxia type 2 in a family with full CAG repeat expansions of ATXN2. JAMA neurology. 70**,** 1302-4.
Teixeira, D., Sheth, U., Valencia-Sanchez, M. A., et al., 2005. Processing bodies require RNA for assembly and contain nontranslating mRNAs. RNA. 11**,** 371-82.
Tezenas du Montcel, S., Charles, P., Goizet, C., et al., 2012. Factors influencing disease progression in autosomal dominant cerebellar ataxia and spastic paraplegia. Archives of neurology. 69**,** 500-8.
Tezenas du Montcel, S., Durr, A., Bauer, P., et al., 2014. Modulation of the age at onset in spinocerebellar ataxia by CAG tracts in various genes. Brain : a journal of neurology. 137**,** 2444-55.

Tollervey, J. R., Curk, T., Rogelj, B., et al., 2011. Characterizing the RNA targets and position-dependent splicing regulation by TDP-43. Nature neuroscience. 14**,** 452-8.

Toyoshima, Y., Tanaka, H., Shimohata, M., et al., 2011. Spinocerebellar ataxia type 2 (SCA2) is associated with TDP-43 pathology. Acta neuropathologica. 122**,** 375-8.

Trapnell, C., Williams, B. A., Pertea, G., et al., 2010. Transcript assembly and quantification by RNA-Seq reveals unannotated transcripts and isoform switching during cell differentiation. Nature biotechnology. 28**,** 511-5.

Tsoi, H., Yu, A. C., Chen, Z. S., et al., 2014. A novel missense mutation in CCDC88C activates the JNK pathway and causes a dominant form of spinocerebellar ataxia. Journal of medical genetics. 51**,** 590-5.

Tsunematsu, R., Nishiyama, M., Kotoshiba, S., et al., 2006. Fbxw8 is essential for Cul1-Cul7 complex formation and for placental development. Molecular and cellular biology. 26**,** 6157-69.

Turkmen, S., Guo, G., Garshasbi, M., et al., 2009. CA8 mutations cause a novel syndrome characterized by ataxia and mild mental retardation with predisposition to quadrupedal gait. PLoS genetics. 5**,** e1000487.

Turnbull, V. J., Storey, E., Tarlac, V., et al., 2004. Different ataxin-2 antibodies display different immunoreactive profiles. Brain research. 1027**,** 103-16.

Uryu, K., Nakashima-Yasuda, H., Forman, M. S., et al., 2008. Concomitant TAR-DNA-binding protein 43 pathology is present in Alzheimer disease and corticobasal degeneration but not in other tauopathies. Journal of neuropathology and experimental neurology. 67**,** 555-64.

van Blitterswijk, M., Mullen, B., Heckman, M. G., et al., 2014. Ataxin-2 as potential disease modifier in C9ORF72 expansion carriers. Neurobiology of aging. 35**,** 2421 e13-7.

van de Loo, S., Eich, F., Nonis, D., et al., 2009. Ataxin-2 associates with rough endoplasmic reticulum. Experimental neurology. 215**,** 110-8.

van de Warrenburg, B. P., van Gaalen, J., Boesch, S., et al., 2014. EFNS/ENS Consensus on the diagnosis and management of chronic ataxias in adulthood. European journal of neurology : the official journal of the European Federation of Neurological Societies. 21**,** 552-62.

Vance, C., Rogelj, B., Hortobagyi, T., et al., 2009. Mutations in FUS, an RNA processing protein, cause familial amyotrophic lateral sclerosis type 6. Science. 323**,** 1208-11.

Velazquez-Perez, L., Rodriguez-Labrada, R., Garcia-Rodriguez, J. C., et al., 2011. A comprehensive review of spinocerebellar ataxia type 2 in Cuba. Cerebellum. 10**,** 184-98.

Velazquez-Perez, L., Seifried, C., Santos-Falcon, N., et al., 2004. Saccade velocity is controlled by polyglutamine size in spinocerebellar ataxia 2. Annals of neurology. 56**,** 444-7.

Verkhratsky, A., Toescu, E. C., 1998. Calcium and neuronal ageing. Trends in Neurosciences. 21**,** 2-7.

von Coelln, R., Dawson, V. L., Dawson, T. M., 2004. Parkin-associated Parkinson's disease. Cell and tissue research. 318**,** 175-84.

Wadia, N. H., Swami, R. K., 1971. A new form of heredo-familial spinocerebellar degeneration with slow eye movements (nine families). Brain : a journal of neurology. 94**,** 359-74.

Waelter, S., Boeddrich, A., Lurz, R., et al., 2001. Accumulation of mutant huntingtin fragments in aggresome-like inclusion bodies as a result of insufficient protein degradation. Molecular biology of the cell. 12**,** 1393-407.

Wang, C., Xu, Y., Feng, X., et al., 2015. Linkage analysis and whole-exome sequencing exclude extra mutations responsible for the parkinsonian phenotype of spinocerebellar ataxia-2. Neurobiology of aging. 36**,** 545.e1-545.e7.

Wang, H., Chen, Y., Lin, P., et al., 2014. The CUL7/F-box and WD repeat domain containing 8 (CUL7/Fbxw8) ubiquitin ligase promotes degradation of hematopoietic progenitor kinase 1. The Journal of biological chemistry. 289**,** 4009-17.

Wang, H. L., Yeh, T. H., Chou, A. H., et al., 2006. Polyglutamine-expanded ataxin-7 activates mitochondrial apoptotic pathway of cerebellar neurons by upregulating Bax and downregulating Bcl-x(L). Cellular signalling. 18**,** 541-52.

Watase, K., Barrett, C. F., Miyazaki, T., et al., 2008. Spinocerebellar ataxia type 6 knockin mice develop a progressive neuronal dysfunction with age-dependent accumulation of mutant CaV2.1 channels. Proceedings of the National Academy of Sciences of the United States of America. 105**,** 11987-92.

Watase, K., Weeber, E. J., Xu, B., et al., 2002. A long CAG repeat in the mouse Sca1 locus replicates SCA1 features and reveals the impact of protein solubility on selective neurodegeneration. Neuron. 34**,** 905-19.

Weber, J. J., Sowa, A. S., Binder, T., et al., 2014. From Pathways to Targets: Understanding the Mechanisms behind Polyglutamine Disease. BioMed research international. 2014**,** 701758.

Wellington, C. L., Singaraja, R., Ellerby, L., et al., 2000. Inhibiting caspase cleavage of huntingtin reduces toxicity and aggregate formation in neuronal and nonneuronal cells. The Journal of biological chemistry. 275**,** 19831-8.

Whaley, N. R., Fujioka, S., Wszolek, Z. K., 2011. Autosomal dominant cerebellar ataxia type I: a review of the phenotypic and genotypic characteristics. Orphanet journal of rare diseases. 6**,** 33.

Wilczynska, A., Aigueperse, C., Kress, M., et al., 2005. The translational regulator CPEB1 provides a link between dcp1 bodies and stress granules. Journal of cell science. 118**,** 981-92.

Wils, H., Kleinberger, G., Janssens, J., et al., 2010. TDP-43 transgenic mice develop spastic paralysis and neuronal inclusions characteristic of ALS and frontotemporal lobar degeneration. Proceedings of the National Academy of Sciences of the United States of America. 107**,** 3858-63.

Wu, L. S., Cheng, W. C., Hou, S. C., et al., 2010. TDP-43, a neuro-pathosignature factor, is essential for early mouse embryogenesis. Genesis. 48**,** 56-62.

Xu, X., Sarikas, A., Dias-Santagata, D. C., et al., 2008. The CUL7 E3 ubiquitin ligase targets insulin receptor substrate 1 for ubiquitin-dependent degradation. Molecular cell. 30**,** 403-14.

Xu, Y. F., Gendron, T. F., Zhang, Y. J., et al., 2010. Wild-type human TDP-43 expression causes TDP-43 phosphorylation, mitochondrial aggregation, motor deficits, and early mortality in transgenic mice. The Journal of neuroscience : the official journal of the Society for Neuroscience. 30**,** 10851-9.

Yamanaka, T., Wong, H. K., Tosaki, A., et al., 2014. Large-scale RNA interference screening in mammalian cells identifies novel regulators of mutant huntingtin aggregation. PloS one. 9**,** e93891.

Yamashita, C., Tomiyama, H., Funayama, M., et al., 2014. The evaluation of polyglutamine repeats in autosomal dominant Parkinson's disease. Neurobiology of aging. 35**,** 1779 e17-21.

Yang, C. M., Chung, H. J., Huang, Y. H., et al., 2014a. Standardized analysis of laparoscopic and robotic-assisted partial nephrectomy complications with Clavien classification. Journal of the Chinese Medical Association : JCMA. 77**,** 637-41.

Yang, H., Li, J. J., Liu, S., et al., 2014b. Aggregation of polyglutamine-expanded ataxin-3 sequesters its specific interacting partners into inclusions: implication in a loss-of-function pathology. Scientific reports. 4**,** 6410.

Yokoshi, M., Li, Q., Yamamoto, M., et al., 2014. Direct binding of Ataxin-2 to distinct elements in 3' UTRs promotes mRNA stability and protein expression. Molecular cell. 55**,** 186-98.

Yoo, S. Y., Pennesi, M. E., Weeber, E. J., et al., 2003. SCA7 knockin mice model human SCA7 and reveal gradual accumulation of mutant ataxin-7 in neurons and abnormalities in short-term plasticity. Neuron. 37**,** 383-401.

Young, J. E., Gouw, L., Propp, S., et al., 2007. Proteolytic cleavage of ataxin-7 by caspase-7 modulates cellular toxicity and transcriptional dysregulation. The Journal of biological chemistry. 282**,** 30150-60.

Yu, Y. C., Kuo, C. L., Cheng, W. L., et al., 2009a. Decreased antioxidant enzyme activity and increased mitochondrial DNA damage in cellular models of Machado-Joseph disease. Journal of neuroscience research. 87**,** 1884-91.

Yu, Z., Wang, A. M., Robins, D. M., et al., 2009b. Altered RNA splicing contributes to skeletal muscle pathology in Kennedy disease knock-in mice. Disease models & mechanisms. 2**,** 500-7.

Zeddies, S., Podliesna, S., di Summa, F., et al., The rna-binding protein ataxin-2 regulates the onset of megakaryocytic differentiation. 42nd Annual Scientific Meeting of the ISEH – Society for Hematology and Stem Cells, Vol. 41. Experimental Hematology, Vienna, Austria, 2013, pp. 68.

Zhang, Y., Ling, J., Yuan, C., et al., 2013. A role for Drosophila ATX2 in activation of PER translation and circadian behavior. Science. 340**,** 879-82.

Zhang, Y., Snider, A., Willard, L., et al., 2009a. Loss of Purkinje cells in the PKCgamma H101Y transgenic mouse. Biochemical and biophysical research communications. 378**,** 524-8.

Zhang, Y. J., Xu, Y. F., Cook, C., et al., 2009b. Aberrant cleavage of TDP-43 enhances aggregation and cellular toxicity. Proceedings of the National Academy of Sciences of the United States of America. 106**,** 7607-12.

Zhou, L., Wang, H., Chen, D., et al., 2014. p62/sequestosome 1 regulates aggresome formation of pathogenic ataxin-3 with expanded polyglutamine. International journal of molecular sciences. 15**,** 14997-5010.

Zoghbi, H. Y., Orr, H. T., 2009. Pathogenic mechanisms of a polyglutamine-mediated neurodegenerative disease, spinocerebellar ataxia type 1. The Journal of biological chemistry. 284**,** 7425-9.

Zuccato, C., Valenza, M., Cattaneo, E., 2010. Molecular mechanisms and potential therapeutical targets in Huntington's disease. Physiological reviews. 90**,** 905-81.

9 Appendix

9.1 Contributions to this thesis

The following internships and master thesis were accomplished in the context of this doctoral thesis and contributed experimental data:

1) Master thesis: Tanja Stehning, "Identification and characterization of interaction partners of Ataxin-2", February 2014
2) Internship: Julia Konovalova, January 2014
3) Internship: Anna Krauss, August 2013
4) Internship: Tanja Stehning, September 2012

9.2 Supplementary Figures and Tables

9.2.1 Supplementary Figures

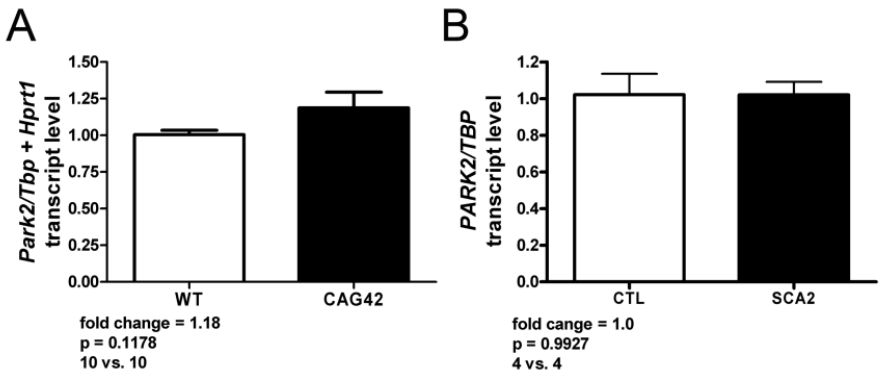

Supplementary Figure 1. Park2 transcript levels are not significantly changed in Atxn2-CAG42-KIN mice and SCA2 patient fibroblasts. Transcript levels of Park2 were assayed via real-time RT-qPCR in cerebellum of 18-month-old WT and *Atxn2*-CAG42-KIN mice (A) as well as in SCA2 patient skin fibroblasts vs. healthy controls (B). Park2 did not show any significant change.

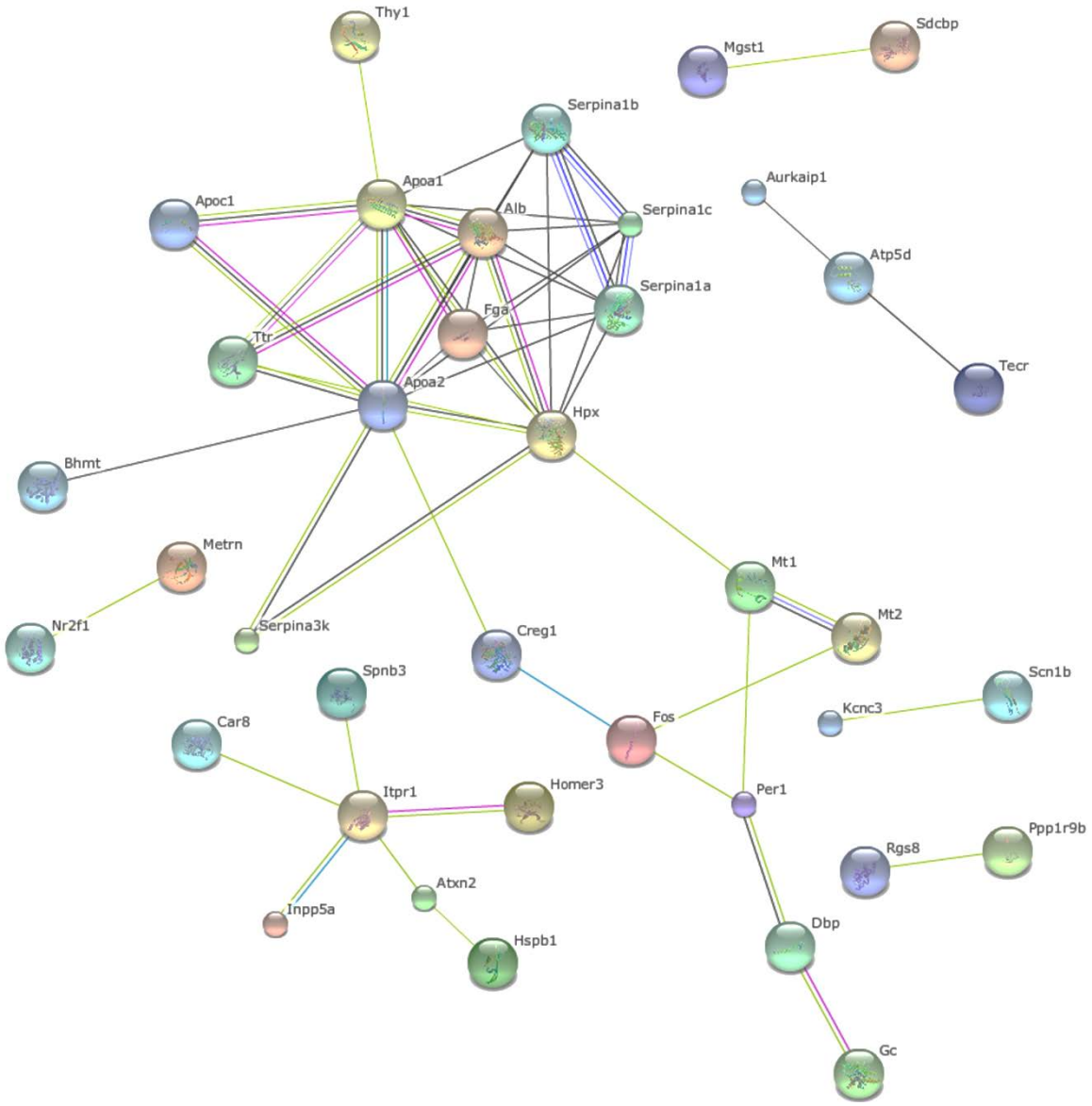

Supplementary Figure 2. Overview of the 100 most downregulated transcripts revealed by RNAseq in Atxn2-KO cerebellum. Downregulated transcripts are depicted as an interaction network. Illustration via STRING 9.05 (GeneXPro).

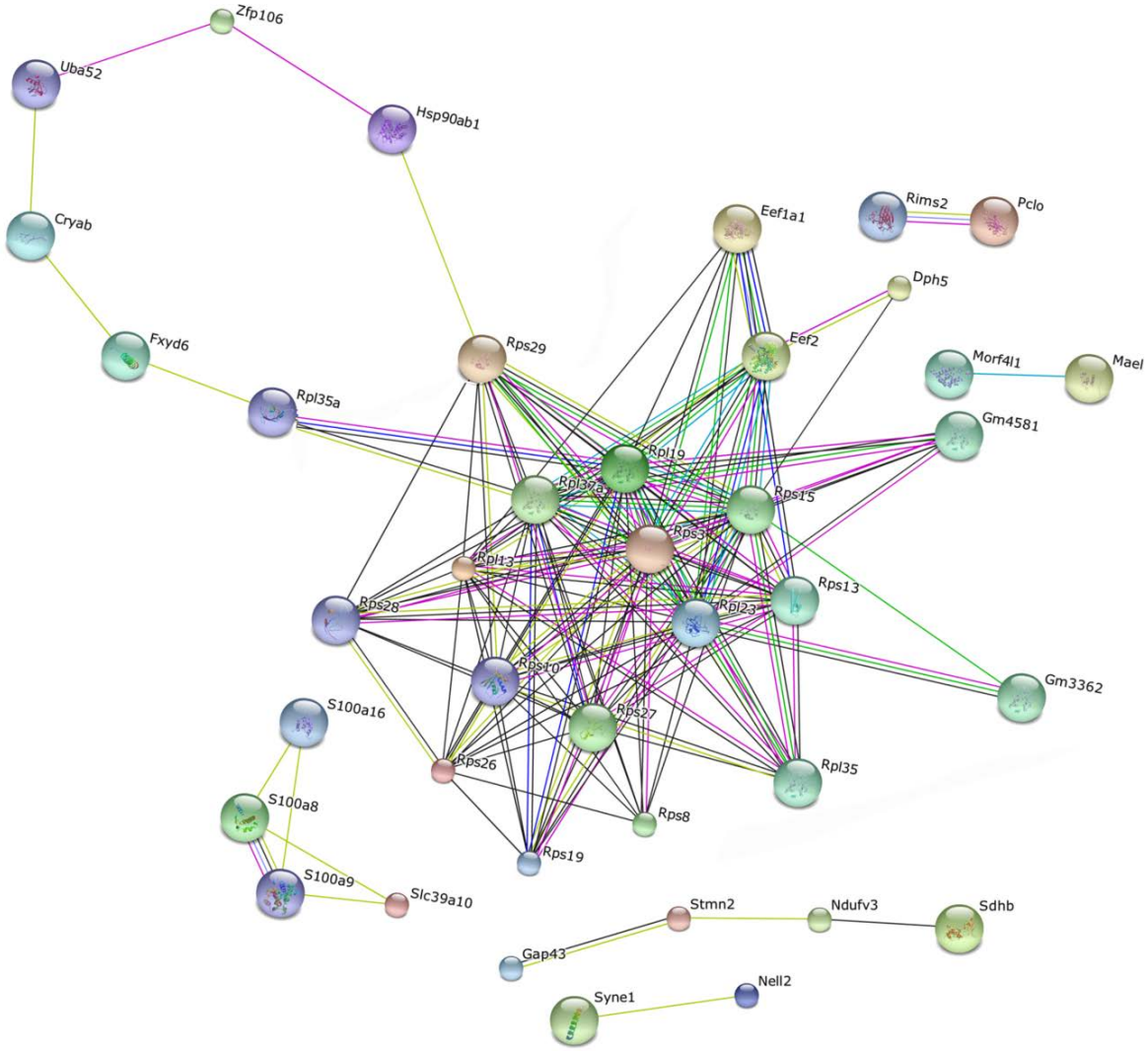

Supplementary Figure 3. Overview of the 100 most upregulated transcripts revealed by RNAseq in Atxn2-KO cerebellum. Upregulated transcripts are depicted as an interaction network. Illustration via STRING 9.05 (GeneXPro).

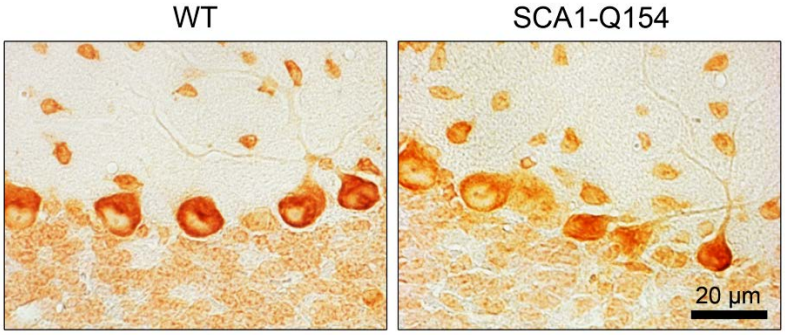

Supplementary Figure 4. ATXN2 does not show aggregation in Atxn1-Q154-KIN mice. Brain slices of 20-week-old WT and HOM animals were stained for ATXN2 and microscopic pictures of Purkinje neurons were taken. ATXN2 was distributed equally in the cytoplasm of WT and HOM mice.

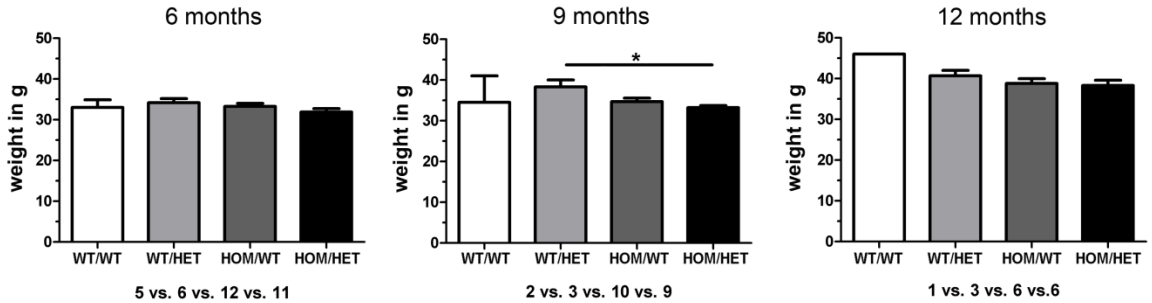

Supplementary Figure 5. Weight analyses in male double mutants do not reveal any consistent changes. Body weight was measured in male animals of all genotypes at 6, 9, and 12 months of age. No consistent changes were observed (n = 1-5 for WT/WT, 3-6 for WT/HET, 6-12 for HOM/WT, and 6-11 for HOM/HET animals).

9.2.2 Supplementary Tables

Supplementary Table 1. Microarray transcriptome profiling reveals significant dysregulation of Fbxw8 in Atxn2-CAG42-KIN cerebellum. Whole genome analysis was conducted using cerebellum of 3 WT vs. 3 *Atxn2*-CAG42-KIN mice at 6 months of age and of 4 WT vs. 4 *Atxn2*-CAG42-KIN mice at 18 months of age. The table shows only an abstract of the complete data.

Gene Symbol	Gene Name	Oligo Spot ID	Fold Change Cerebellum	
			6 months	18 months
Fbxw8	F-box and WD-40 domain protein 8	1426944_at	1.89	2.54
		1436732_s_at	2.40	2.50

Supplementary Table 2. RNAseq confirms upregulation of Fbxw8 in Atxn2-CAG42-KIN cerebellum. For RNAseq 3 WT vs. 3 *Atxn2*-CAG42-KIN animals at 18 months of age were used. The table shows only an abstract of the complete data.

Gene Symbol	Gene Name	Isoform	Fold Change Cerebellum 18 months
Fbxw8	F-box and WD-40 domain protein 8	ENSMUSG00000032867:001	1.48
		ENSMUSG00000032867:006	1.98
		ENSMUSG00000032867:005	1.69

Supplementary Table 3. Microarray transcriptome profiling data for Atxn2-KO mice. Transcriptome profiling was performed using cerebellum and liver of WT and *Atxn2*-KO animals at the ages 6, 12, and 24 weeks. Oligo spots for *Atxn2* are only mentioned in case of significant downregulation in all tissues and at all ages. For calcium homeostasis factors only transcripts with dysregulation at both ages in cerebellum are shown. For translation regulation only transcripts with significant changes in both tissues and at both ages are depicted and *Pabpc1*. The table shows only an abstract of the complete data (n = 3 vs. 3 per age).

Gene Symbol	Gene Name	Oligo Spot ID	Fold Change Cerebellum		Fold Change Liver	
			6 weeks	6 months	6 weeks	6 months
Atxn2 loss						
Atxn2	Ataxin-2	1419866_s_at	-29.59	-42.96	-37.40	-60.24
		1438143_s_at	-49.20	-51.99	-49.09	-56.94
		1443516_at	-1.41	-1.77	-1.77	-2.01
		1459363_at	-1.80	-1.46	-1.30	-1.37

Gene Symbol	Gene Name	Oligo Spot ID	Fold Change Cerebellum		Fold Change Liver	
			6 weeks	6 months	6 weeks	6 months
		1460653_at	-10.00	-14.00	-7.99	-13.71
Calcium homeostasis						
Atp2a2	ATPase, Ca++ transporting, cardiac muscle, slow twitch 2	1416551_at	-1.20	-1.16	-1.28	-1.21
		1452363_a_at	-1.21	-1.23	-1.21	-1.25
Inpp5a	Inositol polyphosphate-5-phosphatase A	1433605_at	-1.35	-1.48	-1.47	-1.45
Itpr1	Inositol 1,4,5-triphosphate receptor 1	1417279_at	-1.55	-1.70	*n.s.*	*n.s.*
Rora	RAR-related orphan receptor alpha	1424034_at	-1.36	-1.32	*-1.27*	*n.s.*
Translation regulation						
Eef1g	Eukaryotic translation elongation factor 1 gamma	1417364_at	1.16	1.23	1.08	1.15
Eif2s2	Eukaryotic translation initiation factor 2, subunit 2 (beta)	1448819_at	1.60	1.39	1.22	1.31
Gnb2l1 / Rack1	Guanine nucleotide binding protein (G protein), beta polypeptide 2 like 1	1455168_a_at	1.10	1.17	1.10	1.15
Nop10 / Nola3	Nucleolar protein family A, member 3	1423210_a_at	1.16	1.24	1.26	1.10
		1423211_at	1.35	1.18	1.18	1.19
Paip1	polyadenylate binding protein-interacting protein 1	1425521_at	10.85	2.84	14.90	8.71
		1441955_s_at	5.25	2.82	7.09	5.85
Pabpc1	poly A binding protein, cytoplasmic 1	1453840_at	-1.84	*n.s.*	*n.s.*	*n.s.*
Rpl6	Ribosomal protein L6	1416546_a_at	1.08	1.21	1.15	1.19
Rpl8	Ribosomal protein L8	1417762_a_at	1.10	1.15	1.12	1.12
Rpl10	Ribosomal protein L10	1415942_at	1.12	1.14	1.08	1.22
Rpl13	Ribosomal protein L13	1450150_a_at	1.09	1.15	1.09	1.26
Rpl14	Ribosomal protein L14	1438626_x_at	1.21	1.32	1.17	1.14
Rpl18	Ribosomal protein L18	1450372_a_at	1.22	1.16	1.13	1.20
Rpl23	Ribosomal protein L23	1415701_x_at	1.12	1.19	1.12	1.16
		1460680_a_at	1.12	1.20	1.12	1.15
Rpl29	Ribosomal protein L29	1448846_a_at	1.25	1.16	1.15	1.23
		1436046_x_at	1.29	1.19	1.15	1.21
		1455348_x_at	1.24	1.12	1.17	1.18
Rpl41	Ribosomal protein L41	1422623_x_at	1.09	1.11	1.12	1.22
Rpo1-3	RNA polymerase 1-3	1447320_x_at	1.14	1.13	1.18	1.17
		1459657_s_at	1.21	1.17	1.18	1.17
Rps2	Ribosomal protein S2	1431765_a_at	1.18	1.13	1.19	1.28
		1422156_a_at	1.19	1.08	1.16	1.26
Rps10	Ribosomal protein S10	1456497_x_at	1.11	1.13	1.14	1.17
Rps12	Ribosomal protein S12	1416453_x_at	110	1.13	1.13	1.17
Rps15	Ribosomal protein S15	1416088_a_at	1.18	1.14	1.15	1.19

Gene Symbol	Gene Name	Oligo Spot ID	Fold Change Cerebellum		Fold Change Liver	
			6 weeks	6 months	6 weeks	6 months
		1416089_at	1.13	1.10	1.08	1.16
Rps16	Ribosomal protein S16	1416404_s_at	1.14	1.17	1.10	1.13
Rps18	Ribosomal protein S18	1435712_a_at	1.12	1.16	1.13	1.23
		1448739_x_at	1.14	1.14	1.18	1.24
Rps26	Ribosomal protein S26	1415876_a_at	1.13	1.17	1.23	1.20
Rpsa	Ribosomal protein SA	1448245_at	1.24	1.29	1.13	1.17
TBC1 domain family members						
Tbc1d8b	TBC1 domain family, member 8B	1430133_at	-1.25	-1.24	-1.80	-1.32
Tbc1d9b	TBC1 domain family, member 9B	1428596_at	*-1.26*	*-1.26*	*-1.26*	-1.28

Supplementary Table 4. Differentially regulated transcripts identified by microarray transcriptome analysis in Tia1-KO mice. Cerebellum and spinal cord of *Tia1*-KO and C57BL/6J WT animals at 12 and 24 weeks of age were analyzed via microarray transcriptome analysis. The table shows only an abstract of the complete data (n = 3 vs. 3 per age).

Gene Symbol	Gene Name	Oligo Spot ID	Fold Change Cerebellum	
			12 weeks	24 weeks
Tia1 loss				
Tia1	Cytotoxic granule-associated RNA binding protein 1 (TIA1)	1431708_PM_a_at	-3,6	-3,45
Lipid storage and membrane trafficking				
Angptl4	Angiopoietin-like 4	1417130_PM_s_at	2,05	1,79
Cntn4	Contactin 4	1438782_PM_at	-2,32	-2,61
Mfsd2a	Major facilitator superfamily domain containing 2A	1428223_PM_at	1,58	1,49
Plin4	Perilipin 4	1418595_PM_at	2,62	2,11
Pnpla2	Patatin-like phospholipase domain containing 2	1428143_PM_a_at	1,4	1,2
Pnpla7	Patatin-like phospholipase domain containing 7	1451361_PM_a_at	1,28	1,37
Tbc1d24	TBC1 domain family, member 24	1448028_PM_at	1,95	1,54
		1442325_PM_at	1,73	1,55
Wdfy1	WD repeat and FYVE domain containing 1	1424749_PM_at	1,38	2,94
		1437358_PM_at	1,31	2,91
		1435588_PM_at	1,39	2,75

Supplementary Table 5. Almost no transcript changes of TBC1 domain family members in Atxn2-CAG42-KIN mice. Analysis of transcript levels via real-time RT-qPCR revealed almost no changes for WT vs. HOM cerebellar tissue between 6 weeks and 18 months of age, as well as in cortical tissue of 18-month-old animals (n = 3-8 WT vs. 3-8 HOM animals).

Gene symbol	WT vs. HOM Cb 18 months	WT vs. HOM Cx 18 months	WT vs. HOM Cb 6 months	WT vs. HOM Cb 6 weeks
Tbc1d1	-1.02-fold *n.s.*	-1.05-fold *n.s.*	-1.05-fold *n.s.*	-1.13-fold *n.s.*
Tbc1d8b	+1.00-fold *n.s.*	-1.07-fold *n.s.*	-1.01-fold *n.s.*	+1.01-fold *n.s.*
Tbc1d9b	+1.02-fold *n.s.*	-1.05-fold *n.s.*	-1.07-fold *n.s.*	-1.03-fold *n.s.*
Tbc1d24	+1.01-fold *n.s.*	-1.05-fold *n.s.*	-1.12-fold *	-1.22-fold **

Supplementary Table 6. Transcriptional dysregulations of ataxia genes in Atxn2-KO, Atxn2-CAG42-KIN and Atxn2-CAG100-KIN cerebellum. Transcript levels were assessed in WT vs. HOM cerebellum of 6-month-old *Atxn2*-KO, 18-month-old *Atxn2*-CAG42-KIN and 10-week-old *Atxn2*-CAG100-KIN animals. Downregulations are highlighted in green, upregulations in red. Transcripts with dysregulations in more than two mouse lines are written in bold (n = 4-11 WT vs. 3-12 HOM for *Atxn2*-KO, 3-11 WT vs. 3-10 HOM for *Atxn2*-CAG42-KIN, and 4-8 WT vs. 4-8 HOM for *Atxn2*-CAG100-KIN animals).

Gene symbol	*Atxn2*-KO WT vs. HOM Cb 6 months	*Atxn2*-CAG42 WT vs. HOM Cb 18 months	*Atxn2*-CAG100 WT vs. HOM Cb 10 weeks
***Atxn1* (SCA1)**	↓*	↓*	*n.s.*
***Atxn2* (SCA2)**	↓***	*n.s.*	↓*
Atxn3 (SCA3)	↓***	*n.s.*	*n.s.*
Sptbn2 (SCA5)	*n.s.*	-	*n.s.*
Cacna1a (SCA6)	*n.s.*	*n.s.*	↑*
Atxn7 (SCA7)	*n.s.*	*n.s.*	-
Atxn10 (SCA10)	*n.s.*	*n.s.*	*n.s.*
Ttbk2 (SCA11)	*n.s.*	*n.s.*	↓**
Ppp2r2b (SCA12)	*n.s.*	*n.s.*	*n.s.*
Kcnc3 (SCA13)	*n.s.*	*n.s.*	↓*
Prkcg (SCA14)	*n.s.*	*n.s.*	*n.s.*
***Itpr1* (SCA15)**	↓*	↓*	↓*
Pdyn (SCA23)	*n.s.*	*n.s.*	-
Fgf14 (SCA27)	*n.s.*	↓T	*n.s.*
Afg3l2 (SCA28)	*n.s.*	↑*	*n.s.*
***Bean1* (SCA31)**	↓*	↑*	*n.s.*
Tgm6 (SCA35)	*n.s.*	*n.s.*	*n.s.*
Nop56 (SCA36)	*n.s.*	*n.s.*	-
Fxn	↑***	*n.s.*	↑*

Supplementary Table 7. Open field behavior of WT, HET and HOM Atxn2-CAG100-KIN animals at different ages. Open Field analysis was performed at 10, 20, and 30 weeks of age as well as at age 12 and 14 months. Decreased performance is highlighted in green, increased in red. Significances are indicated for WT vs. HET and WT vs. HOM animals (n = 11-23 WT, 8-16 HET, and 12-22 HOM).

Parameter	10 weeks		20 weeks		30 weeks		12 months		14 months	
	HET	HOM	HET	HOM	HET	HOM	HET	HOM	HET	HOM
Movement Time	*n.s.*	**↑	**↓	n.s.	n.s.	n.s.	n.s.	n.s.	*↑	*↑
Rest Time	*n.s.*	**↓	**↑	n.s.	n.s.	n.s.	n.s.	n.s.	*↓	*↓
Horizontal Activity	*n.s.*	*↑	*↓	n.s.	n.s.	n.s.	n.s.	n.s.	*↑	*↑
Horizontal Movements	*n.s.*	**↑	*↓	n.s.	n.s.	*↑	n.s.	n.s.	**↑	*↑
Vertical Activity	*n.s.*	*n.s.*	*↓	n.s.	n.s.	n.s.	n.s.	*↓	n.s.	n.s.
Vertical Movements	*n.s.*	*n.s.*	*↓	n.s.	n.s.	**↓	n.s.	***↓	n.s.	T↓
Vertical Time	*↓	*n.s.*	*↓	n.s.	n.s.	**↓	n.s.	***↓	n.s.	n.s.
Total Distance	*n.s.*	*↑	*↓	n.s.	n.s.	n.s.	n.s.	n.s.	*↑	*↑
Stereotype Counts	*n.s.*	*↑	T ↓	n.s.	n.s.	n.s.	n.s.	T↑	n.s.	T ↑
Stereotype Time	T ↑	*n.s.*	n.s.	n.s.	n.s.	n.s.	n.s.	*↑	*↑	*↑

9.3 List of Figures

9.4 List of Tables

9.5 Abbreviations

µg	Microgram
µl	Microliter
µm	Micrometer
µM	Micromolar
129Sv	Inbred mouse strain
1C2	Antibody against polyglutamine repeats >38
3', 5'	3 prime end, 5 prime end
A2BP1	Ataxin-2 binding protein 1
A315T	Nucleotide transition from Adenosine to Thymidine at position 315
ABC	Avidin-Biotin complex
AD	Alzheimer's disease
ADCA	Autosomal dominant cerebellar ataxia
AFG3L2	AFG3 ATPase Family Member 3-Like 2, SCA28
ALS	Amyotrophic lateral sclerosis
AMPA	α-amino-3-hydroxy-5-methyl-4-isoxazolepropionic acid
ANOVA	Analysis of variance
APS	Ammonium persulfate
AR	Androgen receptor
ARCA	Autosomal recessive cerebellar ataxia
AT	Ataxia telangiectasia
ATM	Ataxia telangiectasia mutated
ATN1	Atrophin-1
ATP	Adenosine-tris-phosphate
ATP2A2	ATPase slow twitch 2
ATP2B2	ATPase plasma membrane 2
ATXN	Ataxin
b-ACTIN	Beta Actin
BEAN1	Brain expressed, associated with NEDD4, 1 , SCA31

BOAT	Brother of Ataxin-1
bp	Base pair
BSA	Bovine serum albumin
C57BL/6J	Inbred mouse strain
C9ORF72	Chromosome 9 open reading frame 72
CA8	Carbonic anhydrase 8
CAA	Cytosine-adenine-adenine
CACNA1A	Calcium channel, voltage-dependent, P/Q type, alpha 1A subunit, SCA6
CAG	Cytosine-adenine-guanine
CALB1	Calbindin 1
CALM1	Calmodulin 1
CCDC88	Coiled-coil domain containing 88, SCA40
CCND1	Cyclin D1
cDNA	Complementary DNA
CIC	Capicua transcriptional repressor
cm	Centimeter
CNS	Central nervous system
Co-IP	Co-immunoprecipitation
Cre	Cyclization recombination
Ct	Cycle threshold
CTG	Cytosine-thymine-guanine
CTL	Control
CUL	Cullin
DAG	Diacylglycerole
dATX2	Drosophila Ataxin-2
DDX6	DEAD/H-box helicase 6
DM	Myotonic dystrophy
DMSO	Dimethyl sulfoxide
DNA	Deoxyribonucleic acid
dNTP	Deoxyribonucleic triphosphates
DRPLA	Dentatorubral pallidoluysian atrophy
DTA	Diphtheria toxin A
DTT	Dithiothreitol
e.g.	Exempli gratia
EAAT4	Excitatory Amino Acid Transporter 4 (=SLC1A6)
ECL	Enhanced chemiluminescence
EDTA	Ethylenglycoltetraacetic acid
EEF	Eukaryotic elongation factor
EGF	Epidermal growth factor
EGFR	Epidermal growth factor receptor
EGTA	Ethylenglycoltetraacetic acid
EIF	Eukaryotic initiation factor
ELOVL	Elongation of very long chain fatty acids protein
EP300	E1A binding protein P300
ER	Endoplasmic reticulum
ES cell	Embryonic stem cell
et al.	Et alii

FBS	Fetal bovine serum
FBXW8	F-box and WD repeat domain containing 8
FELASA	Federation of Laboratory Animal Science Associations
FGF14	Fibroblast growth factor 14, SCA27
Flp	Flippase
FRAXA	Fragile site, folic acid type, rare, fra(X)(q27.3) A
FRAXE	Fragile site, folic acid type, rare, fra(X)(q28) E
FRDA	Friedreich ataxia
FRT	Flippase recognition target
FTD	Frontotemporal dementia
FUS	Fused in sarcoma
FXTAS	Fragile X-associated tremor/ataxia syndrome
g	Earth's gravitational acceleration
G418	Geniticin
GABA	γ-Aminobutyric acid
GLUT4	Glucose transporter type 4
GNAQ	Guanine nucleotide binding protein (G protein), q polypeptide
GNB2L1	Guanine nucleotide binding protein (G protein), beta polypeptide 2-like 1
GRASP65/GORASP1	Golgi reassembly stacking protein 1, 65kDa
GRIA	Glutamate receptor, ionotropic, AMPA
GRID2	Glutamate receptor, ionotropic, delta 2
GRM	Glutamate receptor, metabotropic
GWAS	Genome wide association study
h	Hour
HD	Huntington's disease
HECT	Homologous to the E6-AP Carboxyl Terminus
HEK293	Human embryonic kidney 293 cell line
HeLa	Cervical cancer cells derived from the patient Henrietta Lacks
HEPES	4-(2-hydroxyethyl)-1-piperazineethanesulfonic acid
HET	Heterozygous
hnRNP	Heterogeneous nuclear ribonucleoproteins
HOM	Homozygous
HPK1	Hematopoietic progenitor kinase 1
HPRT1	Hypoxanthine-guanine phosphoribosyltransferase 1
HRP	Horseradish peroxidase
HTT	Huntingtin
i.a.	Inter alia
ICMT	Isoprenylcysteine carboxyl methyltransferase
IHC	Immunohistochemistry
INPP5A	Inositol polyphosphate-5-Phosphatase
IP2	Inositol diphosphate
IP3	Inositol trisphosphate
IRS1	Insulin receptor substrate 1
ITPR1	Inositol trisphosphate receptor 1, SCA15
kb	Kilo bases
KCNC3	Potassium voltage-gated channel, Shaw-related subfamily, member 3, SCA13
KCND3	Potassium voltage-gated channel, Shal-related subfamily, member 3, SCA19

kDa	Kilo Dalton
KIN	Knock-in
KITL	C-Kit ligand
KO	Knock-out
KpnI	Restriction site
LA	Long arm of homology
LANP	Acidic (Leucine-Rich) nuclear phosphoprotein 32 family, member A
LoxP	Locus of crossover in P1
Lsm	Like Sm
LsmAD	Like Sm associated domain
Lys	Lysin
M	Molar
MBP	Myelin basic protein
ME31B	Ortholog of DDX6 in *Drosophila melanogaster*
MEM	Modified eagle medium
mg	Milligram
MGRN1	Mahogunin ring finger 1
min	Minutes
MIRAS	Mitochondrial recessive ataxia syndrome
miRNA	Micro RNA
MJD	Majado Joseph Disease
ml	Milliliter
mm	Millimetre
mM	Millimolar
MRI	Magnetic resonance imaging
mRNA	Messenger RNA
n.a.	Not analyzed
n.s.	Not significant
NCBI	National Center for Biotechnology Information
NEAA	Non-essential amino acids
NEDD4	Neural precursor cell expressed, developmentally down-regulated 4
Neo	Neomycin
ng	Nanogramm
NII	Neuronal intranuclear inclusions
NLS	Nuclear localization signal
nM	Nanomol
NMDA	N-Methyl-D-aspartate
NOP	Nucleolar protein
NP40	Nonyl phenoxypolyethoxylethanol
Nr	Number
OD	Optical density
p62/SQSTM1	Sequestosome 1
PAB1	Ortholog of PABP in *Saccharomyces cerevisiae*
PABPC1	Polyadenylate- binding protein, cytoplasmic 1
PAGE	Polyacrylamid gel electrophoresis
PAIP	Poly(A) binding protein interacting protein
PAM	PABP interacting motif

PARK2	Parkin
P-bodies	Processing body
PBP1	Pab binding protein 1, ortholog of ATXN2 in *Saccharomyces cerevisiae*
PBS	Phosphate-buffered saline
PBST	Phosphate-buffered saline, Tween
PCP	Purkinje cell protein
PCR	Polymerase chain reaction
PD	Parkinson's disease
PDYN	Prodynorphin, SCA23
Pen/Strep	Penicillin/Streptomycin
PFA	Paraformaldehyde
PIP2	Phosphatidylinositol 4,5-bisphosphate
PLCB4	Phospholipase C, beta 4
PLCG1	Phospholipase C, gamma 1
PLEKHG4	Pleckstrin homology domain containing, family G member 4
pmol	Picomolar
PMSF	Phenylmethylsulfonyl fluoride
Poly(A)	Polyadenine
polyQ	Polyglutamine
PPP2R2B	Protein phosphatase 2, regulatory subunit B, beta, SCA12
PRD	Proline-rich domain
PRKCG	Protein kinase C, gamma, SCA14
PVALB	Parvalbumin
PVDF	Polyvinylidene fluoride
Rab	Ras related protein
RBFOX	RNA binding protein, fox homolog (C. elegans)
RBM17	RNA binding motif protein 17
RBX1	Ring-box 1
rER	Rough endoplasmic reticulum
RING	Really interesting new gene (structural domain)
RIPA	Radioimmunoprecipitation assay
RNA	Ribonucleic acid
RNAseq	RNA deep sequencing
RORA	RAR-related orphan receptor A
RPL	Ribosomal protein large subunit
rpm	Revolutions per minute
RPS	Ribosomal protein small subunit
RRM	RNA recognition motif
rRNA	Ribosomal RNA
RT	Room temperature
RYR1	Ryanodine receptor 1
s	Seconds
S860/S864	Serine at position 860/864
SA	Short arm of homology
SBMA	Spinal bulbar muscle atrophy
SCA	Spinocerebellar Ataxia
Sca2-/-	Sca2 deficient

SCAR	Spinocerebellar ataxia autosomal recessive
SCASI	Spinocerebellar ataxia with saccadic intrusions
SCF	SKP1-CUL1-F-Box complex
SDS	Sodium dodecyl sulfate
SEM	Standard error of means
SG	Stress granule
SH3	Src homology 3
shRNA	Small hairpin RNA
SKP1	S-phase kinase-associated protein 1
SLC1A6	Excitatory Amino Acid Transporter 4 (=EAAT4)
SOD1	Superoxide dismutase 1
SphI	Restriction site
SPTBN2	Spectrin, beta, non-erythrocytic 2, SCA5
SYNE1	Spectrin repeat containing, nuclear envelope 1
T	Trend
TARDBP/TDP43	Transactive response DNA binding protein 43 kDa
TBC1	Tre-2/USP6, BUB2, cdc16
TBP	TATA box binding protein, SCA17
TGM6	Transglutaminase 6, SCA35
TH	Tyrosin hydroxylase
TIA1	T-cell restricted intracellular antigen-1
TIAR	TIA1 related protein
TIP60	K(Lysine) Acetyltransferase 5
TMEM240	Transmembrane protein 240, SCA21
Tris	Tris(hydroxymethyl)-aminomethane
TRPC3	Transient receptor potential cation channel, subfamily C, member 3
TTBK2	Tau tubulin kinase 2, SCA11
U	Units
U2AF65	Splicing Factor U2AF 65 KD
UBQ	Ubiquitin
UPS	Ubiquitin-proteasome system
UTR	Untranslated region
V	Volt
VCP	Valosin containing protein
vol	Volume
WB	Western blot
WD40	Structural domain
WT	Wild type
ZFE	Central animal facility (Zentrale Forschungseinrichtung)

12 Publications and Presentations

Publications

Parts of this work are published in:

2012 Damrath E, Heck MV, Gispert S, Azizov M, Nowock J, Seifried C, Rüb U, Walter M, Auburger G. ATXN2-CAG42 sequesters PABPC1 into insolubility and induces FBXW8 in cerebellum of old ataxic knock-in mice. PLoS Genetics.

2014 Heck MV, Azizov M, Stehning S, Walter M, Kedersha N, Auburger G. Dysregulated expression of lipid storage and membrane dynamics factors in Tia1 knockout mouse nervous tissue. Neurogenetics.

2015 Fittschen M, Lastres-Becker I, Halbach MV, Damrath E, Gispert S, Azizov M, Walter M, Müller S, Auburger G. Genetic ablation of ataxin-2 influences global ribosomal translation. Neurogenetics.

2015 Halbach MV, Stehning T, Damrath E, Jendrach M, Şen NE, Başak N, Auburger G. Both ubiquitin ligases FBXW8 and PARK2 are sequestrated into insolubility by ATXN2 polyQ expansions, but only FBXW8 expression is dysregulated. PLoS One.

Further publications:

2014 Auburger G, Gispert S, Lahut S, Ömürr Ö, Damrath E, Heck M, Başak N. 12q24 locus association with type 1 diabetes: SH2B3 or ATXN2? World Journal of Diabetes.

Under revision:

Halbach MV, Stehning T, Damrath E, Walter M, Auburger G. Atxn2 knock-out and CAG42-knock-in cerebellum shows similarly dysregulated expression of calcium homeostasis factors.

Zeddies S, Meiners M, Podliesna S, di Summa F, Damrath E, Halbach MV, Auburger G, Gutierrez L, von Lindern M, Thijssen-Timmer DC. Ataxin-2 is crucial for protein accumulation in megakaryocytes and proper platelet functionality.

Manuscripts in preparation:

Meierhofer D, Halbach MV, Sen NE, Gispert S, Auburger G. Metabolome- and proteome- profiling demonstrates deficiency of Atxn2 to modulate branched chain amino acids and fatty acids pathways, as well as the citric acid cycle.

Halbach MV, Gispert S, Damrath E, Seidel K, Kern B, Azizov M, Meierhofer D, Auburger G. The Atxn2-CAG100-KnockIn mouse with ataxia leading to death by age 14 months shows strong cytoplasmic aggregation and strong calcium factor alterations in cerebellum.

Oral Presentations

mRNA processing in neurodegenerative diseases: The interaction of Ataxin-2 with TDP-43. 2012. RNA Club, Goethe University, Frankfurt am Main, Germany.

The E3 ubiquitin protein ligase component FBXW8 binds and degrades pathological ATXN2. 2014. Young investigators colloquium, Frankfurt am Main, Germany.

Poster Presentations

M. Heck, E. Damrath, S. Gispert, M. Azizov, G. Auburger. 2013. The E3 ubiquitin ligase complex component *Fbxw8* degrades pathological *Ataxin-2.* New frontiers in neurodegenerative disease research, Keystone Symposia on Molecular and Cellular biology, Santa Fe, New Mexico, USA.

M. Heck, E. Damrath, S. Gispert, M. Azizov, G. Auburger. 2013. Fbxw8 is involved in expansion-dependent degradation of ATXN2, 10th International Conference on Alzheimer's and Parkinson's Diseases and Related Neurological Disorders, Florence, Italy.

M. Heck, E. Damrath, T. Stehning, S. Gispert, M. Azizov, G. Auburger. 2013. Fbxw8 is elevated in an Atxn2-CAG42 knock-in mouse model and degrades expanded Ataxin-2, Gordon research seminar on CAG triplet repeat disorders, Waterville Valley, New Hampshire, USA.

M. Heck, E. Damrath, T. Stehning, S. Gispert, M. Azizov, G. Auburger. 2013. Fbxw8 is elevated in an Atxn2-CAG42 knock-in mouse model and degrades expanded Ataxin-2, Gordon research conference on CAG triplet repeat disorders, Waterville Valley, New Hampshire, USA.